THE BEST OF NIMBUS

MARCH 1971
CONTRACT NO. NAS 5-10343

prepared for
NATIONAL AERONAUTICS AND SPACE ADMINISTRATION
GODDARD SPACE FLIGHT CENTER
GREENBELT, MARYLAND

ALLIED RESEARCH ASSOCIATES, INC.
VIRGINIA ROAD · CONCORD, MASSACHUSETTS

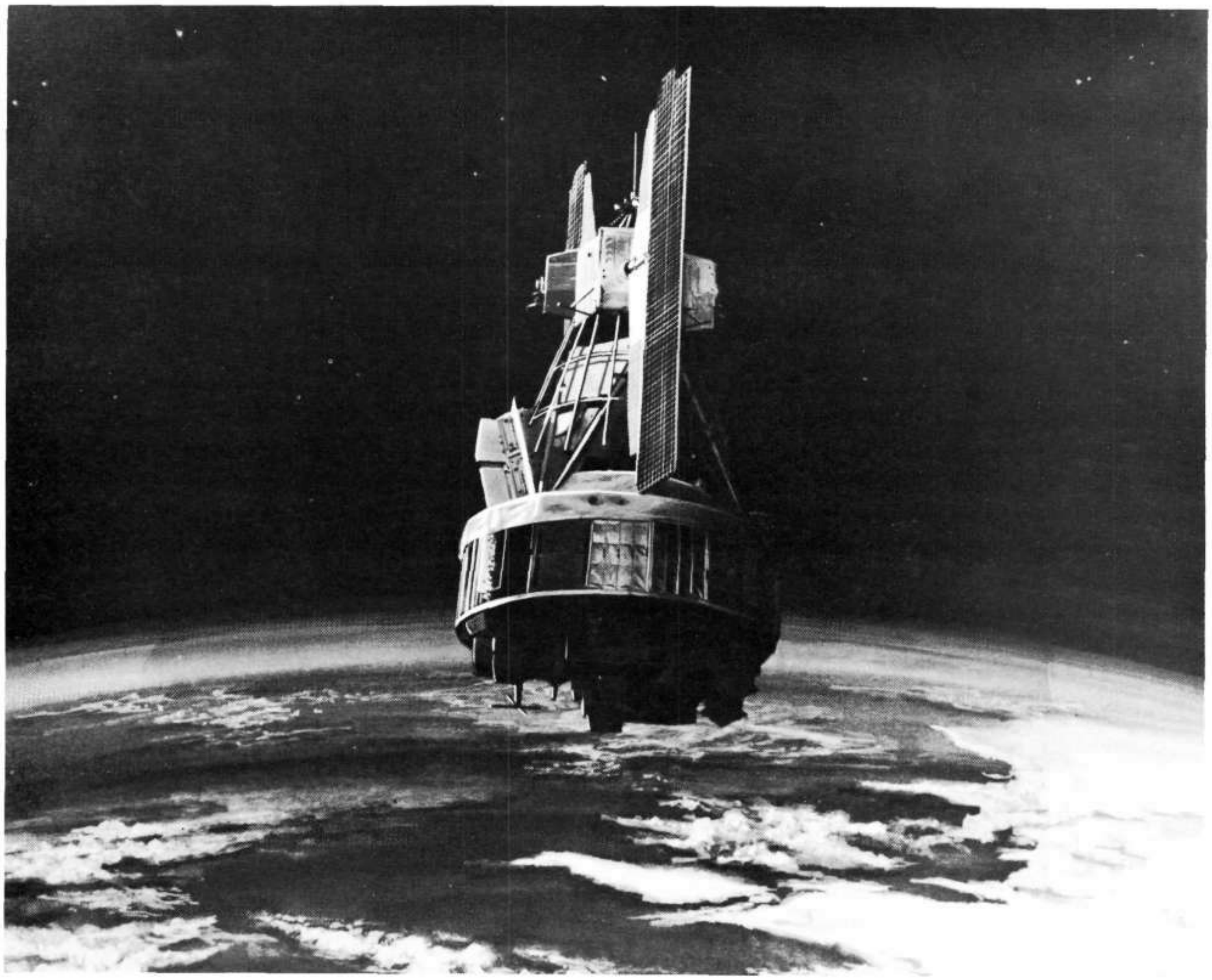

Nimbus

9G45-80

THE BEST OF NIMBUS

MARCH 1971

CONTRACT NO. NAS 5-10343

prepared for

NATIONAL AERONAUTICS AND SPACE ADMINISTRATION

GODDARD SPACE FLIGHT CENTER

GREENBELT, MARYLAND

ALLIED RESEARCH ASSOCIATES, INC.
VIRGINIA ROAD · CONCORD, MASSACHUSETTS

FOREWORD

The past decade has seen the opening of a new era in meteorology. The use of satellites as remote sensing platforms to observe the earth's weather has significantly increased our understanding of our atmospheric environment and its mechanisms. The TIROS satellites which were first launched in April of 1960 were primarily intended to serve the operational needs of the meteorologists in the detection and tracking of storms, frontal systems and similar phenomena by means of their associated cloud patterns. Nimbus, NASA's "second-generation" meteorological satellite, has further advanced the application of such observations to meteorological research and to other fields of geophysics. In the past six years, four Nimbus satellites have been successfully launched, carrying increasingly complex scientific instruments. From their sun-synchronous near-polar orbits these earth-oriented satellites have returned to earth a wealth of new data applicable to meteorology, as well as significant data of interest for oceanography, geology, geography and hydrology.

The successive contributions of the Nimbus program to the field of meteorology have included: near continuous high-resolution global television cloud and storm mapping photography, direct readout of television picture data to local users, high-resolution infrared photography for nighttime cloud mapping, and for surface and cloud top temperature determination, and wind determination by means of satellite tracking of drifting balloons. Of major significance has been the recent demonstration and application of satellite techniques for making quantitative measurements of atmospheric structure. Specifically, the measurement of the three-dimensional distribution of atmospheric temperature and humidity, which began with Nimbus III, marks a major new capability for weather observation. These data and these new techniques are now being rapidly exploited in order to achieve improved and longer range weather forecasts.

This book reviews some of the highlights of the Nimbus six-year history. From the hundreds of thousands of pictures and other results available, we have attempted to select those which best represent the many data types and application areas. These results thus provide a capsule summary of the history and achievements of the Nimbus program.

ACKNOWLEDGEMENTS

This book was prepared by the Geophysics and Aerospace Division of Allied Research Associates, Inc., Concord, Massachusetts, under contract NAS 5-10343 with the Goddard Space Flight Center, National Aeronautics and Space Administration, Greenbelt, Maryland.

The initial picture selection was conducted by Daniel A. Ball in collaboration with NASA officials and with members of the Nimbus Data Utilization Center. Mr. John E. Sissala provided the analysis of many of the photographs with graphical assistance by Hans J. Ackerman. The main text was written by James R. Greaves who was also responsible for the picture grouping and final editing of the figure captions. Mr. John Lindstrom, NASA manager of the NADUC, lent immeasurable assistance and motivation throughout the preparation of this report.

The annotated maps used in a number of illustrations were drawn from the following atlases:

The Times, 1958: The Times Atlas of the World, J. Bartholomew (ed), Houghton-Mifflin Company.

National Geographic Society, 1963: National Geographic Atlas of the World, National Geographic Society.

American Geographical Society, 1964: Physical-Geographic Atlas of the World, Moscow.

Rand McNally and Company, 1960: Goode's World Atlas, E. B. Espenshade (ed).

McGraw-Hill Company, 1963: McGraw-Hill International Atlas, W. Bormann (dir).

Odyssey Books, 1966: The Odyssey World Atlas.

TABLE OF CONTENTS

Preceding page blank

LIST OF ILLUSTRATIONS

PRECEDING PAGE BLANK NOT FILMED

LIST OF ILLUSTRATIONS, contd.

LIST OF ILLUSTRATIONS, contd.

LIST OF ILLUSTRATIONS, contd.

INTRODUCTION

In the late summer of 1964, a new generation of weather satellites was born. Named after the Latin word for raincloud, NASA's Nimbus I * was sucessfully lifted into earth orbit during the pre-dawn hours on the 28th of August. This launch represented the culmination of years of research and planning as the Nimbus concept evolved from the earlier TIROS ** experiments.

Because of the important role played by the Nimbus project in our nation's continuing space program, this publication attempts to review some of its more significant accomplishments during the past six years. A selection of the best of anything is always a subjective procedure, and with hundreds of thousands of pictures and other data displays to choose from, the task becomes particularly difficult. The primary goal in putting together the current selection was to touch upon all phases of the broad spectrum of data types and application areas.

The new Nimbus satellite system incorporated a number of significant technological advances over its predecessors. Unlike the spin-stabilized TIROS satellites, whose sensors were pointed earthward for less than half of each orbit, the Nimbus satellite employed a three-axis stabilization system which kept its sensors oriented toward the earth at all times. This attitude control system kept the sensor packages of all four Nimbus satellites aligned to within 1° of the local vertical. Equipped with sensors capable of both day and nighttime measurements, Nimbus could thus provide a nearly continuous 24-hour earth surveillance.

Even the Nimbus orbit introduced a new concept for meteorological satellites. By carefully matching the nominal 600 n.mi. orbital altitude with a near-polar inclination, a nearly circular sun-synchronous orbit was achieved. This meant that the satellite's orbital plane completed one revolution per year, always keeping one edge directed toward the sun. Thus, the Nimbus sensors would encounter near local noontime conditions on the northbound, or daytime pass and near local midnight conditions on the southbound nighttime pass. This was a considerable improvement over the nearly haphazard viewing conditions encountered by the early TIROS satellites.

---

* A change from Roman numerals to Arabic numbers has recently been made for designating Nimbus satellites. Preparation of this publication was begun before this change and we have therefore retained the Roman numerals herein.

** Television Infra-Red Observation Satellite

The Nimbus project was originally conceived as a meteorological research and development program. As scientists began to study the data, however, it soon became apparent that these data could also be applied to a number of non-meteorological fields such as oceanography, geology, geography and hydrology. In fact, the data have proved to be of such a high quality that they are now being used in the planning stages of yet another generation of earth-observing satellites, the Earth Resources Technology Satellites, currently being developed by NASA.

The Nimbus project thus continues to lay the groundwork for even more sophisticated satellite programs. In this report, some of the highlights of the Nimbus program to date are reviewed. It will be seen that in its brief seven-year history, the Nimbus satellite series has made important contributions to man's knowledge and understanding of his home planet.

The vital statistics of the individual Nimbus satellites and brief descriptions of the various on-board sensor packages are presented in the following section. More detailed sensor descriptions, as well as information regarding the types and quality of the available data, may be found in the various User's Guides and Data Catalogs listed in a separate section.

THE SATELLITES

This section provides a brief life history of the individual Nimbus satellites and describes in some detail the individual sensor subsystems. The sensor packages and the data production figures are summarized in Tables 1 and 2, respectively.

Nimbus I

The Nimbus I spacecraft was launched at 0852 GMT on the 28th of August 1964. Because of an undetected leak in the fuel transfer equipment, a short second burn of the Agena launch vehicle caused the satellite to go into an elliptical orbit, dipping from an apogee of 504 n. mi. (933 km) to as low as 228 n. mi. (423 km) at perigee. The unexpected low altitude at perigee combined with the high quality of the camera system yielded pictures of remarkable detail and clarity.

The first Nimbus satellite carried three meteorological sensors. The Advanced Vidicon Camera System (AVCS) consisted of three separate cameras aligned in a trimetrogon fashion, perpendicular to the satellite's direction of movement. The data were stored on magnetic tape for subsequent readout to either of two Command and Data Acquisition (CDA) stations, Fairbanks, Alaska or Rosman, North Carolina. These data were then relayed over ground lines to the Goddard Space Flight Center (GSFC) at Greenbelt, Maryland, and to the National Environmental Satellite Service (NESS) at Suitland, Maryland. At Goddard, the data were processed, archived and disseminated.

The Automatic Picture Transmission (APT) system continuously transmitted pictures to local weather users equipped with relatively inexpensive receiving equipment. The local ground station concept was developed as part of the Nimbus program and gave users the world over immediate access to satellite pictures of local weather patterns. Some 65 of these APT stations operated during the Nimbus I lifespan, and proved the value of such a real-time network. By the time of Nimbus IV these APT stations had increased in number to more than 395.

TABLE 1

RADIOMETER EXPERIMENTS, CAMERA SYSTEMS, REAL-TIME SYSTEMS AND COMMUNICATIONS AND TRACKING SYSTEMS

	Camera Systems		Radiometer Systems			Real-Time Systems			Atmospheric Sounding Experiments						Communications and Tracking Experiment
	AVCS	IDCS	HRIR*	MRIR	THIR	APT	DRIR	RTTS	IRIS	SIRS	MUSE	BUV	FWS	SCR	IRLS
N-I	X		X			X									
N-II	X		X	X		X	X								
N-III		X	X	X				X	X	X	X				X
N-IV		X			X			X	X	X	X	X	X	X	X

*HRIR was primarily a nighttime sensor on Nimbus I and Nimbus II, although some daytime imagery was recorded. Nimbus III was also equipped with a specifically designed daytime HRIR system to sense reflected radiation.

TABLE 2

NIMBUS DATA COLLECTION FIGURES

		Last Effective Orbit
Nimbus I (Launch - 28 August 1964)		
AVCS	11,600 pictures	369
APT	2,000 pictures	354
HRIR	100 hours	368
Nimbus II (Launch - 15 May 1966)		
AVCS	114,003 pictures	1,444
APT	148,810 pictures	13,029
HRIR	2,190 hours	2,455
MRIR	1,313 hours	985
DRIR	1,370 hours	2,455
Nimbus III (Launch - 14 April 1969) (Data through 25 September 1970)		
IDCS	41,494 pictures	3,840
HRIR	5,684 hours	3,922
MRIR	3,268 hours	3,975
DRID	72,075 pictures	7,095
DRIR	12,745 hours	7,095
IRIS	1,738 hours	1,332
SIRS	8,389 hours	7,143
MUSE	8,521 hours	7,143
IRLS	21,190 data frames	5,934
Nimbus IV (Launch - 8 April 1970) (Data through 28 February 1971)		
IDCS	30,656 pictures	To date
THIR (11.5 μm)	4,819 hours	"
THIR (6.7 μm)	2,801 hours	"
DRID	Selected Coverage	"
DRIR	Selected Coverage	"
IRIS	6,372 hours	"
SIRS	6,684 hours	"
MUSE	6,784 hours	"
BUV	6,627 hours	"
FWS	1,316 hours	815
SCR	6,784 hours	To date
IRLS	22,027 data frames	"

Both camera systems described above provided only daytime data. At night, a High Resolution Infrared Radiometer (HRIR) measured emitted thermal radiation from clouds and from the earth's land and water surfaces. This sensor operated in a cross-track scanning mode and provided daily temperature maps of the earth's surface on a global scale. The approximate spatial resolution at the subpoint was varied from 1.8 to 4.0 n.mi. Daytime temperature measurements were not possible because the Nimbus I HRIR sensor operated in the 3.4 to 4.2 μm atmospheric "window" region which is contaminated by reflected solar radiation during daylight hours. (An atmospheric "window" is any portion of the electromagnetic spectrum where attenuation by atmospheric constituents is minimal.)

On September 23, 1964, after 26 days of operation, the drive mechanism of the satellite's large solar paddles jammed, preventing the acquisition of an adequate power supply to run the essential attitude control system and the sensor arrays. Seven orbits after failure of the drive mechanism, the on-board telemetry system failed.

Nimbus II

Nimbus II was launched into a near-perfect orbit on the 15th of May 1966. Like Nimbus I, it carried on-board the AVCS, APT and HRIR sensor systems. The striking success of the Nimbus I HRIR in recording nighttime cloudiness and surface temperature patterns, led to a modification of the APT system so that the HRIR data could also be read out by local users in a real-time mode. This system was referred to as the Direct Readout Infrared Radiometer (DRIR) system.

An additional experiment was added to the Nimbus II satellite which was designed to measure electromagnetic radiation emitted and reflected from the earth and its atmosphere in five selected wavelength intervals. The Medium Resolution Infrared Radiometer (MRIR) operated in a scanning mode as did HRIR and had a ground resolution of approximately 30 n.mi. at the subpoint. The five wavelength regions, each with a brief description of its purpose, were as follows:

- 5.4 to 6.9 μm - This channel covered the 6.7 μm water vapor absorption band. Its purpose was to provide information on water vapor distribution in the upper troposphere and, in conjunction with the other channels, to provide data concerning relative humidities at these altitudes.
- 10 to 11 μm - Operating in an atmospheric "window", this channel measured surface or near-surface temperatures over clear portions of the atmosphere. It also provided cloud cover and cloud height information (day and night).

- 14 to 16 μm - This channel, centered about the strong absorption band of CO_2 at 15 μm, measured radiation which emanated primarily from the stratosphere. The information gained here was of primary importance in following seasonal stratospheric temperature changes.

- 5 to 30 μm - This channel measured the emitted long wavelength infrared energy and, in conjunction with the reflected solar radiation channel, furnished data on the heat budget of the planet.

- 0.2 to 4.0 μm - This channel covered more than 99% of the solar spectrum and yielded information on the intensity of reflected solar energy from the earth and its atmosphere.

The MRIR tape recorder failed during interrogation on the 29th of July 1966 after two and a half months of successful operation. Use of the AVCS data continued normally until a tape recorder malfunction occurred during interrogation on August 31, 1966. Only sporadic operation was possible until the 2nd of September when a complete failure of the tape recorder system terminated the availability of the data. The HRIR tape recorder failed on the 15th of November 1966. APT data, however, were received until April 1968.

Nimbus III

Nimbus III was successfully launched into a circular orbit on the 14th of April 1969, less than a year after an earlier attempt failed when a malfunction in the launch vehicle caused the launch to be aborted in mid-flight on May 18, 1968. The HRIR and MRIR experiments were retained although the 5 to 30 μm MRIR channel on Nimbus II was replaced by a 20 to 23 μm channel designed to measure radiation in the spectral region containing the broad rotational absorption bands of water vapor in the lower atmosphere.

The three-camera AVCS system was replaced by a single Image Dissector Camera System (IDCS) experiment. The advantages of the IDCS over the more conventional vidicon camera systems included: the ability to sense a greater dynamic range (about 100:1), high signal-to-noise ratios, direct relationship between light flux input and electron current output, and the avoidance of a mechanical shutter.

The real-time APT system of Nimbus I and II was replaced by a Real Time Transmission System (RTTS) capable of instantaneously transmitting HRIR and IDCS data to APT stations within satellite acquisition range while simultaneously storing these data on tape for subsequent transmission to a CDA facility. Thus, unlike Nimbus I and II, a separate camera system was not required for the real-time data.

Atmospheric sounder experiments for mapping parameters other than cloud cover were initiated with Nimbus III. Four additional experiments, not flown before, were included in Nimbus III. These were:

IRIS - Infrared Interferometer Spectrometer - Provided information on the vertical structure of the atmosphere and the emissive properties of the surface. The specific intensity measured in the absorption bands and in the more transparent "windows" may be used to derive vertical profiles of temperature, water vapor and ozone, in addition to other parameters of meteorological interest.

SIRS - Satellite Infrared Spectrometer - Indirect determinations of the vertical temperature profiles of the atmosphere. In its ultimate application, the results from this or a comparable instrument would be used to determine the three-dimensional temperature structure of the atmosphere to a height of 30 km or more.

MUSE - Monitor of Ultraviolet Solar Energy - Measured changes with time in the ultraviolet solar flux in five broad bands from 1150 to 3000 Å, to measure the solar flux in these regions, and to measure the atmospheric attenuation at these wavelengths as the sensor views the setting sun after the spacecraft has crossed the terminator in the northern hemisphere.

IRLS - Interrogation, Recording and Location System - Collected geophysical, meteorological and other experimental data from remote unmanned data-collection stations (platforms), to determine the location of the platforms and track mobile platforms such as on balloons, buoys, and ships.

The Nimbus III tape recorders began to malfunction during the fall of 1969. Various sensors recorded their last data on the following dates.

IRIS	-	22 July 1969
IDCS	-	25 January 1970
HRIR	-	31 January 1970
MRIR	-	4 February 1970

The SIRS, MUSE, IRLS and RTTS systems were all still operative on a real-time basis when Nimbus IV was launched in April of 1970.

Global mapping experiments had effectively been demonstrated by the end of Nimbus III. A giant step forward was taken with the launch of Nimbus IV. Major changes to the atmospheric sounder experiments allowed global atmospheric structure measurements to be made.

Nimbus IV

Nimbus IV which was launched on April 8, 1970, achieved the best orbit of the series with only a 6 n.mi. difference between apogee and perigee (average height, 590 n.mi.). The IDCS, RTTS, IRIS, MUSE and IRLS experiments were all essentially the same as those flown on Nimbus III. The Nimbus IV SIRS experiment had the added capabilities of determining the tropospheric water vapor content and a spatial scan for increased area coverage. Global analyses of upper-level pressure and and temperature were begun using SIRS data.

The Nimbus III MRIR and HRIR experiments were replaced by the Temperature Humidity Infrared Radiometer (THIR) experiment designed to provide both day and night cloud top or surface temperatures and to yield information on the moisture content of the upper troposphere and stratosphere. The Nimbus IV Temperature-Humidity Infrared Radiometer (THIR) experiment has a ground resolution at the subpoint of about 4 n.mi. for the temperature channel and 12 n.mi. for the water vapor channel.

Three additional experiments were flown on Nimbus IV. These include:

FWS - The Filter Wedge Spectrometer

The FWS experiment monitors the vertical water vapor content in the atmosphere along a continuous strip 150 km wide under the orbital path. The spectrum is scanned from 3 to 7 μm with a rotating filter wedge. Vertical water vapor distribution is derived from the spectra by mathematical inversion techniques.

BUV - The Backscatter Ultraviolet Spectrometer

The BUV experiment monitors the global distribution of atmospheric ozone by measuring the intensity of ultraviolet radiation backscattered from the earth's atmosphere at 12 wavelengths in the 2500 Å to 3400 Å spectral region. The knowledge of atmospheric ozone distribution on a global scale is needed for studies of the energy balance and photo chemistry of the stratosphere, the mass exchange between the lower stratosphere and troposphere, and the general atmosphere circulation.

SCR - The Selective Chopper Radiometer

The SCR experiment determines the temperature of six successive layers of the atmosphere by radiometric measurements of the emission of carbon dioxide in the 15 μm band. The SCR consists of six channels, each of which contains its own optical and electronic components. The six channels and their filter bandwidths are 668 ± 1.5 cm^{-1}, 755 ± 6 cm^{-1}, 675 ± 5 cm^{-1}, 697 ± 5 cm^{-1}, and 712 ± 5 cm^{-1}. The field of view for the upper channels (1 and 2) is circular and 160 km in diameter. Channels 3 through 6 have a field of view of 110 km square.

Except for the FWS, all Nimbus IV experiments were still providing useful data as of February 1971. Nimbus E and F (to become Nimbus V and VI upon launch) will carry highly advanced meteorological, oceanographic and earth surface sensing experimental payloads. These satellites are currently scheduled to be launched in 1972 and 1974, respectively.

THE VIEW FROM ABOVE

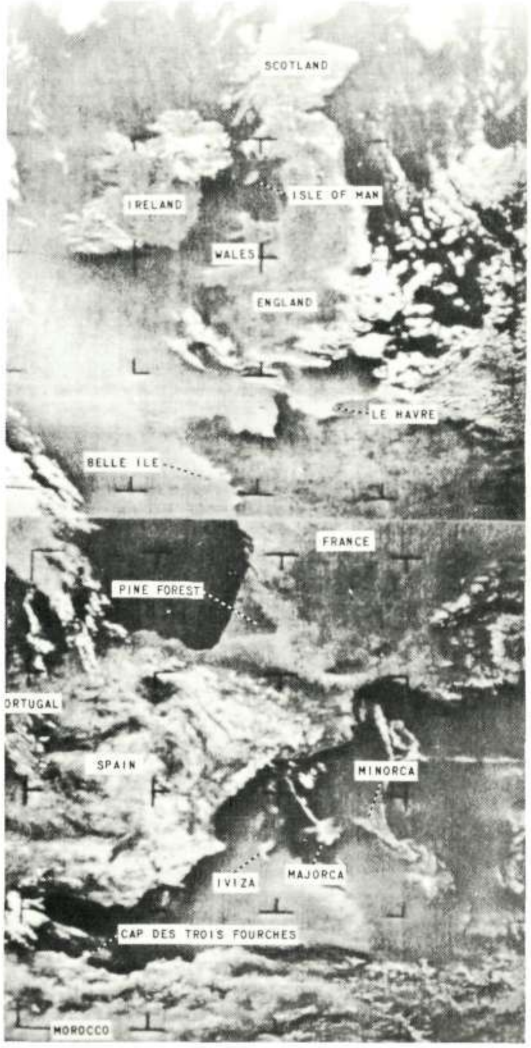

ON A CLEAR DAY ....

Western Europe

This remarkably clear picture of Western Europe was recorded by Nimbus I on 31 August 1964. The picture actually consists of two sequential APT frames read out in real-time by meteorologists in Lannion, France. Of note in the photograph are the darkish highlands of England and Scotland and the pine-forested triangular area of France just north of the French-Spanish border. Pictures such as these provide local meteorologists with instantaneous views of the weather pattern in their immediate area.

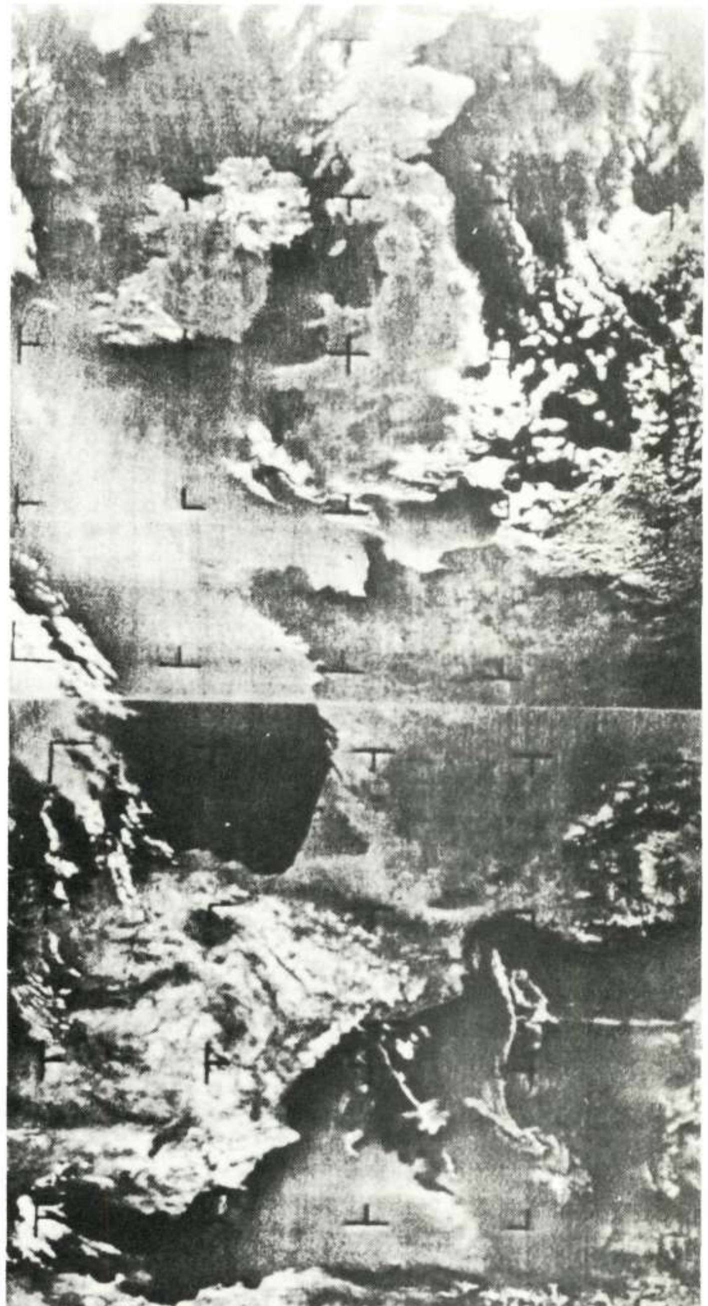

Nimbus I APT 31 August 1964

Northeastern United States

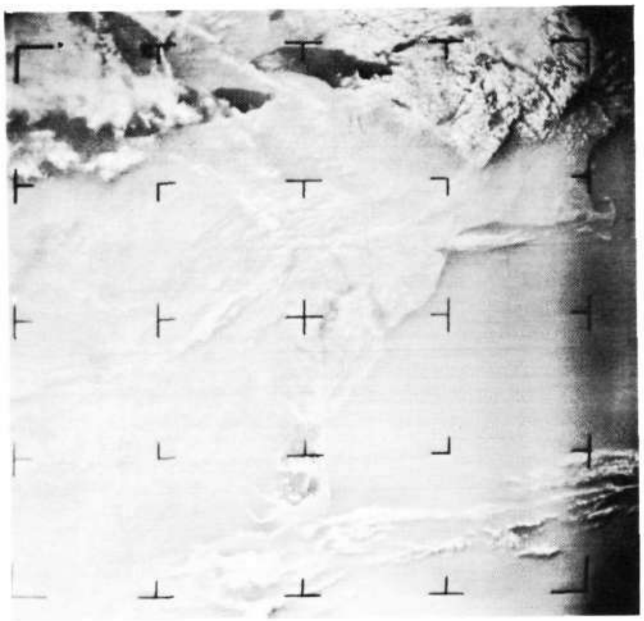

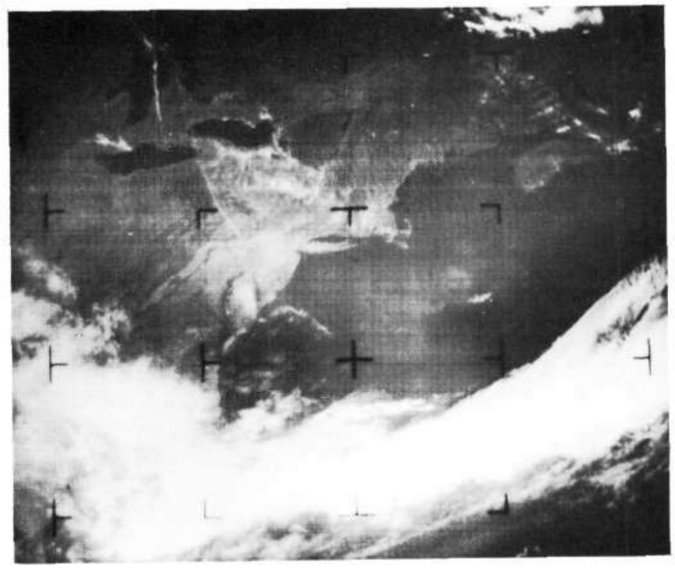

Nimbus I APT 6 September 1964

Nimbus II APT 16 July 1966

In this pair of APT photographs, the Northeastern United States as seen first by Nimbus I and then by Nimbus II nearly two years later is shown. A 230 n.mi. difference in satellite height accounts for the variance in the size of the areas covered. Analysis of the tonal areas in the pictures has produced very close correlations with geologic maps. The lightish area along the coast of the Nimbus II photograph represents some combination of land use, soil, vegetation, and geologic reality enhanced by solar reflection.

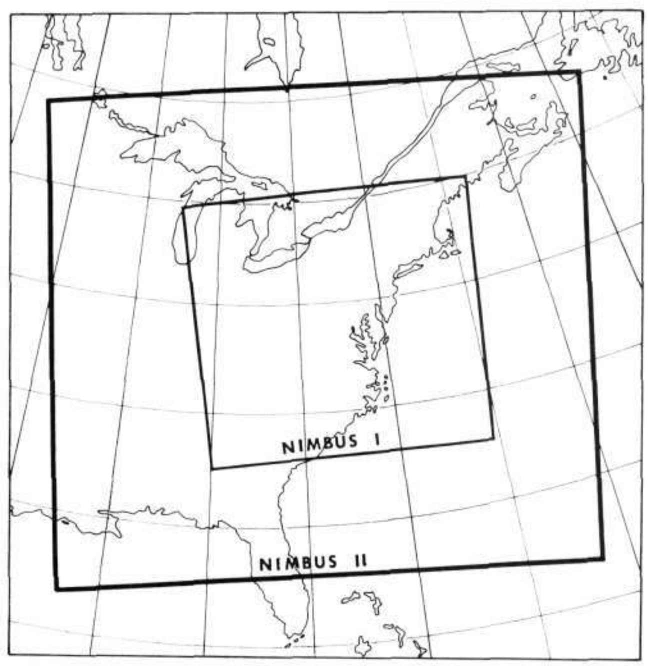

Eastern United States

The bulk of the Nimbus photographic data was first recorded on magnetic tape and then read out to CDA stations at Rosman, North Carolina and Fairbanks, Alaska. This Nimbus I AVCS photograph shows the Eastern United States from just south of Baltimore to Cape Hatteras. Of particular note is the resolution of a man-made object: Interstate Highway 95 from Washington, D. C. to Richmond, Virginia. The road, which appears as a thin white line, is discernible not because of its own width but because of the wide clearing attendant to its construction. The picture was taken shortly after the road was completed and it presents the optimum contrast between lush green vegetation and the newly bared earth. The cities of Washington, Richmond, Petersburg, and Norfolk appear in whitish relief against the surrounding vegetation. Albemarle Sound appears in a bright sunglint area at bottom center.

Nimbus I AVCS
6 September 1964

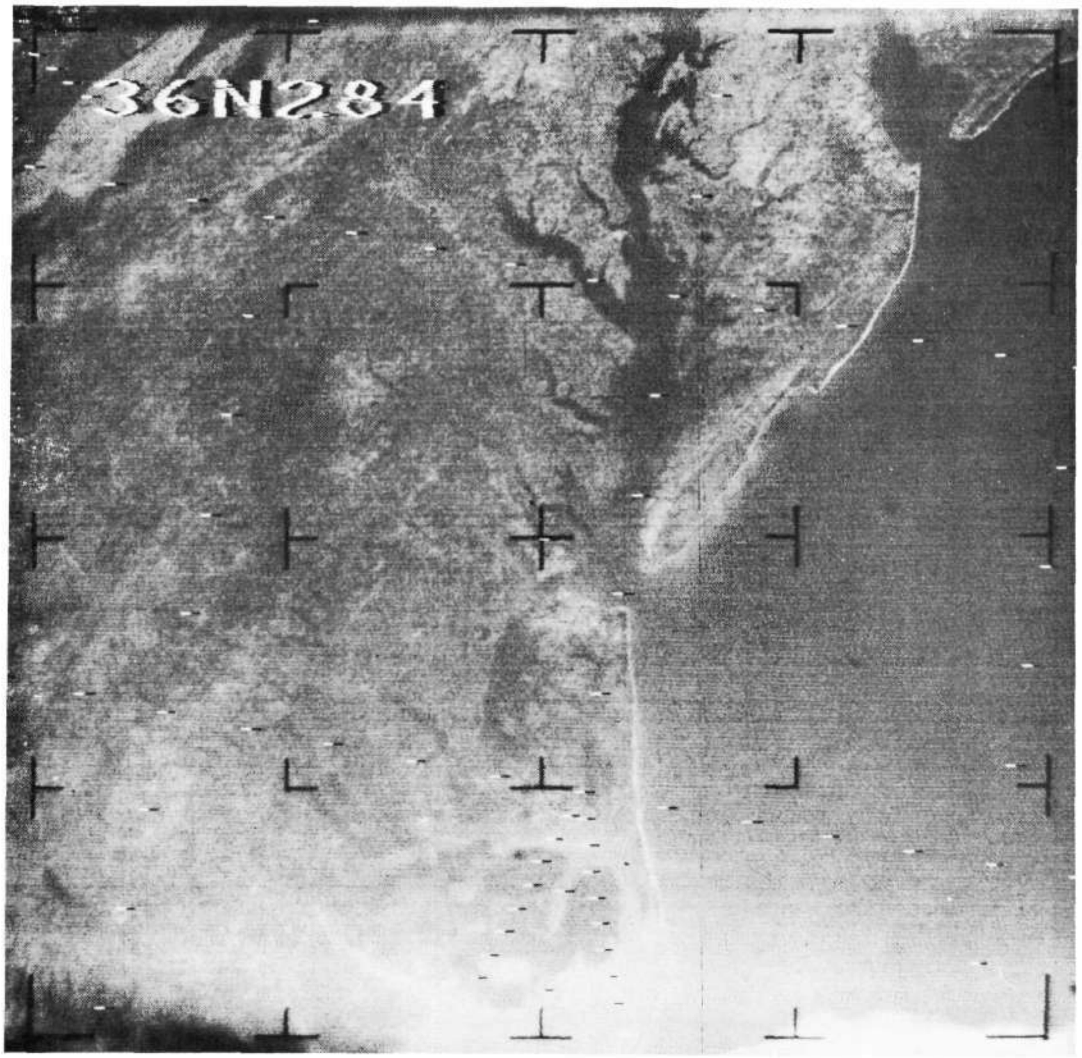

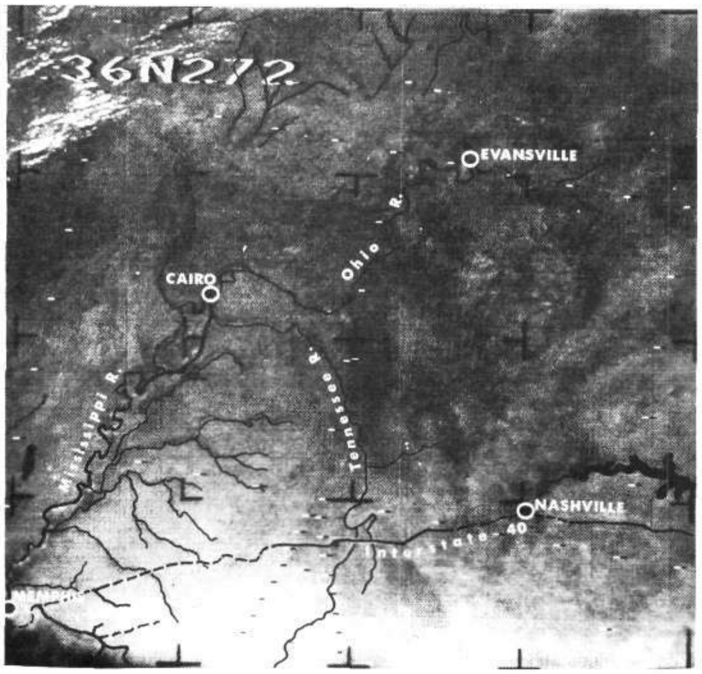

Central United States

The area portrayed in this photograph is from Evansville, Indiana, in the north-central quadrant to Memphis, Tennessee, in the lower left. The Mississippi and its many tributaries are clearly evident as is Memphis itself. Another highway, Interstate 40, is visible for several miles either side of its intersection with the Tennessee River. The juncture of the Ohio and Mississippi Rivers at Cairo, Illinois, is toward the upper left.

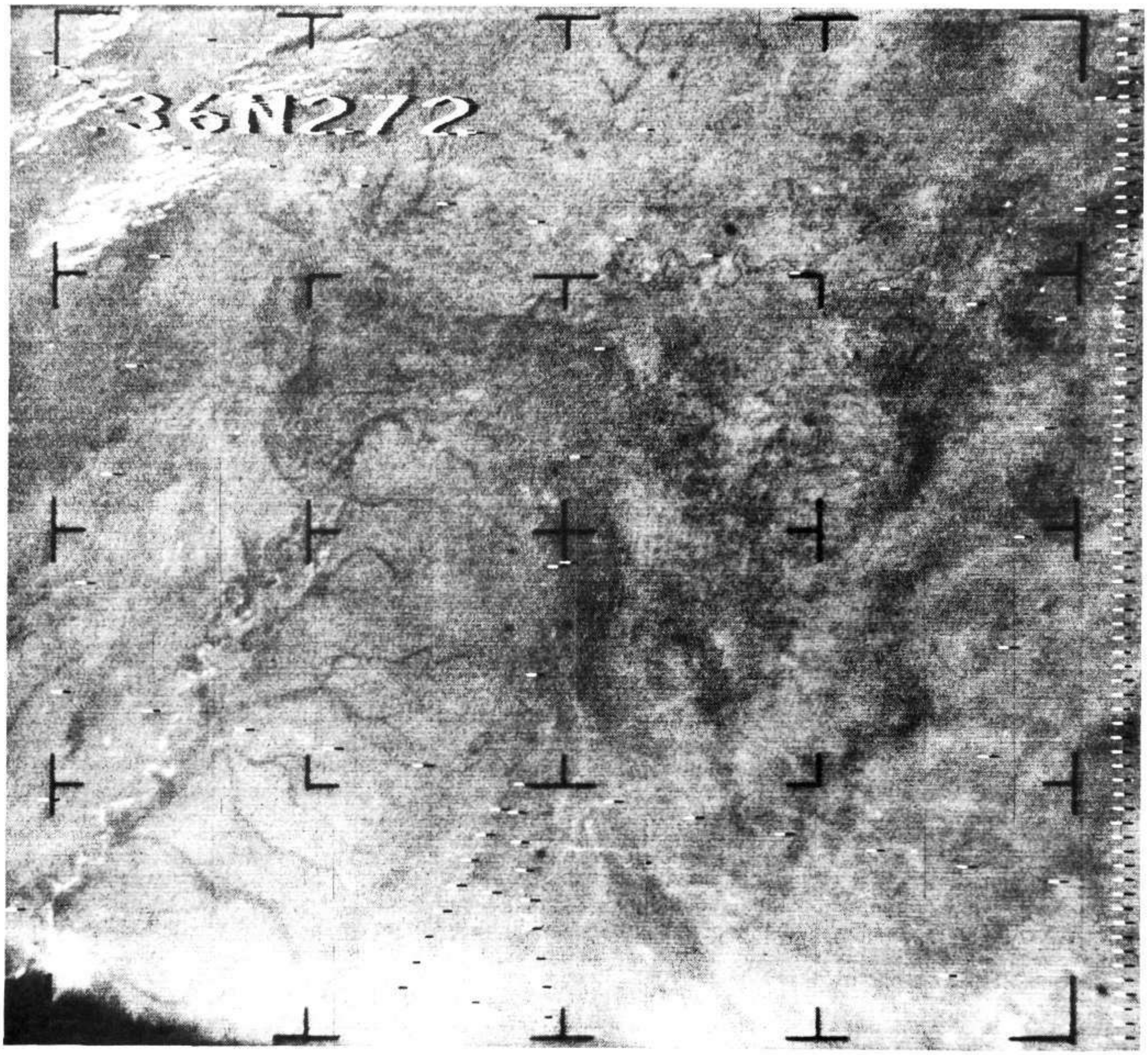

Nimbus I AVCS 10 September 1964

Northwestern United States

Further west, in the states of Washington and Oregon, the Columbia Plateau is dissected by the Columbia River and its tributaries. Reservoirs appear as thicker, darker lines along the river (see map). Snow-peaked mountains (Hood, Adams, and Rainier) appear in the dark Cascade Range at left. Stratus clouds blanket the Willamette Valley and Puget Sound at the extreme left.

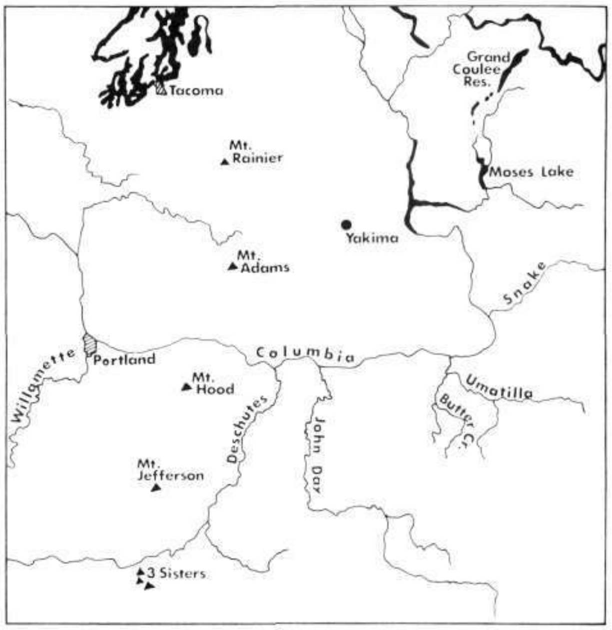

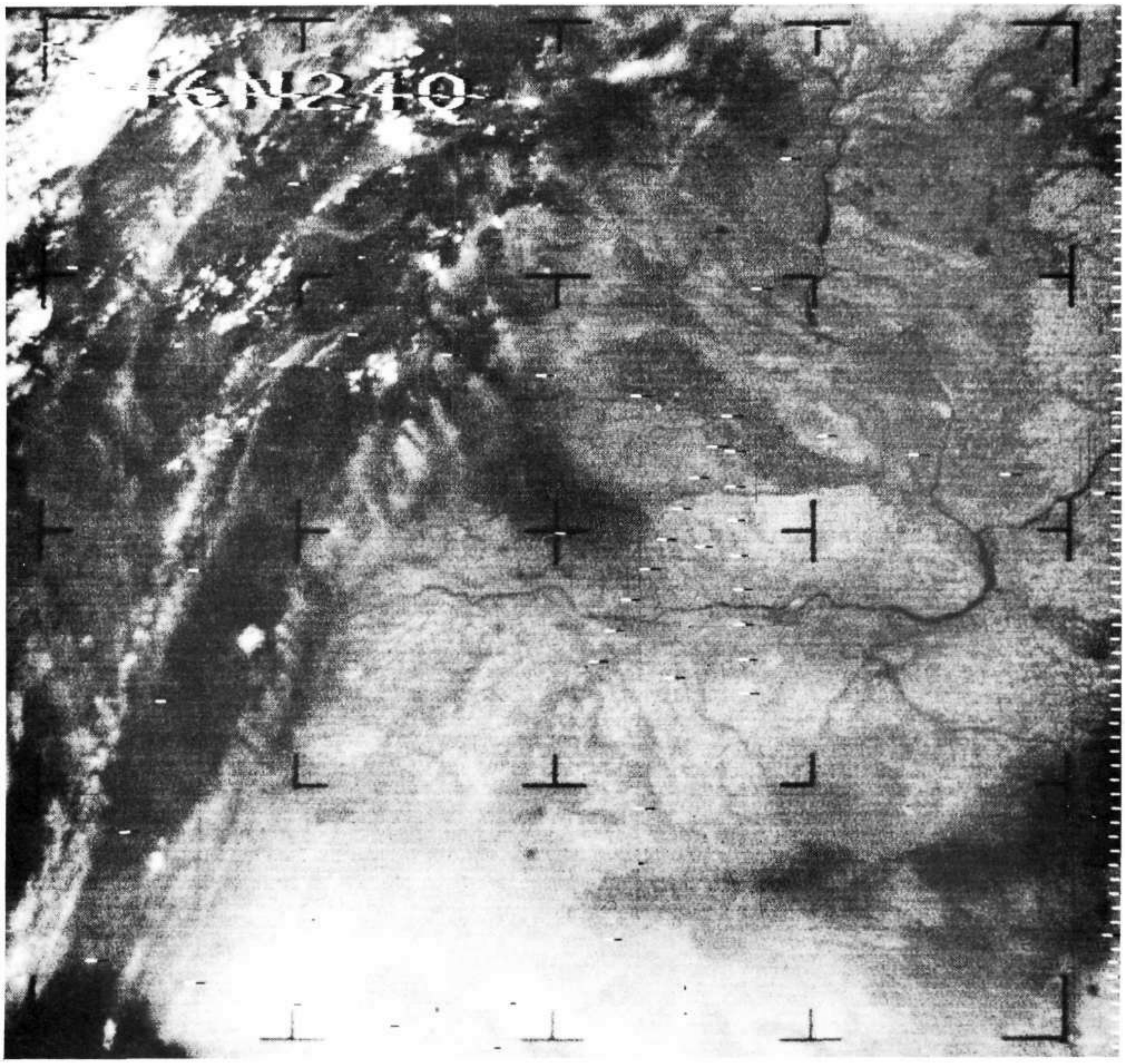

Nimbus I AVCS 16 September 1964

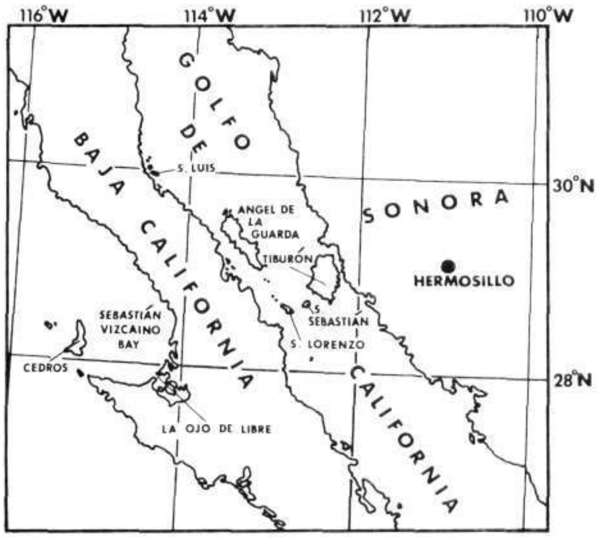

Gulf of California

The data legend of this picture shows that it was recorded at 185052 GMT during orbit 241 of Nimbus I on the 13th of September (the 257th day of 1964, a leap year). For the sake of a clearer presentation format, the legend is omitted from the other figures. Mexico, Baja California, and the Gulf of California are relatively cloud-free but low stratus clouds hug the Pacific shores of the Baja peninsula and scattered cumulus clouds dot the mountains of Mexico. The higher volcanic terrain of Tiburon Island (highest peak 3985 feet) appears darker than its lower slopes, probably because of vegetal cover.

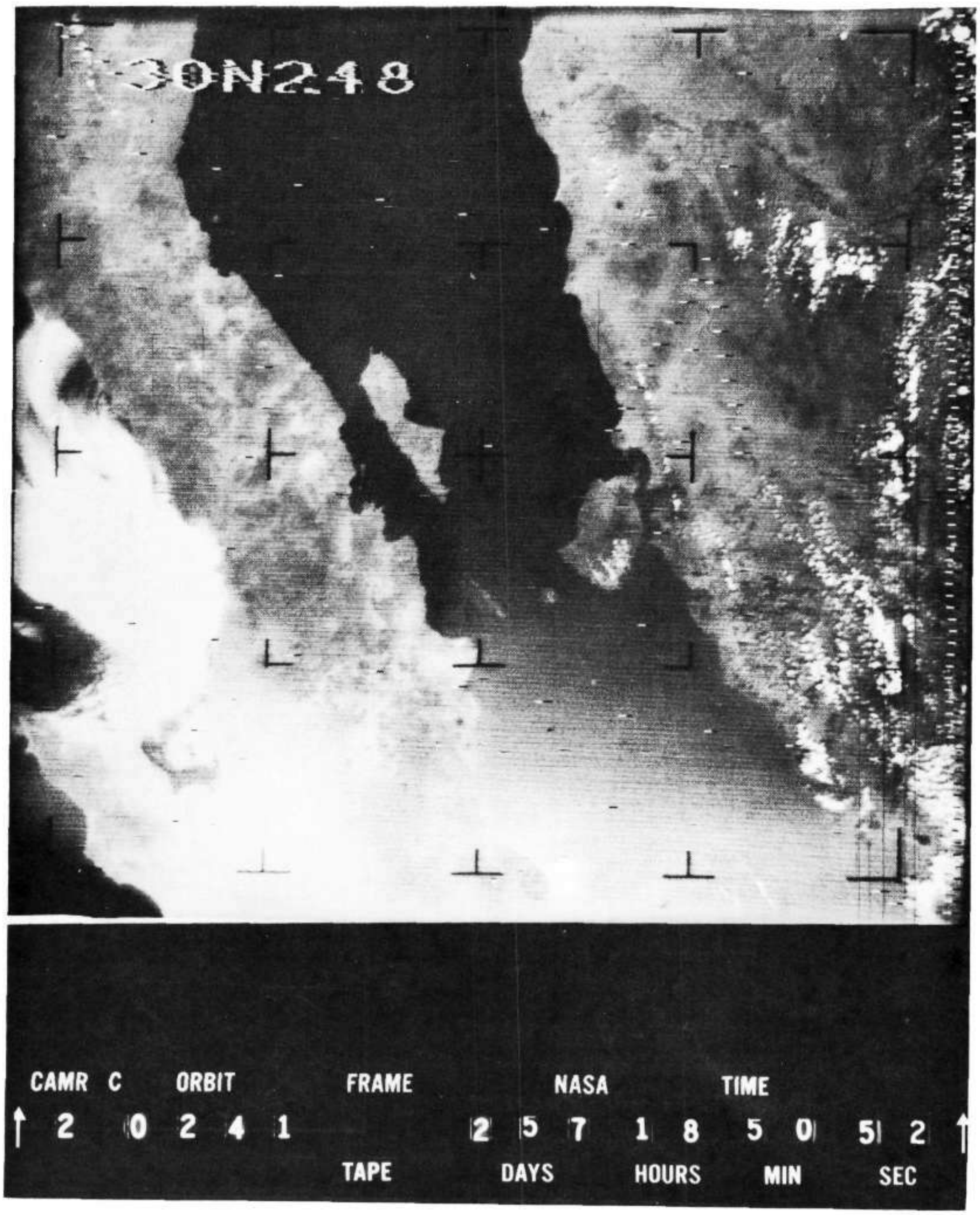

Southern Italy

On the Italian peninsula, the cities of Naples, Salerno, and Taranto appear as light areas against darker backgrounds. Lakes Lesina and Varano, the islands along Yugoslavia's Dalmatian Coast, and the islands of Ischia and Capri are all readily apparent. A small white convective cloud appears to cover parts of Ischia.

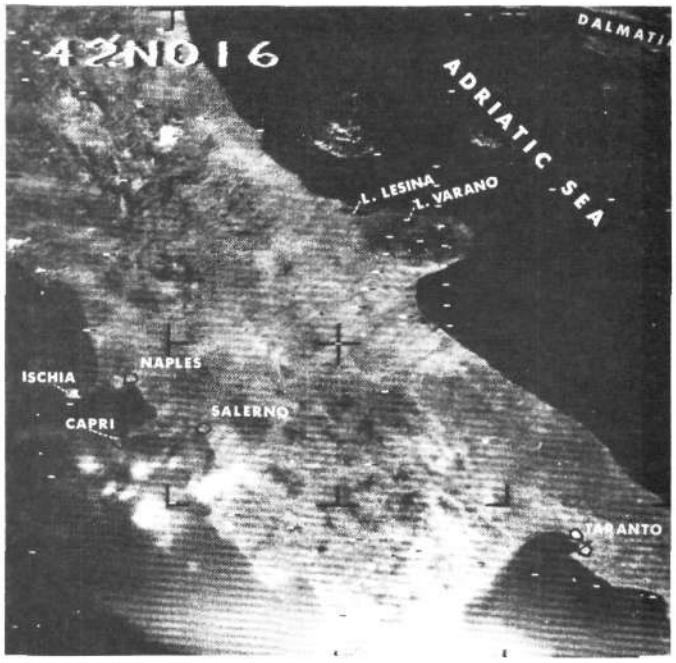

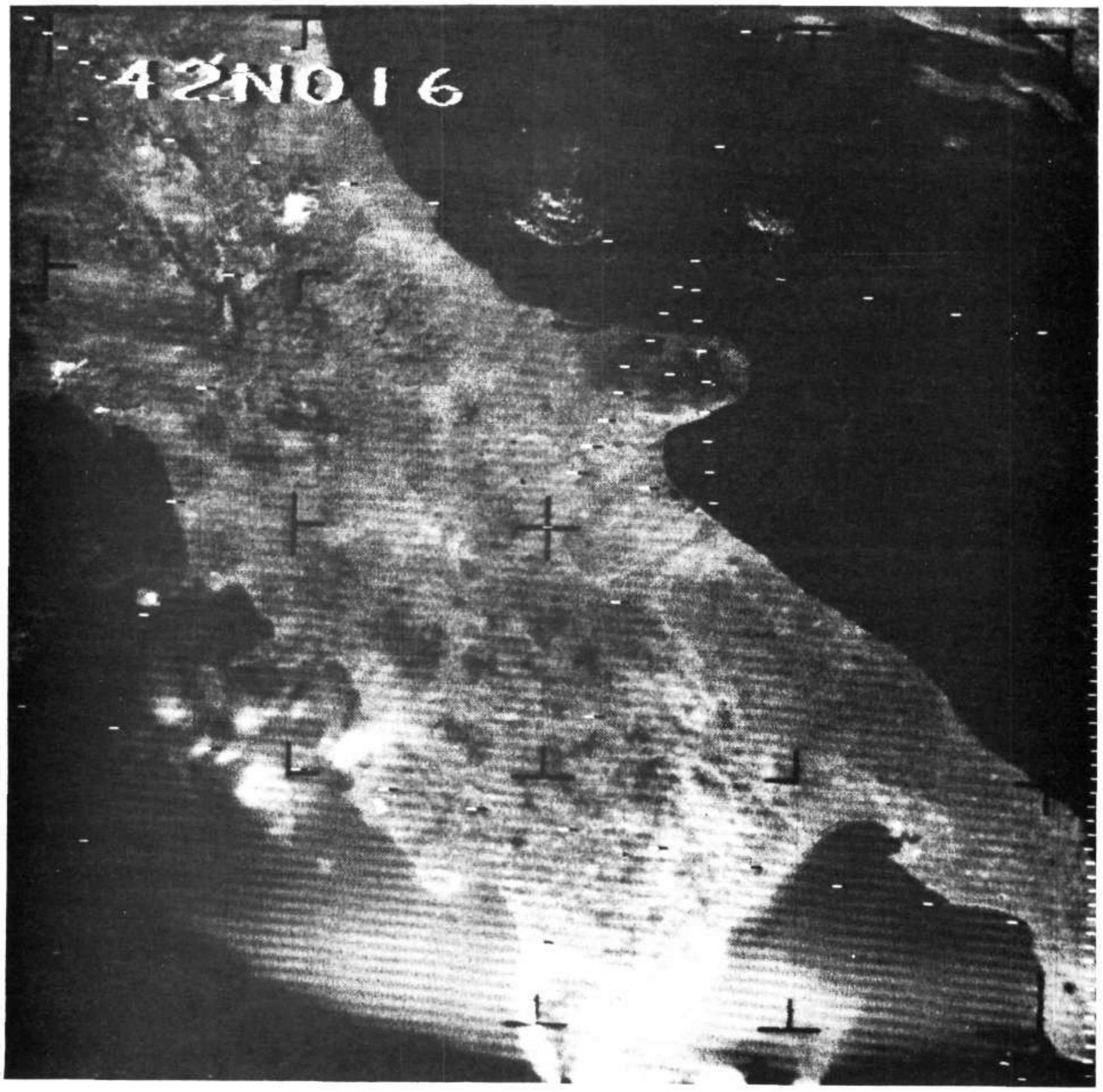

Nimbus I AVCS 12 September 1964

Nile Valley and Red Sea

Further east along the Mediterranean shore, the gross surface characteristics of the typically cloud-free land areas are readily apparent. The Nile Valley appears exceptionally wide because of the rich, irrigated soil along its banks. The dark area at left-center is the El Faiyum depression which contains the Birket Qarun lake. The area is heavily irrigated by canals from the Nile. Owing to its darkness virtually no details are apparent in the fertile Nile Delta north of Cairo.

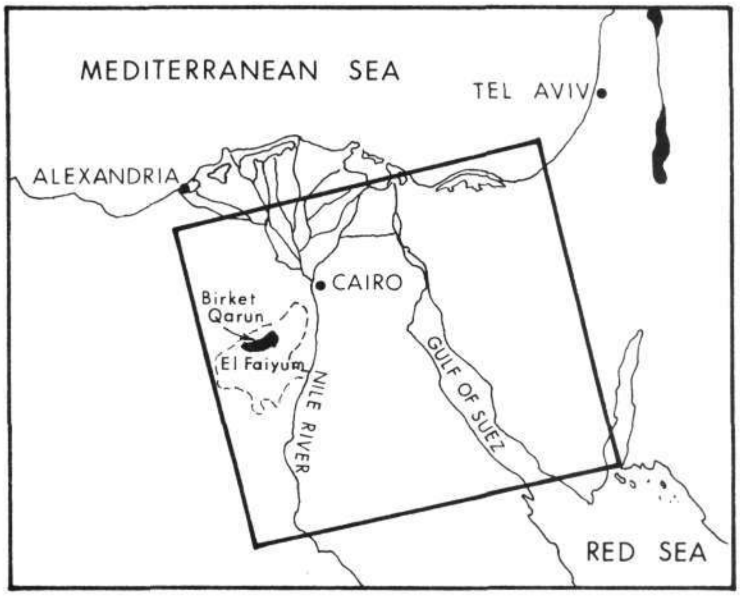

Nimbus I AVCS 16 September 1964

Near East

Just to the northeast of the previous picture, the Dead Sea and the Sea of Galilee may be seen. Visible just southwest of the center fiducial are pearl-like coastal sand beaches. The dark, circular area at upper right center is probably the Al Ghuba salt marsh, although its shape as shown in current charts is more elongated than pictured.

The Gulf of Aqaba, the Dead Sea, and the Sea of Galilee are known to be aligned along one fault line system which is part of the Great Rift Zone. The former interconnection between the present-day water bodies may be inferred by reference to the light linear pattern evident between them.

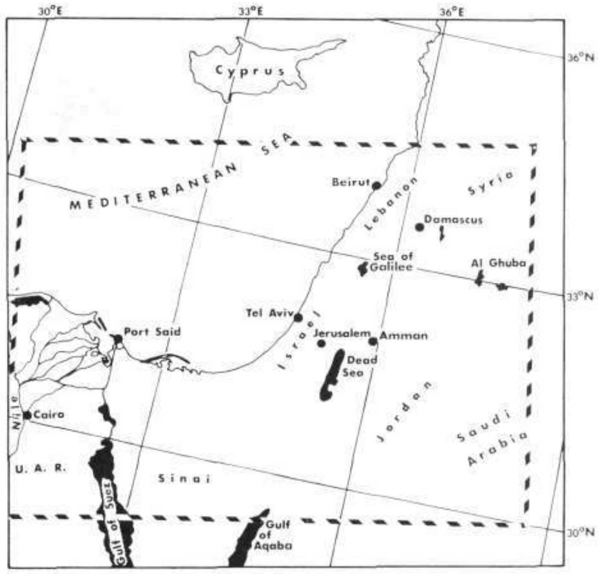

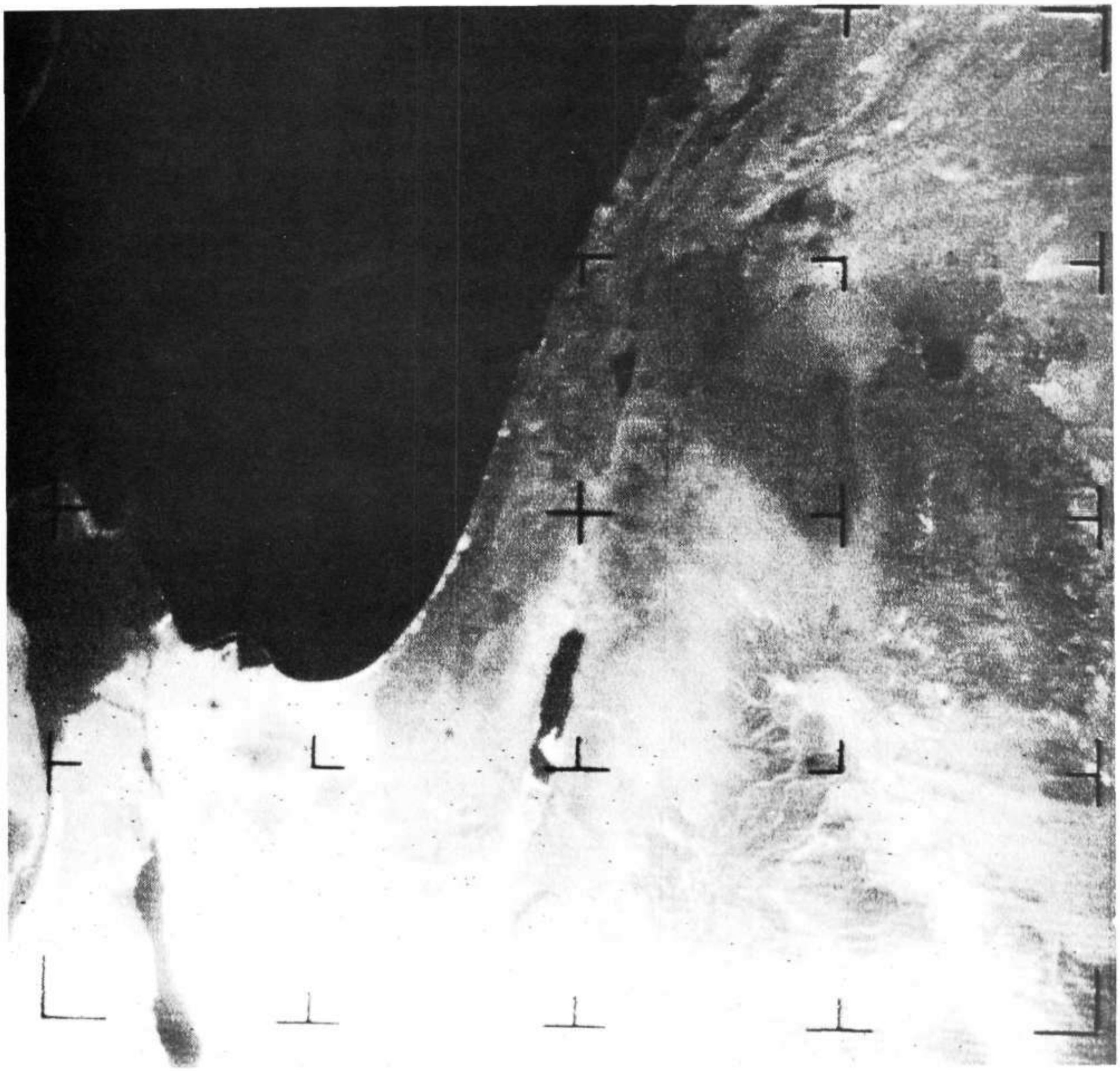

Nimbus I AVCS 15 September 1964

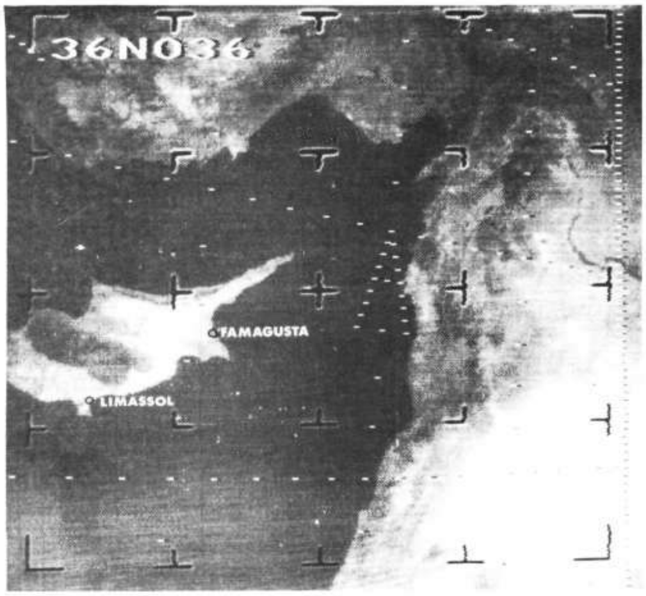

Eastern Mediterranean

Still further north, the topographic features of Cyprus and the Levant are starkly evident as seen through virtually clear skies. Of note is the dark area running east-west through Cyprus which is generally representative of forested elevations above 1000 ft. The lighter areas, on the other hand, are mostly below 500 ft. The dark outlines of the Euphrates River can be seen in Syria at center right.

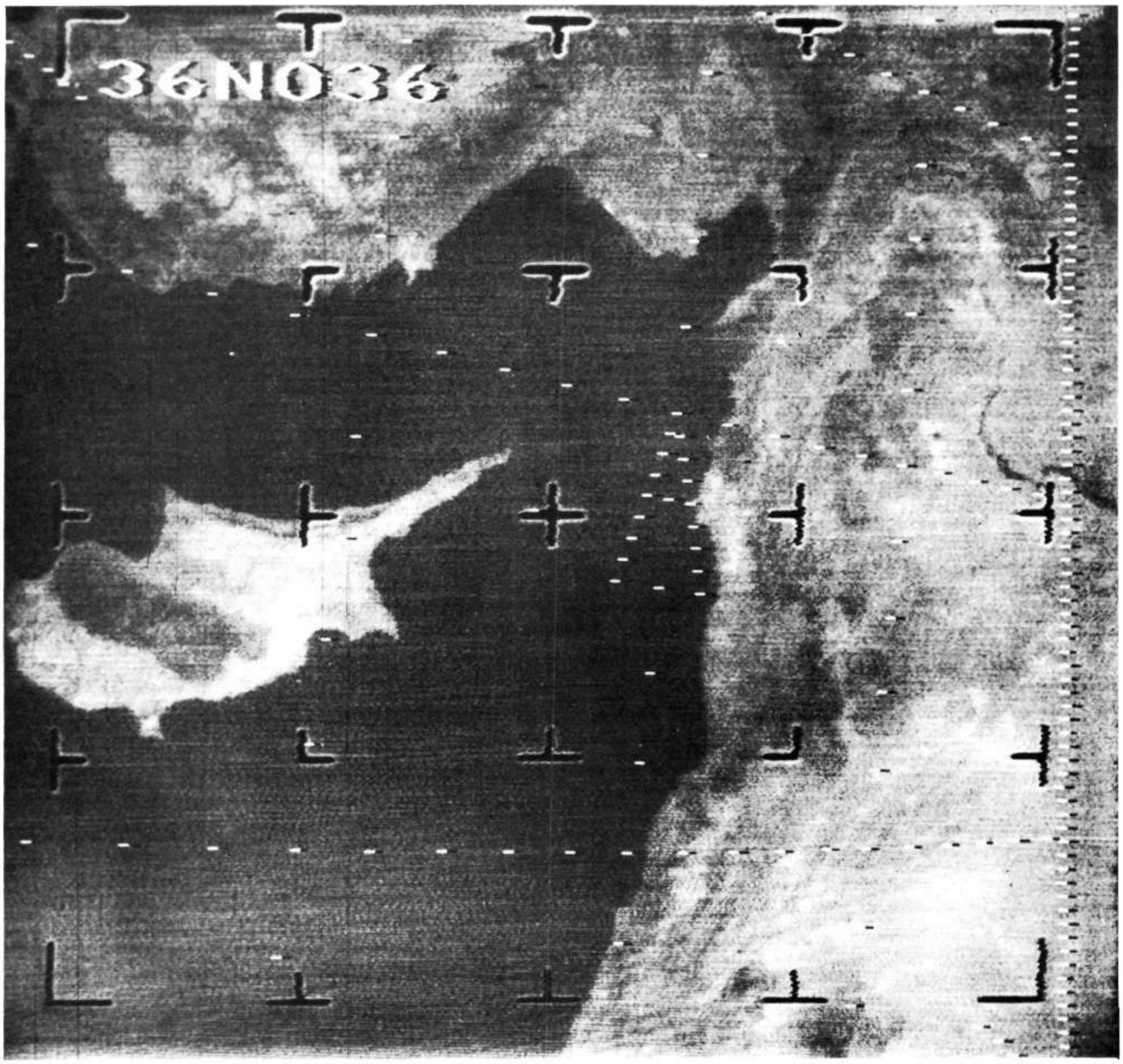

Nimbus I AVCS 16 September 1964

CLOUDS, STORMS and HURRICANES...

Guadalupe Island

Satellite meteorology revealed an order to cloud patterns that had not previously been expected. This is a typical eddy pattern in the clouds to the lee of Guadalupe Island, just west of Baja California. The island acts as a barrier against the uniform wind flow, setting up eddies in the persistent clouds over the area.

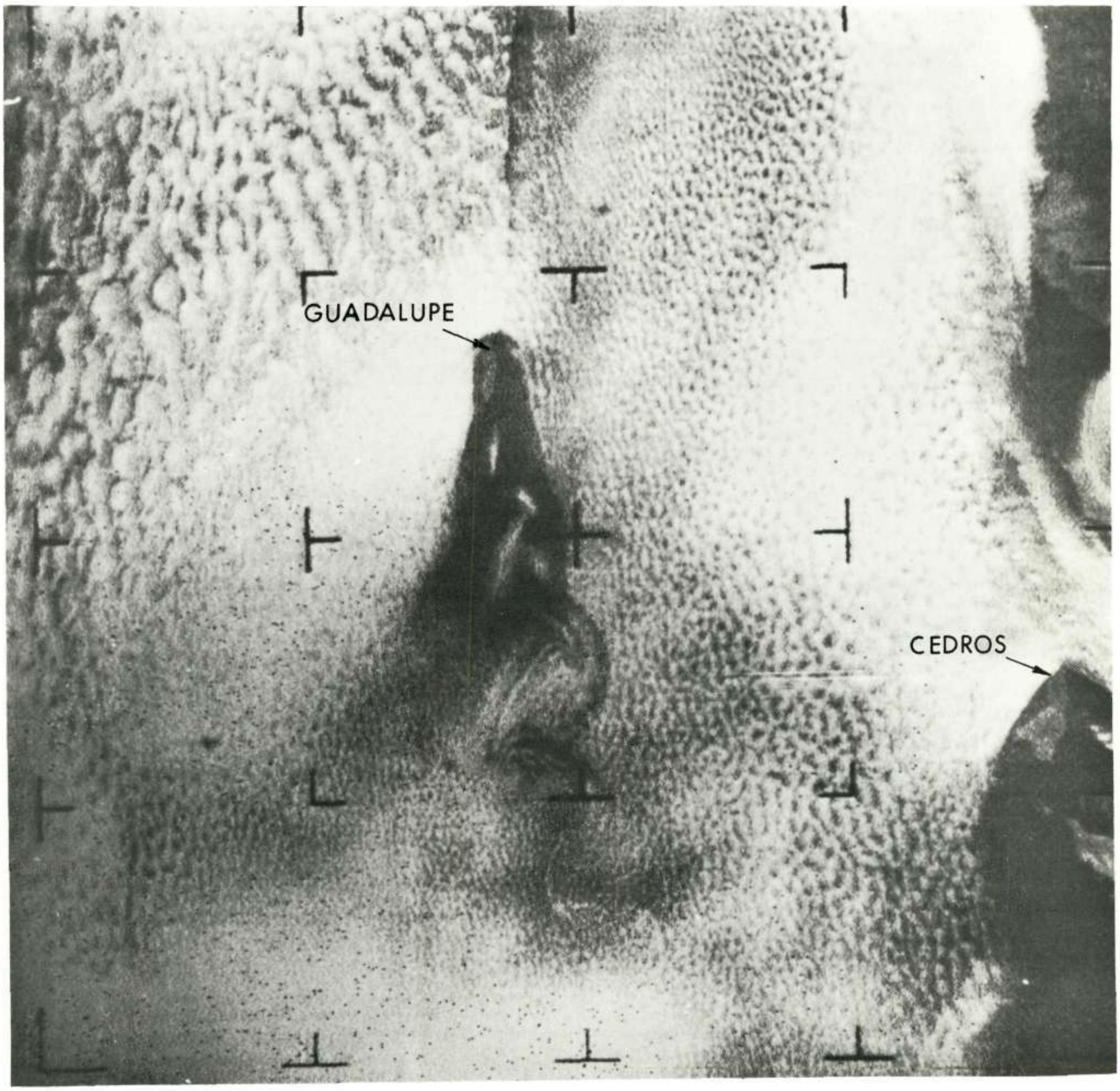

Nimbus I AVCS 13 September 1964

Eastern United States

Although the Nimbus data may be applied to a number of non-meteorological areas (see later figures), the primary emphasis was always on meteorology. This photograph, which was read out directly from the Nimbus III IDCS camera system, demonstrates the value of satellite imagery to the operational meteorologist. A fast-moving cold front had swept through the eastern tier of states and was lying offshore in the Atlantic (lower right corner of the photograph). A large high-pressure system was oriented north-south through the midwest, giving rise to cloudless skies over much of the United States. A weak low-pressure trough accounted for the cloudiness which extended from offshore New York through Maryland (see weather map).

Also of significance in the picture is the snowfall which blankets the Eastern United States. The southern snow boundary runs through Virginia and North Carolina and represents the approximate limits of a one-inch snow cover. The dark line 70 to 80 miles west of Chesapeake Bay delineates the forested ridge upon which lies the Skyline Drive and the white area to its left the Shenandoah Valley and its extensions.

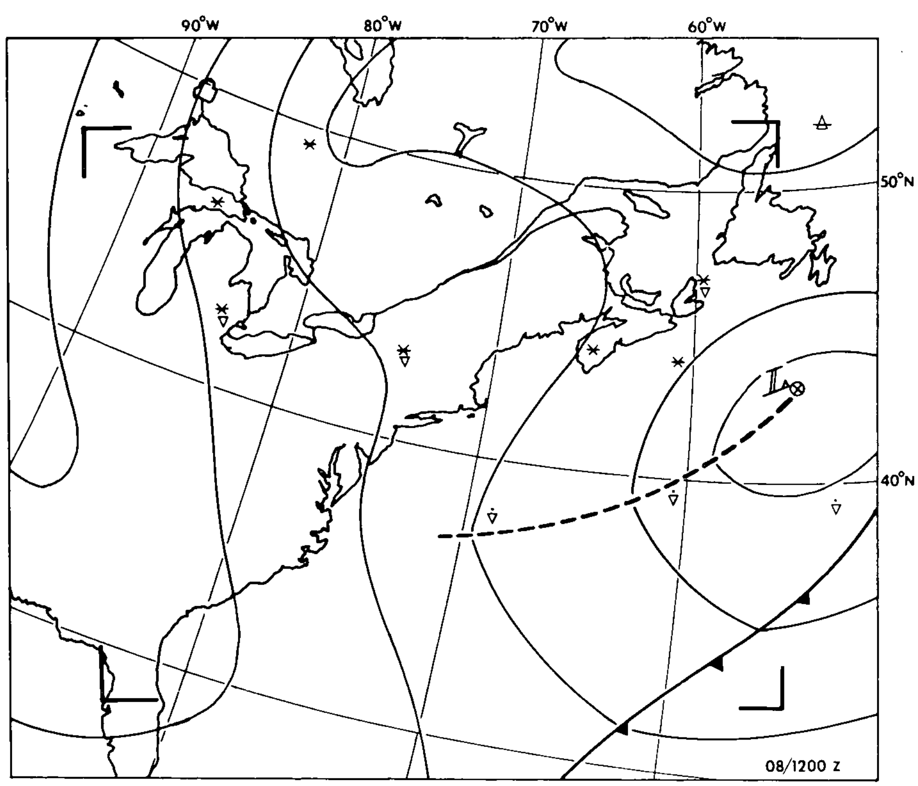

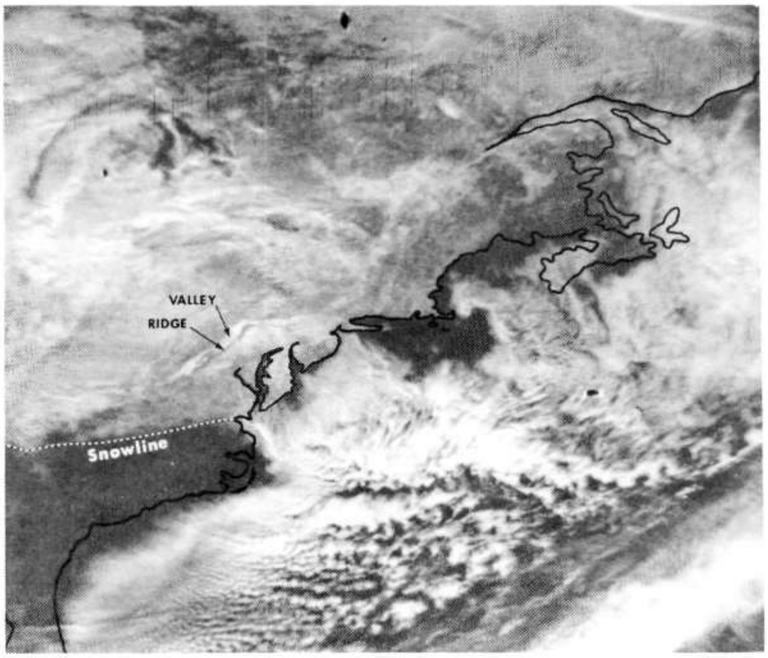
VALLEY
RIDGE
Snowline

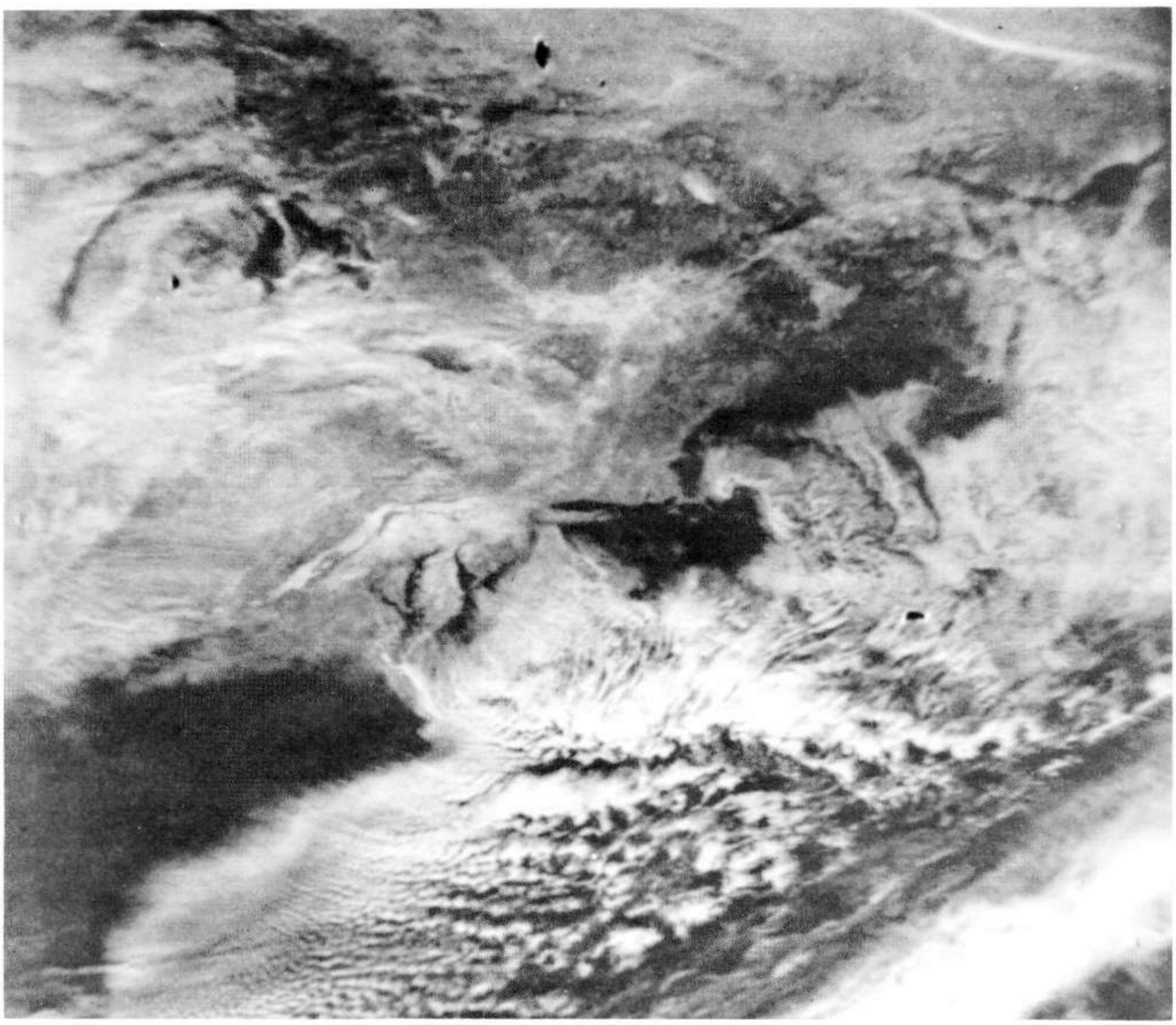

Southeast Asia

This photograph, showing Viet Nam, Thailand, Cambodia, Laos, and the Malay Peninsula, is illustrative of the type of pictures available to local weather forecasters. Such information is available twice daily and is of tremendous benefit in areas with sparsely located weather reporting facilities.

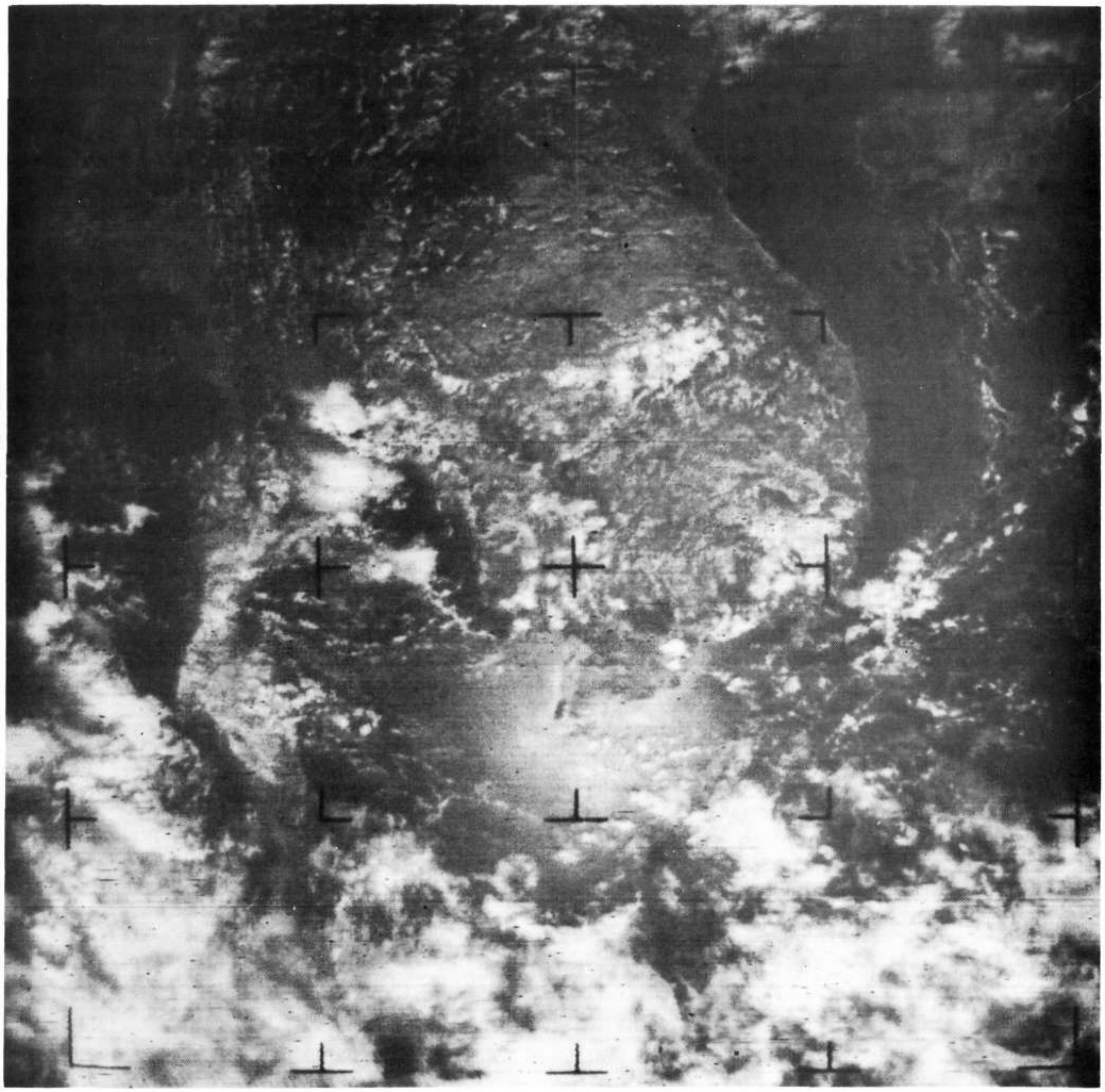

Nimbus II APT 14 October 1966

Argentina and Chile

Lee wave clouds appear as ripples to the east of the Andes Mountains of South America. The Andes in this region reach to 8000 feet with peaks above 10, 000 feet. The average wavelength of the cloud bands is seven nautical miles. The wavelength of such cloud patterns is a function of local wind speeds.

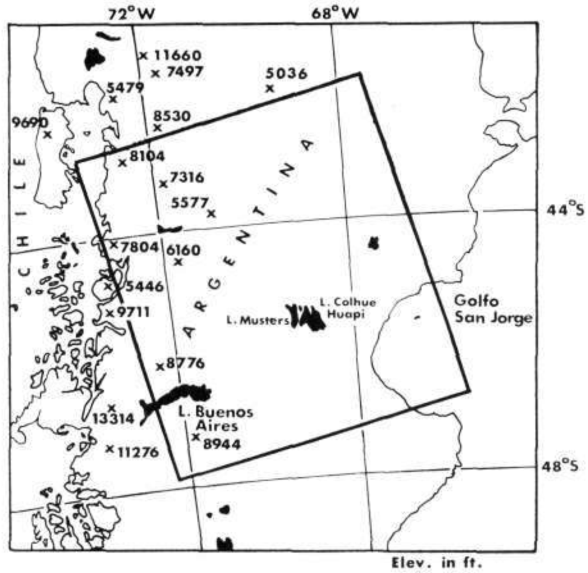

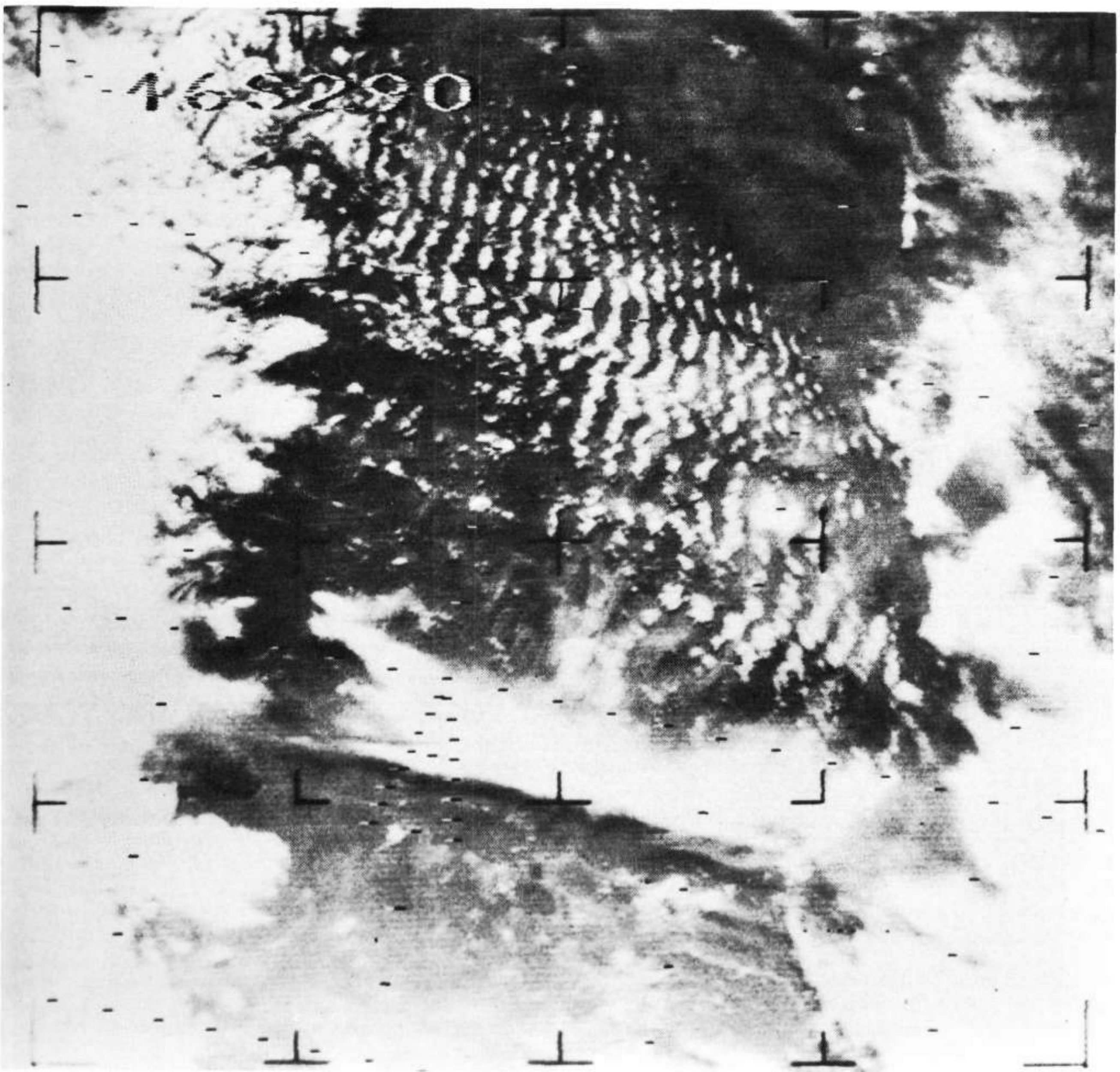

Nimbus I AVCS 13 September 1964

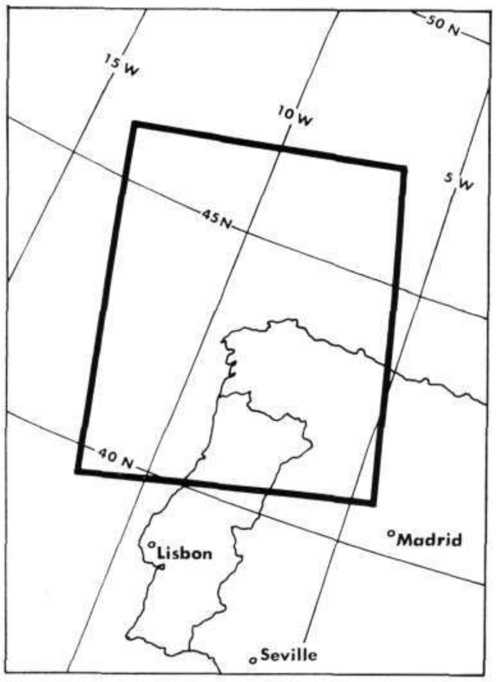

Atlantic Ocean off Spain

Of note in this photograph is the unusual cloud formation at upper left. Speculation has been made as to its origin, ranging from aircraft condensation trails to the condensed smoke of ships' wakes to jet stream cloudiness. The area covered by the phenomenon is approximately 30 x 80 nautical miles. The Iberian Peninsula, nearly invisible in the photograph, appeared more clearly in the original 70 mm film. The vertical lines resulted from a noise interference in the received data.

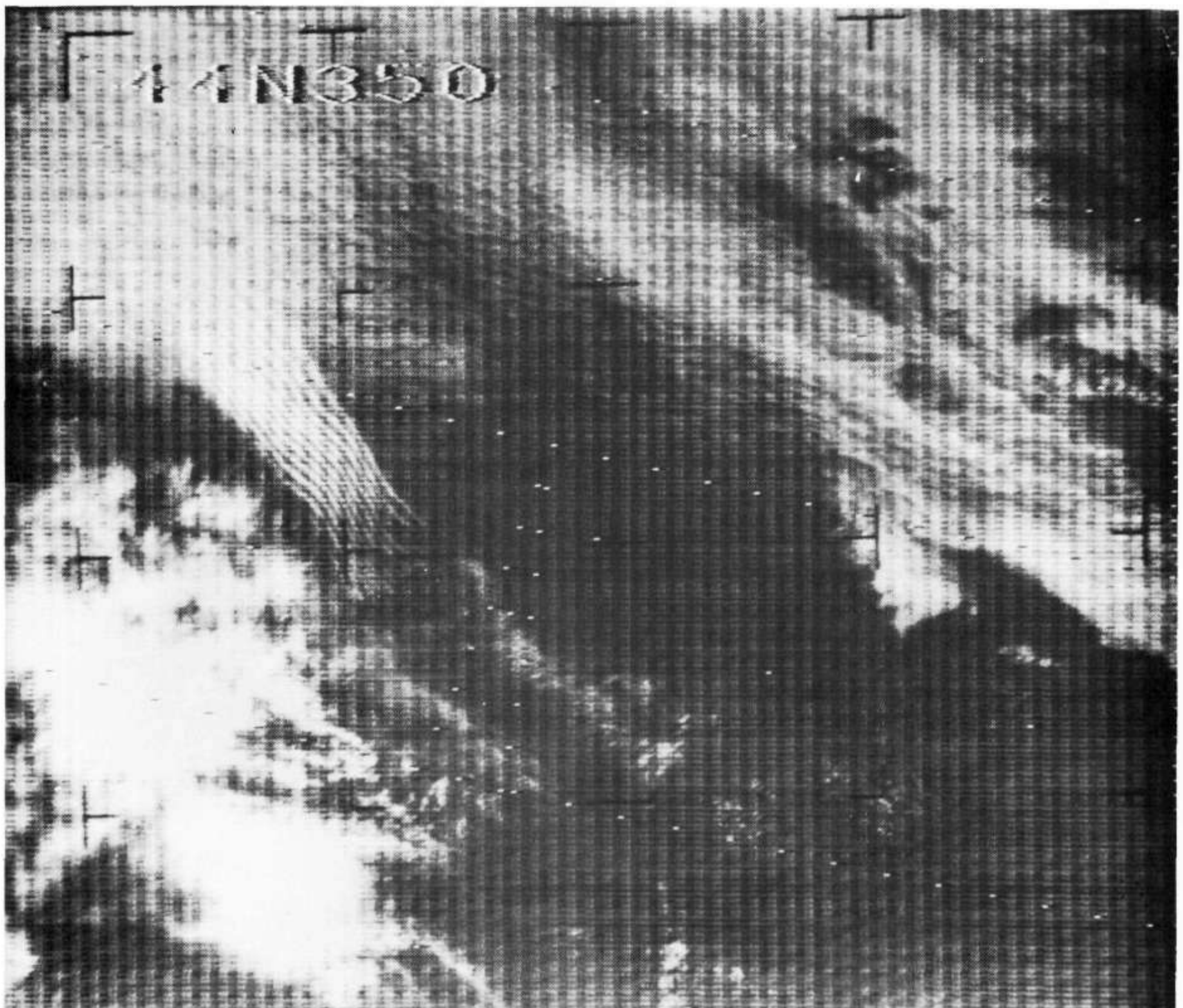

Nimbus II AVCS 27 May 1966

Arabian Sea

Before satellite imagery was available, the tracking of storm centers in remote areas was nearly impossible. In this nighttime "picture" of temperature patterns, a tropical cyclone is shown between the Arabian Peninsula on the left and India on the right. (The gray-scale in this HRIR presentation is proportional to temperature with darker areas representing warmer temperatures. More examples of this type of data will be presented in the next group of figures.) These cyclones are analogous to the hurricanes and typhoons of the Atlantic and Pacific Oceans. This storm moved inland over the eastern tip of the Arabian Peninsula and dissipated a few days after the photograph was taken.

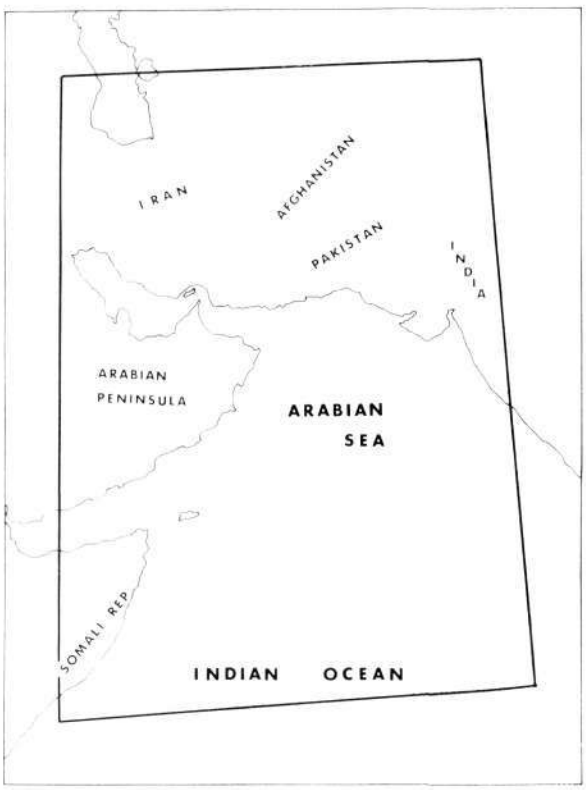

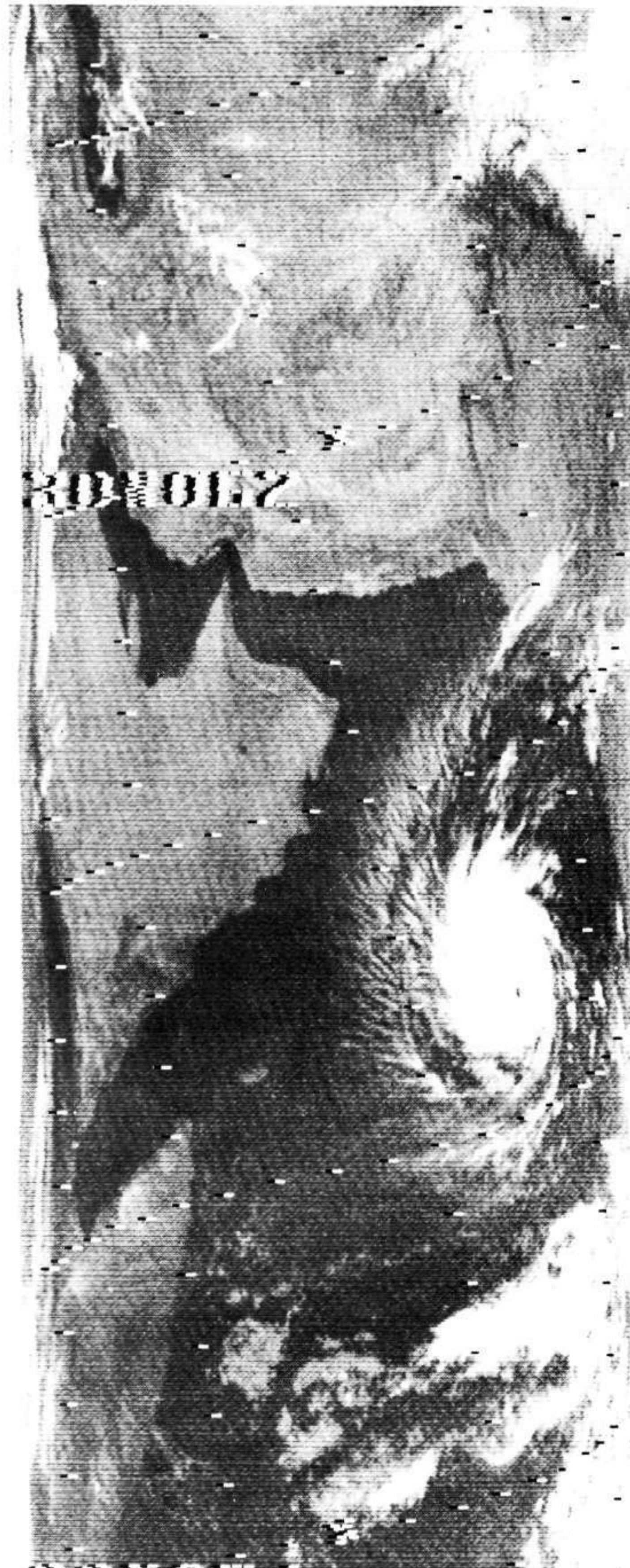

Nimbus II HRIR 8 November 1966

Nimbus III HRIR 7 November 1969

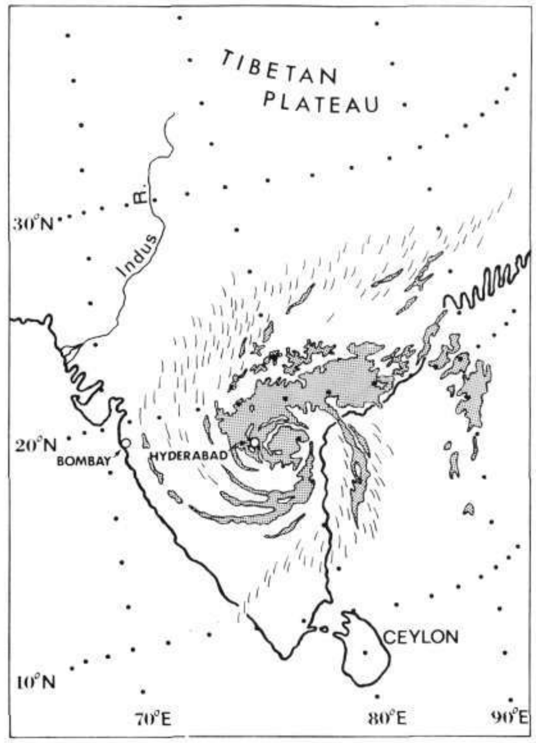

An Indian Ocean Storm

Another tropical storm was observed as it moved east to west across India between the 5th and 10th of November 1969. At the time of the HRIR sequence shown, it was located approximately 70 n.mi. east-northeast of Hyderabad.

Of note is the classical, symmetrical appearance of the clouds associated with the cyclonic indraft of a northern hemisphere storm. The brighter tones represent clouds of higher vertical development (cooler temperatures), probably cumulonimbus.

The grayish Tibetan Plateau is sprinkled with the darker lakes of Tibet and China.

Hurricane Alma

The tracking of potentially dangerous hurricanes is probably the most dramatic meteorological application of the Nimbus satellites. In this picture the 1966 Hurricane Alma is shown over Florida. Of note is the grayish, triangular area along and west of Florida's west coast. Here, it is thought, the shallow coastal waters have been wind-whipped into one huge area of white water. The light tonal effect is caused by higher solar reflectance from wind-whipped shallow waters.

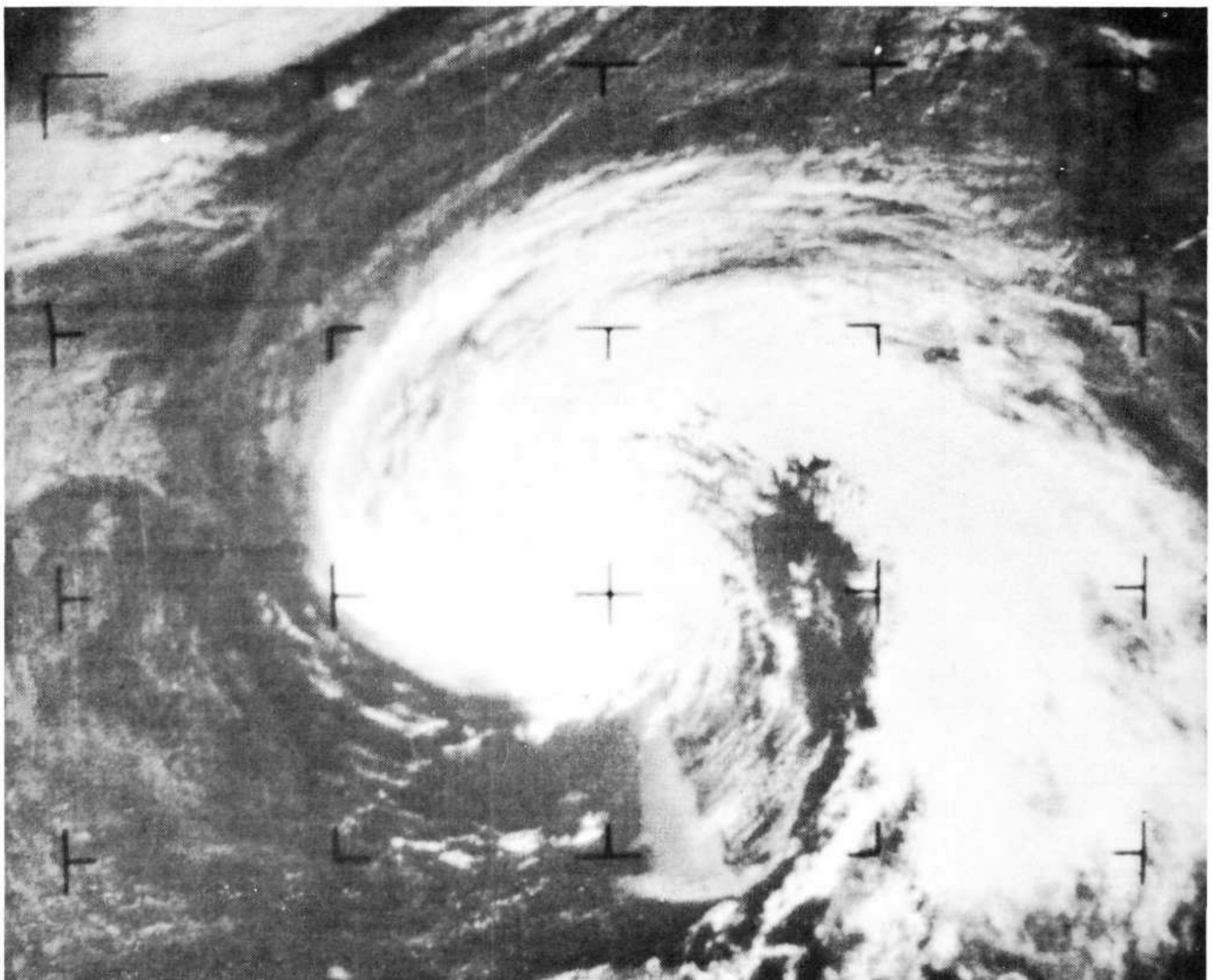

Nimbus II APT 9 June 1966

Hurricane Beulah

This photograph is an enlargement of the fourth picture shown in the following series and offers an example of the quality of Nimbus photography. The large extent of the storm's cloud pattern is evident when judged against the size of Cuba.

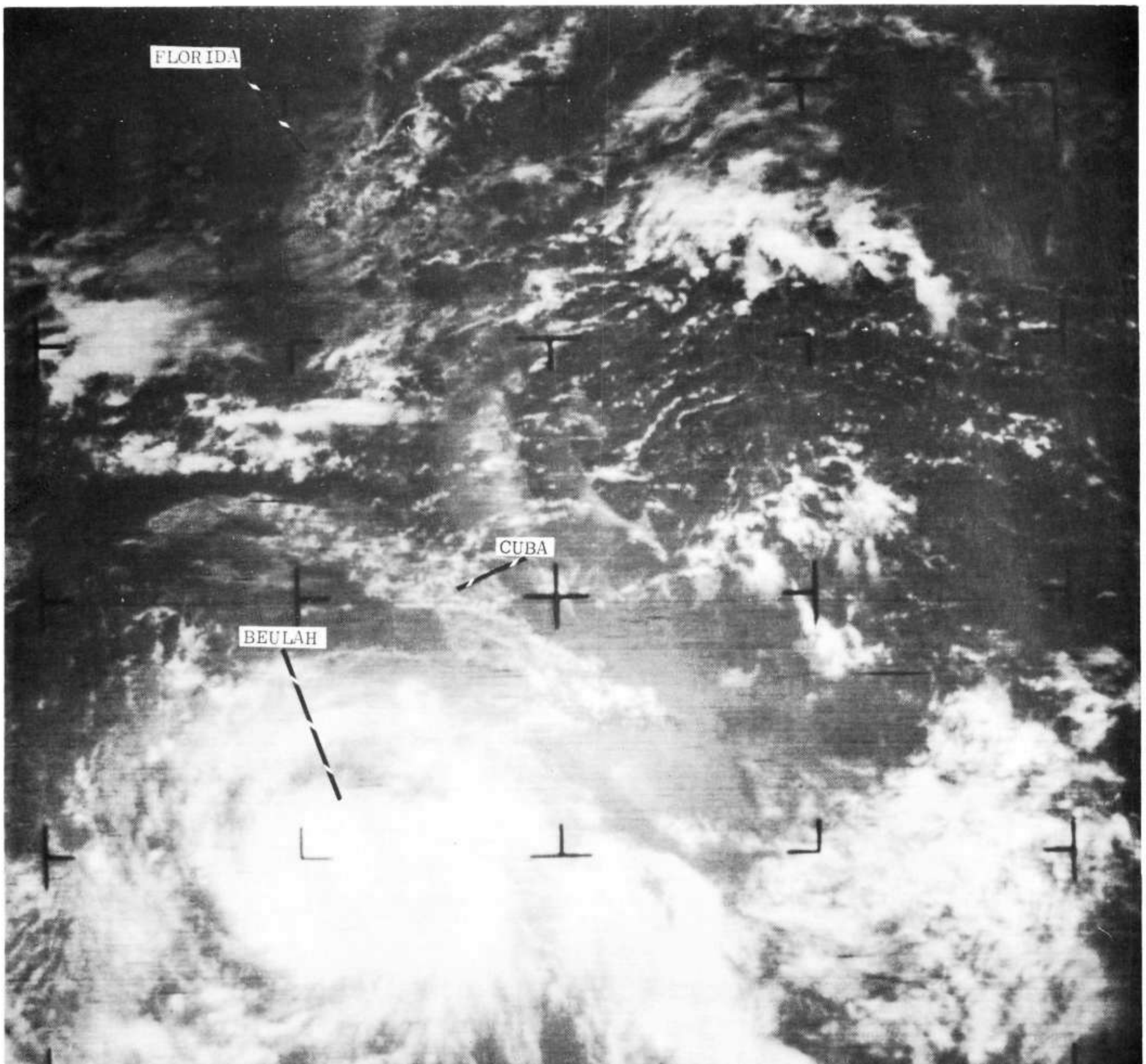

Nimbus II APT 14 September 1967

Hurricane Beulah

A single APT station at Goddard Space Flight Center, Maryland, received these pictures of the westward progression of Hurricane Beulah. Such a receiving capability is especially useful to stations in remote areas where other forms of weather data are sometimes difficult to acquire.

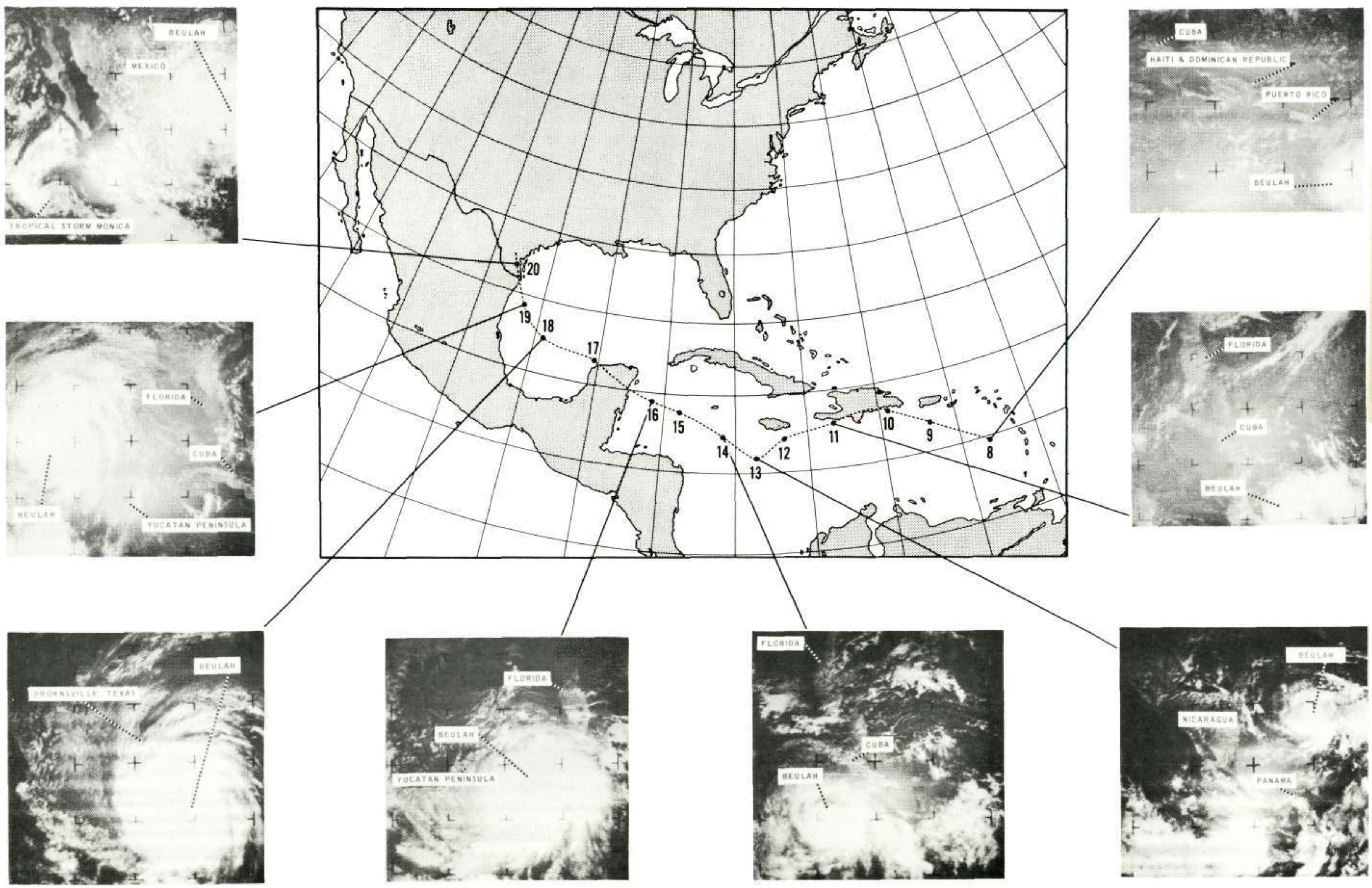

Eastern United States and Atlantic Ocean

After having transmitted some 100,000 APT pictures over a period of 16 months, Nimbus II spotted three tropical disturbances south and east of the United States. In this montage of the Nimbus II APT picture, Beulah, Chloe, and Doria are clearly evident, as are Florida and the Great Lakes. (Doria is imbedded in a frontal system along the east coast.)

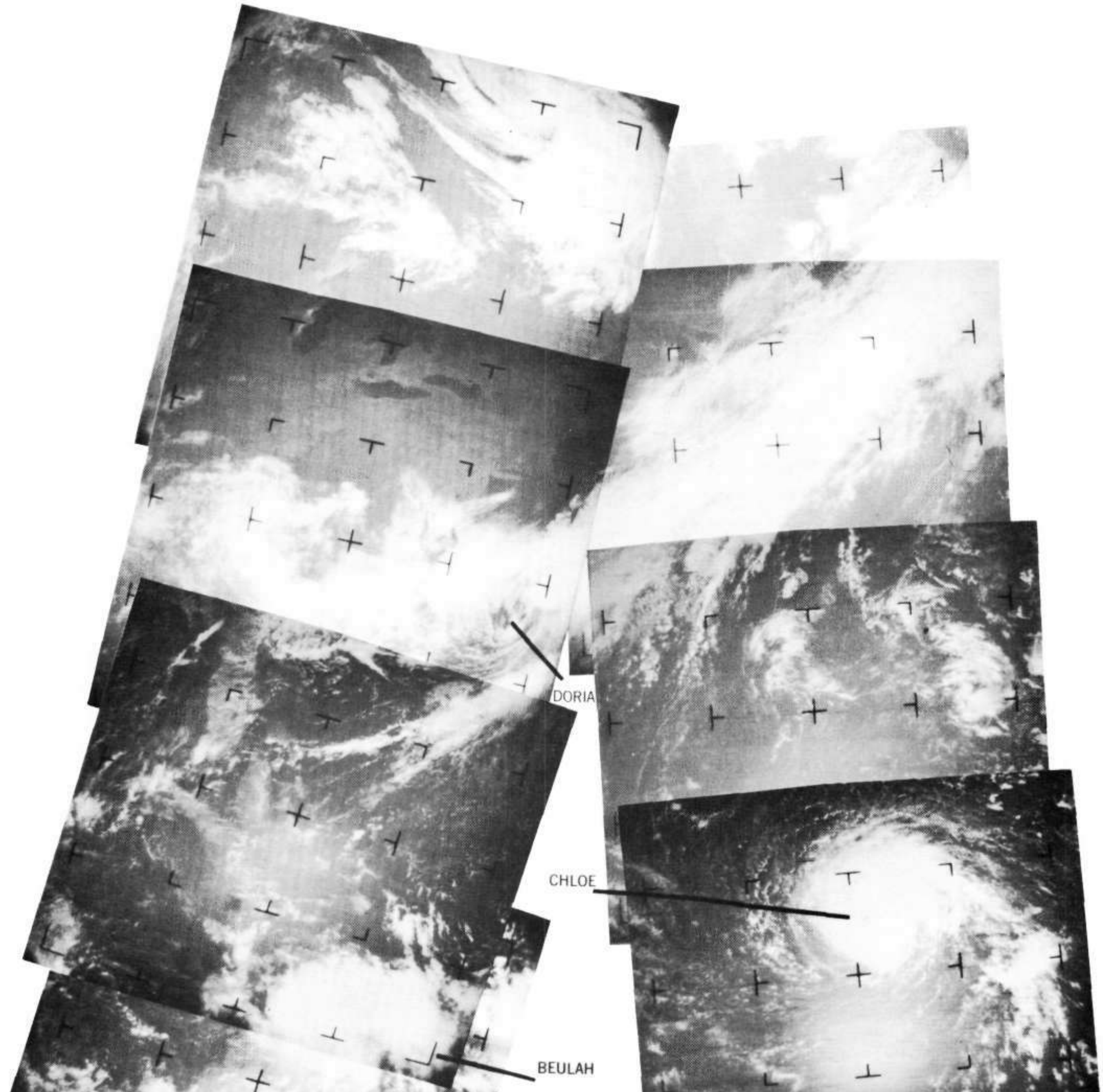

Nimbus II APT 11 September 1967

Hurricane Becky

Becky, the second storm of the 1970 season, is shown some 3 hours before it moved inland over Apalachicola, Florida. Although never particularly strong or well-organized, the hurricane caused considerable amounts of rainfall along its path through the Eastern United States. Tallahassee, Florida, reported 8.18 inches of rain during the 24-hour period ending at noon on the 22nd.

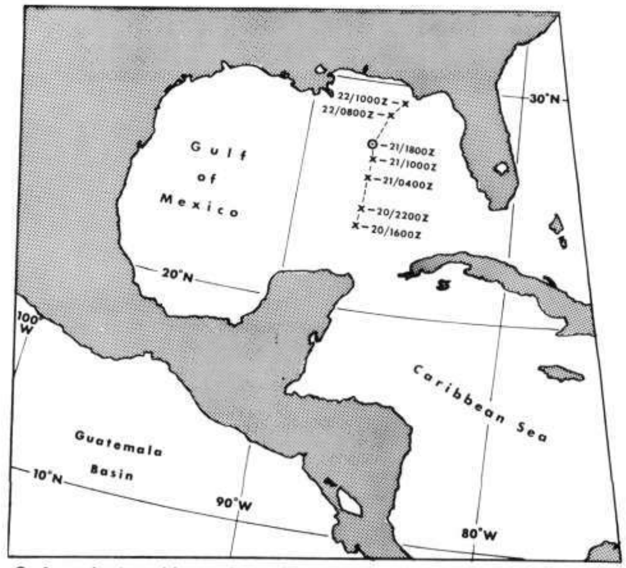

⊙ – Approximate position at picture time

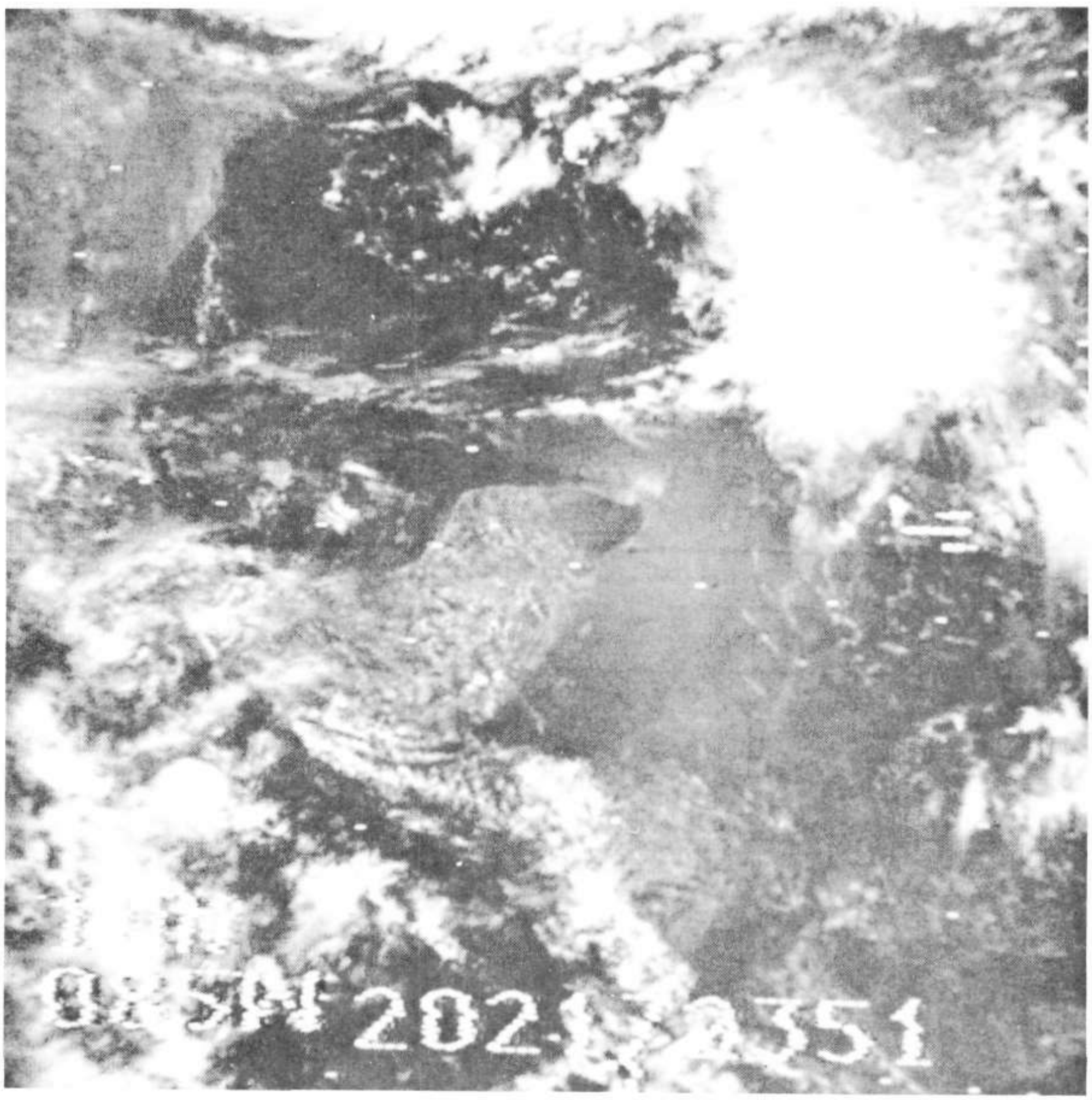

Nimbus IV IDCS 21 July 1970

Hurricane Camille

Photographic coverage of Camille, one of the deadliest hurricanes in recent history, begins with a picture of the storm's infancy on 11 August 1969. Camille was christened a tropical storm on 14 August and reached hurricane strength the following day. It then swept through the southeastern United States and back into the Atlantic where it is shown in the last photo with hurricane Debbie.

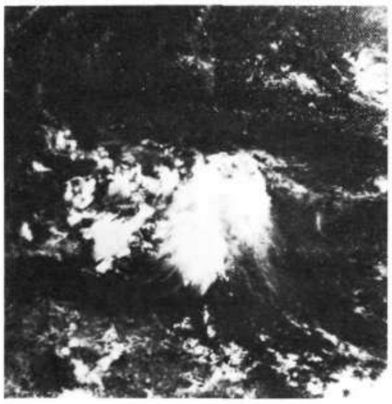

11 AUG

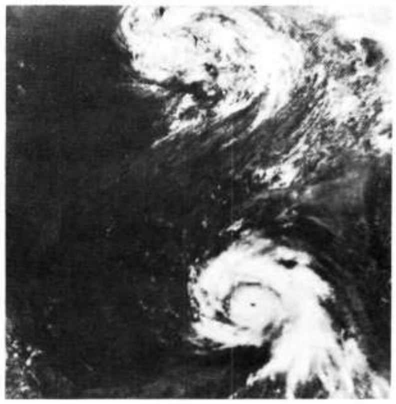

16 AUG

17 AUG

18 AUG

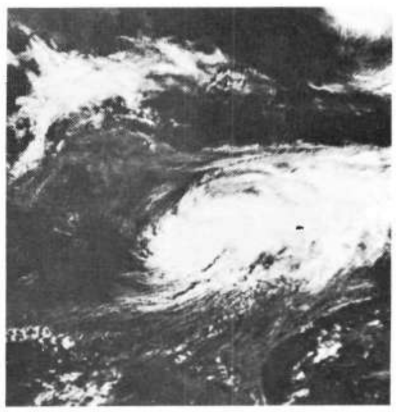

19 AUG

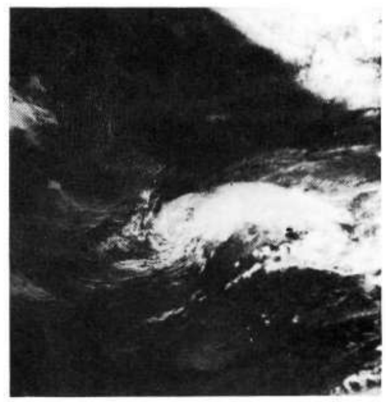

20 AUG

21 AUG

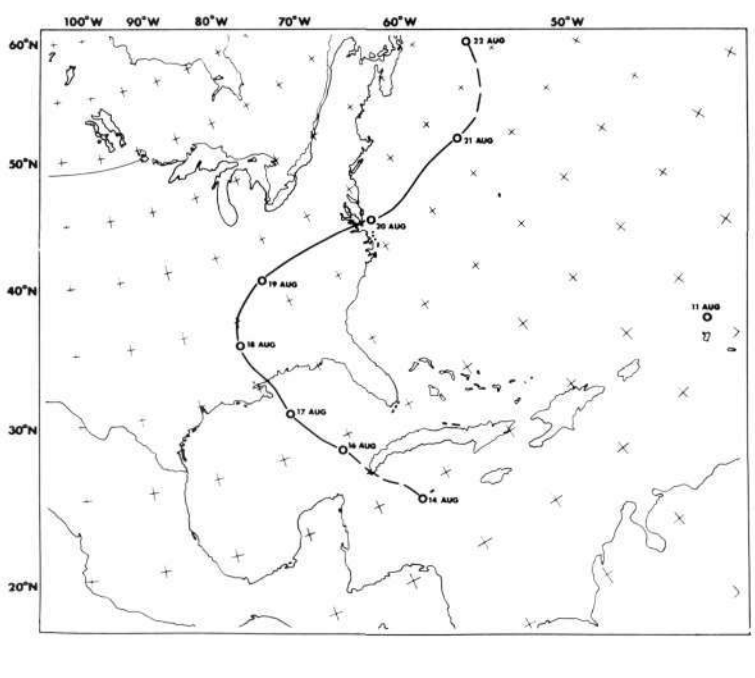

Nimbus III DRID

BEYOND MEN'S EYES ...

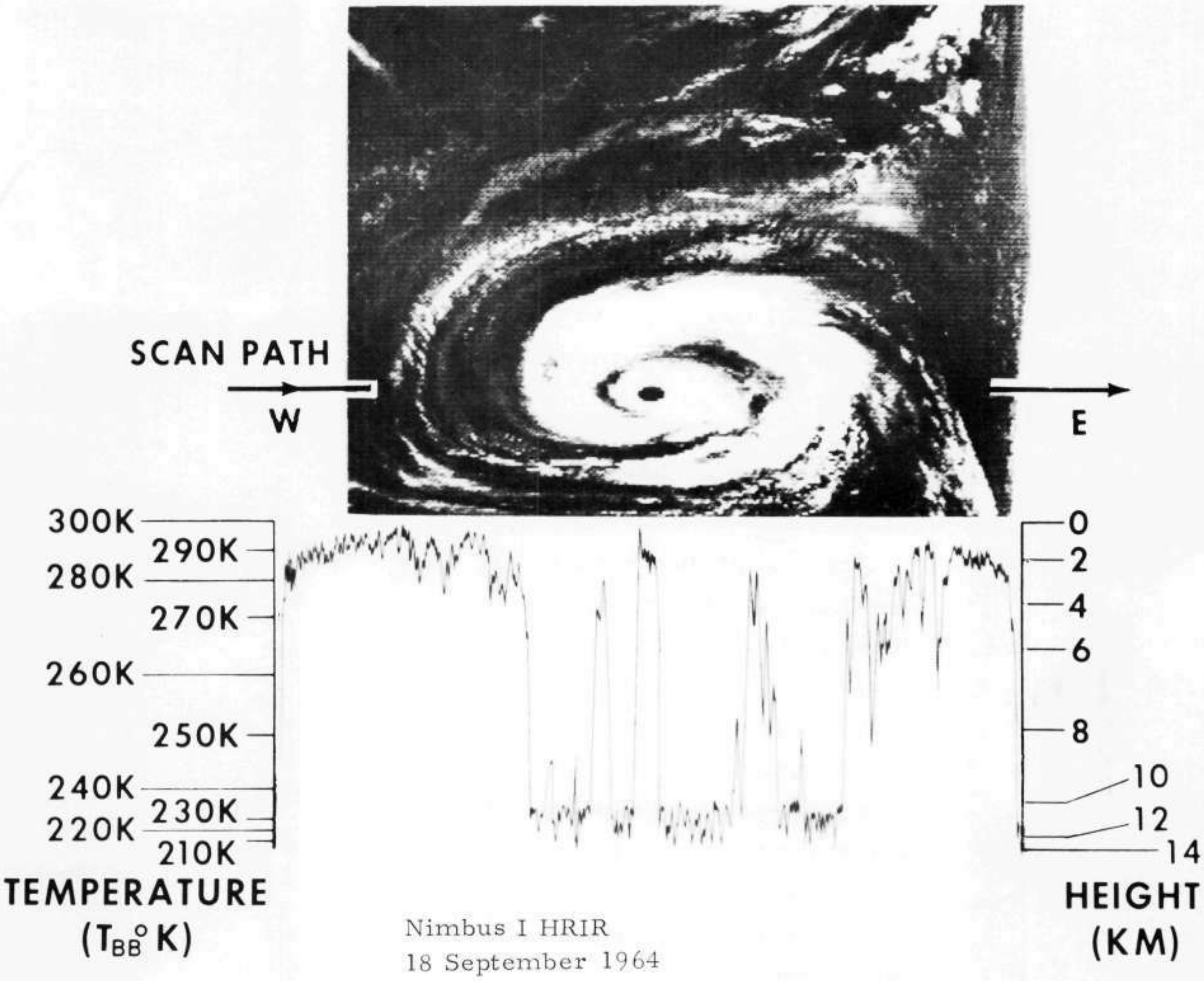

Nimbus I HRIR
18 September 1964

Hurricane Gladys

Our eyes are sensitive to only the relatively narrow "visible" portion of the electromagnetic spectrum. Instruments can be built, however, which are sensitive to almost any wavelength interval. By monitoring infrared wavelengths in the atmospheric "window" regions, we can record surface, cloud or atmospheric temperature patterns. This was the case with the Nimbus I HRIR experiment which operated in the 3.4 to 4.2 μm band.

For detailed analyses of HRIR data, the analog trace of individual scan lines can be used to generate temperature values. These values can then be related to surface temperature patterns and to cloud top heights. Note that the trace follows closely the tonal patterns in this Nimbus I HRIR picture of Hurricane Gladys. The warmer temperatures are associated with the darker cloud-free areas and the colder temperatures with the cloudy areas. An increase of some 85^{O}K occurs passing from the clouds into the cloud-free eye of the storm.

HRIR Comparison

A second channel was added to the Nimbus III HRIR system which enabled daytime measurements of solar reflectance to be made. These two strips of HRIR imagery, taken approximately 12 hours apart, show portions of eastern Africa, the Mediterranean Sea, and Europe. The differences between the day and night pictures are readily apparent when viewed over the same area and at such a short time interval. The daytime photograph, while not giving the same fine cloud definition as the nighttime, emphasizes the physical features of the land areas.

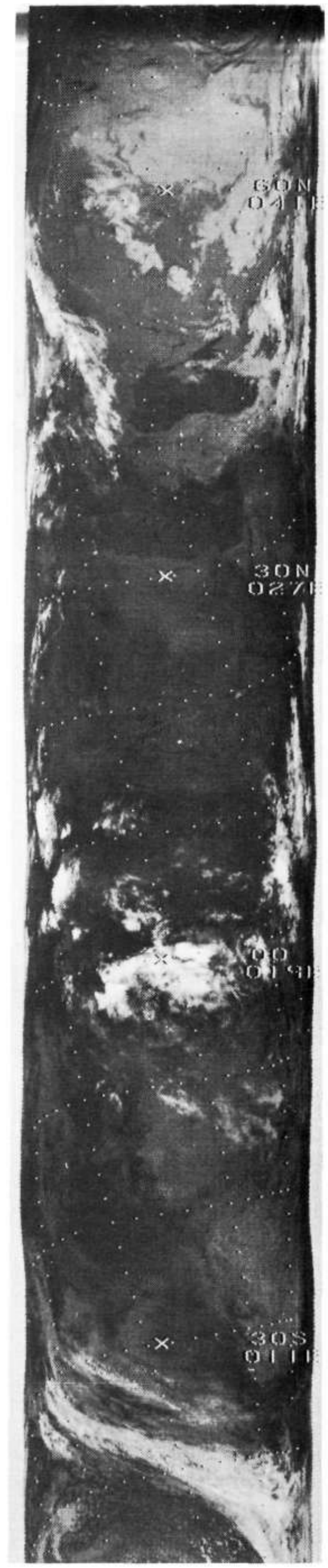

Day

Nimbus III HRIR Night
26 May 1969

Hurricane Alma

A medium resolution five-channel scanning radiometer was included in the Nimbus II sensor package. This example shows how Hurricane Alma appeared in all five channels first over the Gulf Coast in the 9 June photograph and then over the Carolinas in the 13 June picture. The use of the five MRIR bands was described in the previous section.

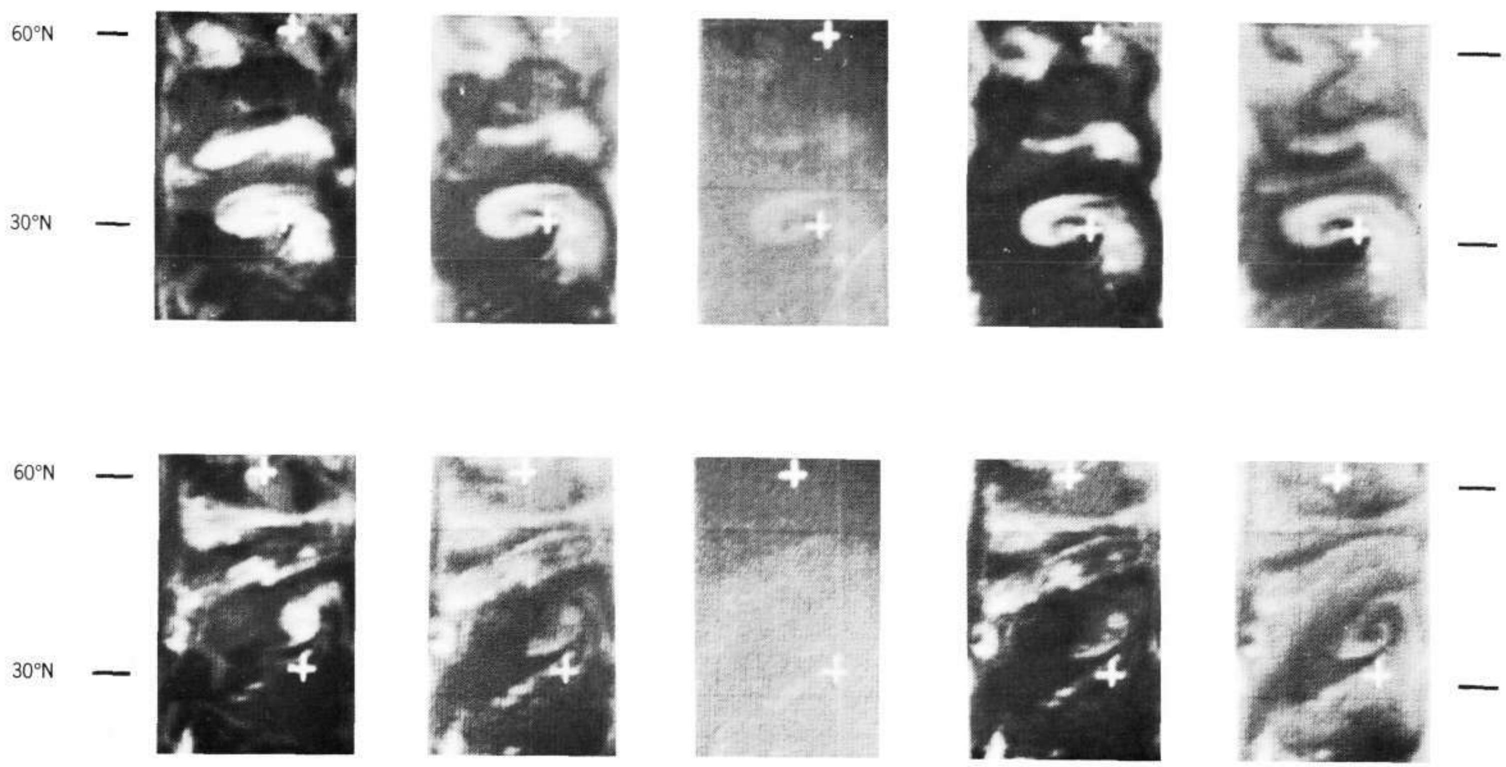

0.2 - 4.0 μm   5 - 30 μm   14 - 16 μm   10 - 11 μm   6.4 - 6.9 μm

Nimbus II MRIR   9, 13 June 1966

Central United States and Canada

The Nimbus II APT system was modified so that HRIR data could be read out directly by local users. DRIR (Direct Readout Infrared) pictures could thus be recorded by anyone after a few modifications to existing APT equipment. These particular pictures were recorded by the Canadian Meteorological Service. The text for each picture was provided by the CMS.

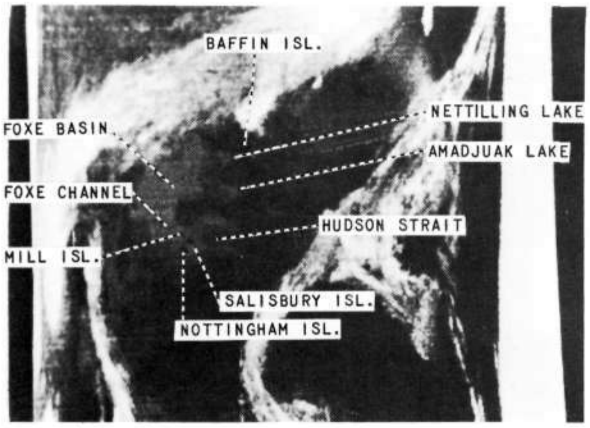

Baffin Island appears dark against the colder waters of Hudson Strait and Foxe Basin. Nettilling and Amadjuak Lakes, being relatively cold, appear lighter. Salisbury, Mill, and Nottingham Islands can be made out in the Foxe Channel.

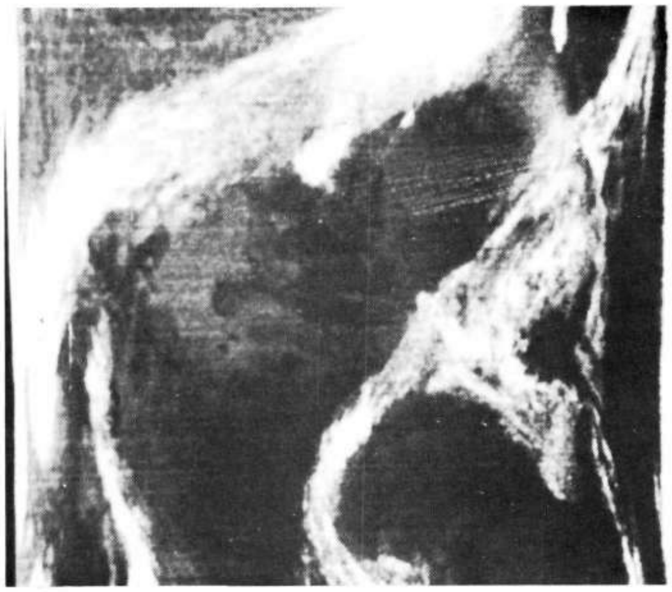

Nimbus II DRIR 22 July 1966

In this picture the warm waters along the edges of James Bay appear darker (warmer) against the colder land and middle waters of James and Hudson Bays. Small lakes such as Abitibi and Kesagami show clearly as do the Great Lakes at the bottom of the photograph.

This picture shows excellent definition of the Great Lakes and their connecting waterways. Even the Mississippi River and its tributaries appear as dark returns against the cooler land.

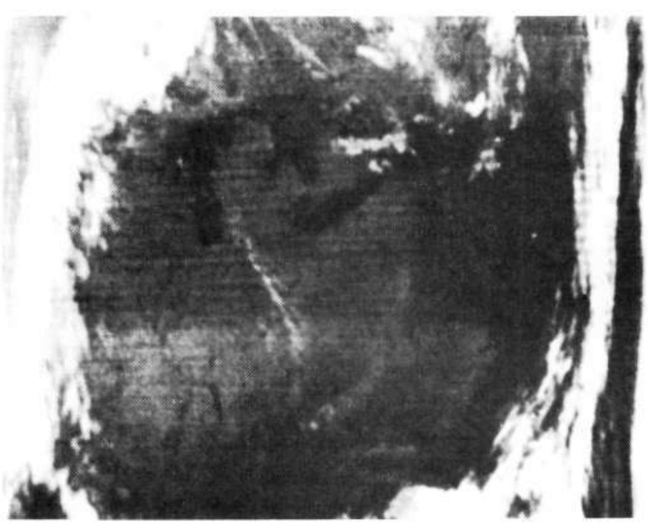

South Pacific off South America

In this nighttime (temperature) HRIR display, the dark area which extends southwestward from the juncture of the 30°S, 90°W coordinates is, in all probability, an open space in the surrounding grayish stratus clouds. The area is some 625 n.mi. west of the coast of Chile.

The varying shades of whites and grays present a study in the relationship between cloud heights and temperatures (and, therefore, shades of gray). The bright whites generally represent clouds of greater vertical development and the lighter grays correspond to thinner and/or lower clouds.

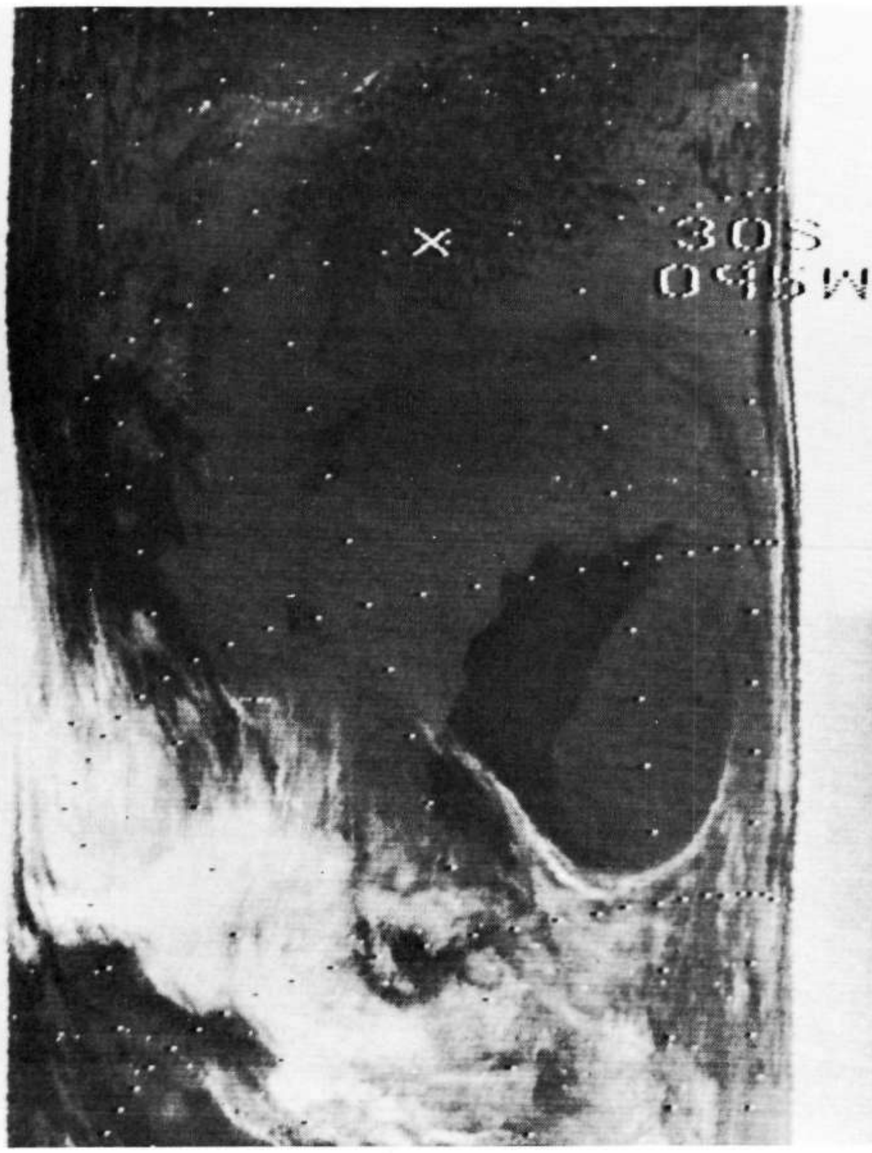

Nimbus III HRIR 8 November 1969

Medium Resolution Infrared Radiometer

The 5 to 30 μm band of the Nimbus II MRIR experiment was replaced in Nimbus III by a 20 to 23 μm water vapor band. The five channels of the Nimbus III MRIR are shown on orbit 1034 as the satellite traveled from Antarctica northward over Central Africa, the Mediterranean Sea, Central Europe, and Norway. The new channel provided data from the spectral region containing broad rotational absorption bands of water vapor and gave information similar to the 6.5 to 7.0 μm channel except that the radiation was largely measured from lower in the atmosphere.

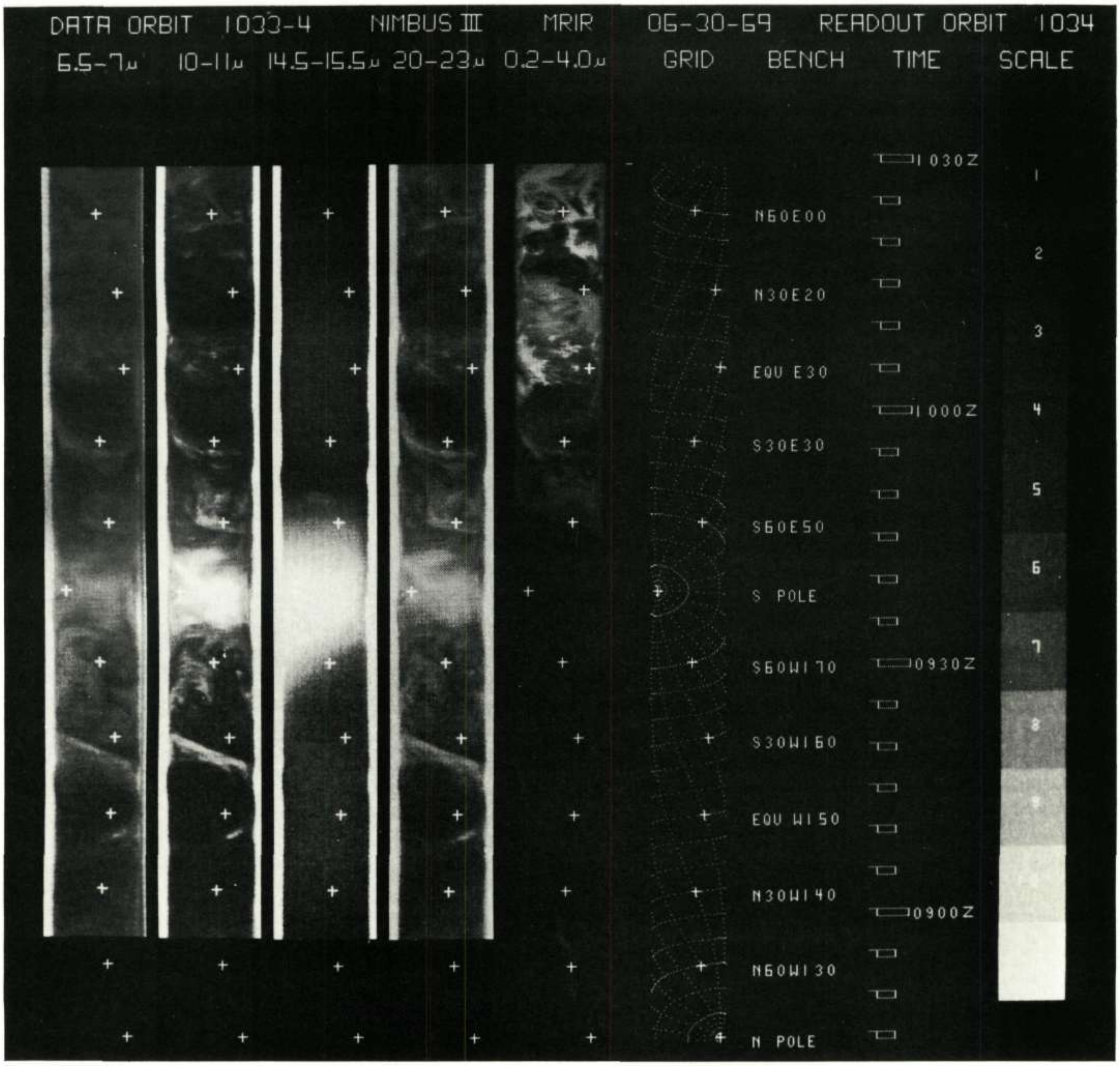

Nimbus III MRIR 30 June 1969

The Atlantic off Africa

The HRIR experiment of Nimbus I, II and III was replaced on Nimbus IV by a two-channel (temperature and water vapor) scanning radiometer. The Cape Verde Islands are spotlighted in this enlargement of a portion of a daytime Temperature-Humidity Infrared Radiometer (THIR) orbit. Although several of the islands are partially or totally obscured, this temperature channel display was used in conjunction with others to help establish the ground resolution of the THIR system. The smallest distance here discernible is about 6 or 7 statute miles, as compared to the theoretical resolution which is a little less than 5 statute miles.

The accuracy of the computer-imposed gridding is frequently checked on the Nimbus imagery as it was on this picture. It is correct in the area of the islands to well within prescribed tolerances.

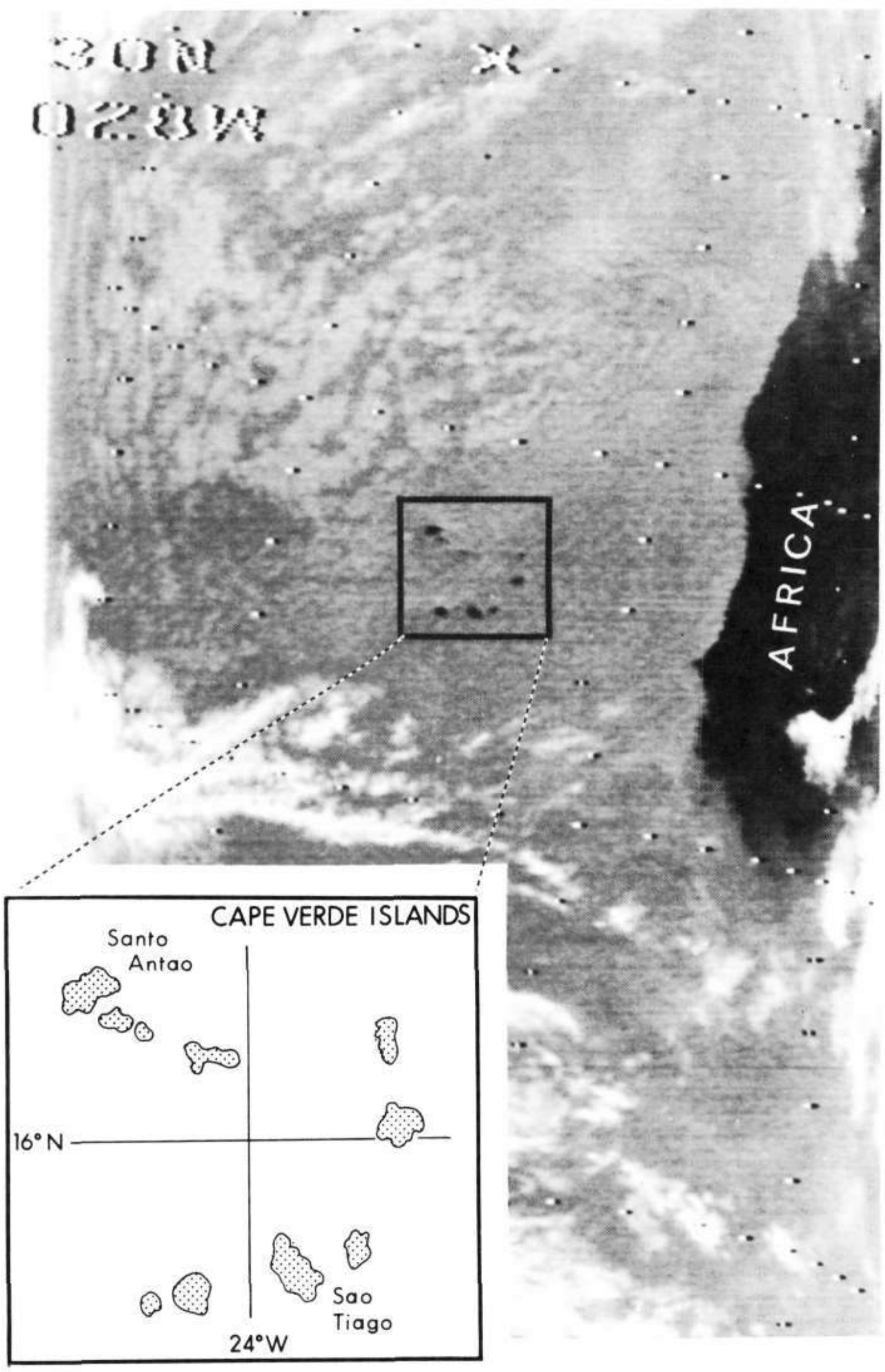

Nimbus IV THIR (D)   10 April 1970

The Eastern Mediterranean

This annotated imagery from THIR's 11.5 μm temperature channel shows a clear view of the Levant. The negatives of this type imagery can be processed, within limits, to accentuate either geological detail or cloud coverage.

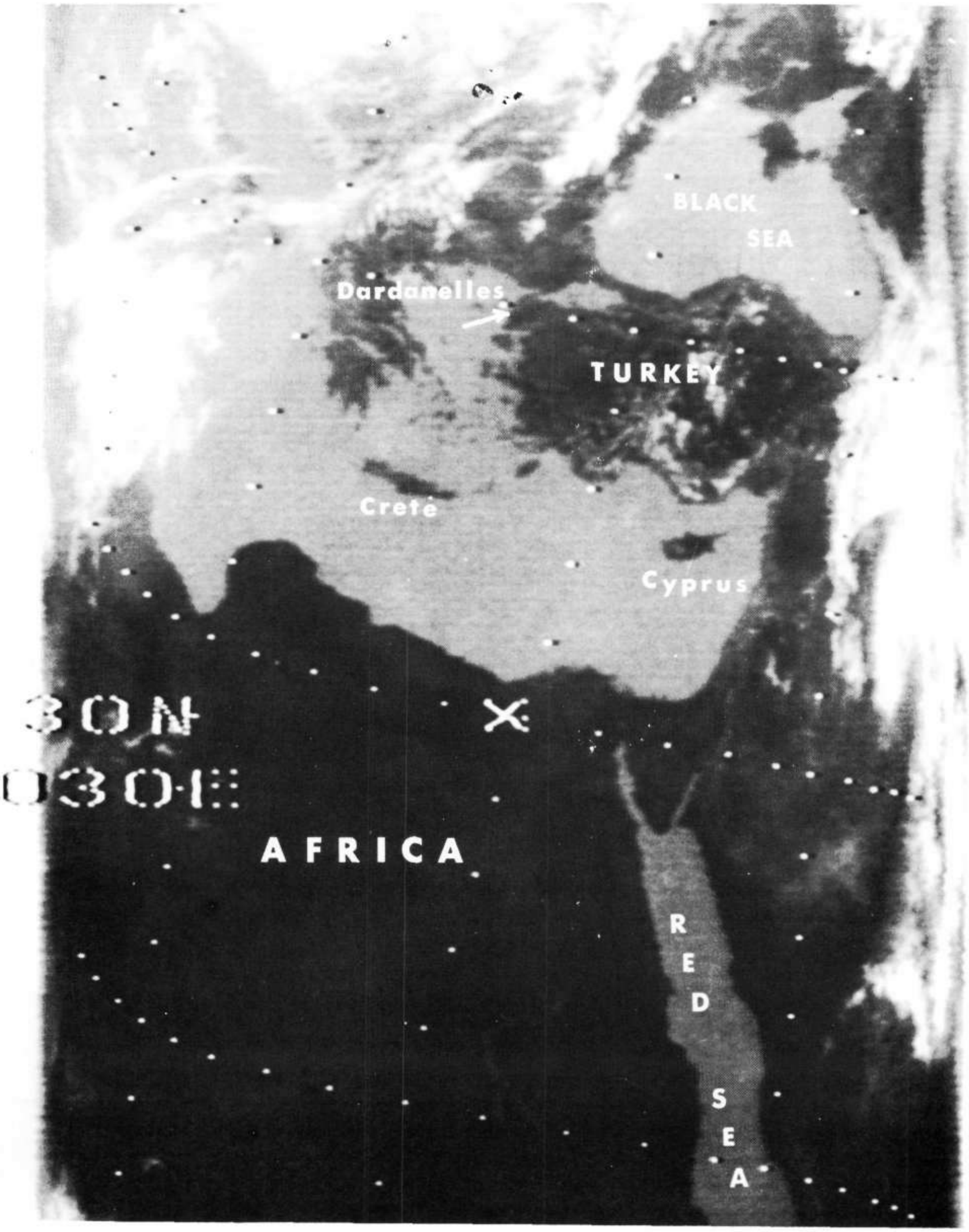

Nimbus IV THIR (D) 29 April 1970

Top of the World

The 11.5 μm temperature channel of the Nimbus IV THIR produced this daytime imagery extending from the Gulf of Alaska across the East Siberian Sea to the Mara Sea. The bottom portions of the imagery were recorded at 1038 local (Alaska) time on 3 July (03/2038 GMT). The top-most portions were recorded 15 minutes later by satellite time but at 0253 local (90°E) time on 4 July (03/2053 GMT). Thus the satellite passed through some 16-1/4 hours "earth time" in 15 minutes transit. The sun's northward summer position accounts for the almost total daylight seen in the imagery.

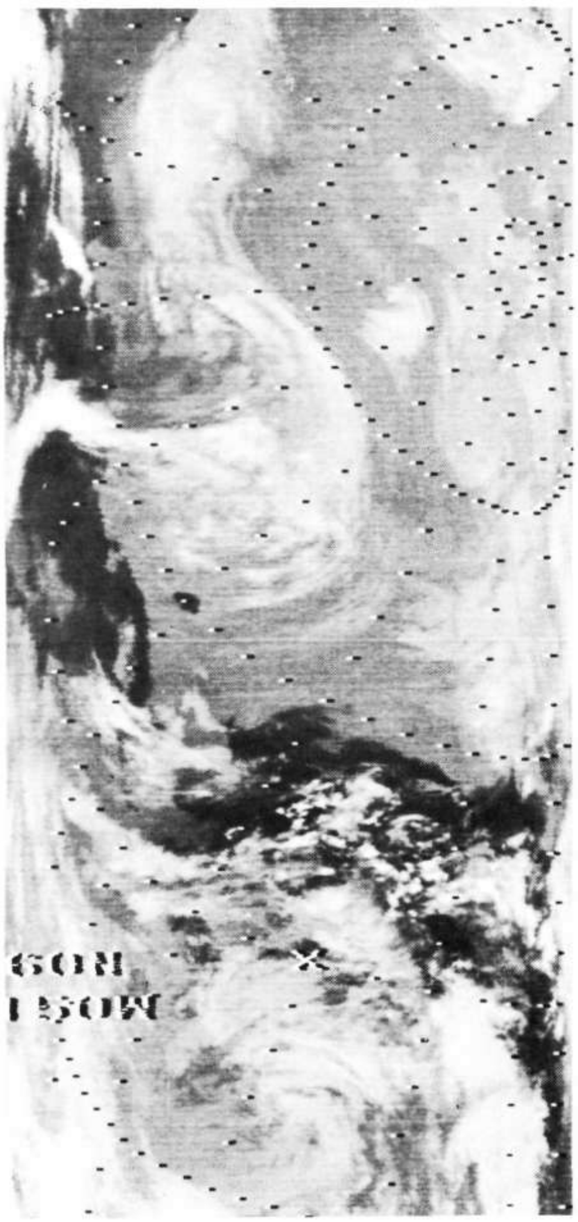

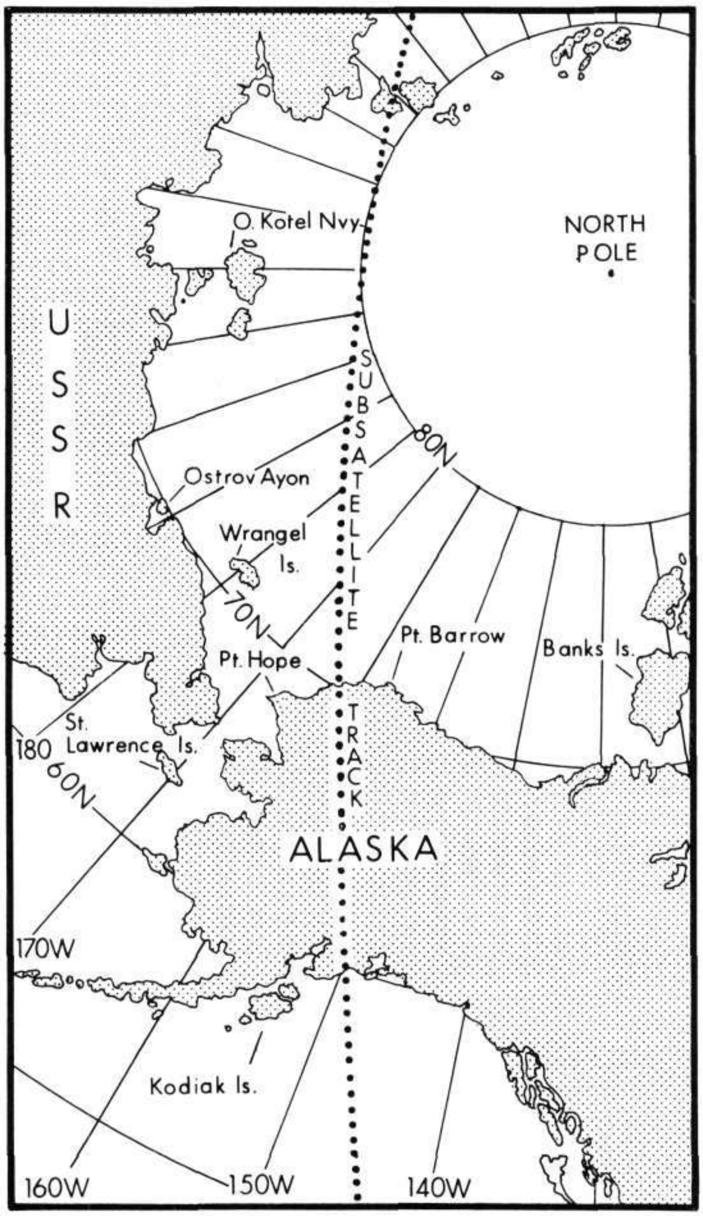

Nimbus IV THIR (D) 3 July 1970

Two Views of Europe

The Temperature-Humidity Infrared Radiometer (THIR) 11.5 μm channel provides temperature readings for cloud tops, land and water surfaces, as in these two striking photographs of Western Europe, the Mediterranean Sea and North Africa.

Land, warming faster than water during daytime, represents the dark, almost black areas compared to the less warm and grayish appearance of the ocean and the Mediterranean Sea. Cloud tops, being of relatively cold temperatures, are designated by lighter gray to absolute white.

Nimbus IV THIR Daytime 14 May, 1970

3 June 1970

IDCS-THIR Comparison, India

In addition to the THIR experiment, Nimbus IV carried a single scanning camera system which had replaced the earlier (Nimbus I and II) AVCS three-camera arrangement. In this comparison between the output of the Image Dissector Camera System (IDCS) and the THIR experiment, it may be seen that the information provided by the two systems is complementary rather than redundant. In the IDCS enlargement, there is much geological detail which is missing in the THIR display. The THIR display, however, which reveals temperature patterns, shows the Indian coastline much more clearly, particularly in the vicinity of the Kathiawar Peninsula which is obscured by haze in the IDCS picture.

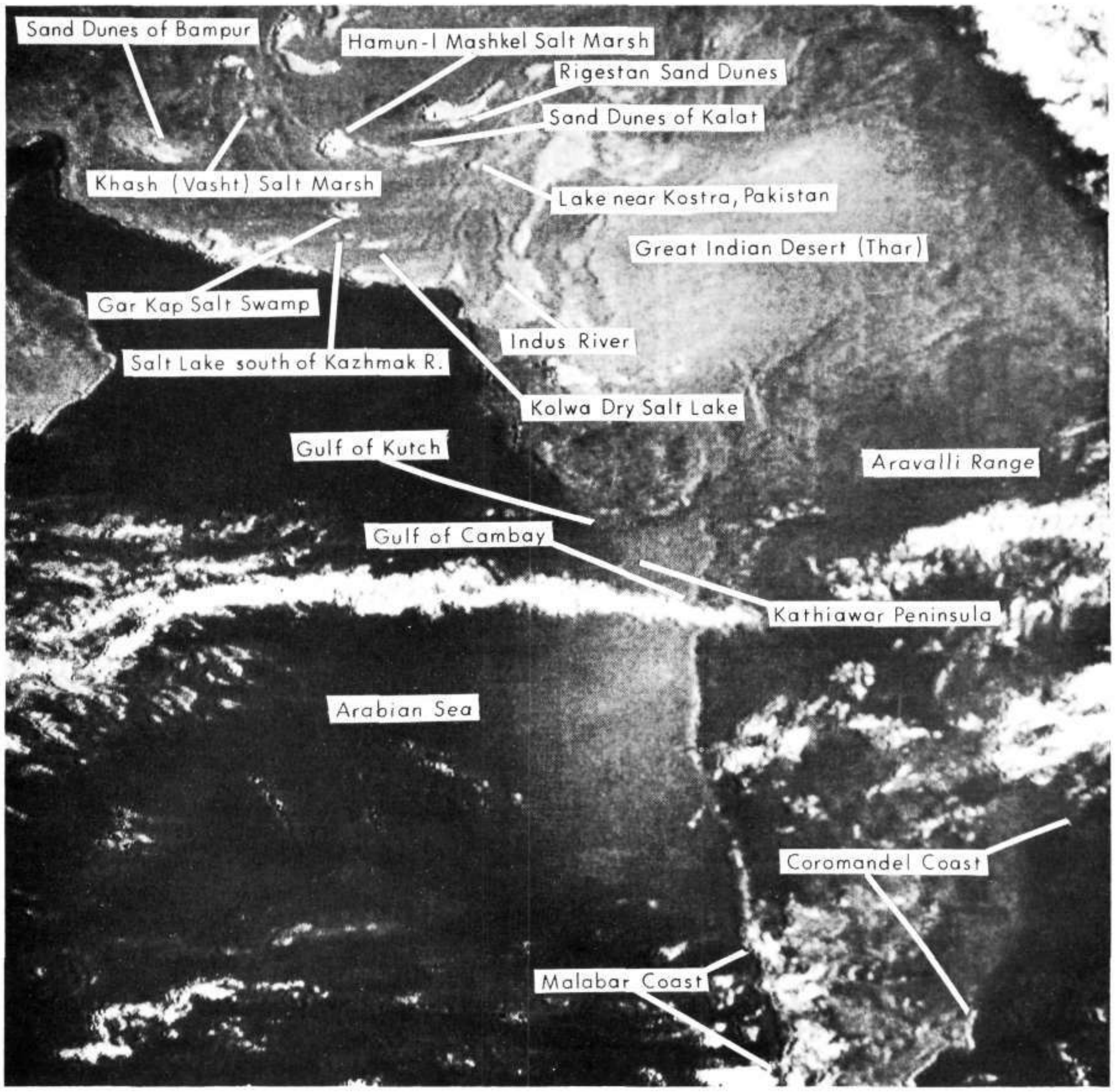

Nimbus IV IDCS 9 April 1970

Nimbus IV THIR (D) 11.5 μm
9 April 1970

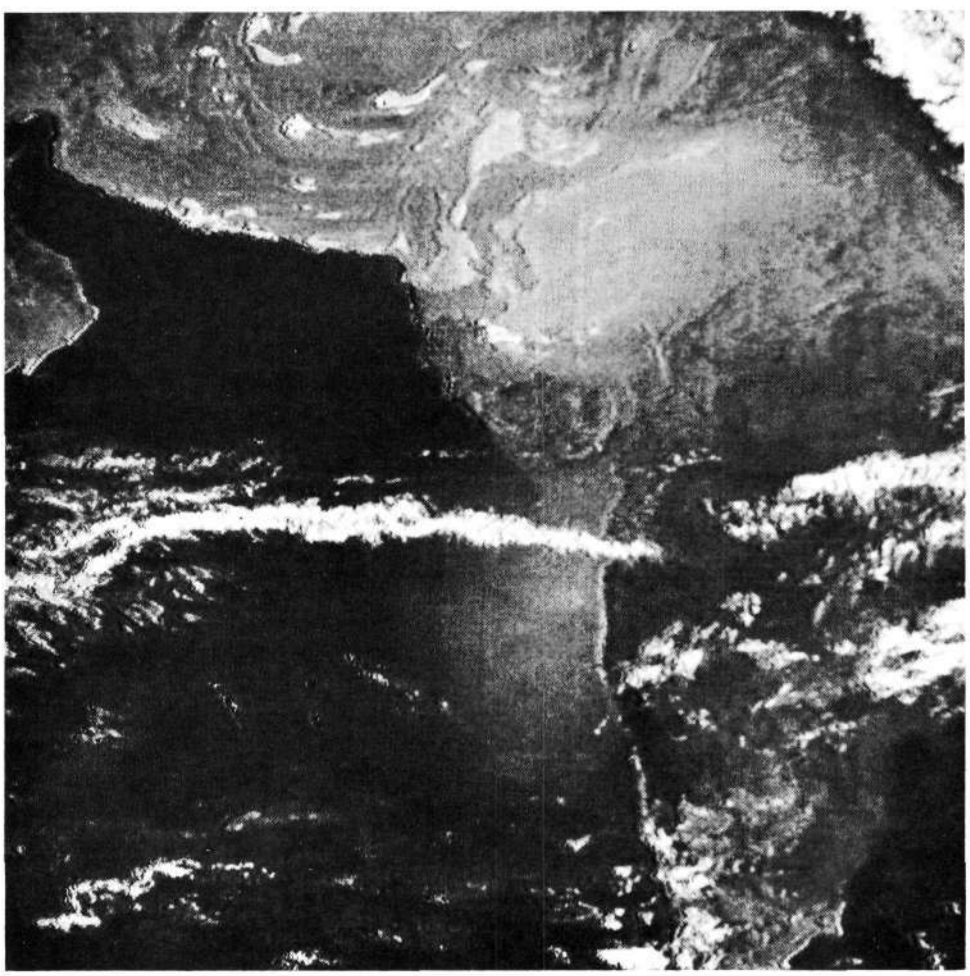

Nimbus IV IDCS
9 April 1970

Daily Montages

The montages shown here are representative of those produced daily from the Nimbus IV THIR sensor. The two channels can be compared side by side or, if desired, superimposed through the use of transparencies. By photographically combining the two negatives and processing the resultant image through a variety of colored filters, areas of thin cloudiness not visible on the 11.5 μm imagery, can be readily seen.

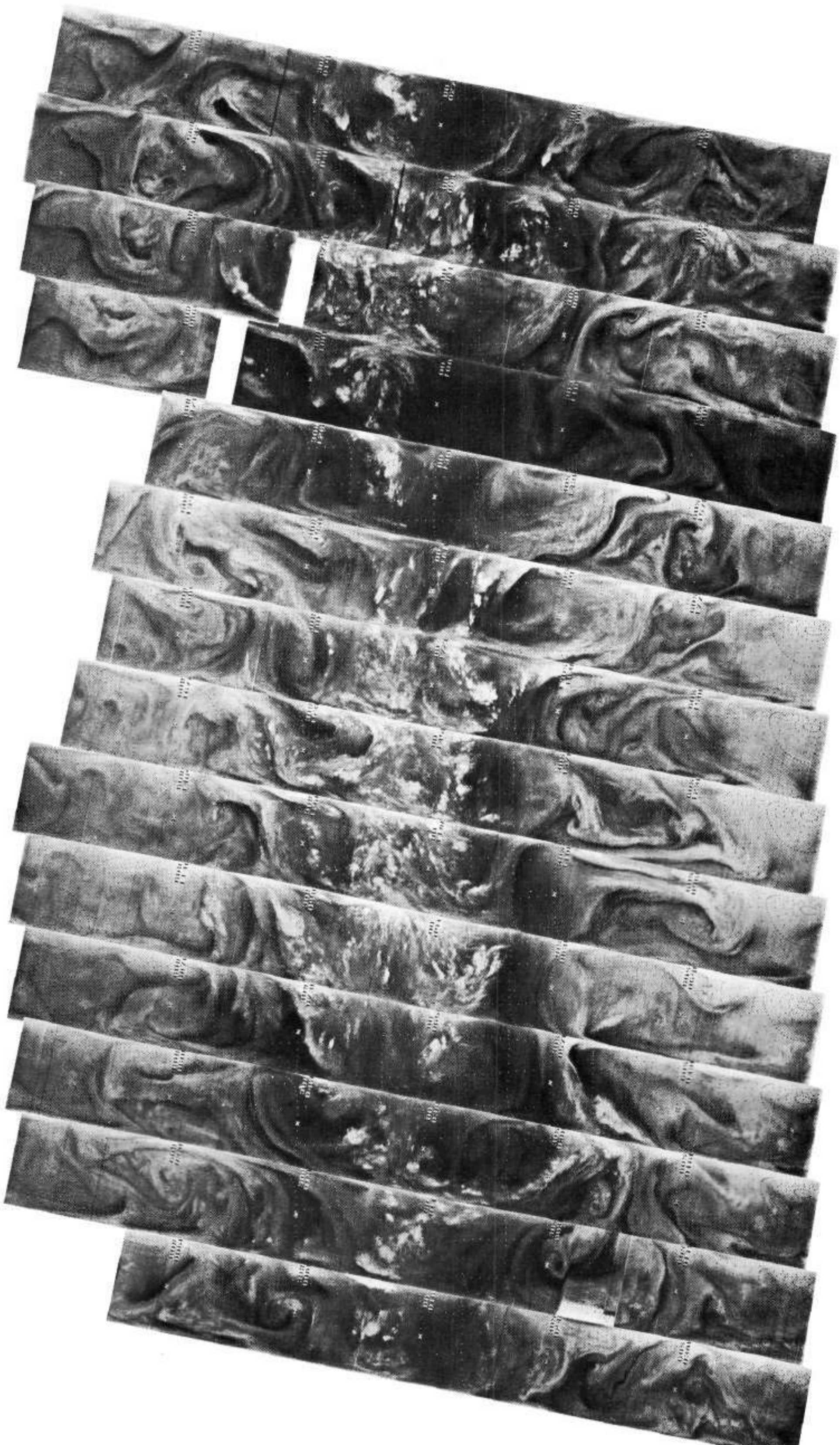

6.7 μm Channel

Nimbus IV THIR 25 September 1970

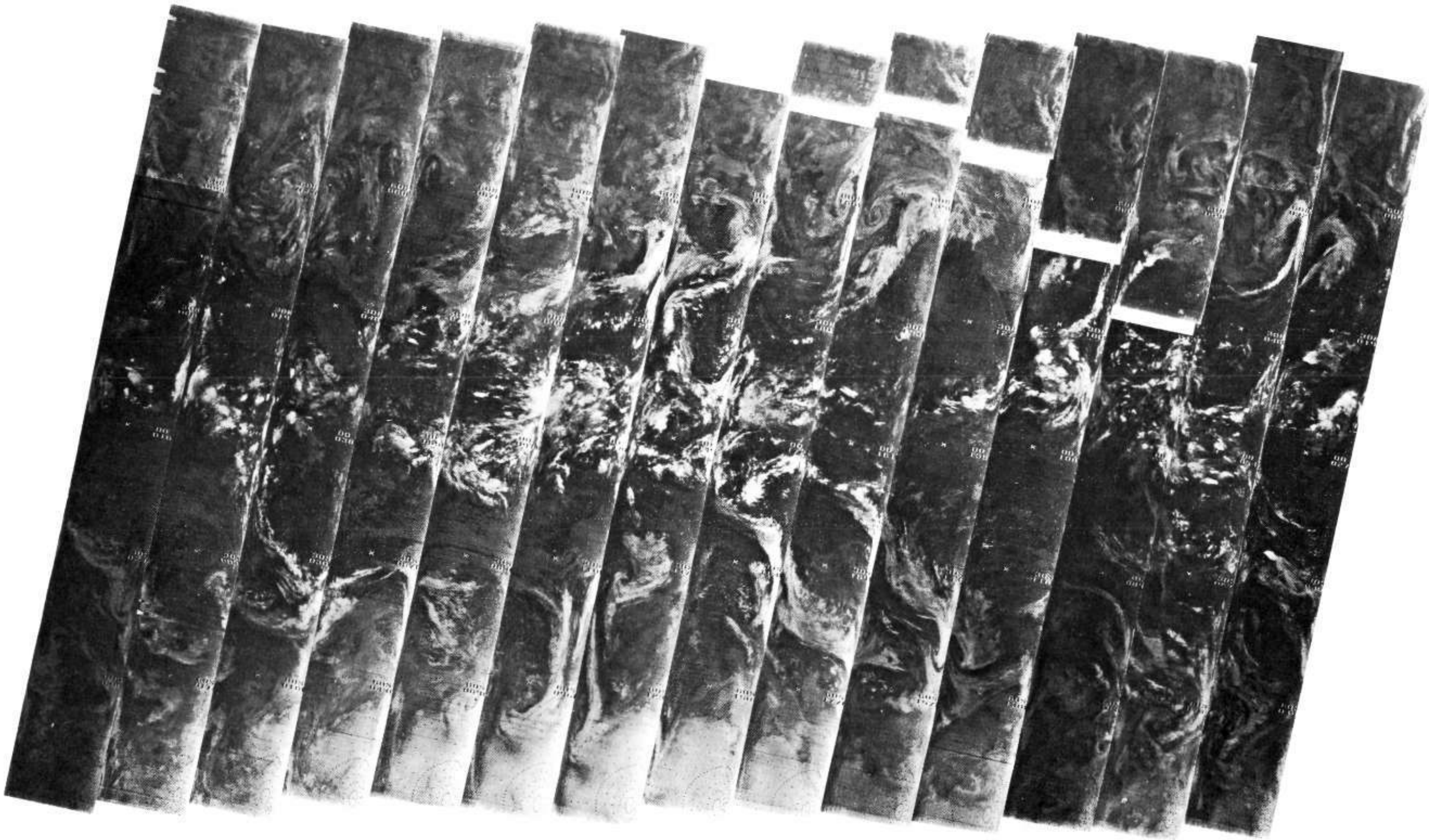

Nimbus IV THIR 25 September 1970 11.5 μm Channel

A Storm in the Bay of Bengal

The meteorological applications of the Nimbus IV THIR imagery become evident in the analysis of pictures such as these. The particular configuration of the clouds associated with each storm system (compare this picture with that of the 7 November 1969 Indian Ocean Storm - page 28) and the coverage obtained through successive orbits enables the meteorologist to prepare much more accurate forecasts than in the presatellite period.

Little in the way of topographic detail is apparent in either picture because of the dense cloud coverage. The Himalaya Mountains, however, appear at the top of both images.

11.5 μm Channel

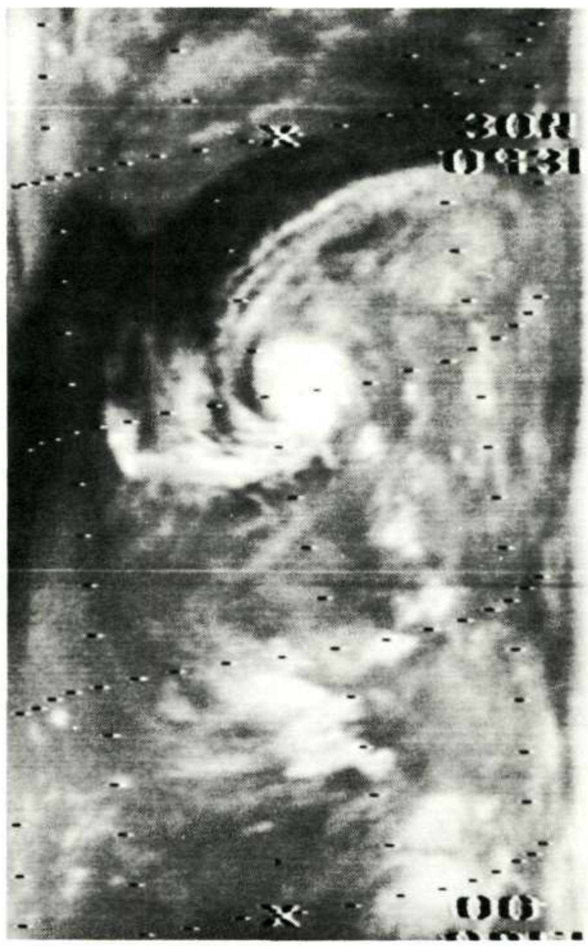

6.7 μm Channel

Nimbus IV THIR 5 May 1970

MOVING a MOUNTAIN...

Mt. Siple, Antarctica

One of the more spectacular applications of the Nimbus AVCS imagery was the relocation of an entire mountain on the Antarctic continent. In 1964, the U. S. Geological Survey utilized AVCS imagery to make this and other changes to the existing maps of Antarctica. Two of the more important changes are shown here:

1) Mount Siple was moved on the charts 2^{o}W from its previous chart position. The 10,000 ft. peak is near the coast and important as a navigational reference.

2) The ice front was updated from its previous best-known position. (This type of relocation has continued periodically since 1964.)

The AVCS data were also used to alter the chart configuration of the Kohler Range of mountains (not seen). Expeditions had reported two groups of mountains where AVCS showed but one.

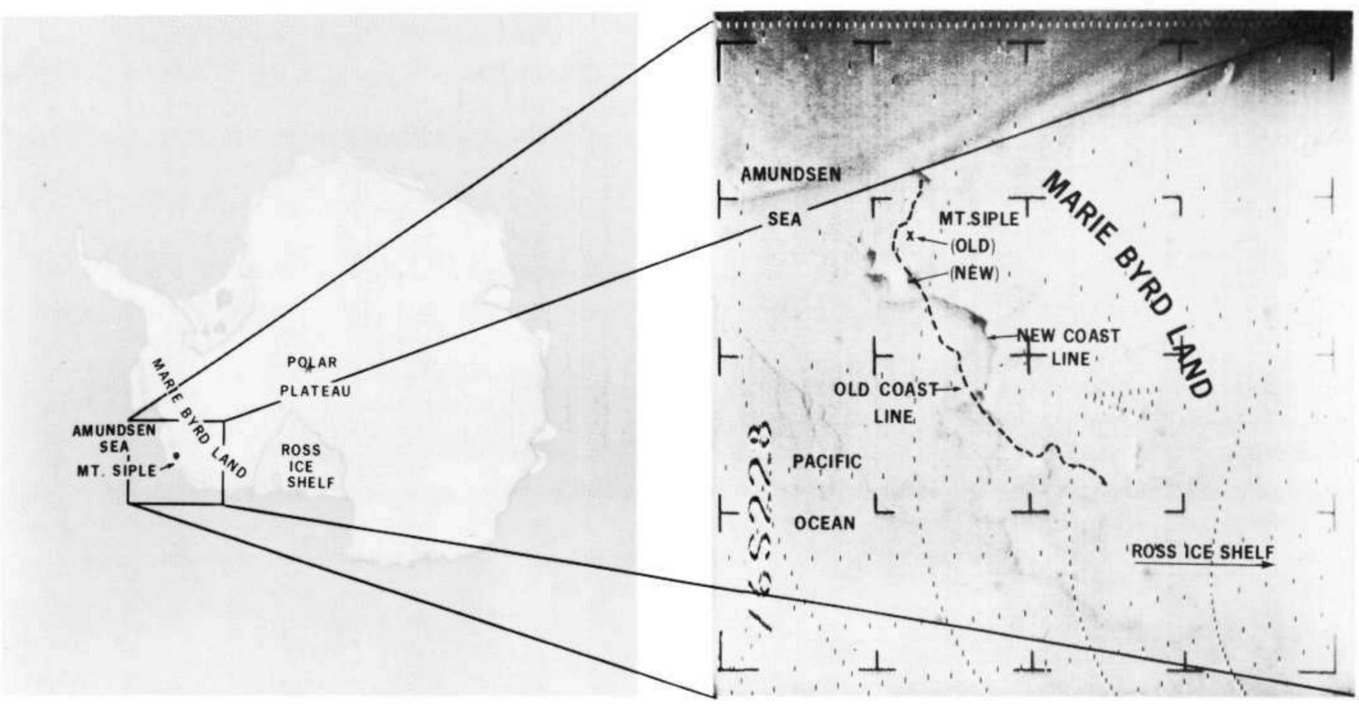

Nimbus I AVCS 9 September 1964

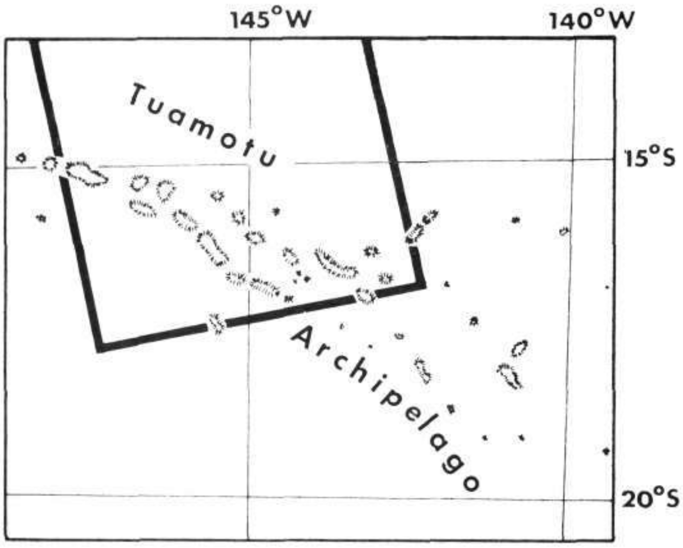

Tuamotu Archipelago

On some occasions, the Nimbus imagery may be used to better locate the many tiny islands and atolls which dot the vast Pacific. This photograph shows several coral atolls just northeast of Tahiti. The whitish rims of the atolls are probably less than a half-mile in width. Finding such areas in a cloud-free state is relatively rare since even the small amount of heat generated by such minute land masses is enough to trigger convective cloudiness.

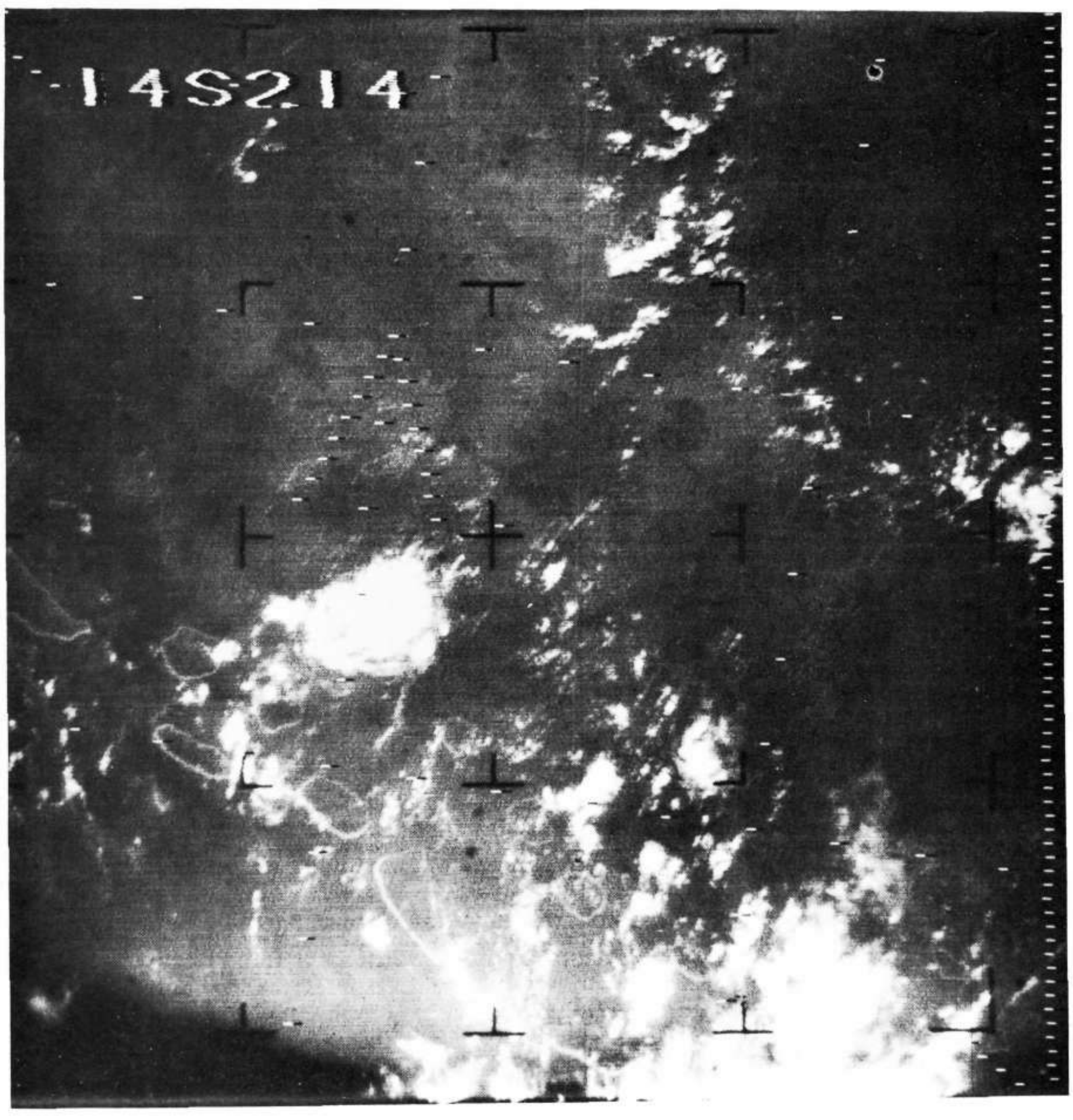

Nimbus I AVCS 15 September 1964

James Bay, Canada

Even underwater features can at times be mapped. In this photograph, Akimiski Island, in west-central James Bay, appears as a half-moon silhouette. C. I. Taggart, a noted Canadian photo-interpreter, was able to determine from this photograph that extensive underwater shoals surround Akimiski Island. The shoals appear as a light band circling the island.

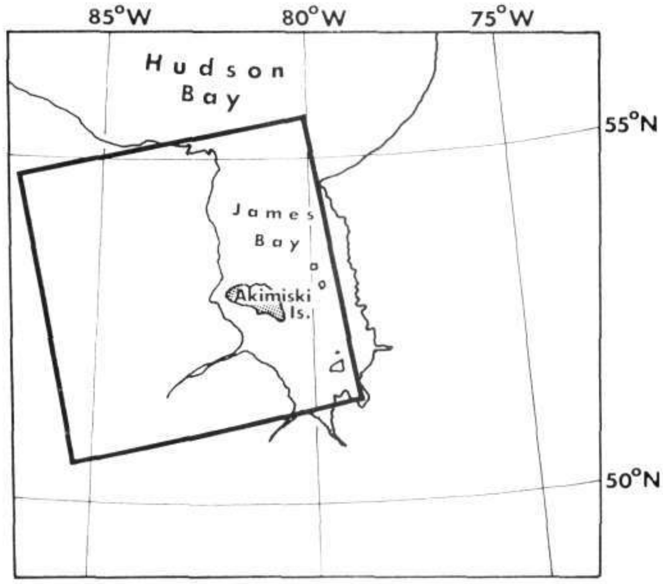

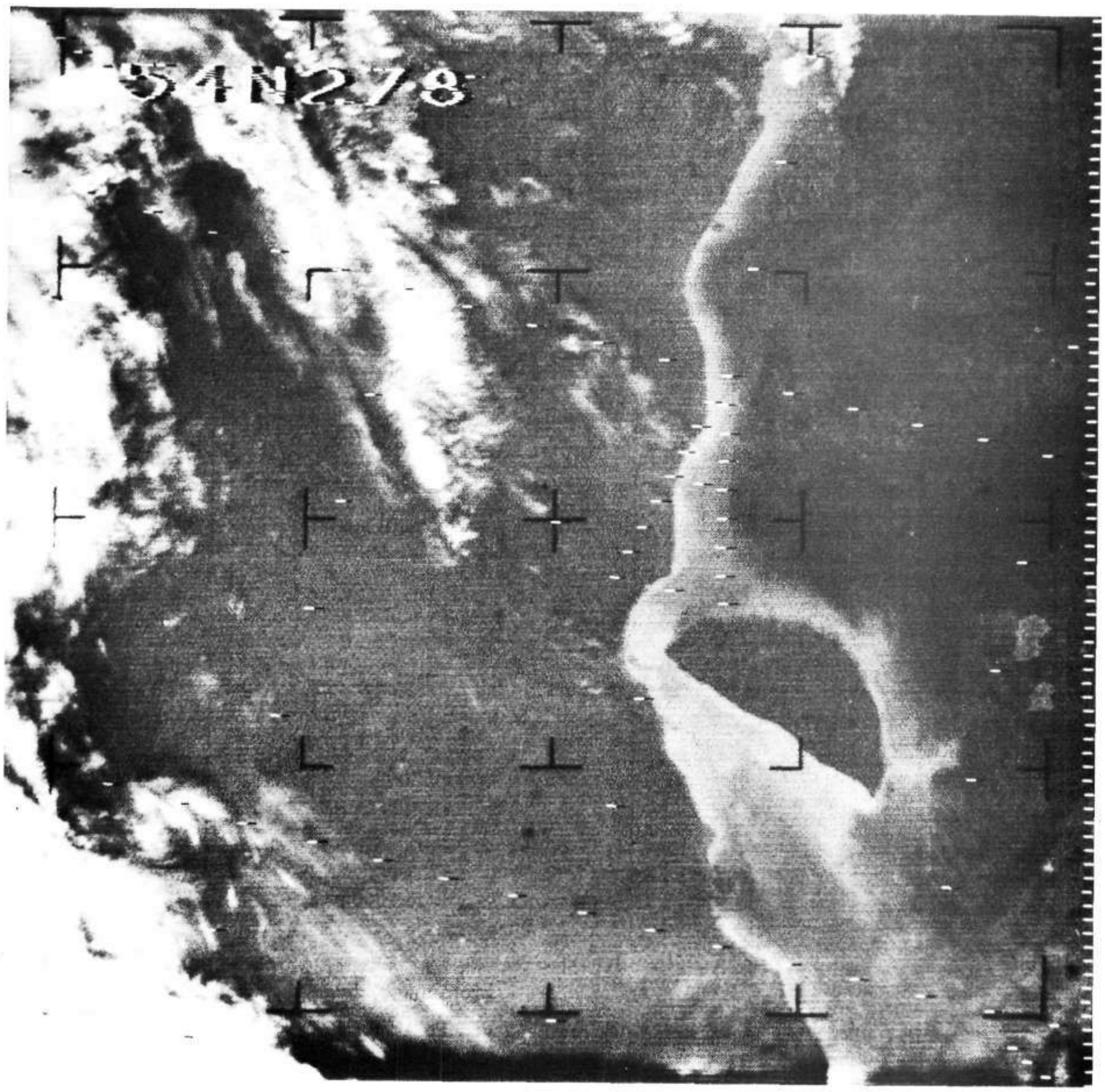

Nimbus I AVCS 6 September 1964

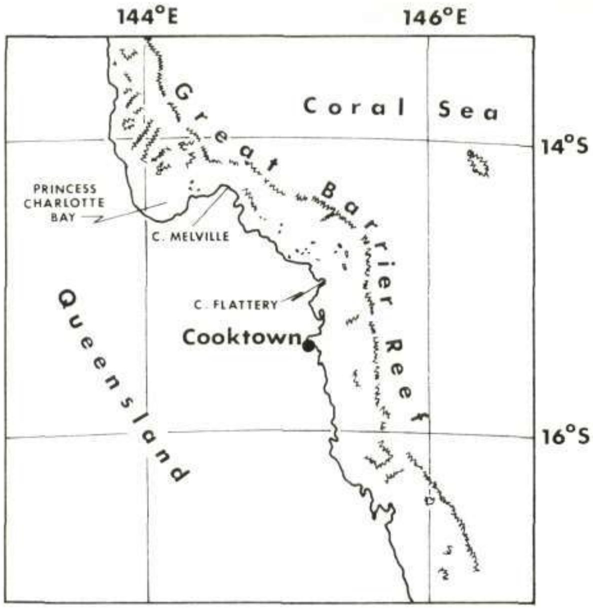

Northeastern Australia

A portion of the Great Barrier Reef of northeastern Australia appears in this photograph as a white, sinuous line running north-south to the right of center. Cape Melville and Princess Charlotte Bay are at top center. The coastline is partially obscured by clouds from Cape Flattery southward.

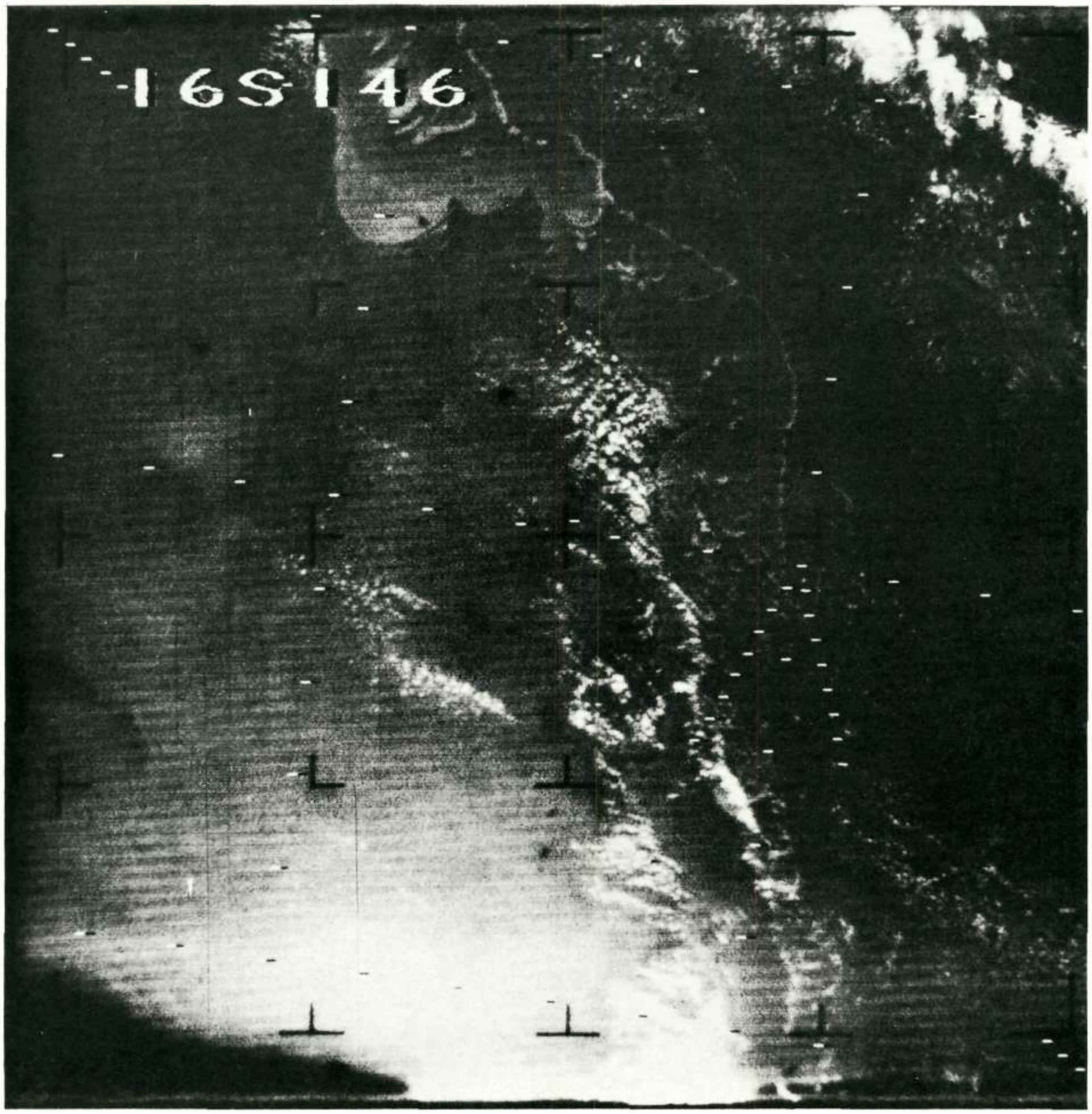

Nimbus I AVCS 21 September 1964

Antarctica

The coastline of Antarctica's Filchner Ice Shelf is shown in this mosaic composed of parts of three AVCS pictures. These and other photographs of the area were used by the U. S. Geological Survey to make coastline changes to their relief models of Antarctica. Leads appear in the mosaic as dark areas along the ice edge. The changes in the ice front during the period 1957-1964 are noted in the map below.

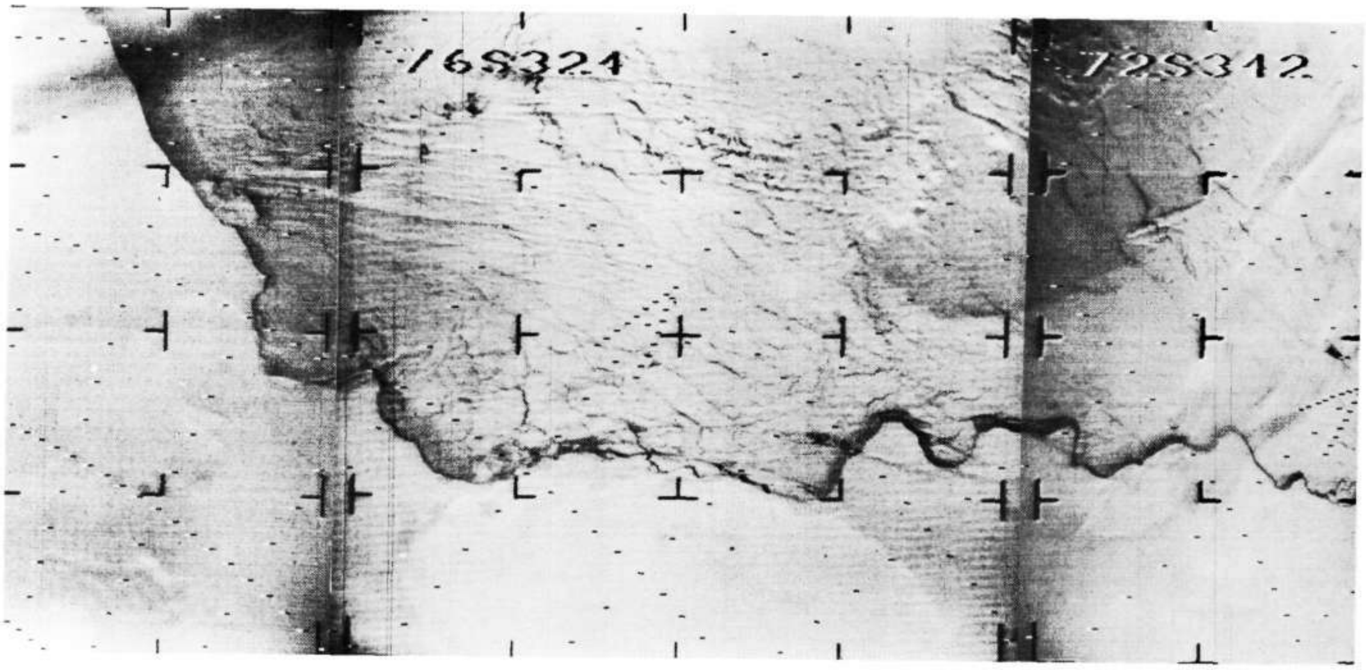

Nimbus I AVCS 9 September 1964

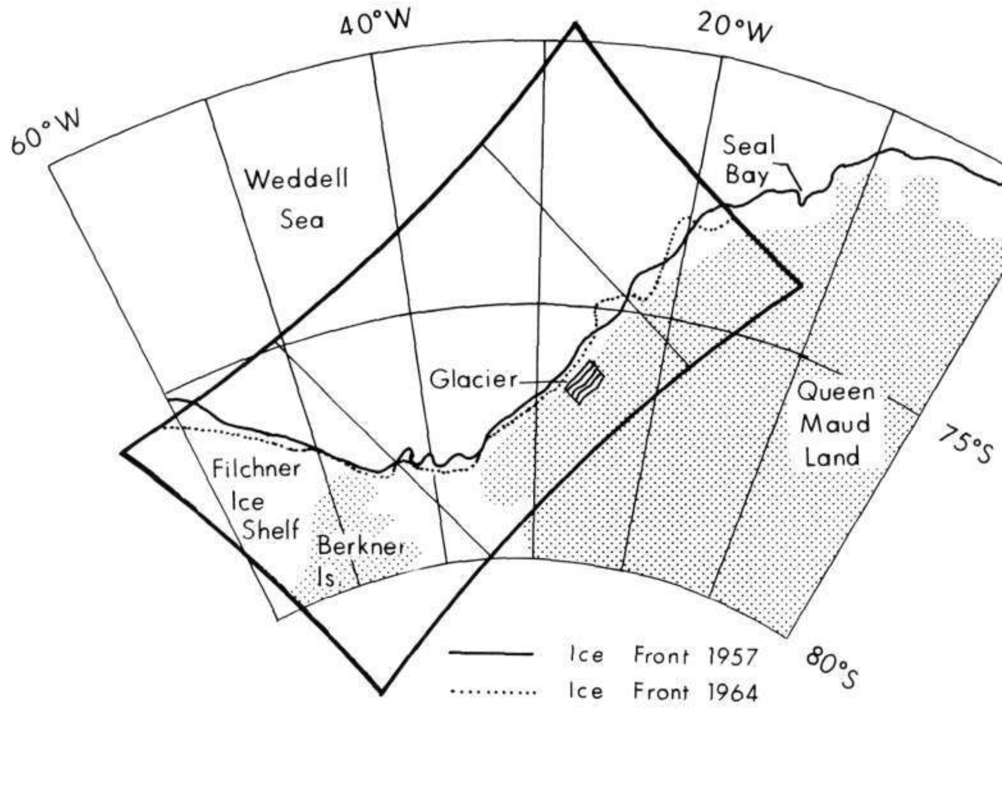

SNOW, GLACIERS and ICEBERGS...

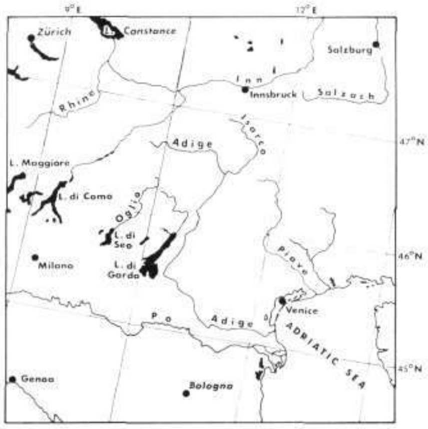

The Italian Alps

Here, the fine, dendritic pattern of an Alpine snowfield outlines the rivers of Italy, Austria and Switzerland. Such photographs, taken on a repetitive basis, are valuable tools in estimating snow depths, areal coverage and rate of melt. Combined with other observations, they could be used to accurately forecast time and extent of spring flooding.

Nimbus I AVCS 15 September 1964

Lake Issyk-Kul

These two AVCS frames show portions of southern Kazakhstan, USSR, and northern Sinkiang Province, China. Lake Issyk-Kul and the drainage pattern of the Tien Shan mountains are readily apparent. The snow and glacier fields in the lower portions of the pictures give fine outline to the rivers. The mountains average some 16,000 feet and are permanently snow-covered in many areas.

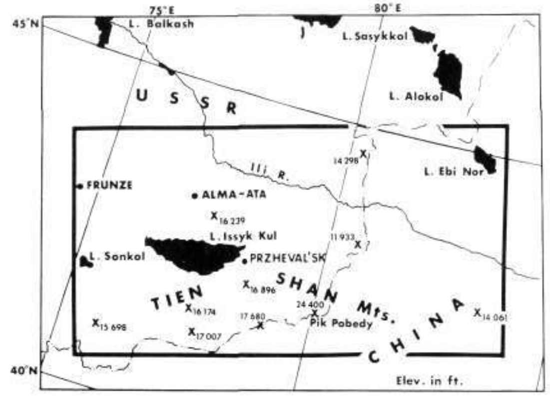

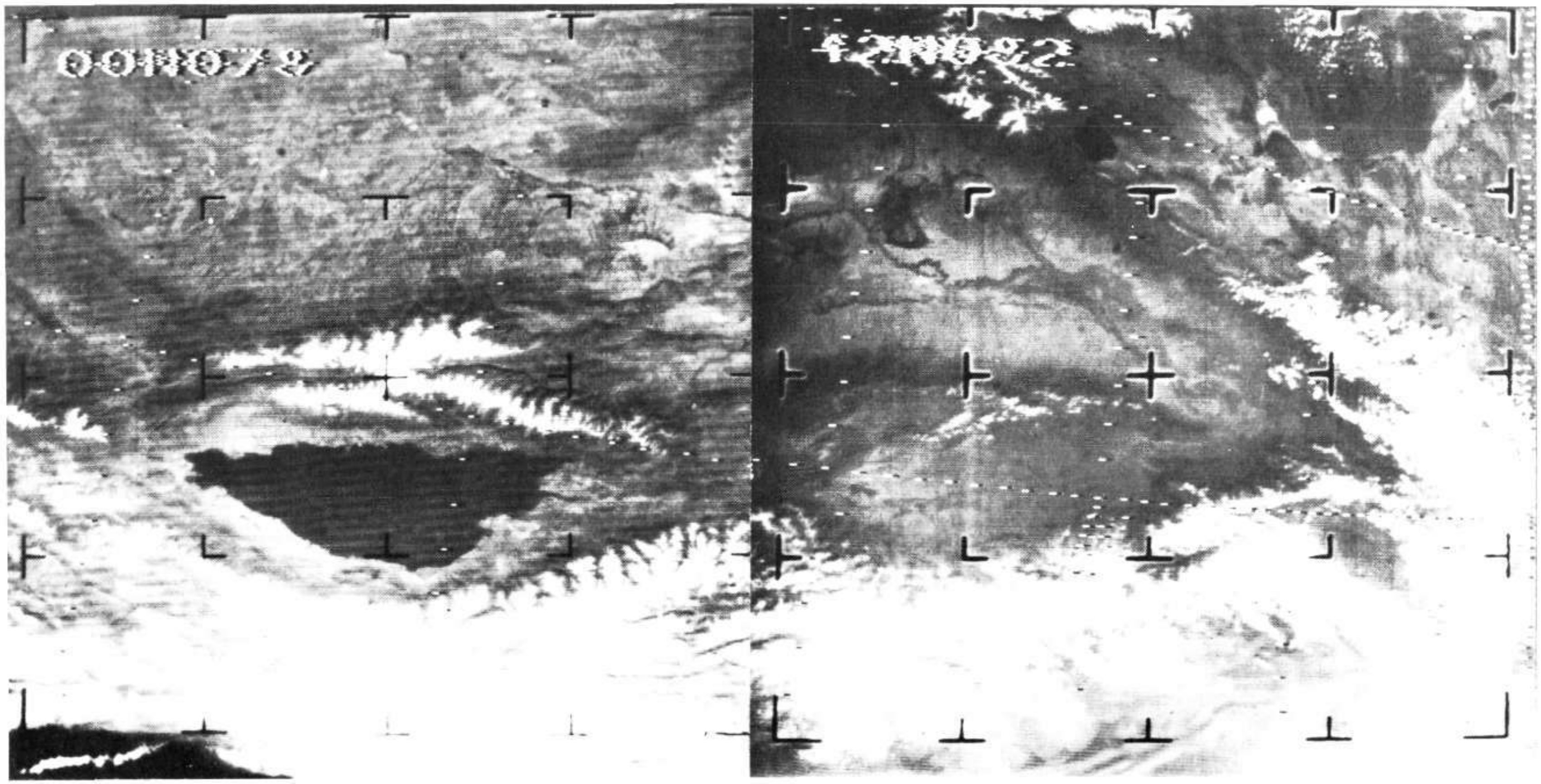

16 September 1964 Nimbus I AVCS

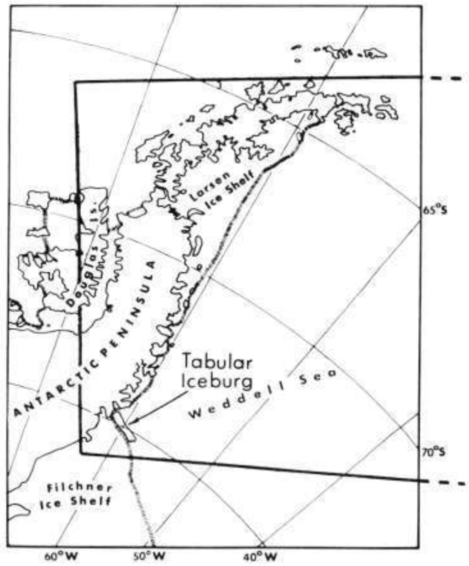

Antarctic Peninsula

A large offshore lead or opening in the ice along the eastern coast of the peninsula appears in this picture as a jagged dark area just off the Larsen Ice Shelf of the Antarctic Peninsula. The same lead was spotted five years later by Nimbus III. (See next picture.) The first tabular iceberg ever observed from space is visible in the extreme lower left corner of the picture. The iceberg, over 70 miles in length, was observed on many occasions over a period of weeks. As these icebergs drift equatorward, their continual reconnaissance by satellites such as Nimbus become extremely important to the shipping industry.

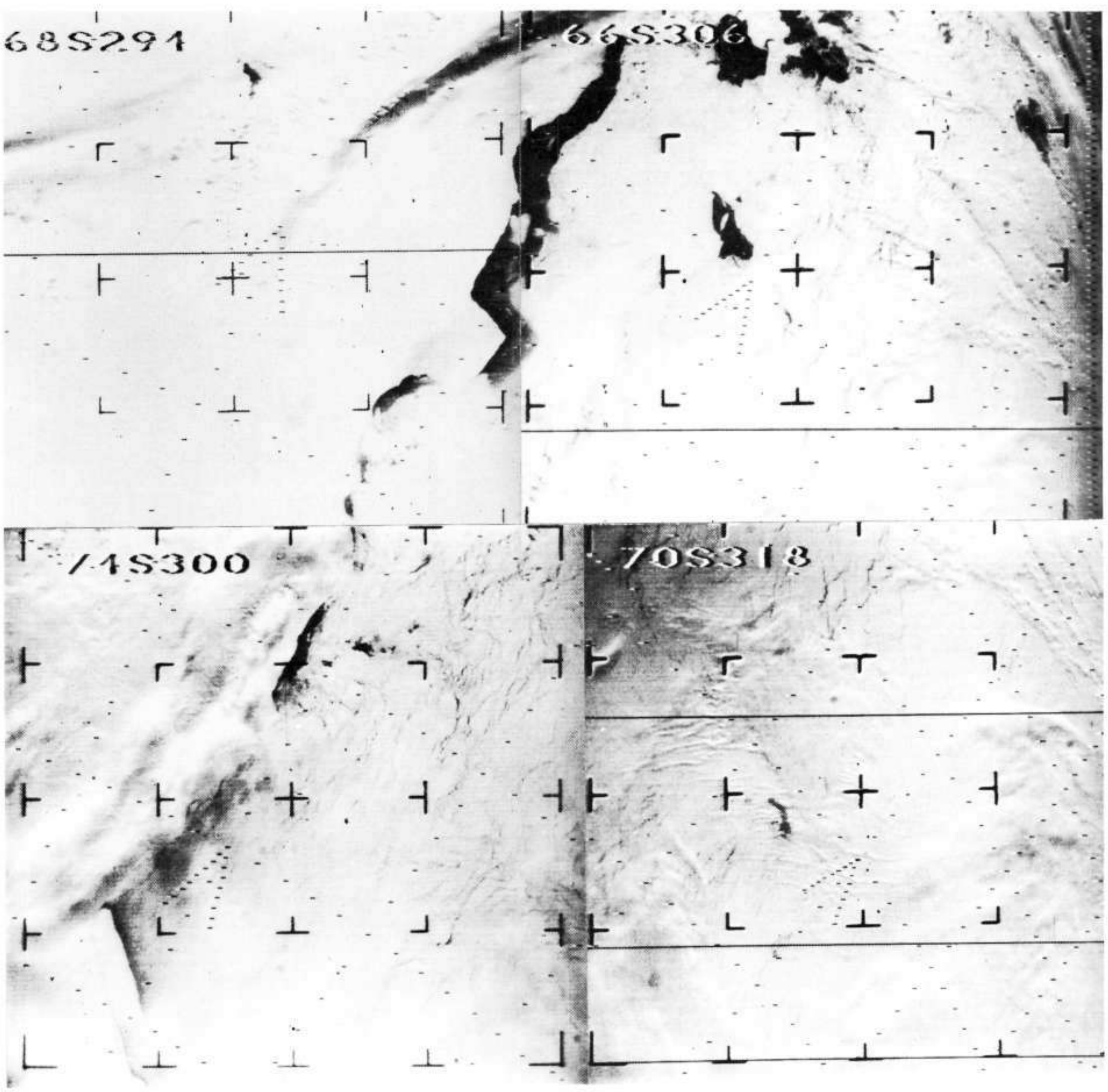

Nimbus I AVCS 9 September 1964

Nimbus III Picks Up a Lead

This series of Nimbus III IDCS satellite pictures recorded during August and September 1969 show the development of an offshore lead along the east coast of the Antarctic Peninsula. The westerly wind helps produce this kind of large lead. Most of the 20 to 30 mile width was produced in a six-day period from 27 August to 2 September. The pack ice boundary can be observed to the north of the peninsula in several of the images. Such ice information can be valuable to ships during their summer resupply efforts.

9 AUGUST

20 AUGUST

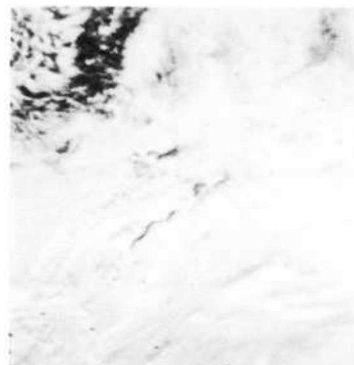

21 AUGUST

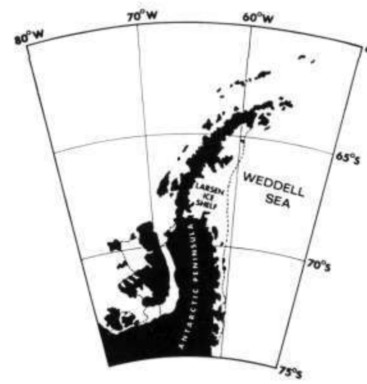

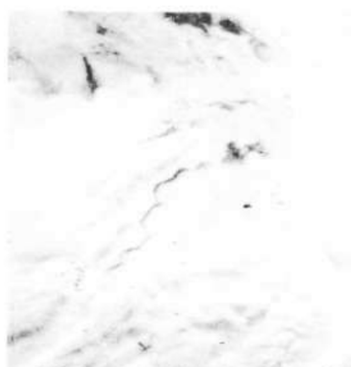

27 AUGUST

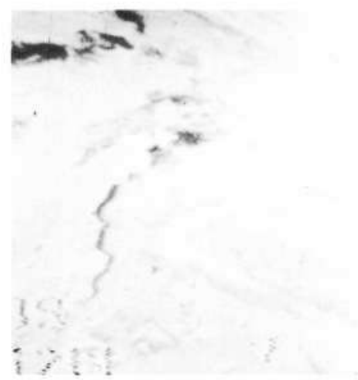

29 AUGUST

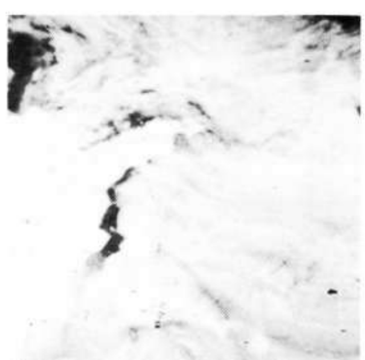

2 SEPTEMBER

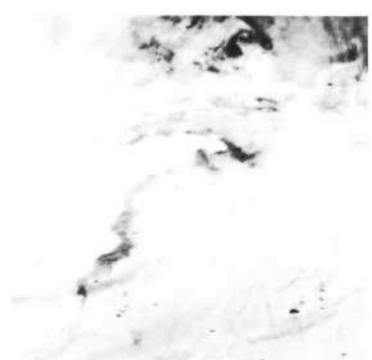

4 SEPTEMBER

Nimbus III IDCS

Mountain Snow Changes

This temporal sequence of Image Dissector Camera System (IDCS) pictures demonstrates the utility of a satellite platform with a two-mile ground resolution to monitor seasonal snow limits. The time and amount of snow melt is an important input for flood and irrigation planning. The daily world coverage from a polar orbiting satellite is an additional data source for this information.

28 APRIL

30 MAY

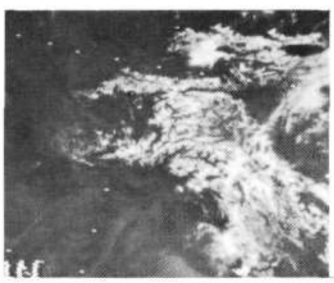

21 JUNE

18 JULY

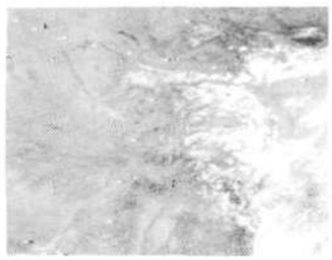

24 AUGUST

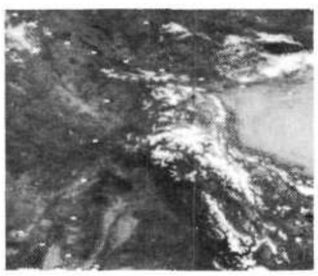

18 SEPTEMBER

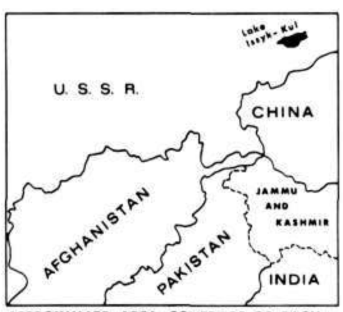

APPROXIMATE AREA COVERAGE OF EACH PICTURE

12 OCTOBER

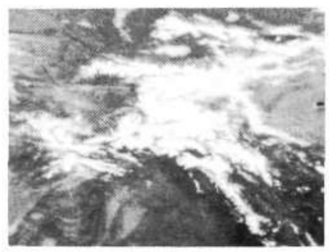

28 NOVEMBER

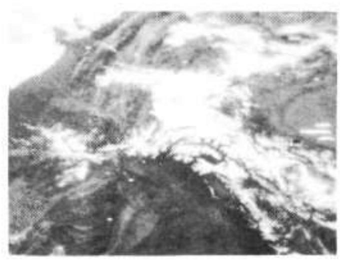

20 DECEMBER

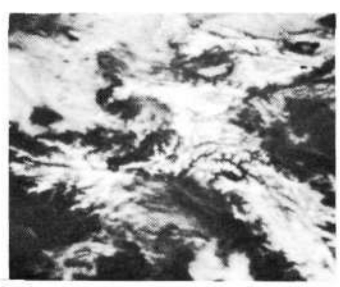

21 JANUARY

1969 - 1970 Nimbus III IDCS

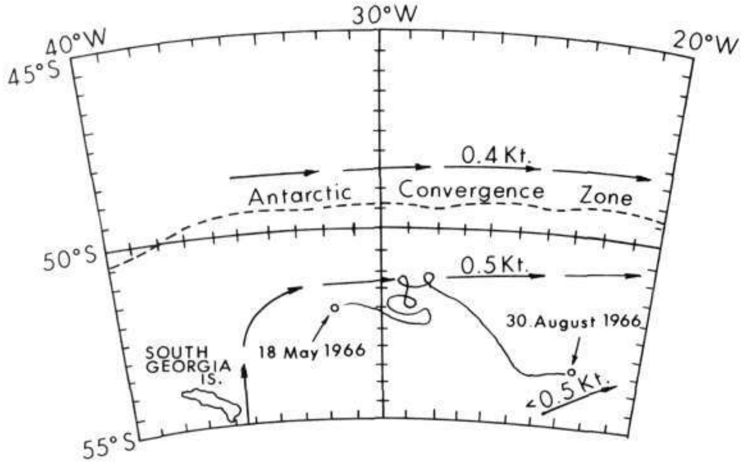

Antarctica

These pictures show the three-month progression through the South Atlantic Ocean of a 25-mile long tabular iceberg. The iceberg was viewed on the average of once every three days during the lifetime of Nimbus II. Ocean current calculations of this remote area were made from the changes in the iceberg's positions.

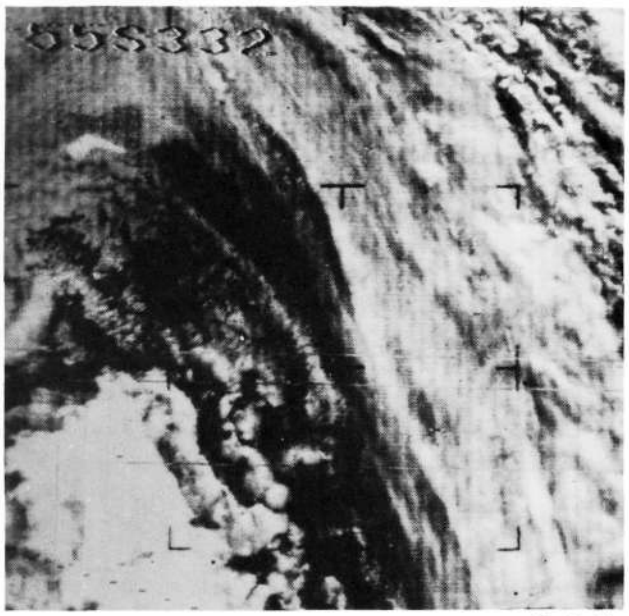

18 MAY

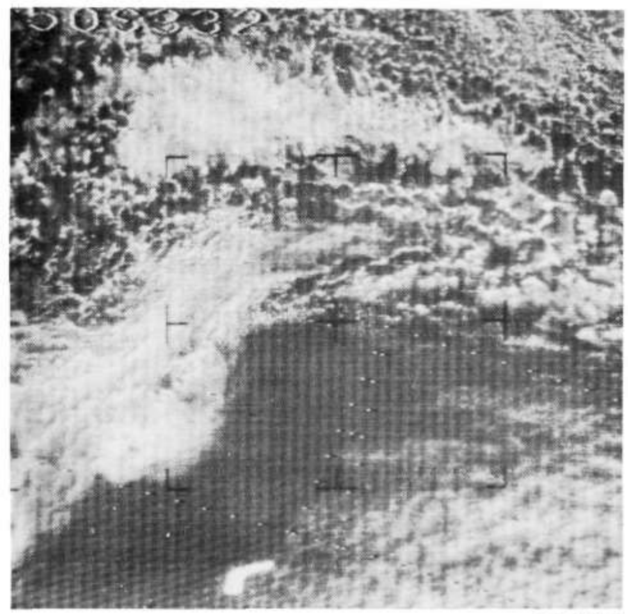

19 JUNE

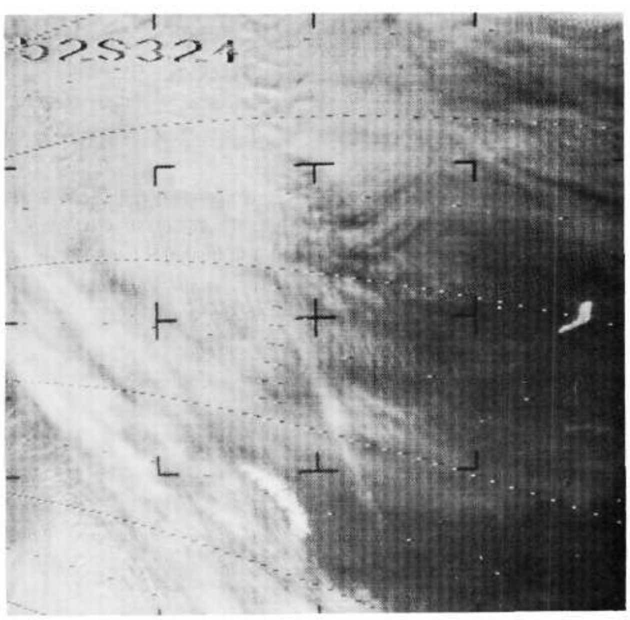

12 JULY

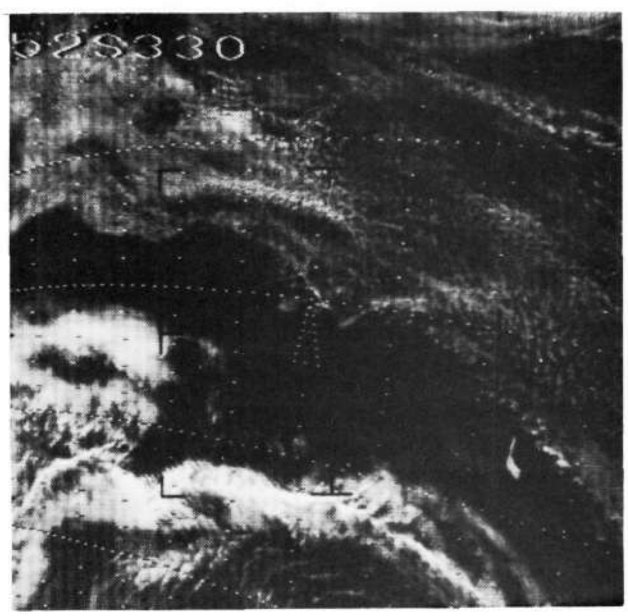

20 AUGUST

East Coast of Greenland

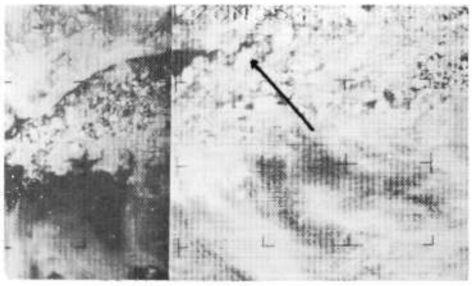

1 June

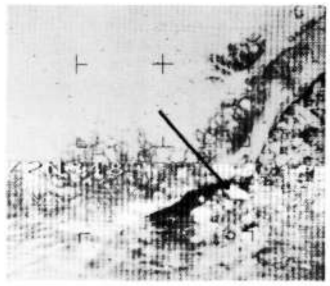

8 June

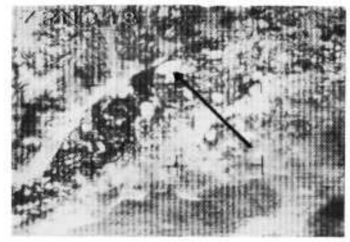

21 June

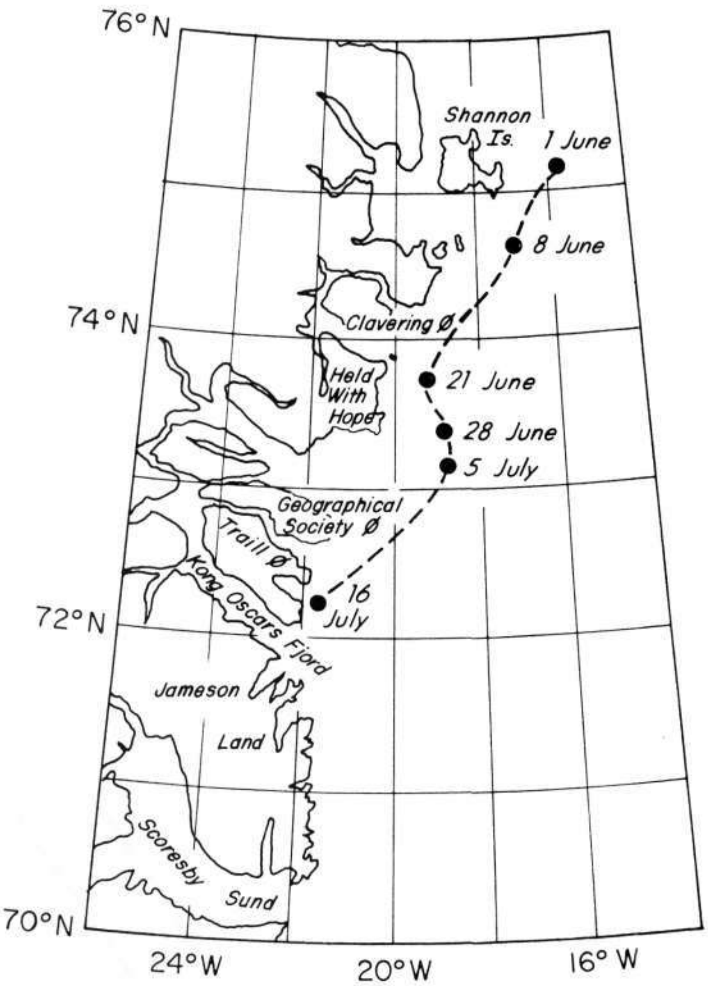

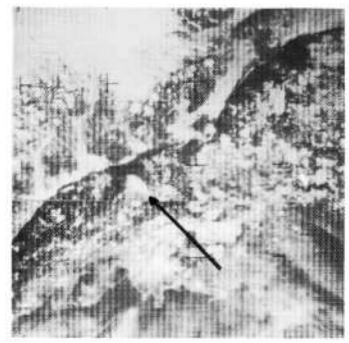

28 June

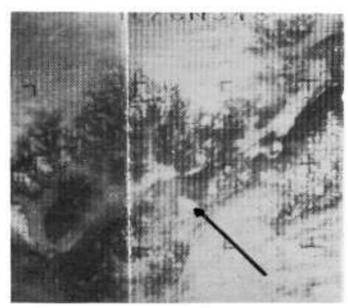

5 July

16 July

This is an example of the use of satellite data to track sea ice. The ice floe is about 17 miles in length and was followed for over six weeks. Note the overall decrease in the amount of sea ice from 1 June to 16 July.

Nimbus II AVCS
June - July 1966

Greenland and Iceland

These two pictures show concurrent coverage by the HRIR and IDCS systems of Nimbus III. The HRIR daytime photograph shows remarkable agreement and fidelity of detail to the IDCS even though the HRIR detects energy in the 0.7 to 1.3 μm band as compared to 0.45 to 0.65 μm for the IDCS. Both show the icepack boundaries between Iceland and Greenland. The resolution of the HRIR is slightly less than the IDCS (4 to 5 n.mi. for the HRIR, 2 to 3 n.mi. for the IDCS).

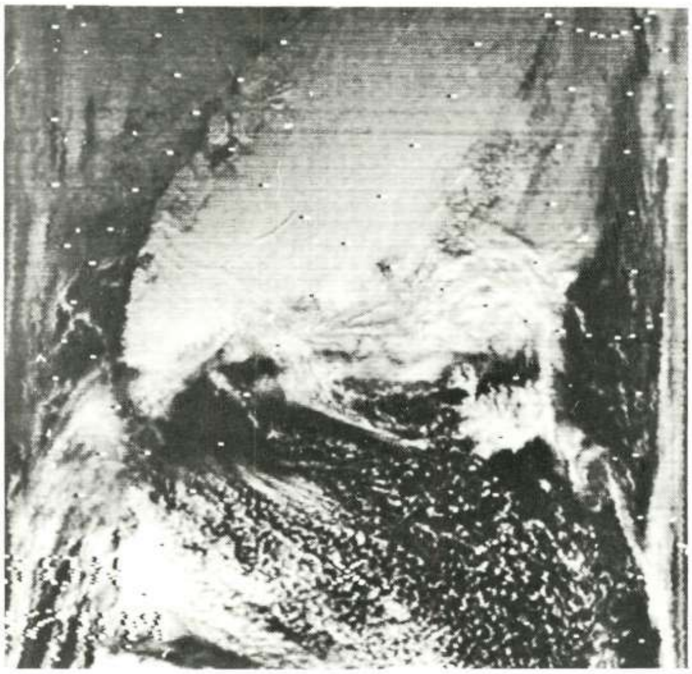

Nimbus III
HRIR (D)

IDCS

15 April 1969

Scandinavia

This classic view of northern Europe demonstrates the versatility of satellite photography. In addition to the fine geologic detail brought out by snow cover, the ice coverage in the Gulf of Bothnia and adjacent waters and the overall cloud portrayal show the many uses of video-type photography. The streaked clouds at top center delineate the western side of a low-pressure system which is off the northeastern side of the photograph in the Barents Sea.

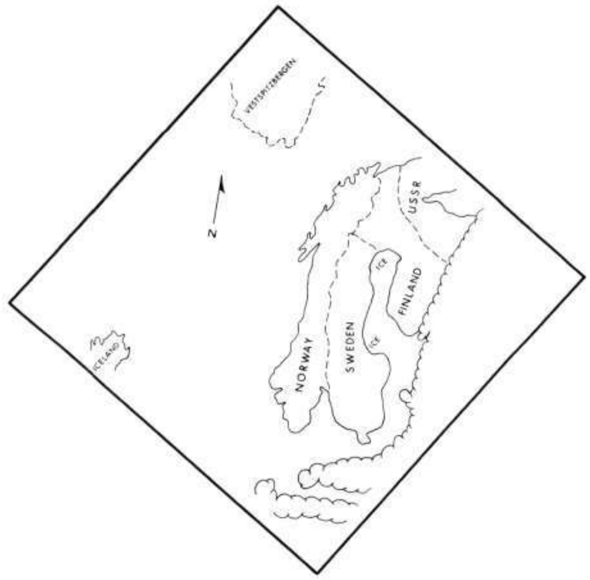

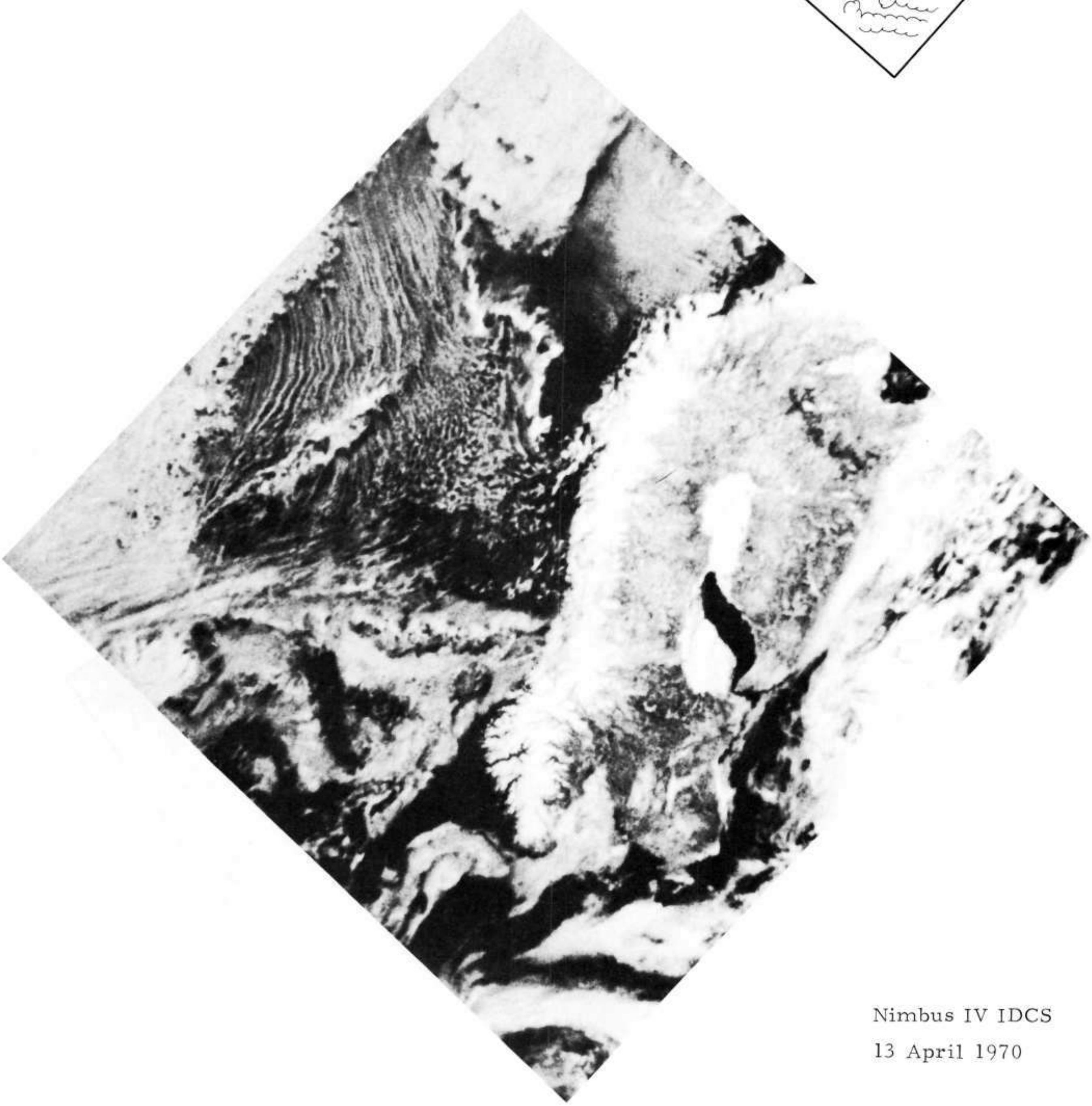

Nimbus IV IDCS
13 April 1970

Snow Melt Surveillance - Kamchatka, U.S.S.R.

These three Nimbus IV IDCS pictures taken over the period of about one month show a rapid decrease in snow cover on the peninsula of Kamchatka. Snow melt begins first in the major river valleys and later spreads to marshland areas. An overall decrease in reflectance is apparent, even in the mountainous areas.

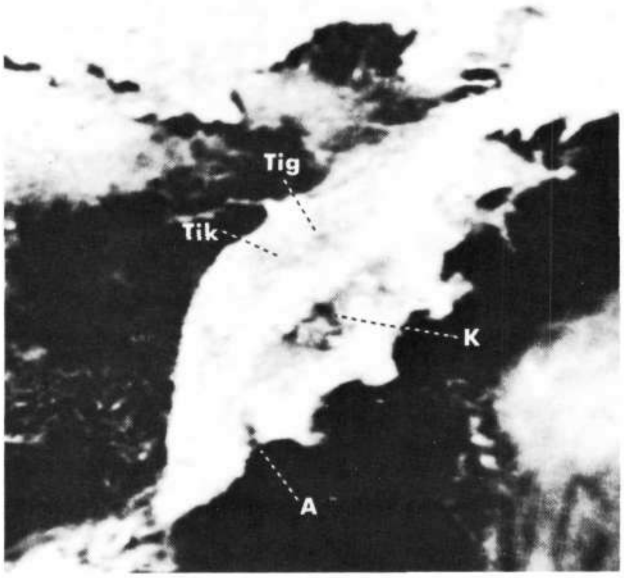

22 April 1970 - Snow melt has begun in the Kamchatka (K), Avacha (A), Tikhaya (Tik), and Tigil (Tig) river valleys.

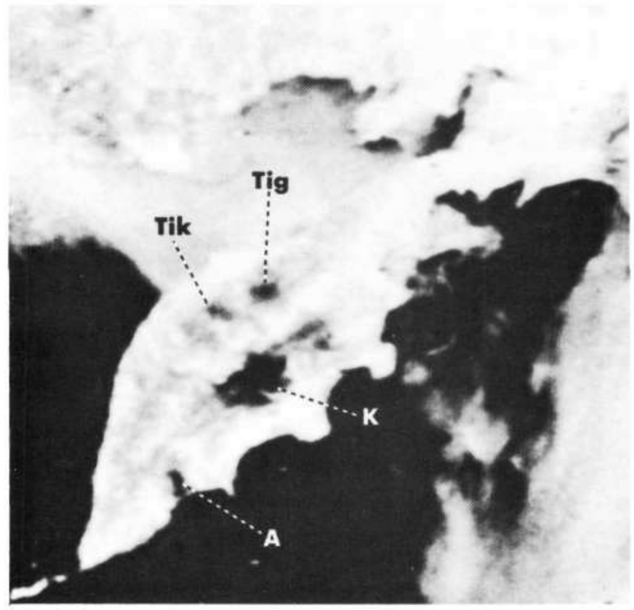

27 April 1970 - Further snow melt in these river valleys is evident. Note also, overall peninsula reflectances have decreased.

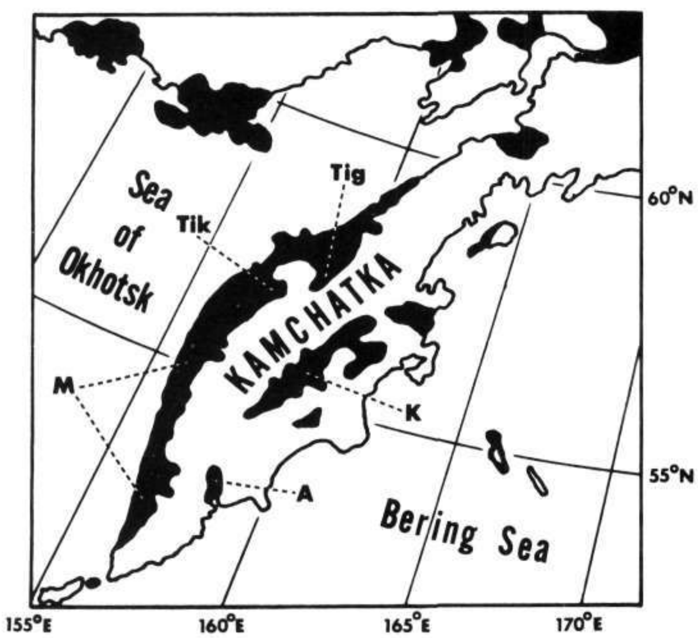

0 - 200 m ▬ river valleys, marshes
200 - 3000 m ▭ mountains

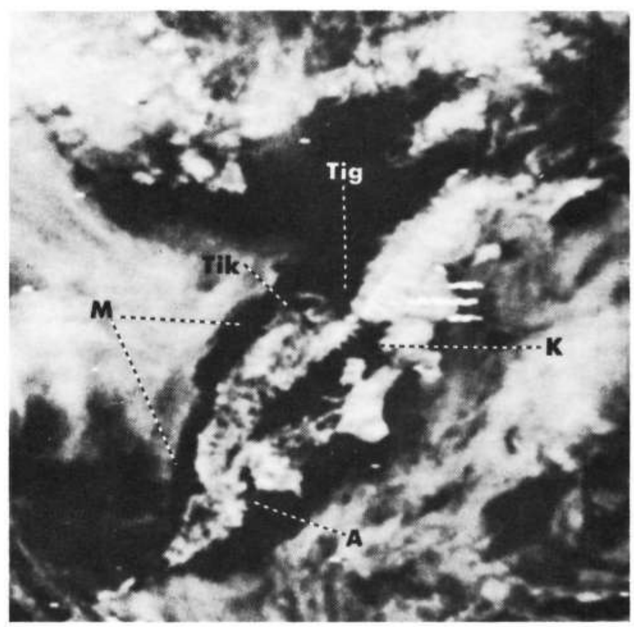

27 May 1970 - All river valleys (K, A, Tik, Tig) and marshland (M) snow cover has melted.

Nimbus IV Image Dissector Camera System (IDCS)

Baffin Bay Reconnaissance

These Nimbus IV IDCS pictures of Baffin Bay are examples of the daily data supplied to the U. S. Navy. They are used in providing sea-ice forecast support and in reducing aerial reconnaissance requirements. Ice boundaries and estimates of concentration have been found to be in close agreement with aerial reconnaissance data.

26 April 1970

25 May 1970

24 June 1970

9 July 1970

31 July 1970

9 August 1970

2 September 1970

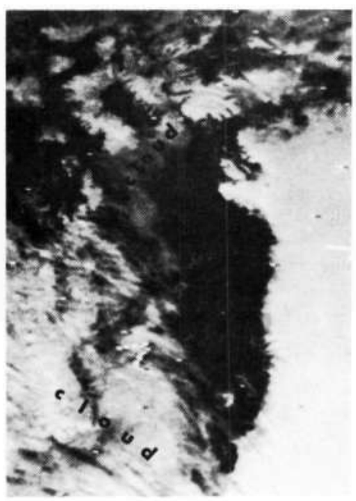

8 September 1970

9 September 1970

Foxe Basin, Northwest Territories

In this late summer photograph, Prince Charles Island, Canada, is surrounded by new ice. A comparison with the annotated photograph suggests that the islands within the basin as well as the edges of the basin are rimmed with ice. New snow, which appears considerably whiter, is also in evidence. The Barnes Icecap in the extreme upper right is stark in its whiteness. Pictures such as these can be used to maintain a daily record of the manageability of near-polar waterways.

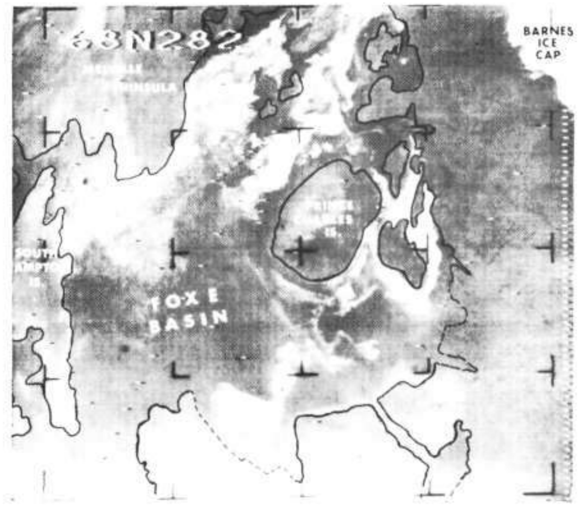

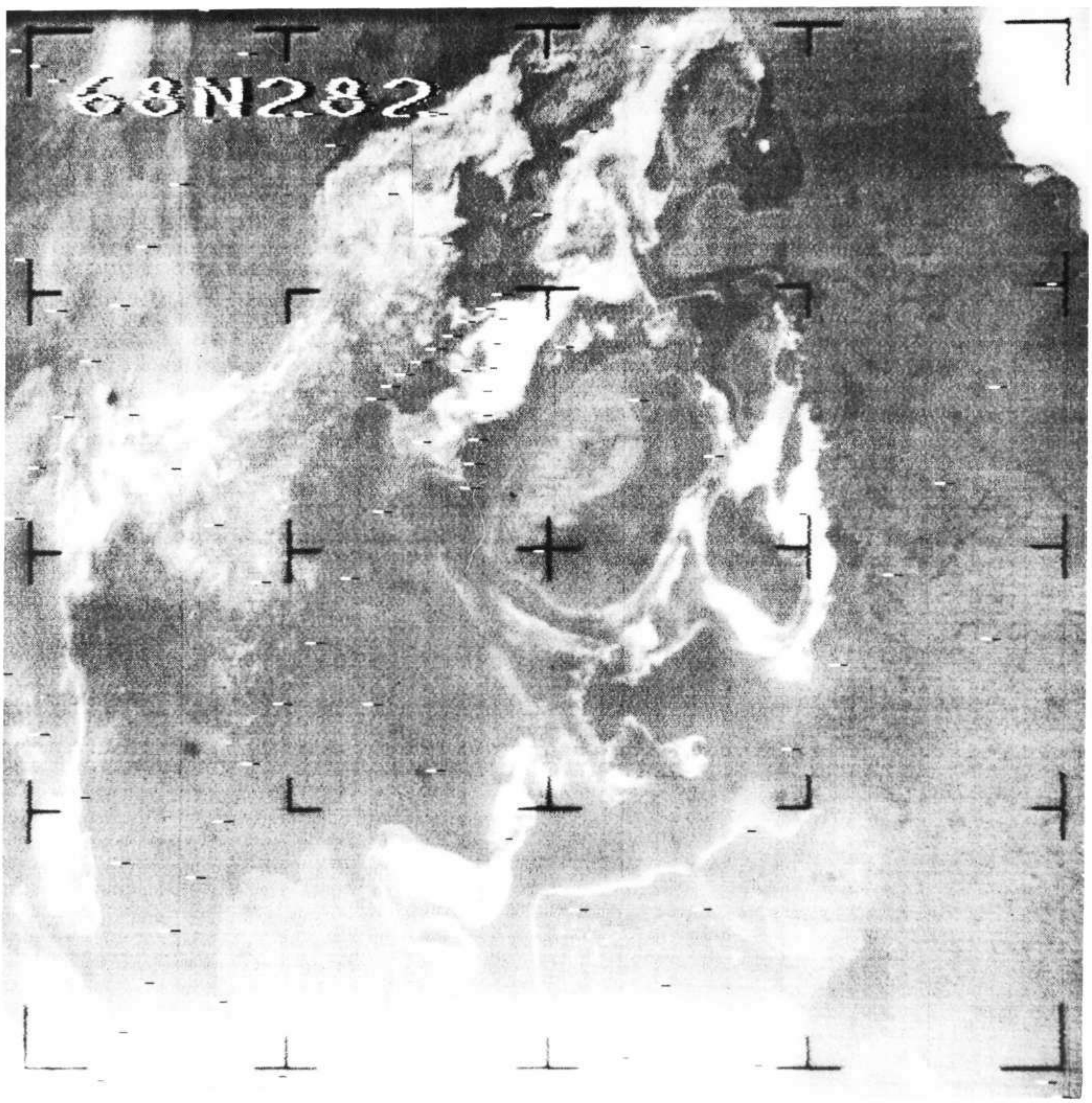

Nimbus I AVCS 31 August 1964

TAKING the OCEAN'S TEMPERATURE...

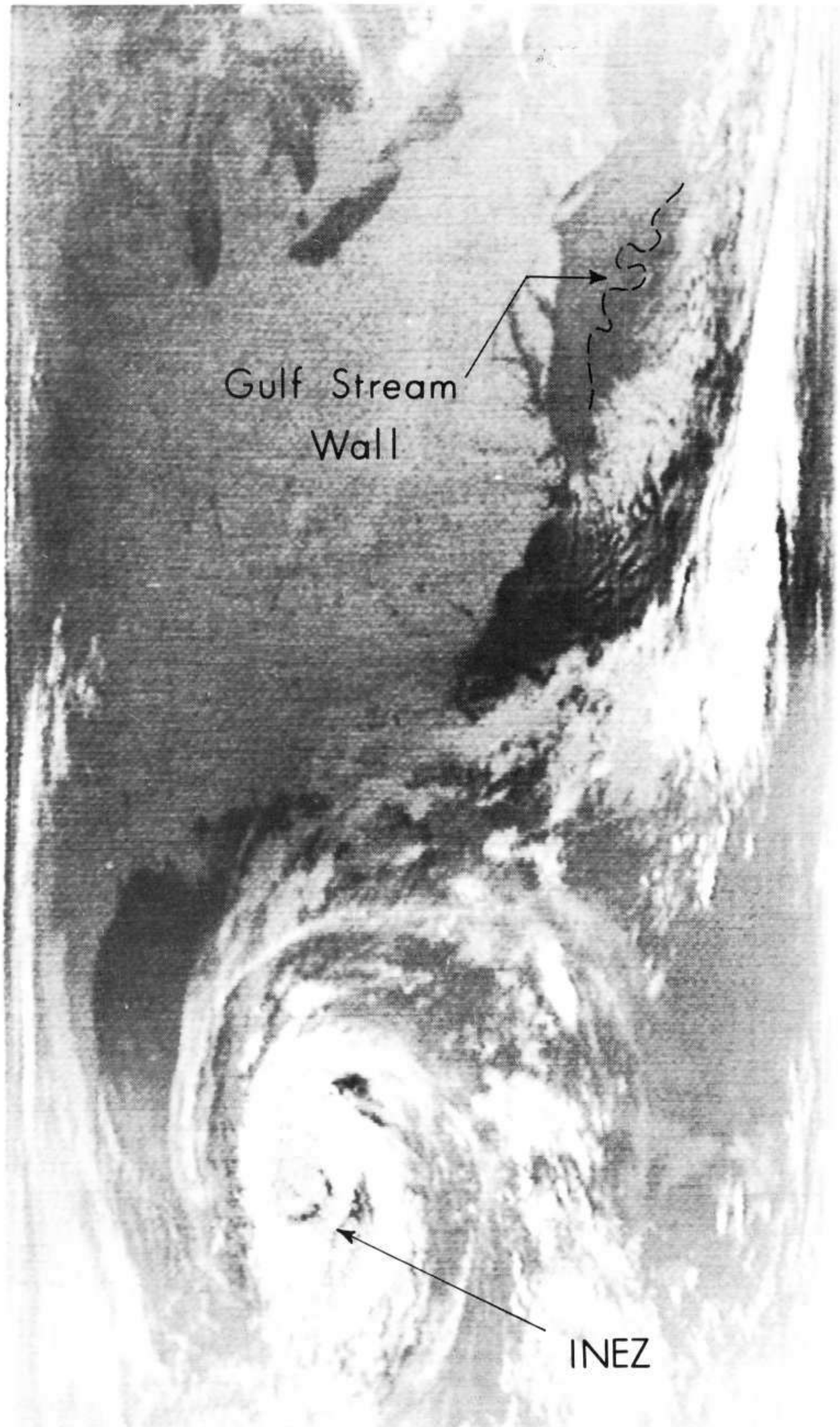

Nimbus II HRIR 7 October 1966

Hurricane Inez and the Gulf Stream

The infrared sensors on all four Nimbus satellites have been used to measure ocean surface temperatures. In this case, Hurricane Inez is shown in the Gulf of Mexico, just off the Yucatan Peninsula. The warm waters (darker tone) of the Gulf Stream can be seen off the eastern coast of the United States from Cape Hatteras to a point where they disappear in a cloud band off New England.

The Gulf Stream

This Direct Readout Infrared photograph was received by the Satellite Data Laboratory, Canadian Department of Transport, Toronto. Of significance is the fine delineation between the warm Gulf Stream and the cooler Atlantic Ocean through which it passes. Lakes Ontario and Erie fail to stand out with their normal contrast to the land because they probably are covered with a thin layer of stratus cloudiness.

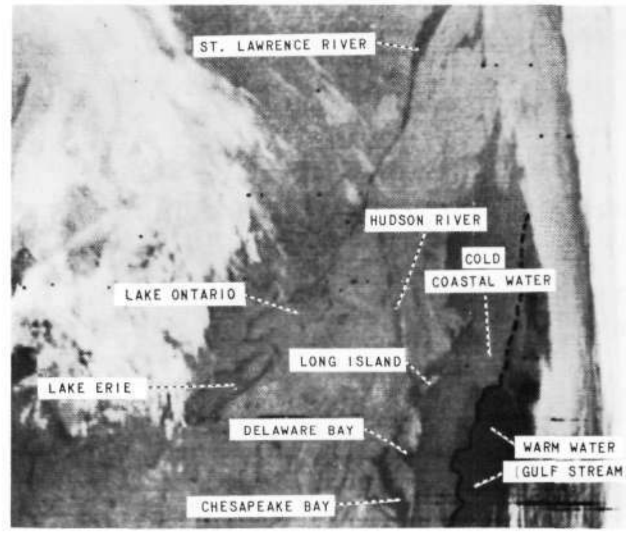

Nimbus III DRIR 24 May 1969

The Gulf Stream

The THIR imagery shown here may be compared with the two previous pictures of the Gulf Stream. Such a sequence of pictures can be used to monitor the movement of the "north wall" of the Gulf Stream and its meanders. The northern wall of the Gulf Stream is denoted by a dashed line in the annotated picture. The line separates the warm Gulf Stream waters from those of the cooler Atlantic Ocean through which the stream travels. The southern wall is less well-defined and is partially obscured by thin clouds. The Nimbus IV THIR was the first sensor capable of making daytime temperature measurements at this resolution.

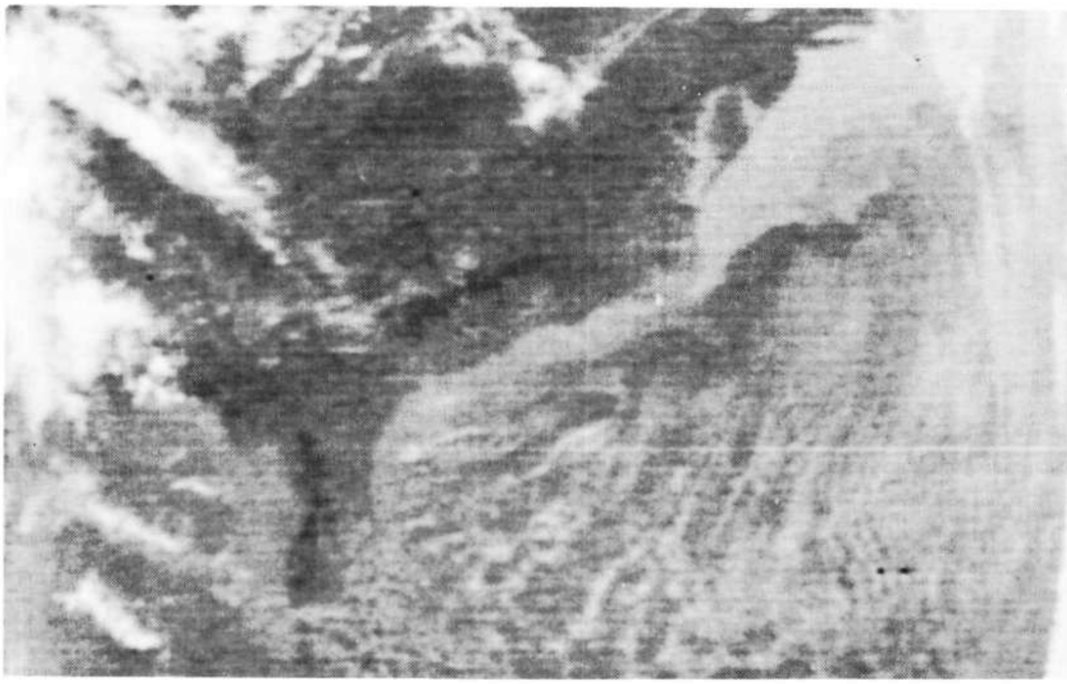

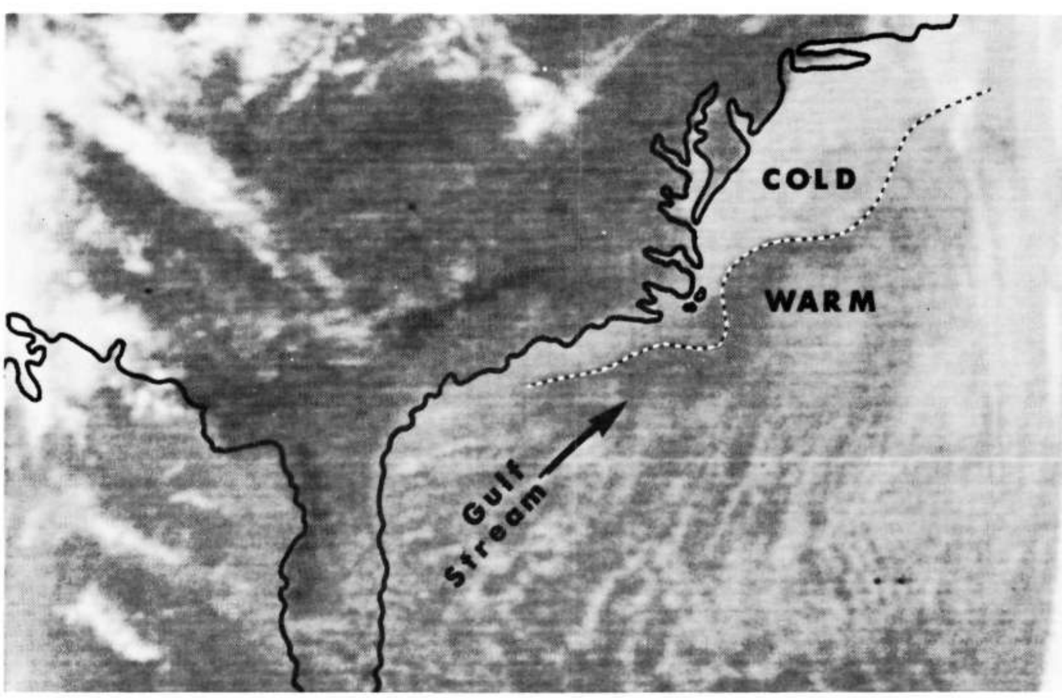

Nimbus IV THIR (D) 8 April 1970

Lake Michigan

The surface temperatures of smaller bodies of water can also be monitored. This is a digitized HRIR temperature map of Lake Michigan. Isotherms have been drawn for 2°K temperature intervals. This type of data display is superior to the photographic display for detailed numerical analysis. Even the relatively small Lake Winnebago, southwest of Green Bay, shows as an area warmer than its surroundings. (Scan lines are parallel to the dashed line running across the lake.)

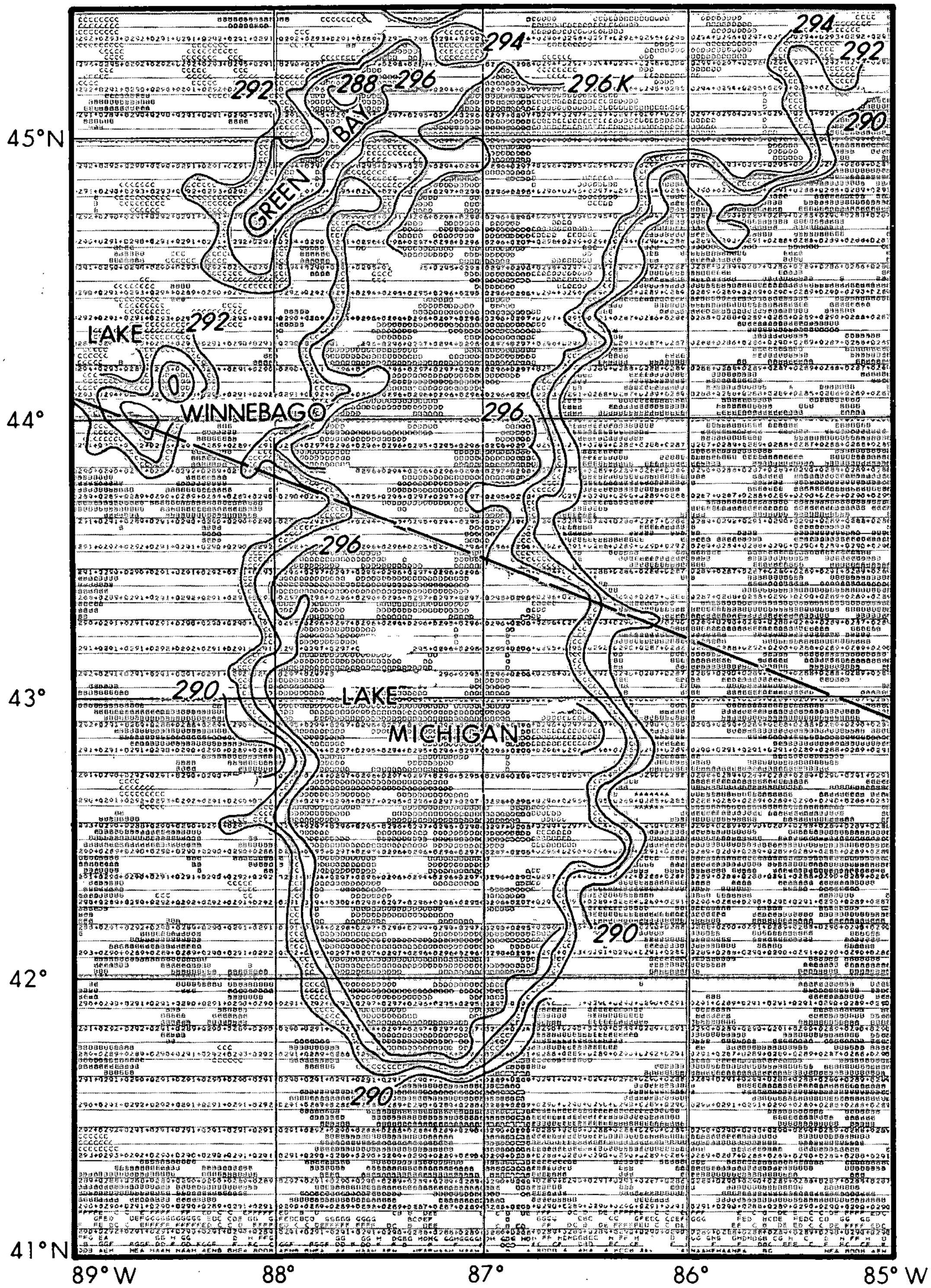

Nimbus II HRIR 6 October 1966

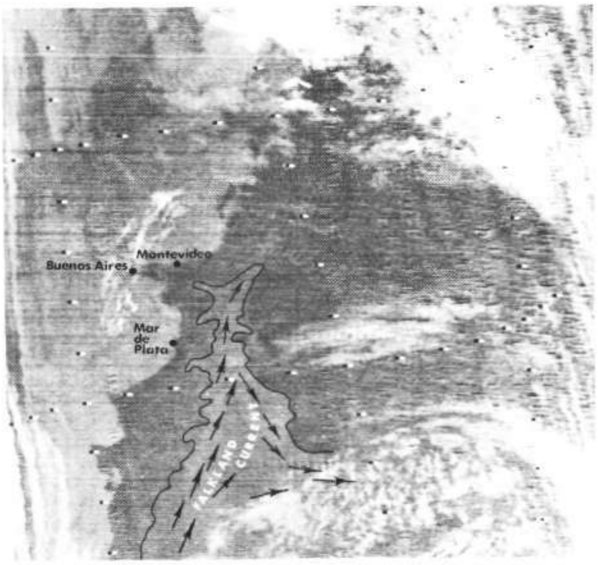

Falkland Current

This picture of the Falkland Current was received during the first week of Nimbus III operation and beautifully illustrates the utility of the nighttime HRIR data. The accompanying map defines the area and the average current directions.

Nimbus III HRIR (N) 22 April 1969

Central France

As has been noted, the Nimbus Project is generally thought of as a meteorological research and development program. Although far removed from the field of meteorology, the sciences of Geology and Agriculture have also benefitted from the Nimbus satellite series. Indications of rock type, fault zones, and the abundance of vegetation have all been observed in the Nimbus data. In this picture, the tonal variations due to chalk and limestone formations of the Paris Basin are clearly visible. The dark lines through the light areas are rivers of central France (see map). Paris, though not visible, lies to the north of the thin white line of clouds at the left.

Geological map notations are:

1) Upper Cretaceous Chalk Formations
2) Lower Cretaceous Sands and Clays
3) Barrios and Langros Plateaus

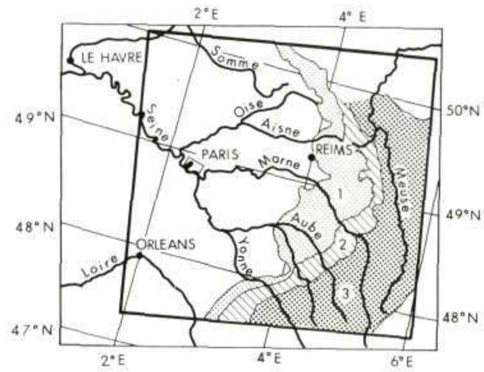

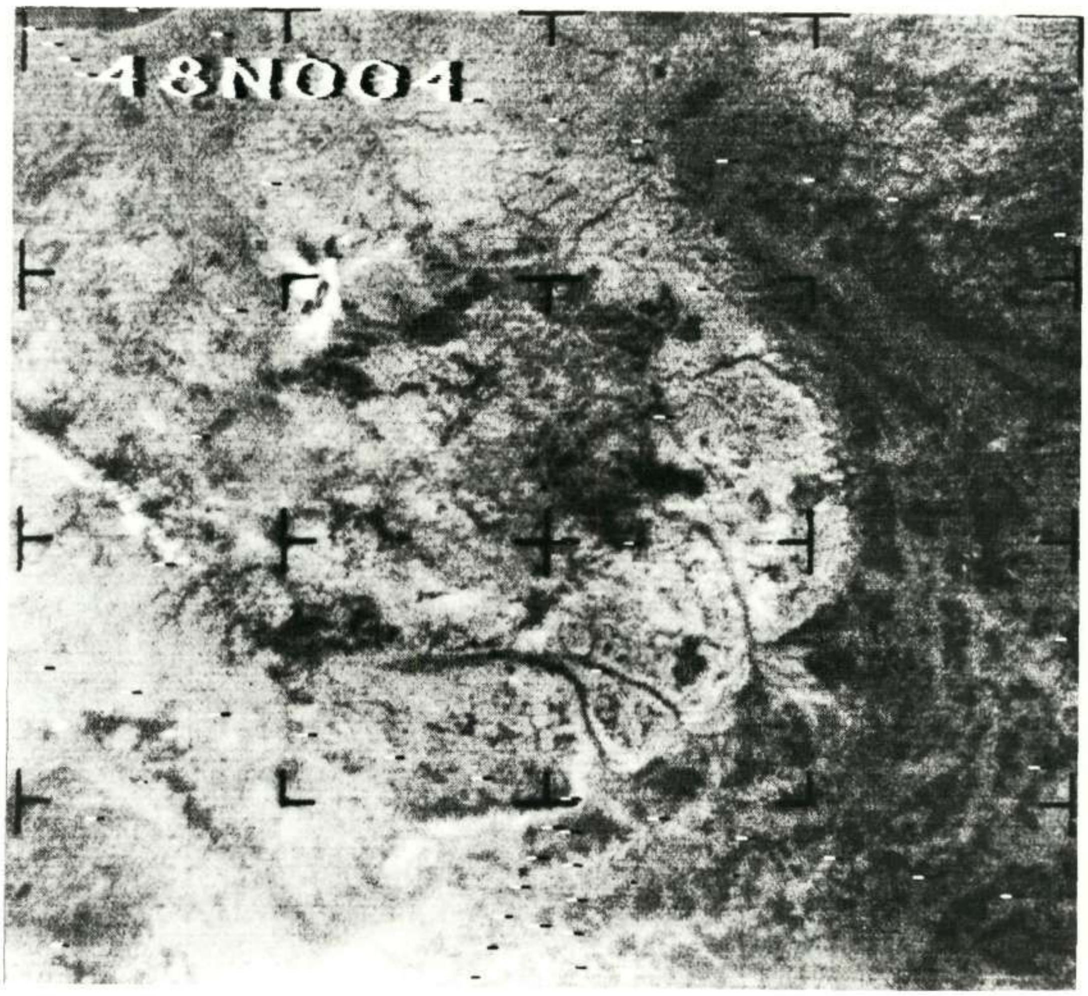

Nimbus 1 AVCS 13 September 1964

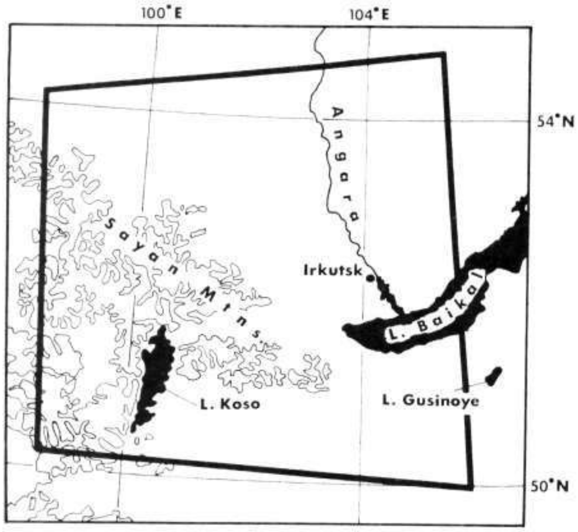

South-central USSR

The snow pattern in this Nimbus I AVCS picture reveals a NW-SE fault zone in the Sayan Mountains of Mongolia-Southern USSR. This information was used by the U. S. Geological Survey to revise a geologic map of the area. Lake Koso, Mongolia, is visible at lower center.

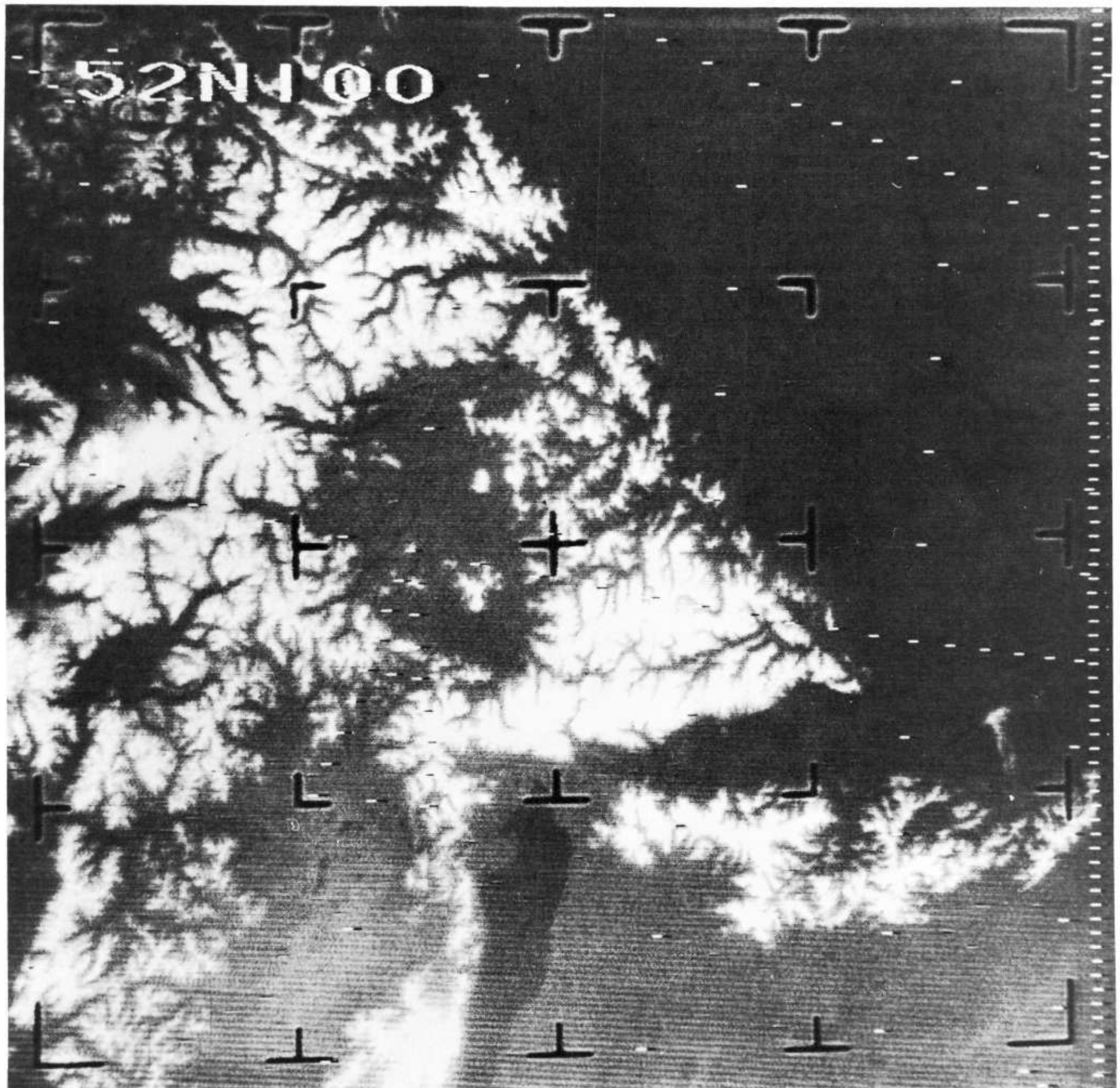

Nimbus I AVCS 19 September 1964

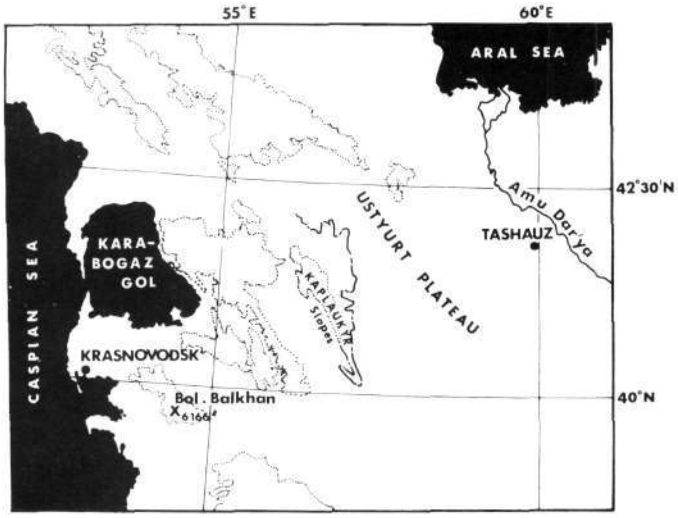

Southwestern USSR

The eastern portions of the Caspian Sea and its adjacent bay of Kara Bogaz appear in this picture. The rapidly growing salt flats of the bay are distinguished in the northeast of this salt water body. Inland toward the Aral Sea (upper right) are the highlands of the Ustyurt Plateau. Especially noteworthy is the hook-like appearance of the Kaplaukyr slopes and the salt flats to their right.

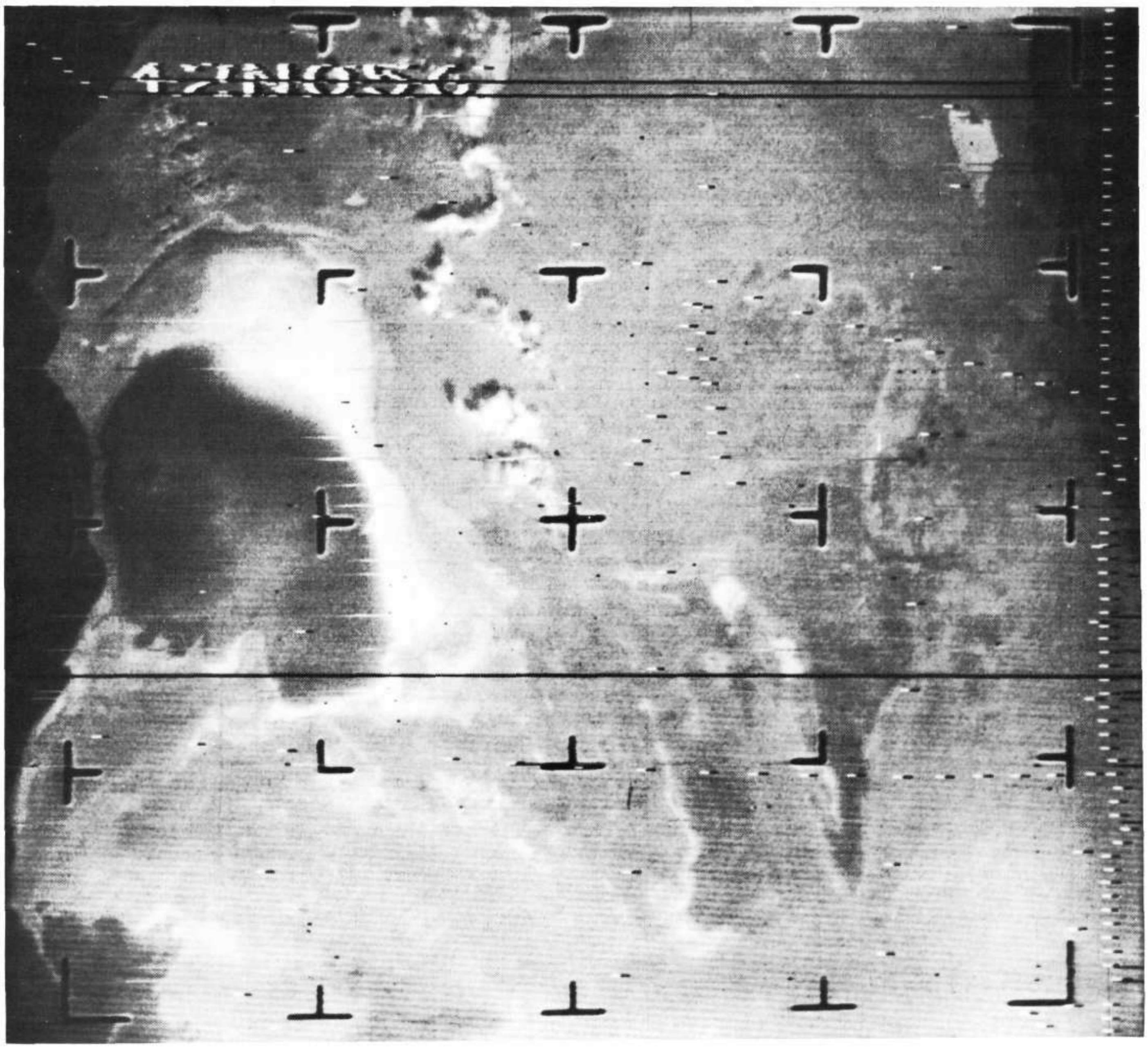

Nimbus I AVCS 19 September 1964

Strait of Gibralter

The Strait of Gibraltar, which separates Spain and Morocco, is a little less than eight miles wide at its narrowest point. The tiny hook-shaped peninsula, upon which lies the fortress of Gibraltar, is clearly evident just northeast of the center fiducial. This photograph reveals the continuation of the El Riff mountain range of Africa into the Sierra range of Spain, illustrating their common geological origin.

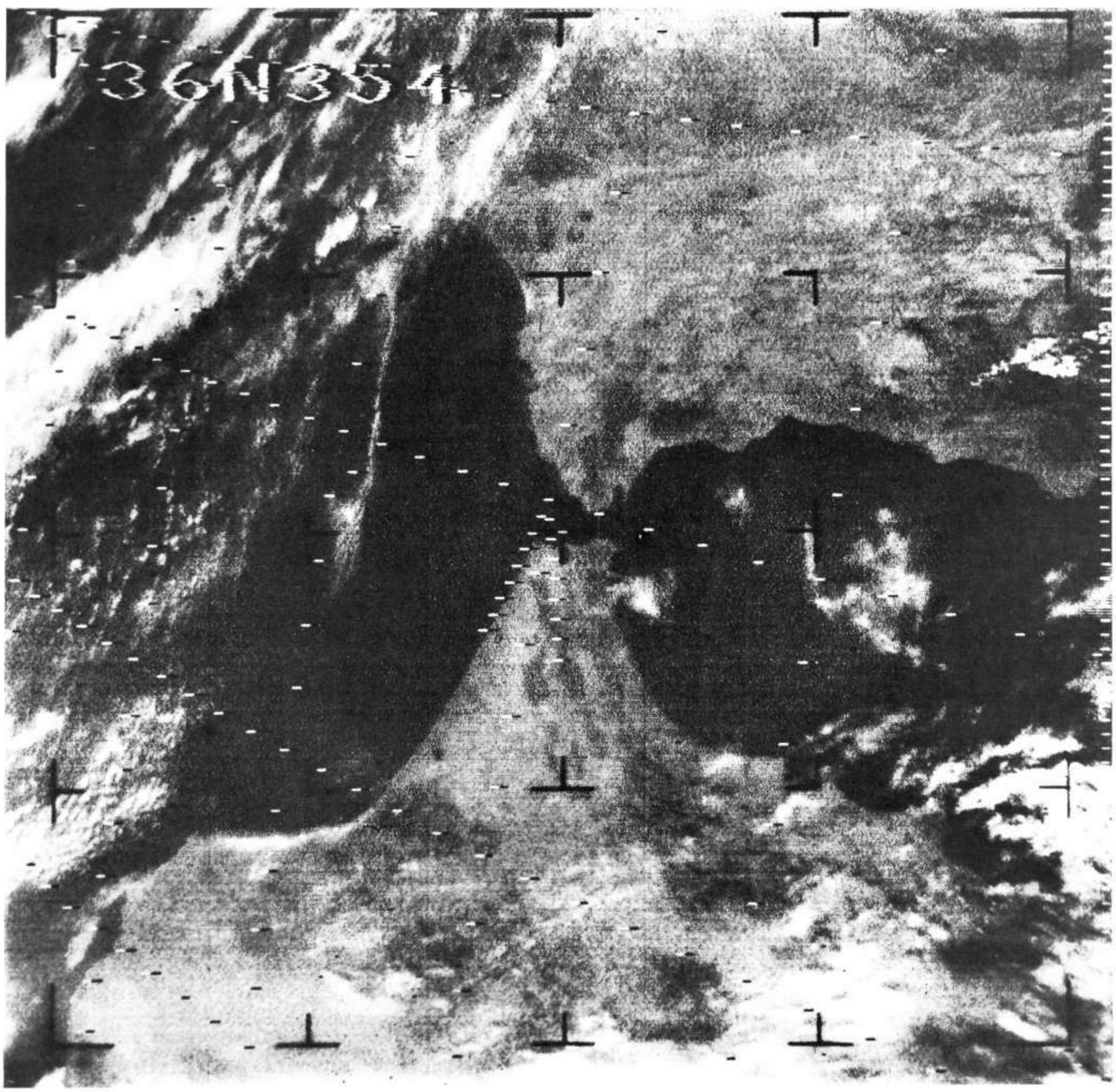

Nimbus I AVCS 3 September 1964

Asia Minor

The sand seas of the central Arabian Peninsula appear in this picture as light-colored, tenuous streaks. Fertile areas along the coast, such as the portion of Muscat at the southeastern tip of Arabia bordering the Gulf of Oman, are darker.

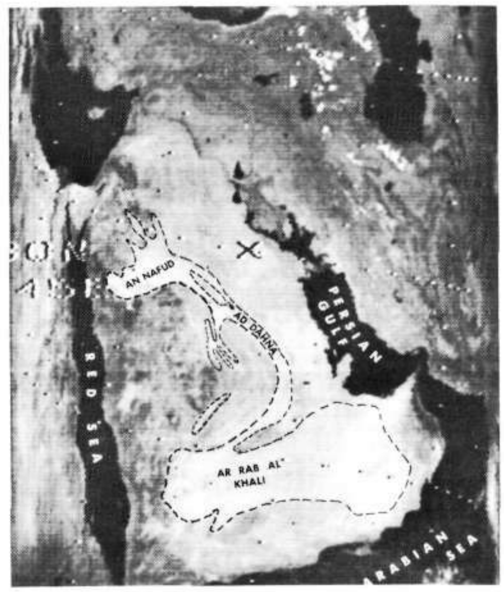

Nimbus III HRIR (D) 6 June 1969

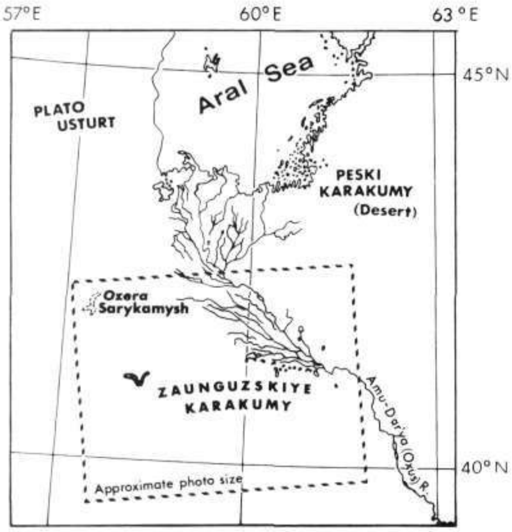

The Amu-Dar'ya River

The dark, heavily vegetated Amu-Dar'ya (Oxus) River valley of the southern USSR can be seen at the upper right portion of this picture. This region just south of the Aral Sea is much darker than the surrounding lands which are characteristically covered by desert shrubs. Of note at center-left is a light-colored "V" shaped depression which is probably a dried lake or river bed. At upper left is Ozero (Lake) Sarykamysh, also below sea level.

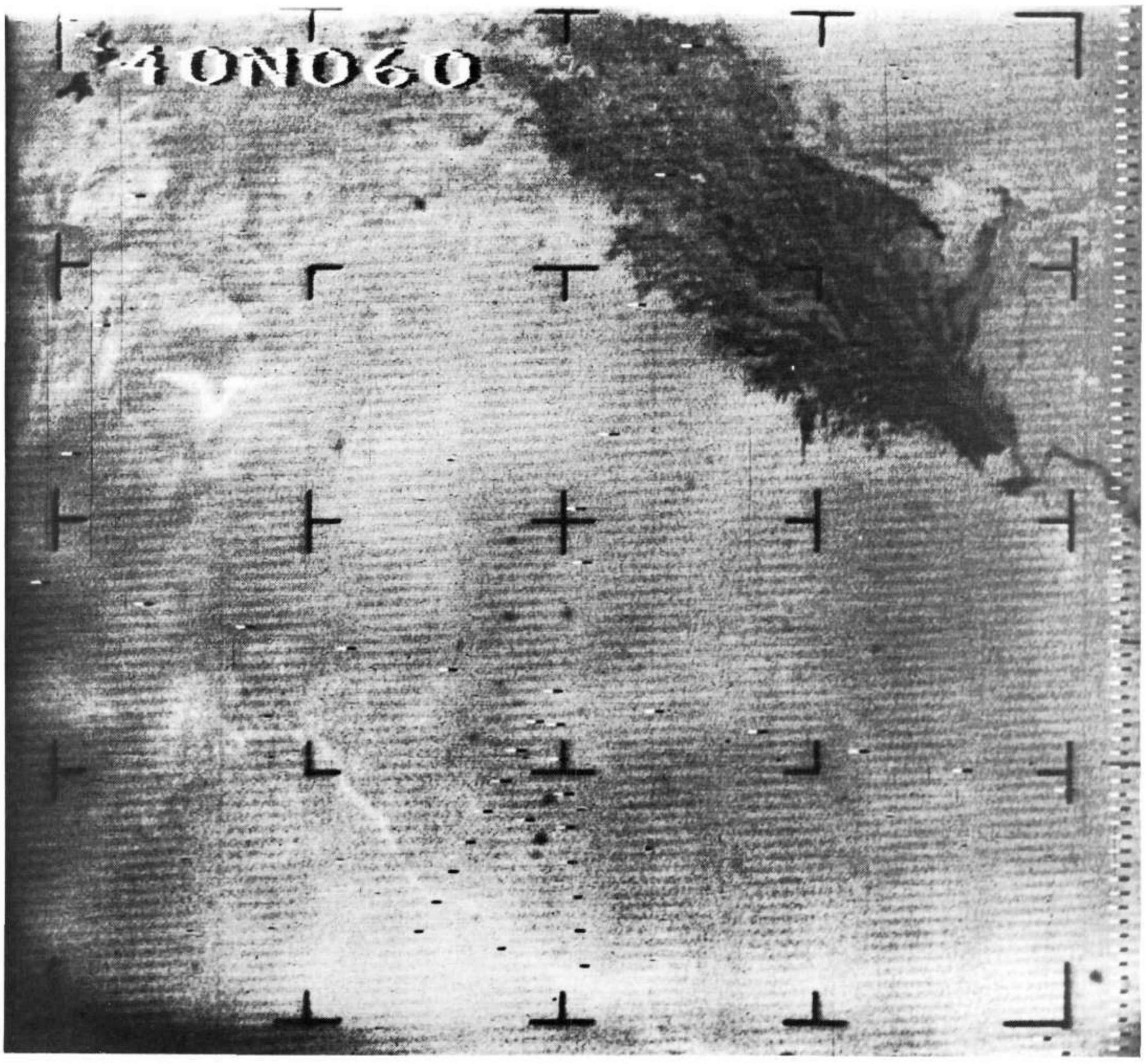

Nimbus I AVCS 18 September 1964

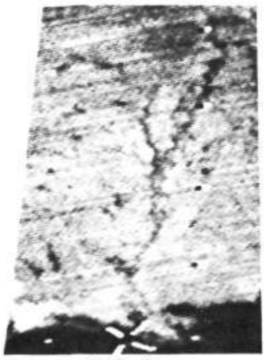

25 April
Seven days since any rainfall

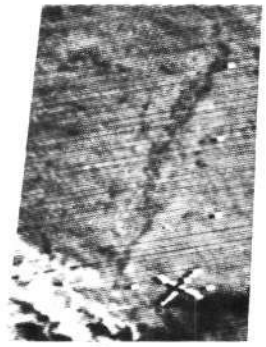

30 April
Rainfall of 0.3 to 1.5 inches on 27th. and 28th.

22 May
Rainfall of 0.5 to 2 inches on 18 May

6 June
Rainfall 0.2 to 1.2 inches in La. and Miss. on 2 June. Light and scattered rainfall elsewhere since 22 May

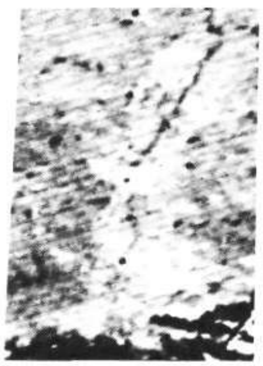

13 July
July 11th. and 12th. rainfall in La. and Miss. Light and scattered rainfall since 2 July elsewhere.

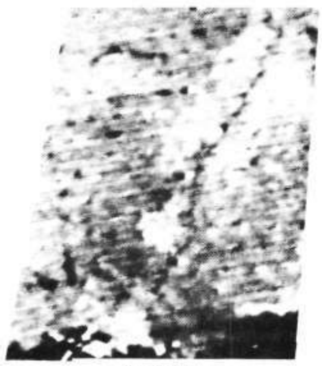

15 July
July 11th. thru 14th. rainfall in La. and Miss. No change elsewhere.

9 August
Almost no rainfall since 28 July. 13 days!

12 September
Generally heavy rainfall from 1 thru 8 September. No rainfall from 9 thru 12 September.

Nimbus III HRIR (D)
April - September 1969

Nimbus III Records Terrestrial Changes

This sequence of 1969 Nimbus III daytime HRIR pictures shows the changing patterns of the 0.7 to 1.3 μm band reflected solar radiation in the lower Mississippi Valley. These reflectance patterns are mainly due to combinations of soil and vegetation conditions. Changes in the elongated bright area along the Mississippi River appear to be due to surface soil moisture changes in the heavily cultivated generally gray alluvial soil. An increase in reflectivity indicated by an increase in brightness is thought to be caused by a decrease in soil moisture during an abnormally dry 1969 summer season.

The Effects of Seasonal Dryness

This time-series demonstrates the effects of the summer precipitation minimum on the rivers of Iraq. In the 30 May imagery, the Euphrates River valley is still dark and wide with vegetation and soil moisture resulting from winter precipitation. As the summer progresses and the precipitation decreases, the river areas assume the appearance of the surrounding steppes and deserts. By 6 August, in the series, the Euphrates in Iraq has become almost indistinct. The graphs show precipitation amounts for Basra and Baghdad, along the river in Iraq, and for Urfa and Mazkirt in the highlands of Turkey near the river's source.

30 May 69

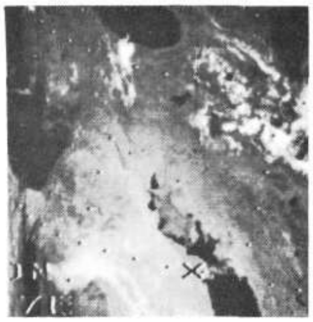

16 Jun 69

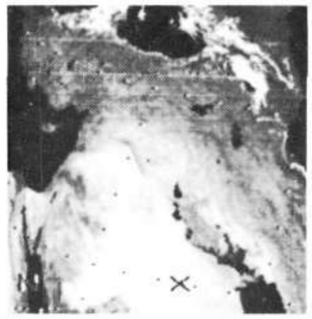

3 Jul 69

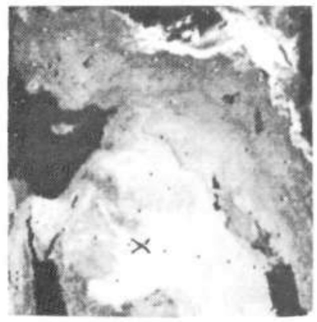

6 Aug 69

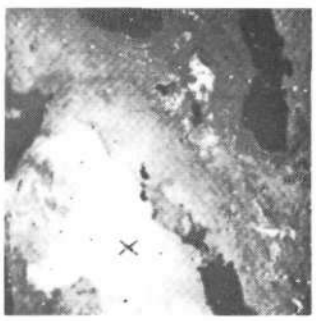

26 Aug 69

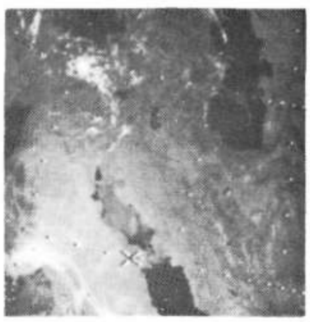

15 Sep 69

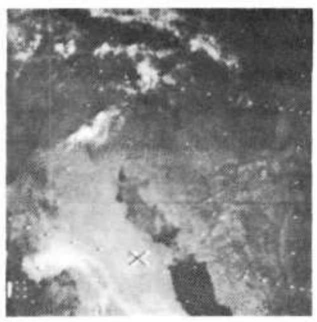

12 Oct 69

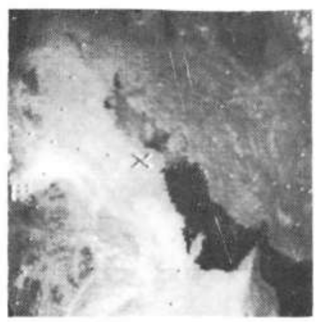

13 Nov 69

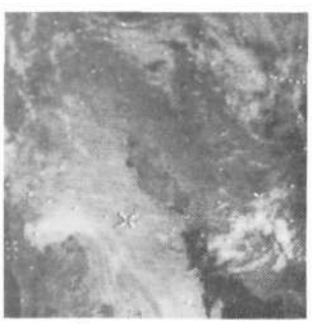

15 Dec 69

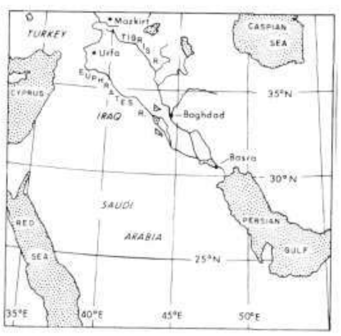

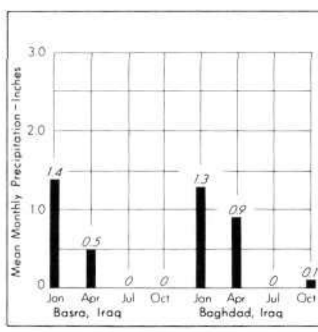

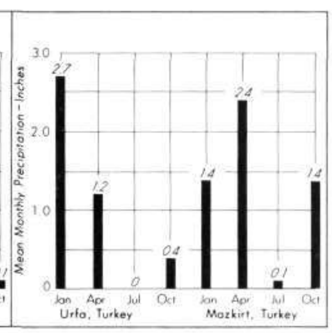

Nimbus III HRIR (D) May - December 1969

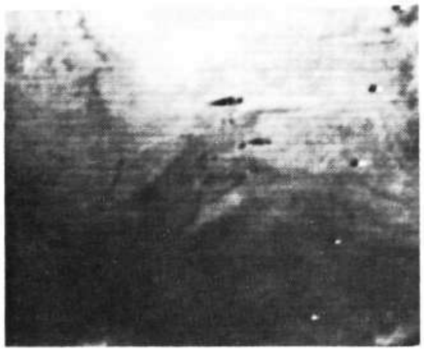

16 June 1969

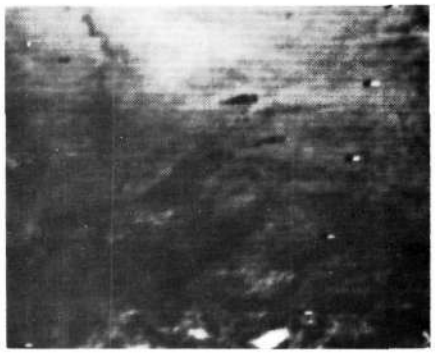

13 July 1969

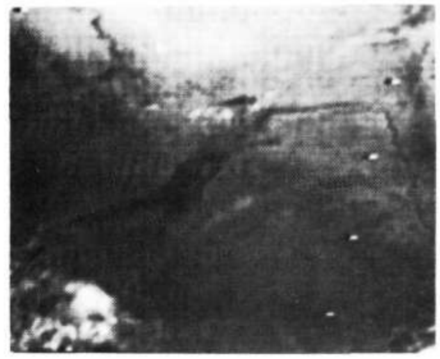

15 September 1969

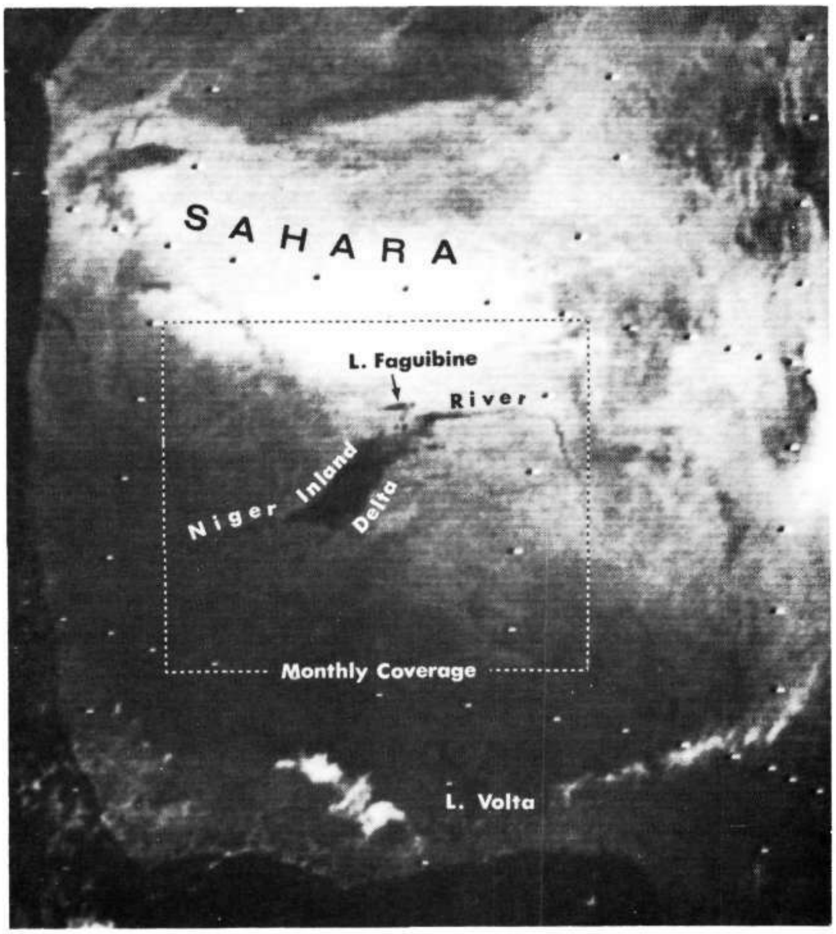

18 November 1969

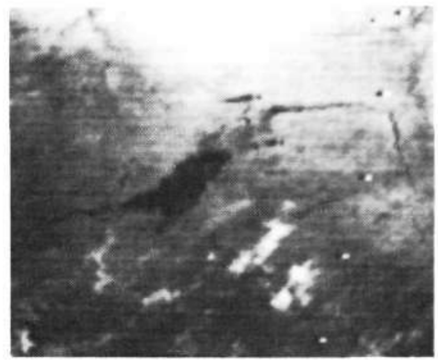

12 October 1969

25 December 1969

31 January 1970

Nimbus III HRIR

Hydrologic Changes

Seasonal soil moisture changes and flooding are believed to account for most of the reflectance variations of the Niger River inland "delta" in these Nimbus III near-infrared (0.7 to 1.3 μm) High Resolution Infrared Radiometer (HRIR) pictures. Rainfall increases each month from May through August and then decreases to almost none by November. Delta reflectances appear to decrease from July through November. Concurrent with a lack of rainfall from November through January is a dramatic increase in the delta reflectance.

Fort Peck Reservoir

The enlarged portion of this Nimbus I Advanced Vidicon Camera System (AVCS) image of the Fort Peck Reservoir in Montana, U.S.A., was recorded on 17 September 1964. Image resolution in this picture is about 1200 feet. Reservoir surface area is within six percent of the area measured on a U. S. Geological Survey Map.

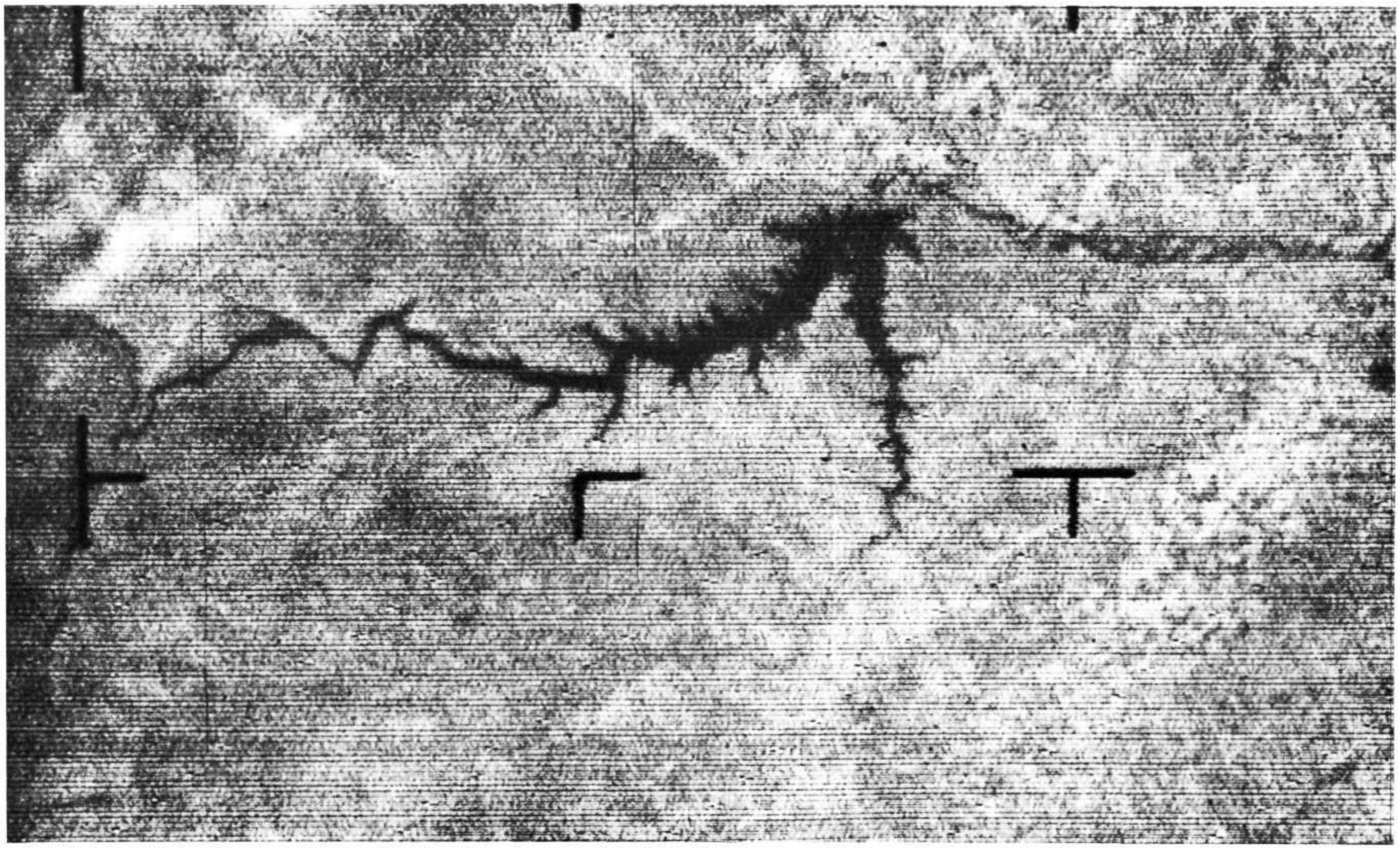

Nimbus I AVCS 17 September 1964

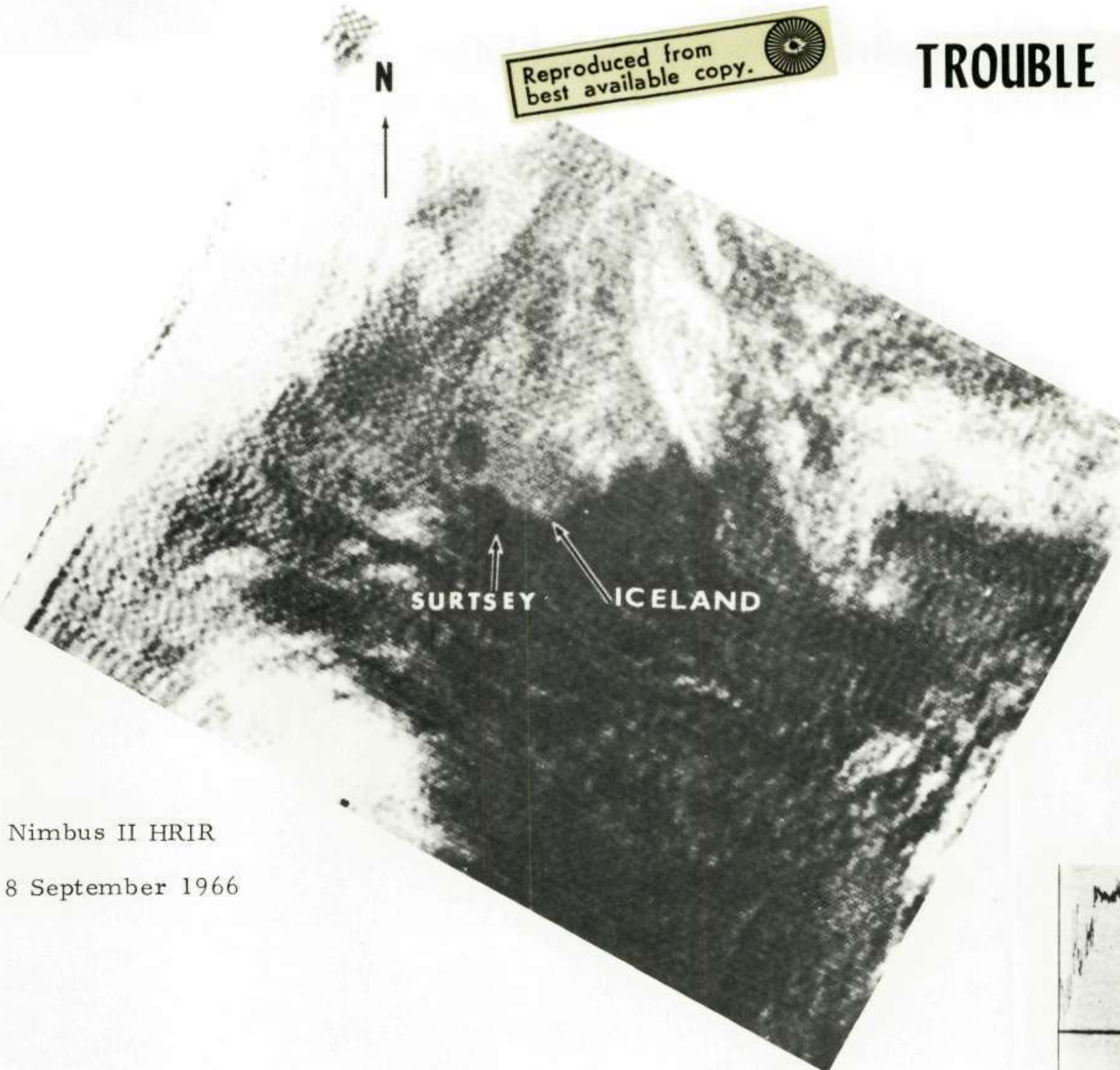

Nimbus II HRIR

8 September 1966

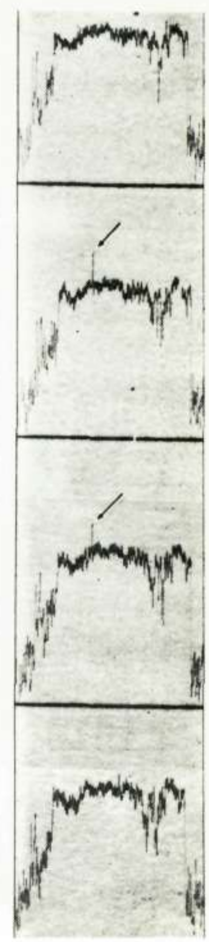

Surtsey Island

Surtsey, a volcanic island 20 miles southwest of Iceland, made its first violent appearance above the surface of the sea on 14 November 1963. The HRIR imagery shows the island as a very dark (hot) spot in relief against the cooler sea. At the time it was but two square kilometers in area but its heat made it readily discernible. It also appears in the diagram as a sharp spike in the middle two scans of the visicorder temperature trace.

Southern California Brush Fire Smoke Plumes

This central portion of a Nimbus IV satellite IDCS picture taken on 27 September 1970 recorded smoke plumes from five of the major brush fires in Southern California. Plume locations are:

1) San Diego - 140,000 acres burning (1 plume)

2) Los Angeles - 105,000 acres burned (3 plumes)

3) Sequoia National Forest - 5,000 acres burning (1 plume)

(For reference - the Great Salt Lake in upper right and Salton Sea just above "1")

Nimbus IV IDCS 27 September 1970

Ash Plume from Beerenberg Volcano

This new eruption of the Beerenberg Volcano on Jan Mayen Island was first observed on the night of 20 September 1970. By noon on 21 September, when this Nimbus IV IDCS picture was taken, the ash plume (within the rectangular area) extended more than 200 miles to the southeast.

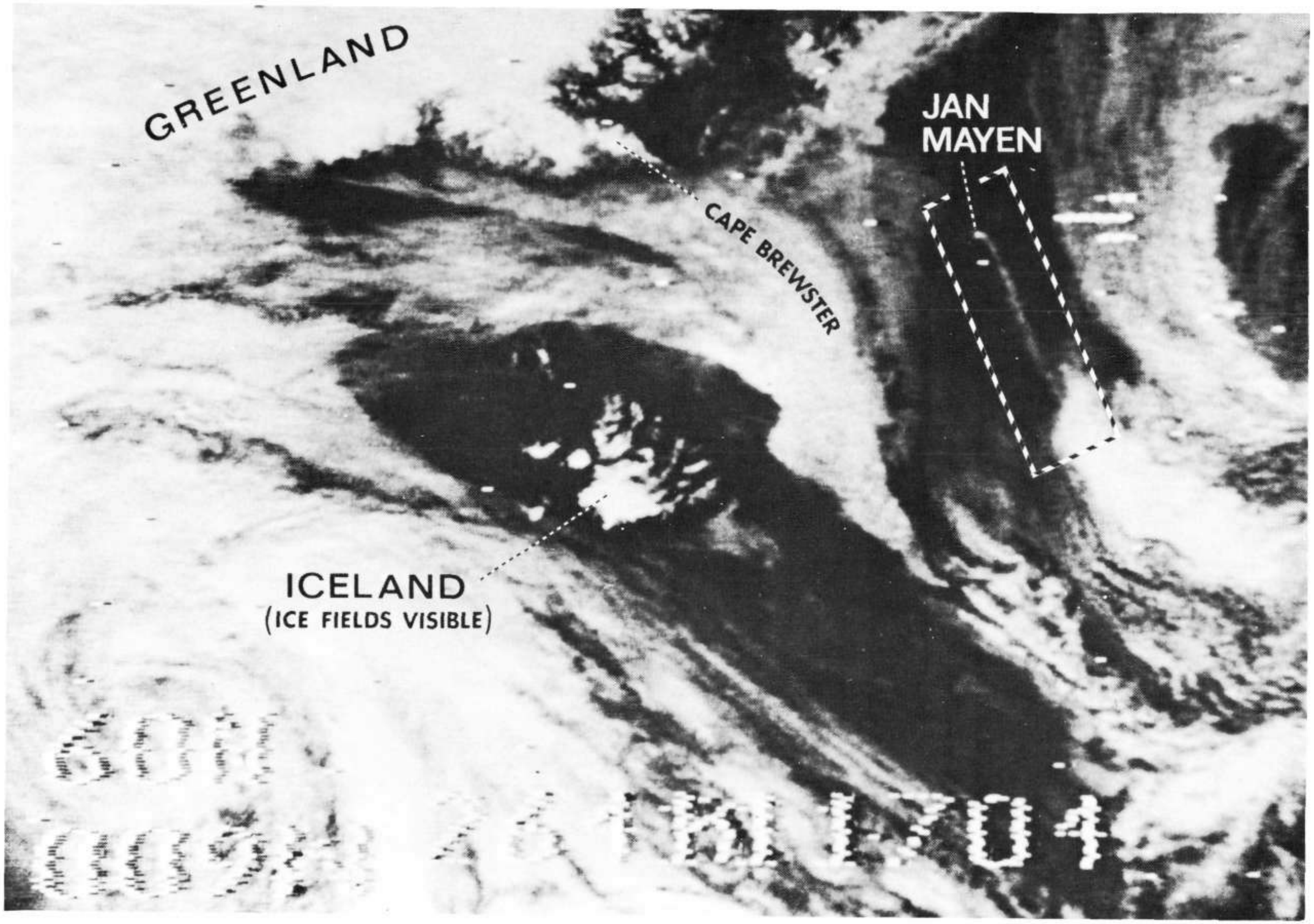

Nimbus IV IDCS 21 September 1970

NEW WAYS of SEEING...

China, Korea and Japan

A new visible/near-infrared channel (0.7 to 1.3 μm) was added to the HRIR experiment on Nimbus III. This channel, operative in the daytime, recorded the reflected solar energy from the earth-atmosphere, with a side-to-side cross-track scan as the satellite moved forward. These two simultaneous pictures are centered over the Sea of Japan and graphically illustrate the differences between the IDCS camera system and daytime HRIR scanning system. Notable among the differences is the greater contrast between land and water in the HRIR imagery. This results from a combination of factors: (1) The HRIR system operates within a spectral band where there are more pronounced differences between land and water reflectivities; (2) the longer HRIR wavelength is conducive to more thorough penetration of underlying haze.

Sunglint appears in the IDCS photograph near the lower center just north of Japan. Because of the differences in viewing geometry between the two systems, sunglint is not apparent in this instance in the HRIR.

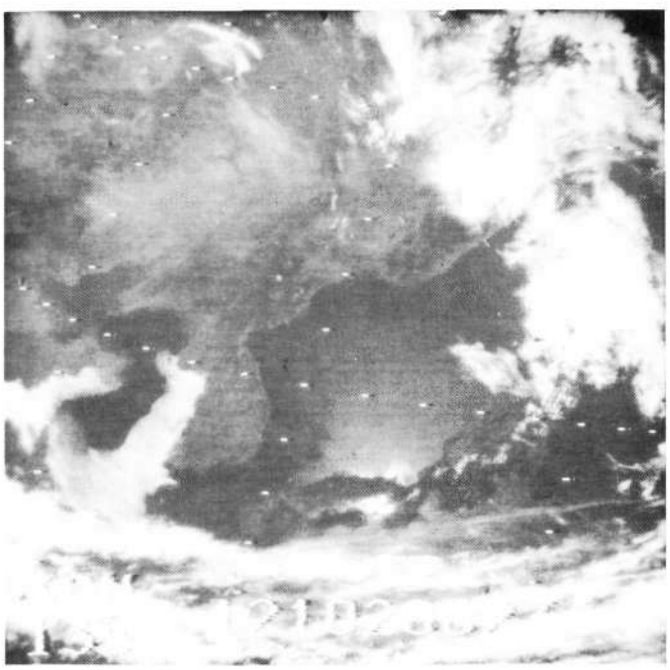

IDCS

HRIR (D)

Nimbus III IDCS/HRIR (D) 1 May 1969

Montage

This montage was assembled only two days after the launch of Nimbus III and provided a good look at the then new daytime HRIR coverage. The HRIR system was operated during daylight on the two previous Nimbus satellites but Nimbus III carried the first scanning sensor specifically designed for daytime use.

Nimbus III HRIR (D) 16 April 1969

2

Hurricane Bernice

Four views of Bernice are shown, just off Mexico's west coast. Interesting comparisons can be made between the two data acquisition systems in these near-simultaneous pictures. The greater distortion along the edges of the HRIR daytime photographs can be attributed to the much larger area covered (approximately 3800 n.mi. across as compared to 1500 n.mi. for the IDCS). Equally apparent is the difference in contrasts over land areas. The IDCS was designed to emphasize the visible portion of the spectrum while the daytime HRIR operates in the near infrared portion.

Apparent on the photograph are the Imperial Valley and the Salton Sea of southern California (see annotated photograph). Also in evidence is the dark, volcanic Cerro del Pinacate, a 4560 ft. peak.

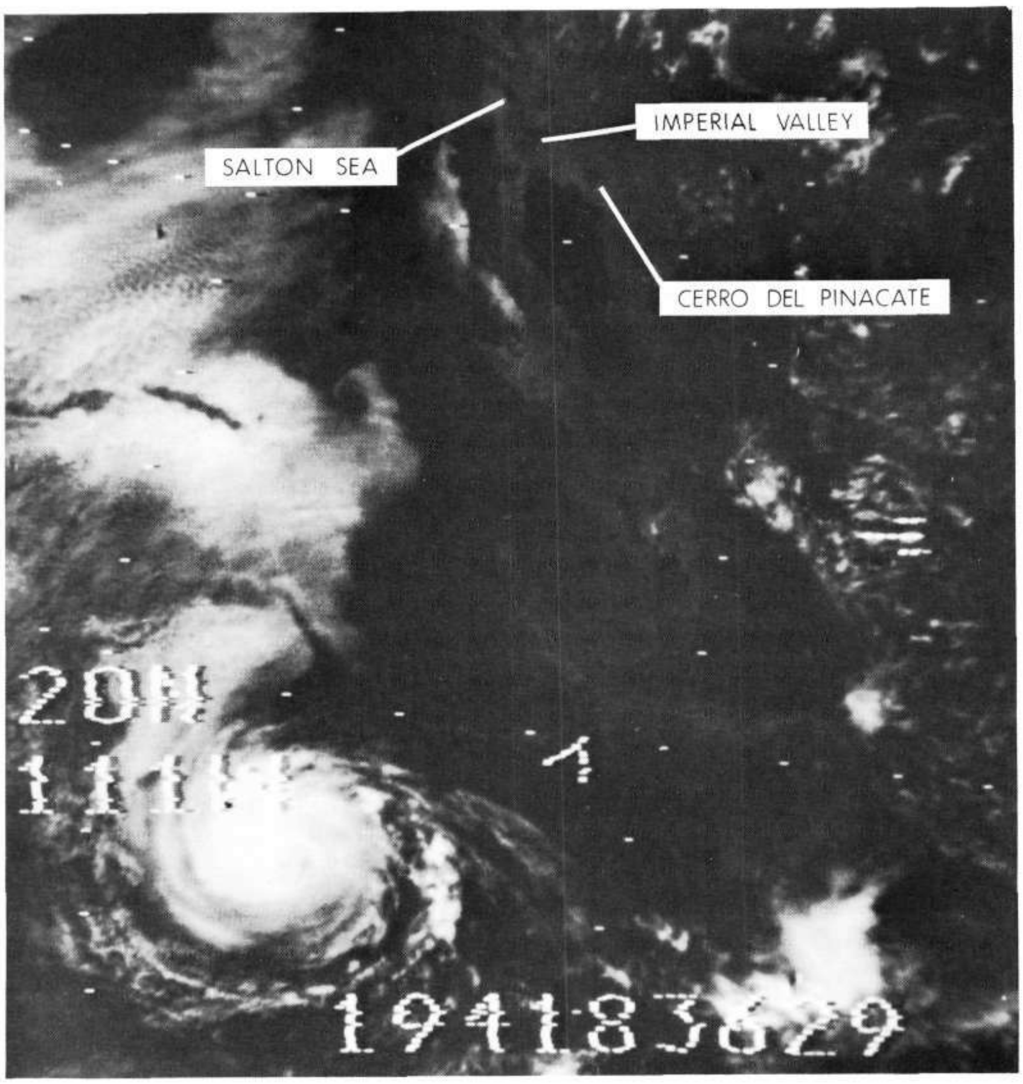

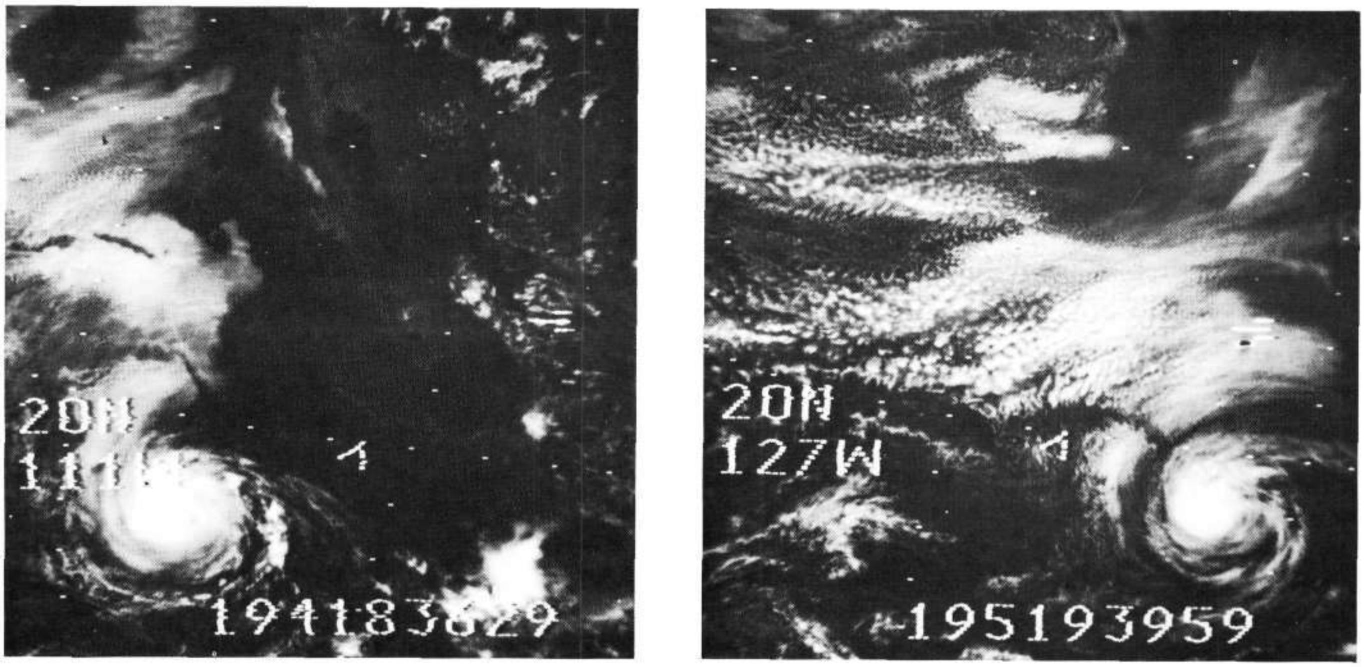

Nimbus III IDCS

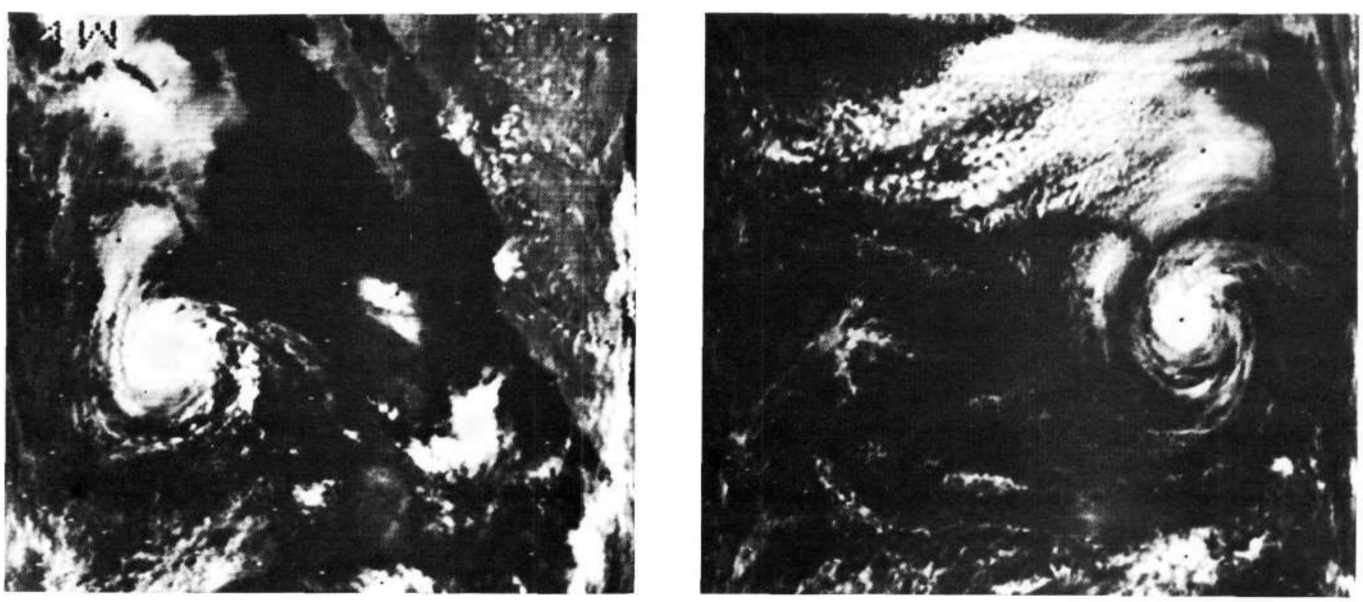

Nimbus III HRIR

13 July 1969

14 July 1969

Southeast Asia

The land masses of Southeast Asia appear in this daytime HRIR image with startling clarity against the darker, less reflective oceans. Typhoon Susan is visible near the right horizon over the Philippines and part of a large cyclonic storm is shown at the top over mainland China. The bright spot at $6^{O}N$, near the center, is sunglint, the specular reflection of the sun from the ocean surface.

Nimbus III HRIR (D) 23 April 1969

Montage of North America

This montage, constructed of two successive orbits, demonstrates the wealth of detail to be found on cloud-free imagery. Selected areas from such photographs may be enlarged many times to be used for studies of changes occurring on the earth's surface. Time-series enlargements are useful in determining changes in vegetal boundaries and coverage, snow coverage and extent of recent precipitation, among other applications.

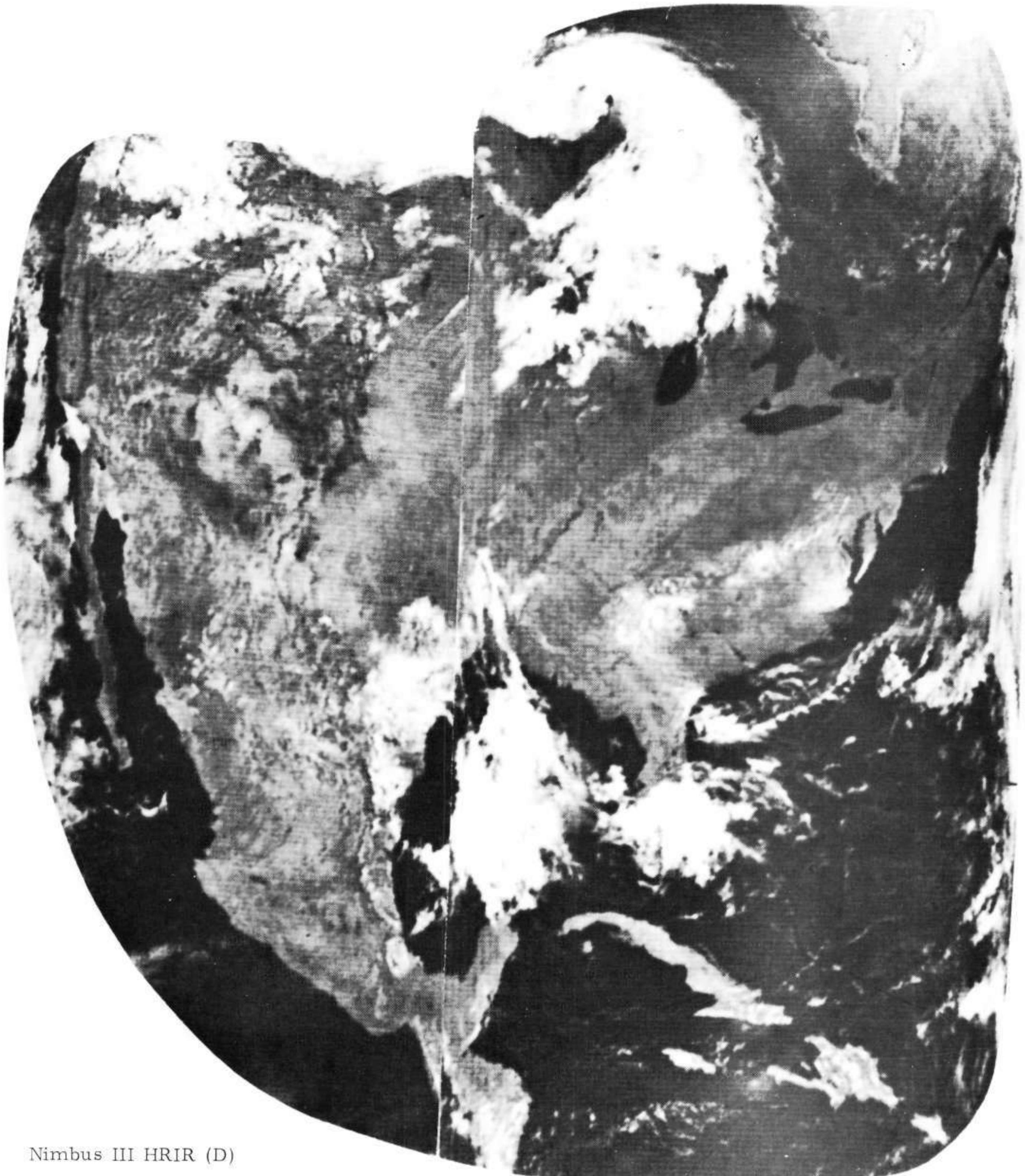

Nimbus III HRIR (D)
1 May 1969

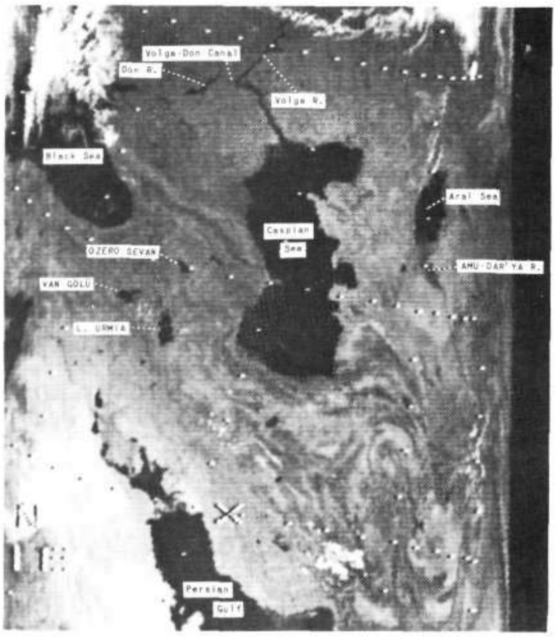

Caspian Sea

A swath of HRIR imagery approximately 2000 miles long runs from near Leningrad at upper left to near Karachi at lower center. The physical characteristics, particularly south of the Caspian Sea, are outstanding in their clarity. The Volga and Don Rivers and the canal connecting them are indicative of the resolution of the HRIR system.

The east-west distortion inherent in the scanning IR system can be appreciated by observing the increased packing of grid "tics" near the edges of the photograph.

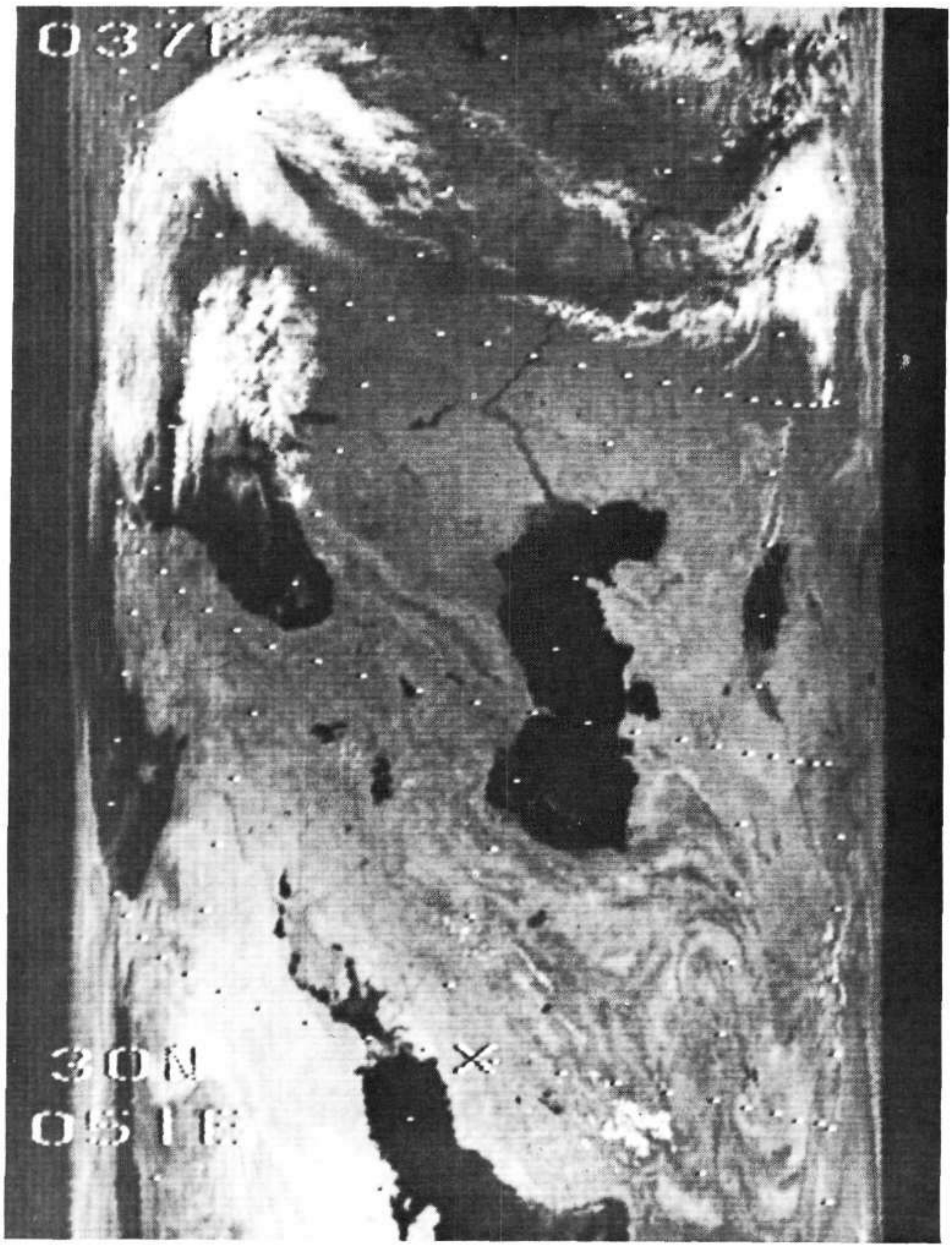

Australia

This montage was constructed from two orbits on succeeding days in order to obtain a relatively cloud-free image. The Great Sandy and Gibson Deserts of northwest Australia stand out as lighter gray against the darker vegetation which surrounds them. Lake Eyre appears as a dark, triangular area about one-third of the way up from the bottom center of the photograph. Groote Eylandt and Wellesley Island in the Gulf of Carpentaria, 50 and 40 miles in length, respectively, lie at upper right-center.

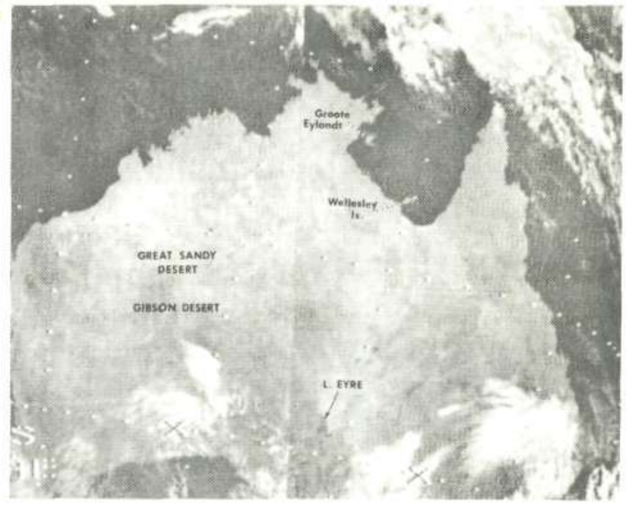

Nimbus III HRIR (D) June 1969

A Unique View of Europe

An unusual combination of meteorological features produced this comparatively rare cloudless view of Europe. A high-pressure system was centered over England and a weak stationary front extended from the Baltic Sea through France and Spain and into the Atlantic. Low-pressure systems account for the cloudiness at the two edges of the photograph.

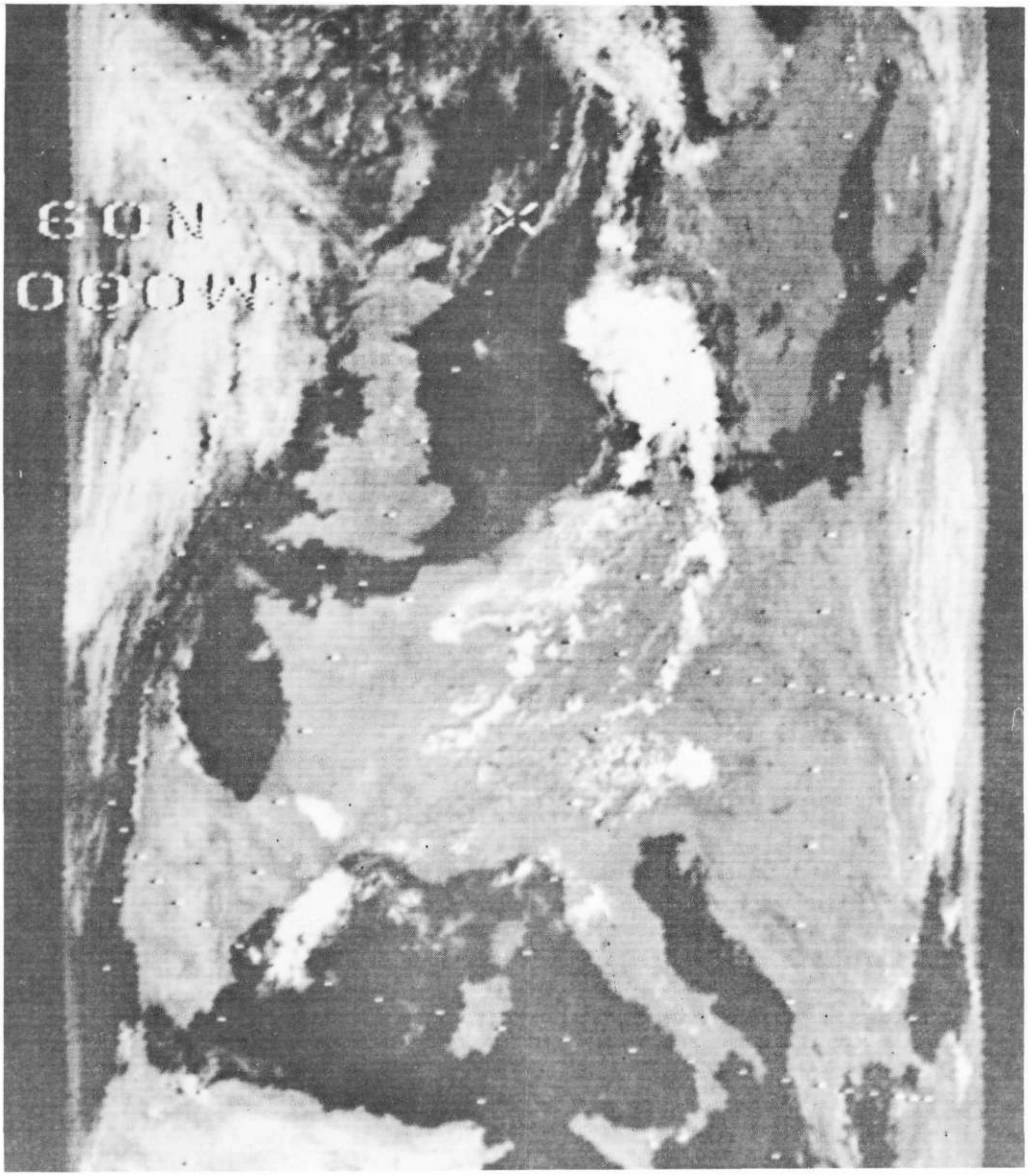

Nimbus III HRIR (D) 6 August 1969

Nimbus III DRIR after 15-1/2 Months

This montage reflects the quality of the direct readout imagery of the daytime HRIR scanner after 15-1/2 months in space (6413 orbits). The pictures, reflecting conditions at approximately local noontime, show a frontal cloud band extending from west of Lake Michigan into Kentucky, another band extending eastward from the northern edge of Lake Superior and still another off the east coast in the Atlantic.

The myriad of visible lakes and rivers attest to the resolution of the system after its lengthy tour of outer space.

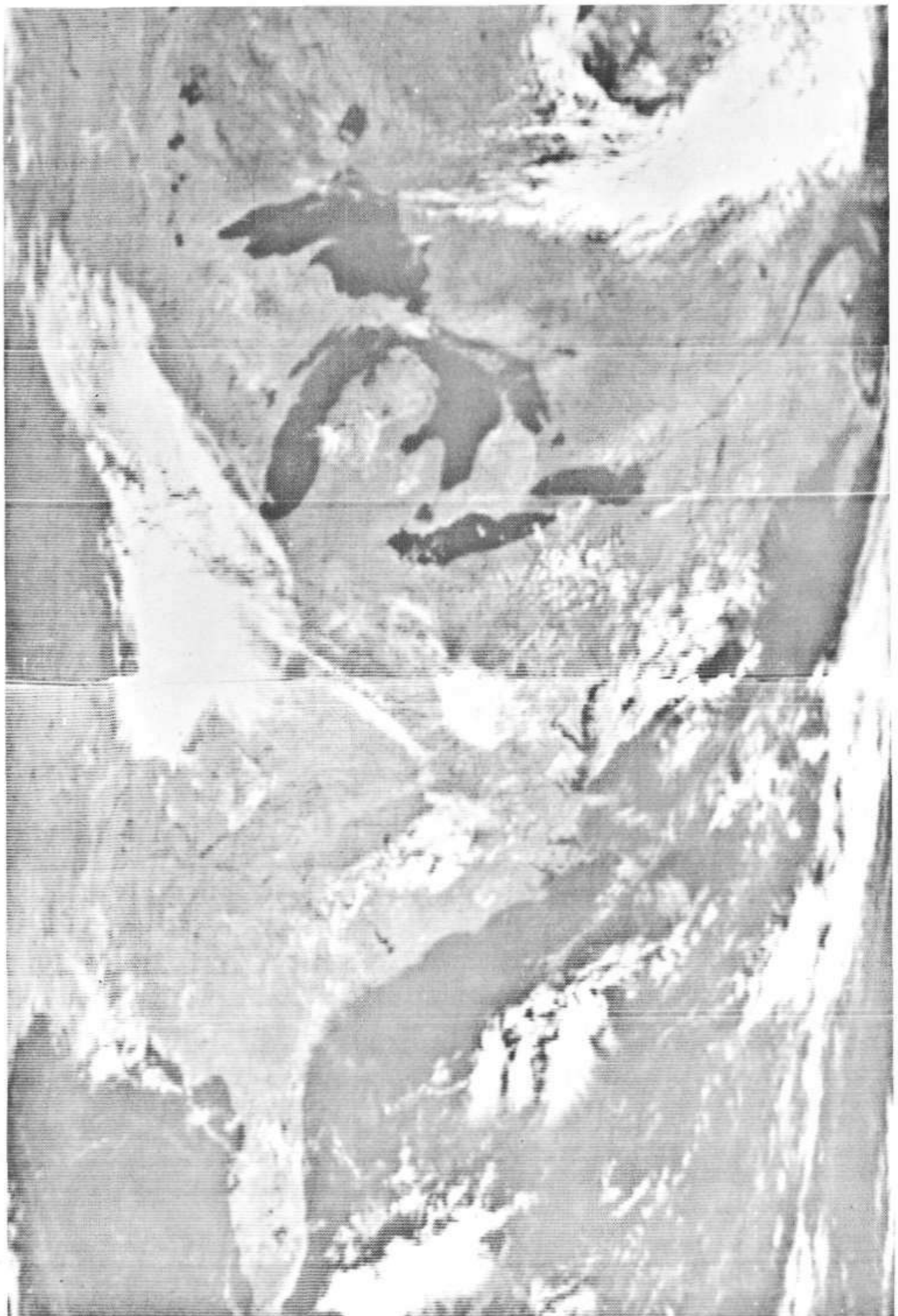

Nimbus III DRIR (D) 5 August 1970

Amateur Reception

This superior high-resolution infrared daytime scanning radiometer picture was received by the amateur APT station at the University of Dundee in Scotland four days prior to the termination of Nimbus III DRIR transmissions, which had been in operation almost 18 months.

The image on the 21st of September 1970 clearly shows the glaciers of Iceland: Langjokull$^{(1)}$, Hofsjokull$^{(2)}$, and Vatnajokull$^{(3)}$. Northeast of Iceland, volcanic activity of Beerenberg, accompanied by a more than 200 mile ash plume$^{(4)}$, is visible on Jan Mayen Island$^{(5)}$.

Further south, on the European continent, geographic areas can be seen such as the Pyrenees$^{(6)}$, the Alps$^{(7)}$, Lake Geneva$^{(8)}$, Lake de Neuchatel$^{(9)}$, Lake Constance$^{(10)}$ and the Rhine river valley$^{(11)}$.

Nimbus III DRIR (D) 21 September 1970

Infrared Interferometer Spectrometer (IRIS) Experiment

The launching of Nimbus III and IV introduced a new generation of meteorological sensors and systems designed to probe the atmosphere to a greater extent than had previously been possible. The experiments reviewed in this section indicate a potential for a giant step forward in obtaining knowledge of our atmosphere.

The IRIS experiment was designed to measure thermal emission in the 5 to 25 μm channel. Temperature, humidity and ozone profiles were developed and compared to radiosonde data and ground-based spectrometers. The lower left and right graphs illustrate the excellent correlations between the IRIS data and that obtained by radiosonde.

The data received from IRIS provide atmospheric information on a scale not before possible. Measurements have been previously received from only a handful of weather ships in both the Atlantic and Pacific Oceans and not at all in many other remote areas. It is now possible to receive, in clear areas, continuous strips of data in a north-south direction separated only by the 27-1/2° of longitude between orbits.

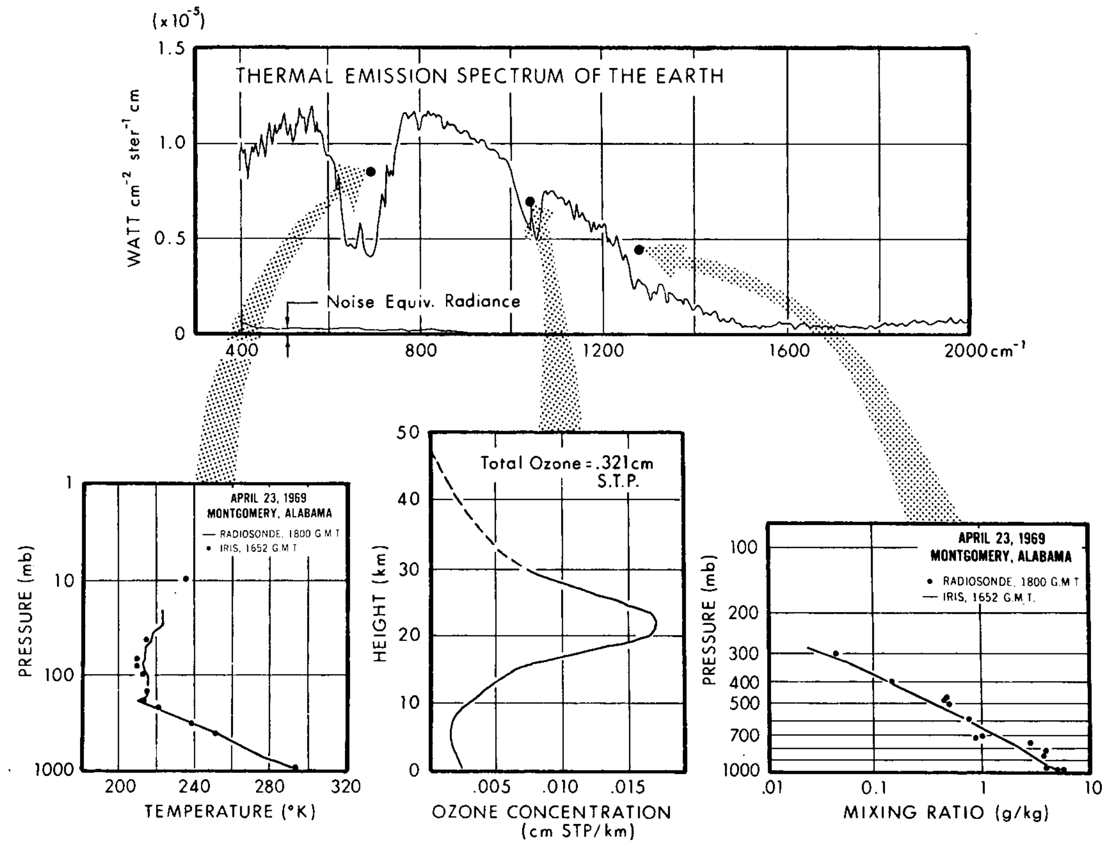

Nimbus III 23 April 1969

A NEW GENERATION OF SENSORS...

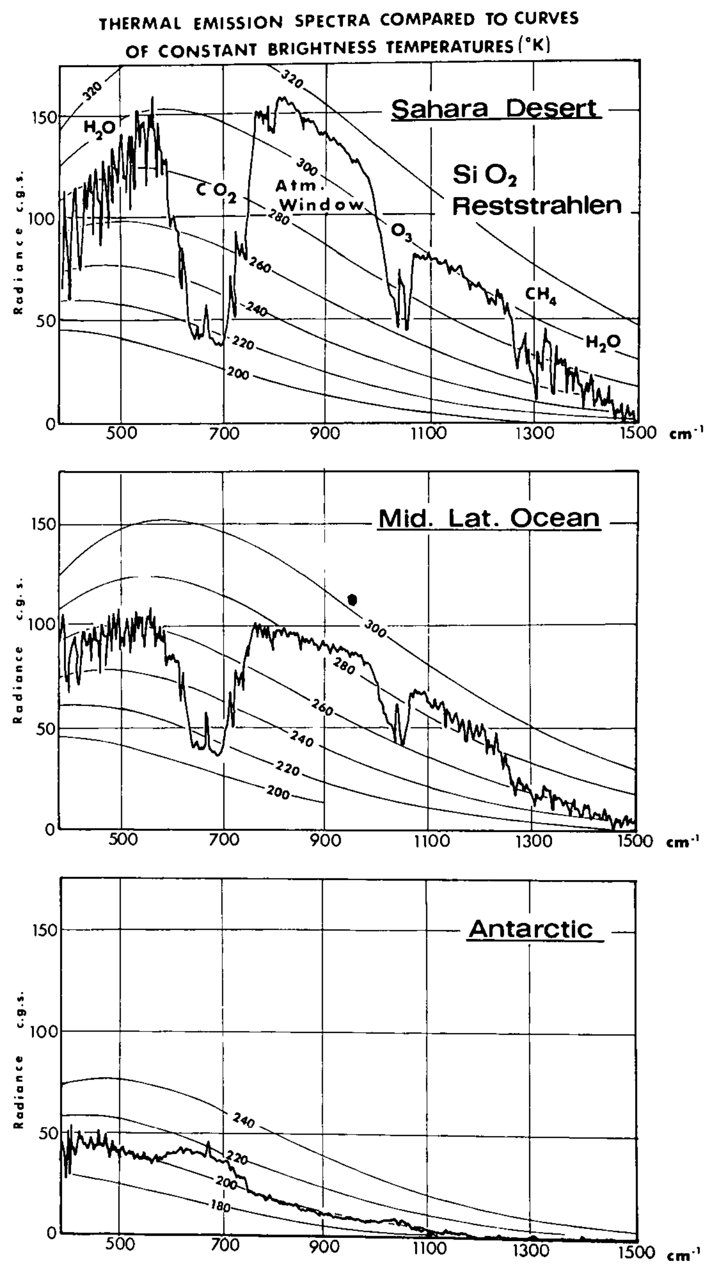

Nimbus IV IRIS 10 April 1970

Thermal Emission Spectra

The thermal emission spectra, as measured by the Nimbus IV IRIS experiment for three representative areas of the world, are compared here to standard "blackbody" curves. The departures from the smooth blackbody curves are due to both atmospheric absorption and changes in the emissivity of the source with wavelength. It can be seen in the figure that at these wave numbers the primary absorption constituents of the atmosphere are water vapor (H_2O), carbon dioxide (CO_2), ozone (O_3) and methane (CH_4). In the "atmospheric windows", from 750 to 950 cm^{-1}, and 1050 to 1250 cm^{-1}, it may be inferred that the surface temperatures for the top, middle and bottom graphs were 312°K, 285°K and 200°K, respectively. The emissivity of silicon dioxide (SiO_2), the predominant component of the desert, drops markedly between the two atmospheric windows. Thus, in the first graph, the apparent surface temperature within the second atmospheric window is only 300°K as compared with 312°K in the first. This difference is significant enough to warrant the inclusion on Nimbus E (scheduled to be launched in 1972) of a sensor specifically designed to measure this difference.

Total Atmospheric Ozone

The Nimbus IRIS experiment has enabled the meteorologist to remotely sense, quite accurately, the total ozone distribution over the globe. The geographic coverage achieved by these data far exceeds any previous ozone measurements.

A close association has been found between the total ozone variation and atmospheric weather systems. The close relationship between total ozone and pressure systems has already been used experimentally to deduce upper air winds. Thus, the IRIS ozone measurements can be immensely valuable for weather prediction in the vast tropical region and southern hemisphere where the conventional meteorological network to gather upper air data is sparse.

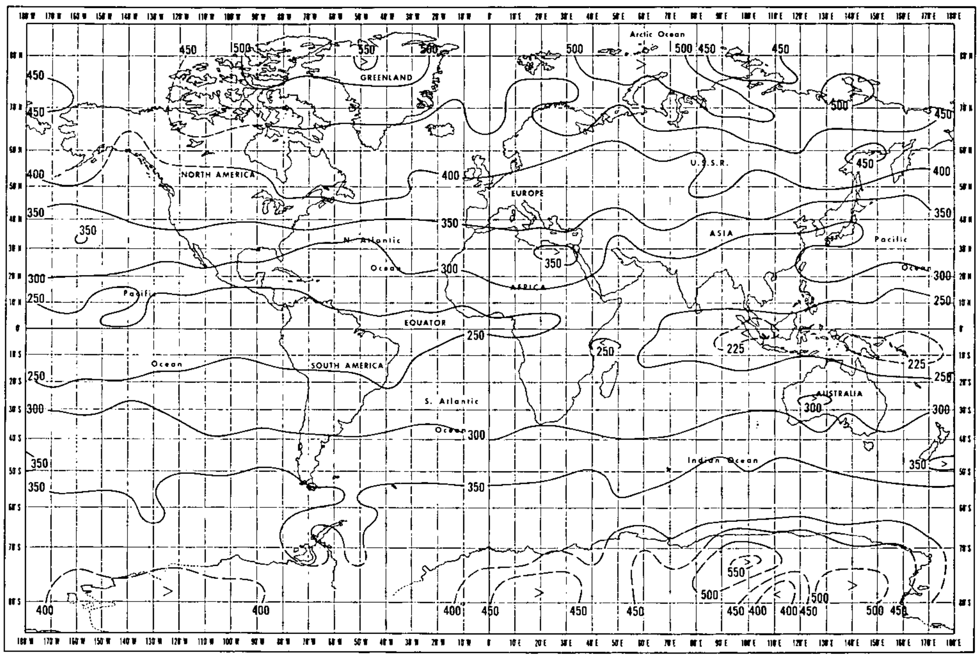

8-Day Mean - April 22-29, 1969

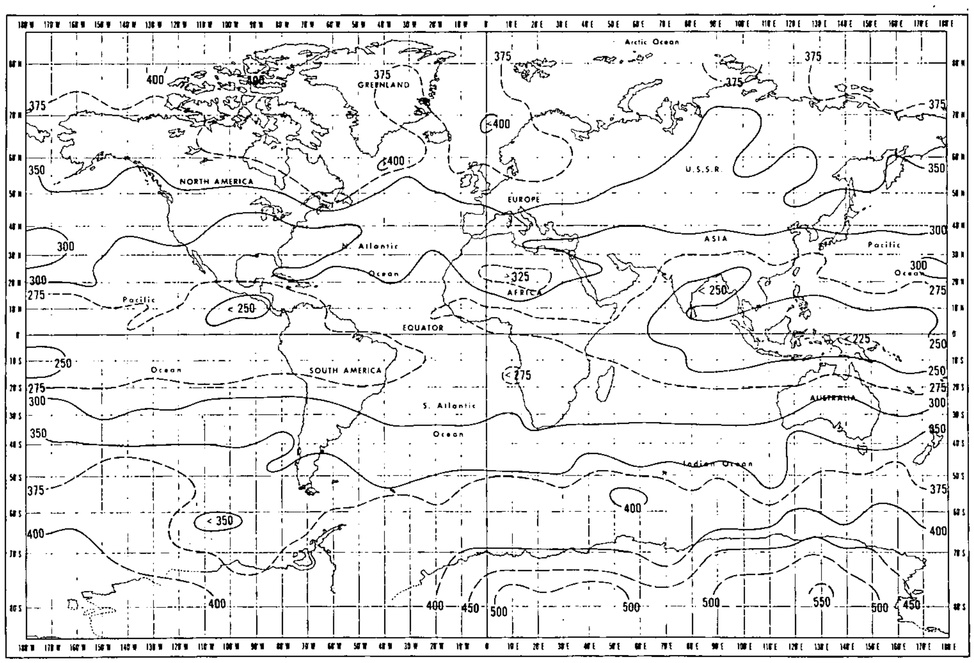

Nimbus III 8-Day Mean - July 3-10, 1969

Total Ozone Content (10^{-3} cm STP)

Satellite Infrared Spectrometer (SIRS)

The Nimbus III Satellite Infrared Spectrometer (SIRS) was a 91-lb instrument designed to measure infrared energy radiated by the atmosphere at seven wavelengths in and near the 15 μm absorption band of carbon dioxide. From these measurements, temperatures at various levels in the atmosphere were derived.

SIRS also sensed the temperatures of cloud tops, when they were present, by means of measurements at an eighth wavelength in the atmospheric "window" at 11 μm. In the absence of clouds, this measurement was used to determine, within a few degrees, the surface temperature.

The figures offer a comparison between a conventionally derived 300-millibar chart and one constructed from values provided by SIRS. The temperatures resulting from the SIRS measurements were computer-converted into height values through entry into various atmospheric equations which relate temperature, density and pressure.

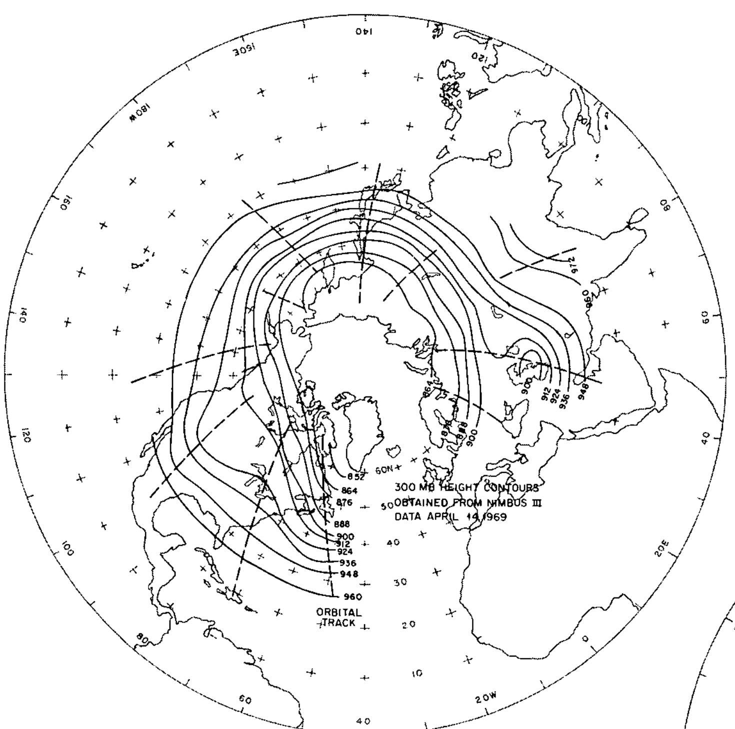

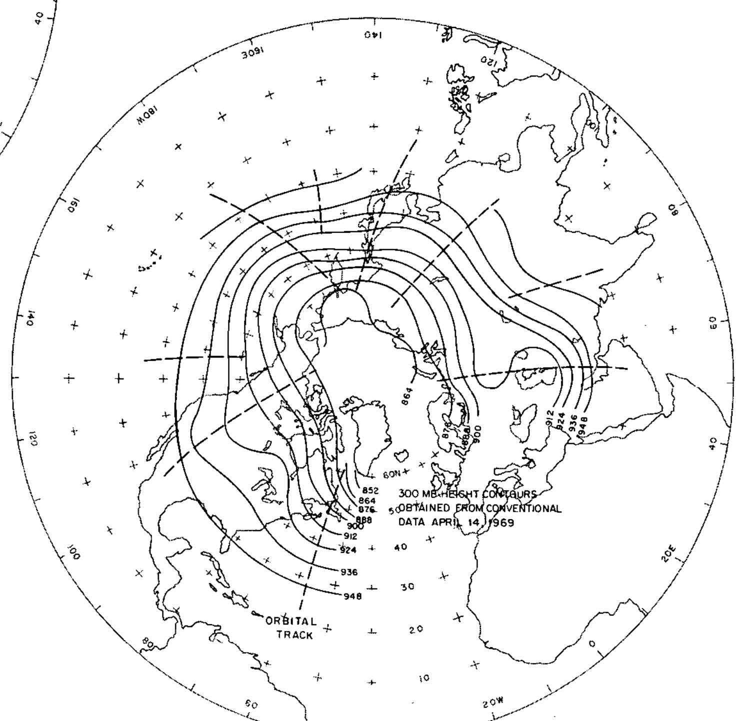

Water Vapor Comparison

This graph shows a comparison between the atmospheric water vapor content as measured by radiosonde and by SIRS over Key West, Florida, and western Cuba, respectively. Mixing ratio (in grams per kilogram) is plotted along the abscissa against pressure (in millibars) along the ordinate. The pressure may be generally related to height; i.e., 1000 millibars is near the earth's surface and 300 millibars averages near 30,000 ft. Mixing ratio is the dimensionless ratio of the mass of water vapor to the mass of dry air.

The SIRS sounding is a smoother, less responsive plot than the radiosonde. Radiosonde moisture determination is generally considered to be more accurate near the surface than aloft.

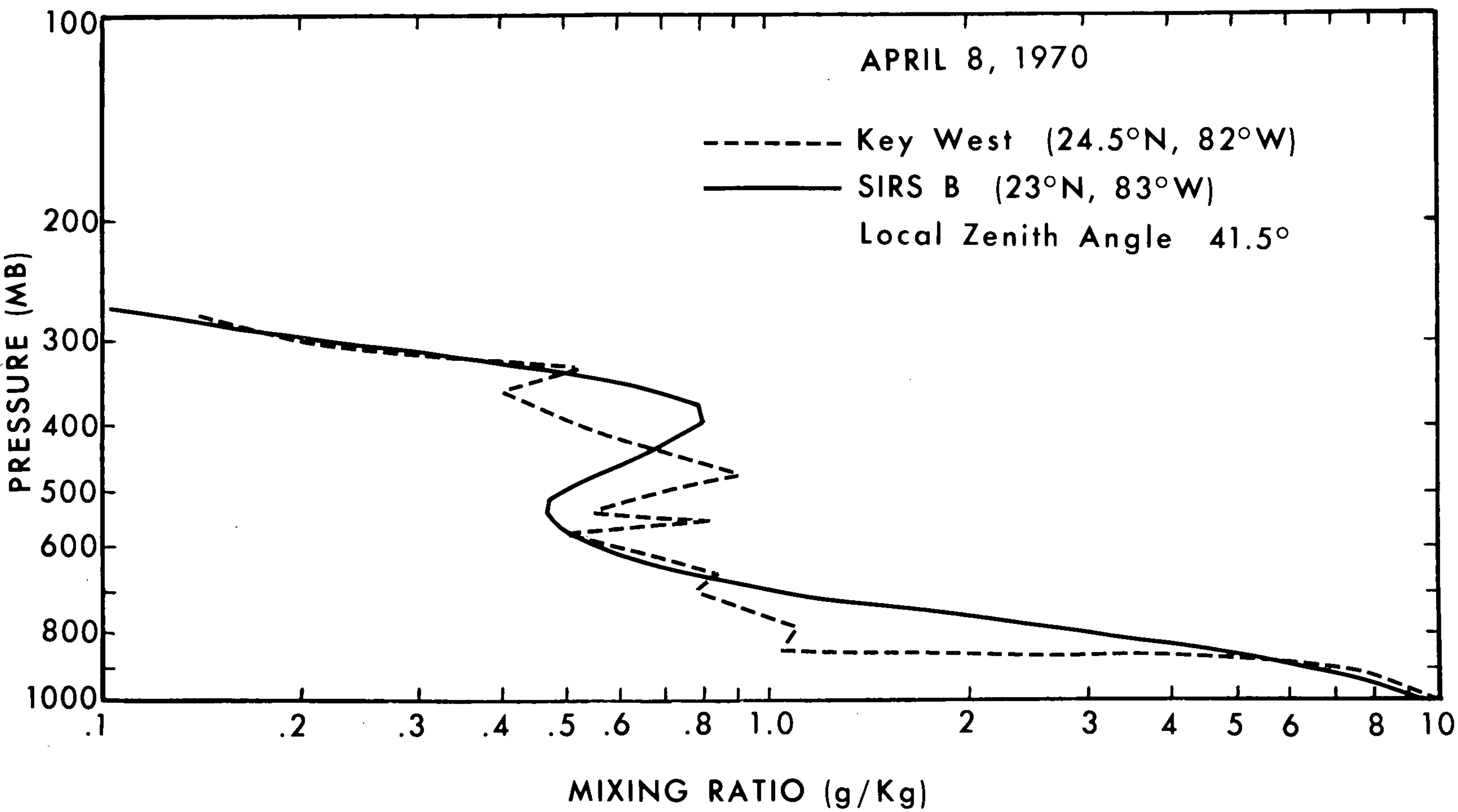

Nimbus IV SIRS 8 April 1970

SIRS A–SIRS B–Radiosonde Comparison

Atmospheric data from the Nimbus III SIRS A and the Nimbus IV SIRS B instruments are compared to radiosonde data for the same area. All three soundings were obtained over Baffin Island in Northern Canada and are remarkably similar.

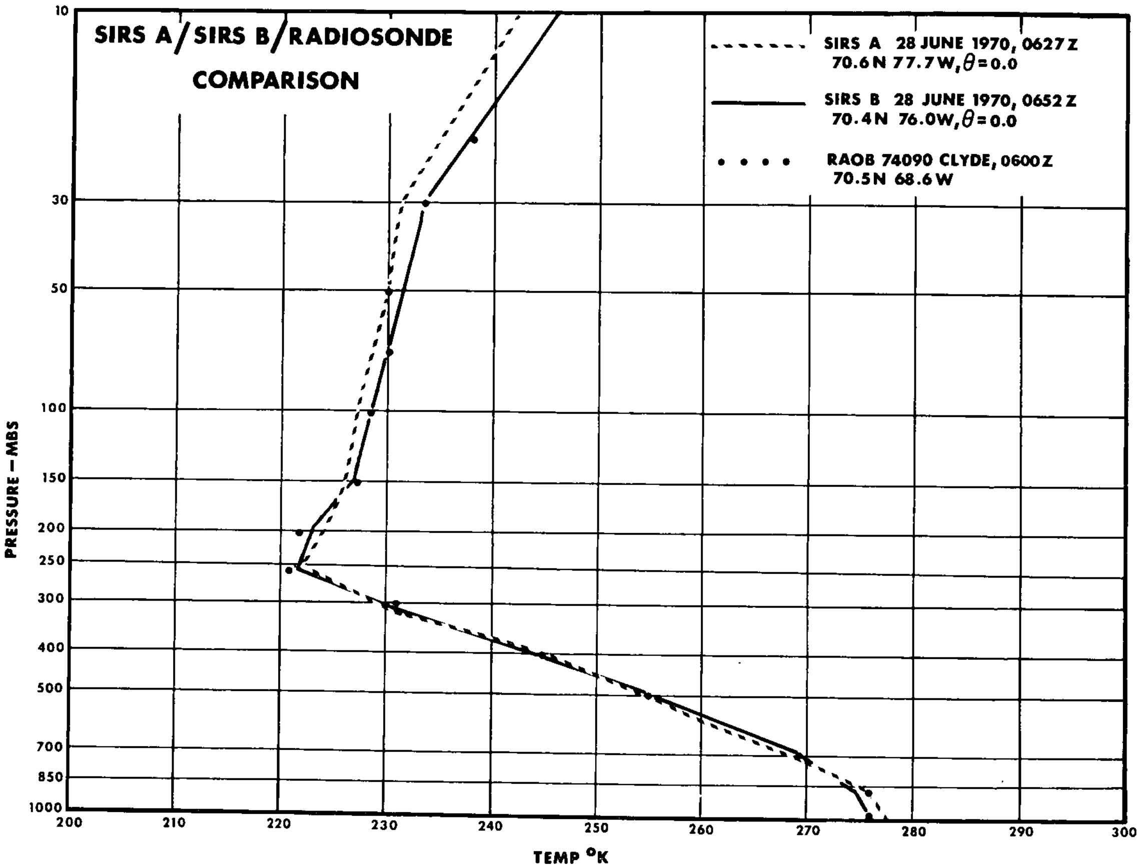

Nimbus SIRS 28 June 1970

SCR Temperature Sounding

The SCR (Selective Chopper Radiometer) determines temperature in six 10-km deep layers and over a horizontal area of approximately 5000 sq. mi. The left figure was produced over the ocean just off the California Coast. A comparison is presented between the SCR and measurements obtained from balloon and rocketborne instruments. In the right figure, a similar comparison between SCR and rocket data is made for the Wallops Island, Virginia, area.

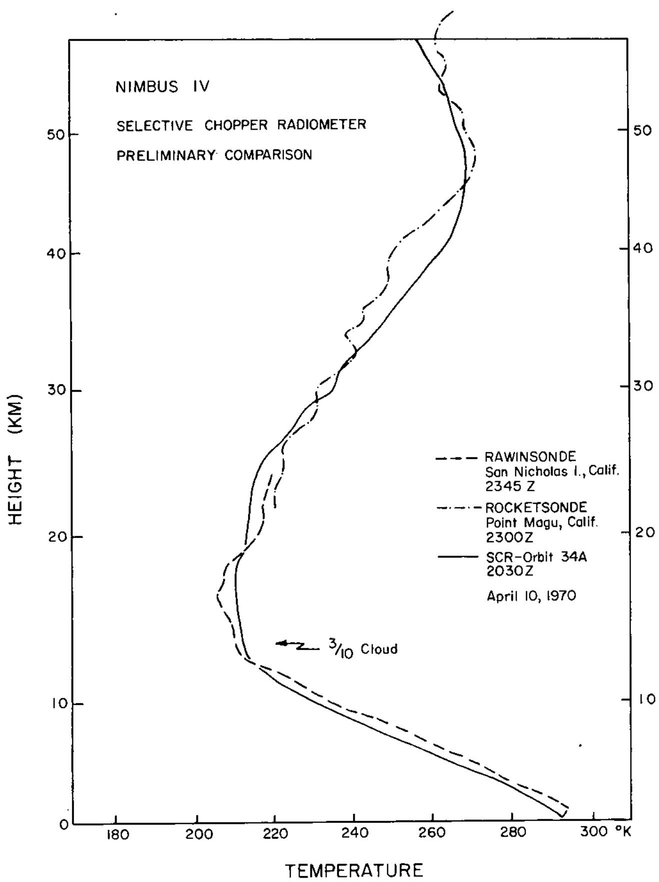

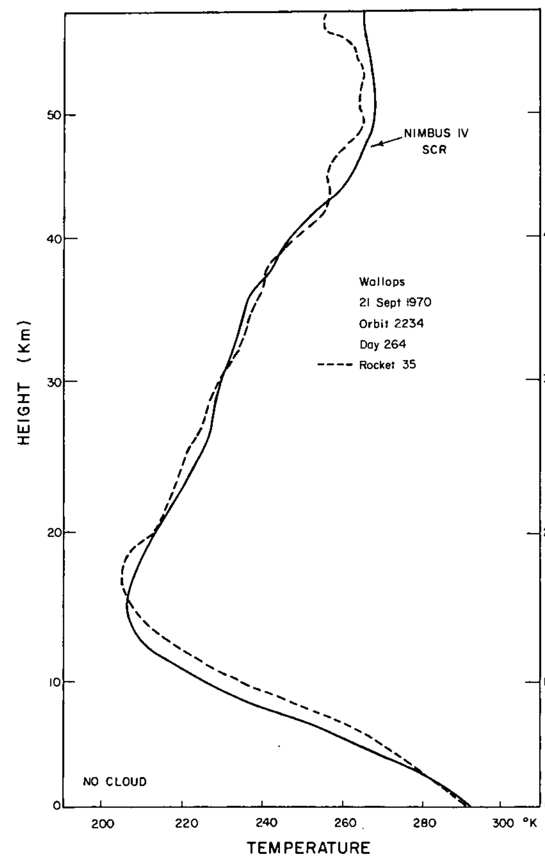

Nimbus IV SCR

Stratospheric Warming

An important feature of the winter stratosphere near the poles is the occurrence of "sudden warmings" where the temperature over a small area may rise by as much as 50°K in a few days, accompanied by a major change in circulation. Observation of these events, dependent on meteorological rocket and radiosonde ascents, has been hampered by the sparsity of data. Now, stratospheric warmings can be observed by the Selective Chopper Radiometer (SCR) on the Nimbus IV satellite. The radiometer has six channels, each accepting infrared radiation emitted by carbon dioxide in the atmosphere at wavelengths of approximately 15 μm. The radiation measured by channel A originates in a layer approximately 20 km thick centered at the 2 mb (42 km) level, while that measured by channel B originates in a layer of similar thickness centered at 20 mb (26 km). Figures A and C are northern hemisphere maps of channel A radiance, while B and D are northern hemisphere maps of channel B radiance.

These radiances can be interpreted in terms of atmospheric temperatures, using the table below.

Equivalent Temperature as a Function of Radiance for A Blackbody

Radiance mW m^{-2} sr^{-1} $(cm^{-1})^{-1}$	Equivalent Temperature (K^{o})
30	201.0
40	213.7
50	224.7
60	234.5
70	243.6
80	251.9
90	259.8
100	267.2
110	274.2
120	281.0

Figures A and B for December 30, 1970, show a warming region developing over central Asia. By January 4, 1971 (Figures C and D) the warm area had intensified and its center moved northeastward over Siberia. Data such as these are being used to monitor other "sudden warmings" to considerably greater heights than has previously been possible.

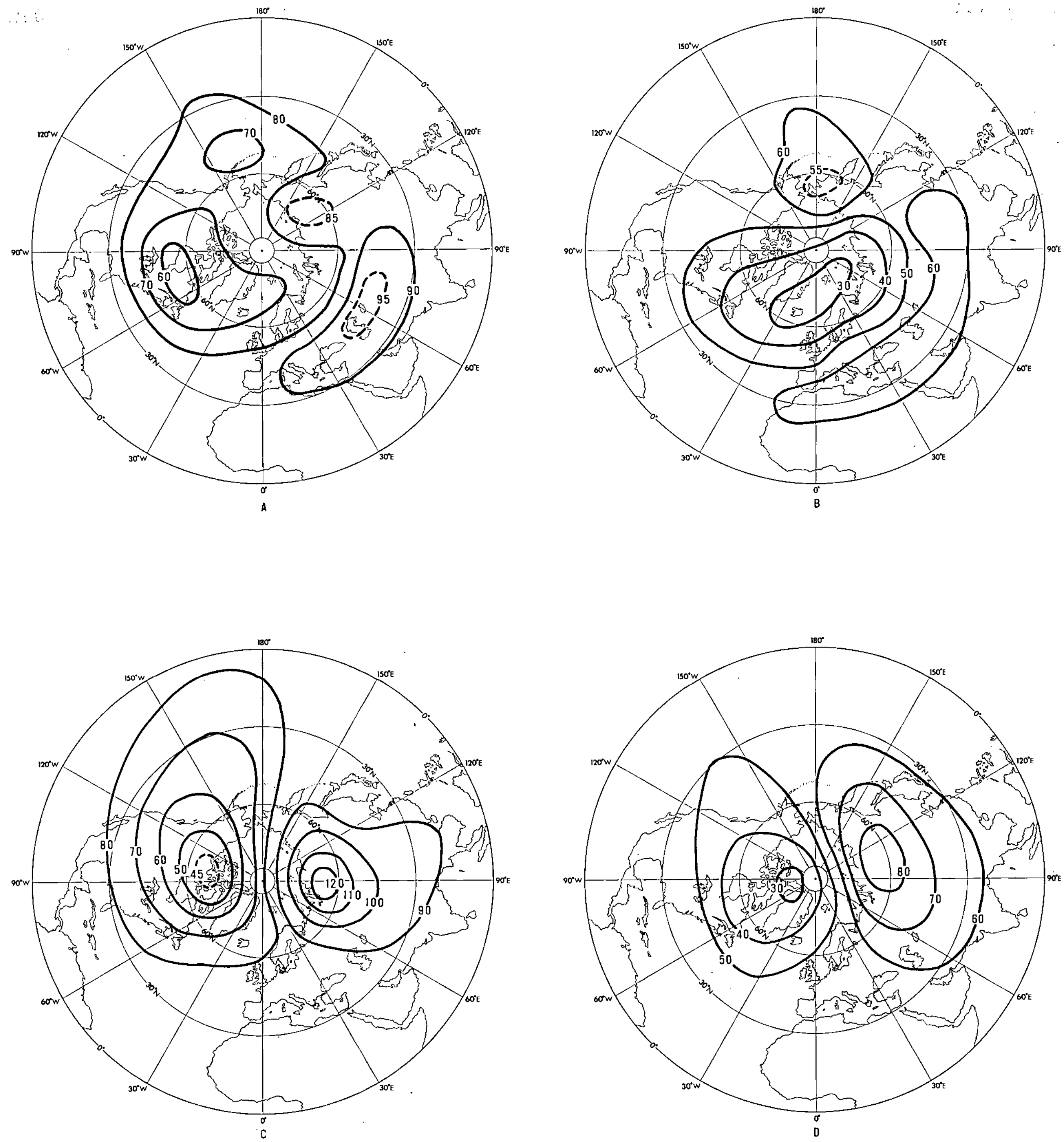

Nimbus IV SCR

Backscatter Ultraviolet Spectrometer (BUV)

The BUV experiment was designed to measure the vertical distribution and total amount of ozone on a global scale. This graph compares atmospheric ozone content as measured by BUV to data previously collected during a NASA mobile experiment. The small circles define the ozone amounts as measured by the Dobson spectrophotometer and the lengths of the bars extending from the circles are indicative of the variability of the data samples. The map shows the orbital track along which the measurements were made.

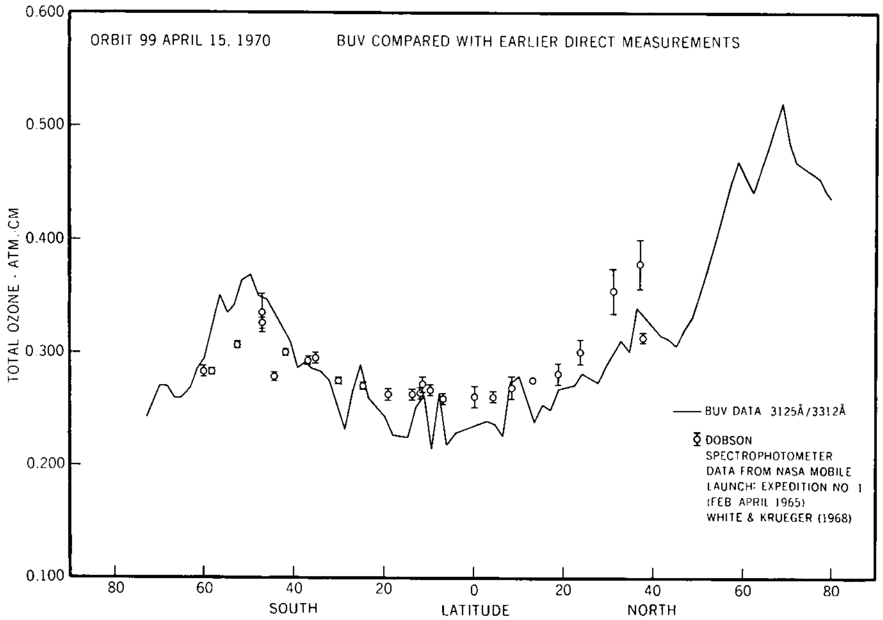

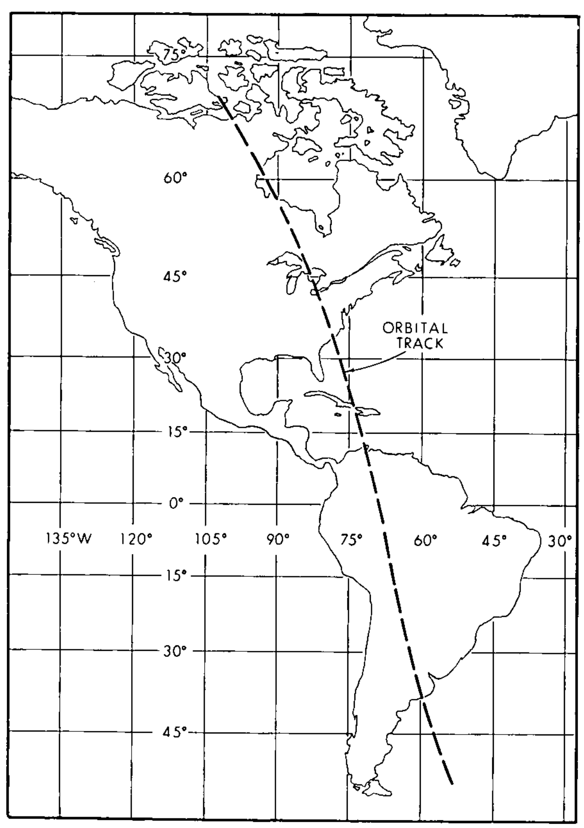

Nimbus IV BUV   15 April 1970

BUV measurements as compared with the standard ultraviolet solar spectrum measured from an aircraft are shown in the graph (top left). The backscattered ultraviolet radiation from the atmosphere measured by the BUV experiment yields the total atmospheric ozone, which in the graph at the upper right is compared to measurements made by the IRIS experiment. The analysis at the bottom of the page is a hemispheric map of total columnar ozone above the surface (in milli-atmosphere centimeters) derived from BUV measurements.

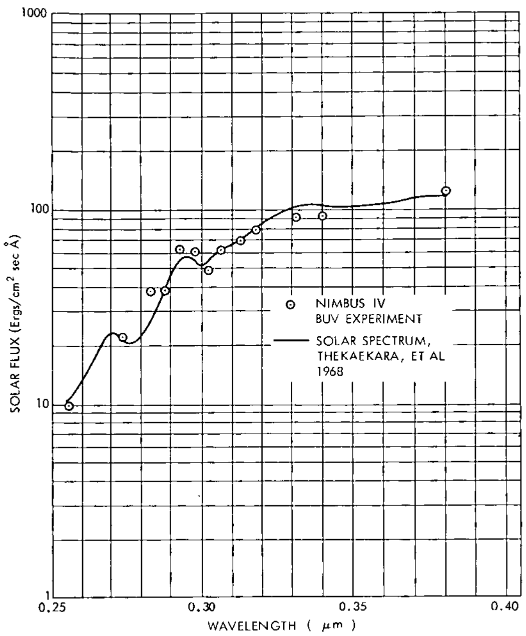

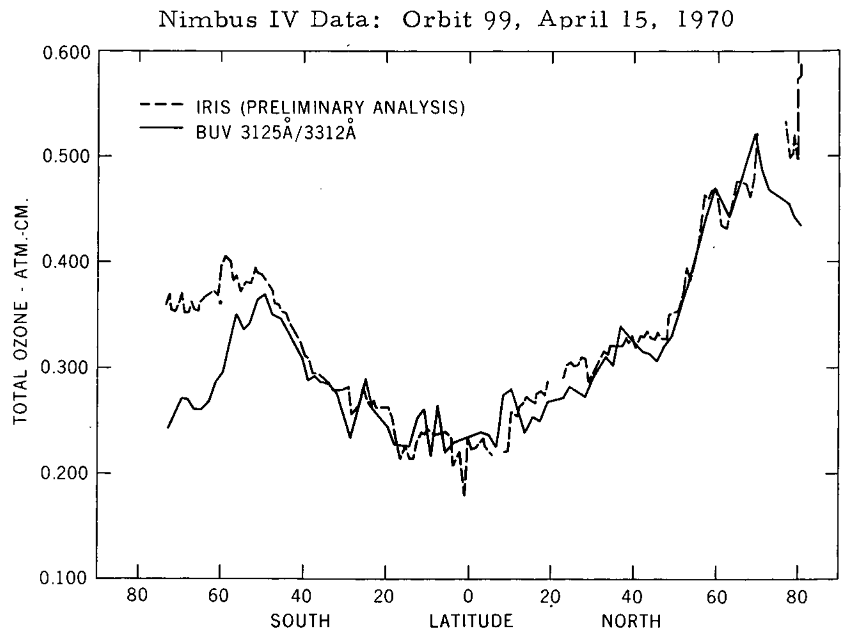

BUV TOTAL OZONE APRIL 30 MAY 1, 1970 ORBITS 294-312

OZONE AMOUNTS IN MILLI ATM-CM

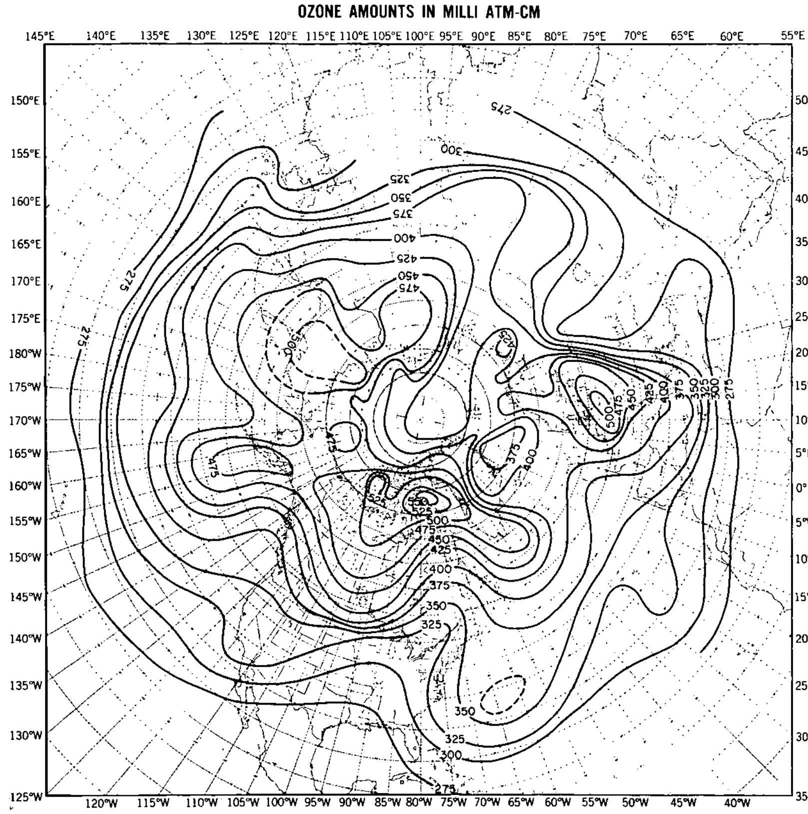

Nimbus III MUSE

This figure shows results obtained over a one-year period from three of the channels of the Nimbus III Monitor of Ultraviolet Solar Energy (MUSE) experiment. The data are compared with earth-based observations of solar coronal activity in the microwave (10.7 cm) region and to variations of the earth's geomagnetic field (Σ Kp).

The spaceborne MUSE experiment measures solar radiation otherwise undetectable at the earth's surface because of the screening effect of the atmosphere that absorbs all energy below 3000 Å. The solar radiation from 1150 to 3000 Å provides the major source of energy input into the upper atmosphere.

The 2750-3150 Å channel measures radiation responsible for the photo-chemical equilibrium that governs the amount and distribution of ozone in the upper stratosphere.

The 1750-1850 Å channel measures radiation originating mostly from the sun's photosphere (sun's surface) which produces atomic oxygen from molecular oxygen at the 90 km level in the atmosphere.

The 1350-1600 Å channel monitors radiation originating from the sun's chromosphere (the layer surrounding the photosphere) which is responsible for the formation of the D region of the ionosphere.

The measurements for the three MUSE channels are given in raw instrument current readings related to actual solar flux in quanta/cm^2 sec (see Nimbus III User's Guide, p. 183). Each point is an average for one day's measurement. The MUSE data clearly show the long-term solar variations with period coincident with the solar rotation rate (approximately 27 days), and correlate well with the standard 10.7 cm measurements of solar coronal activity from ground-based observatories.

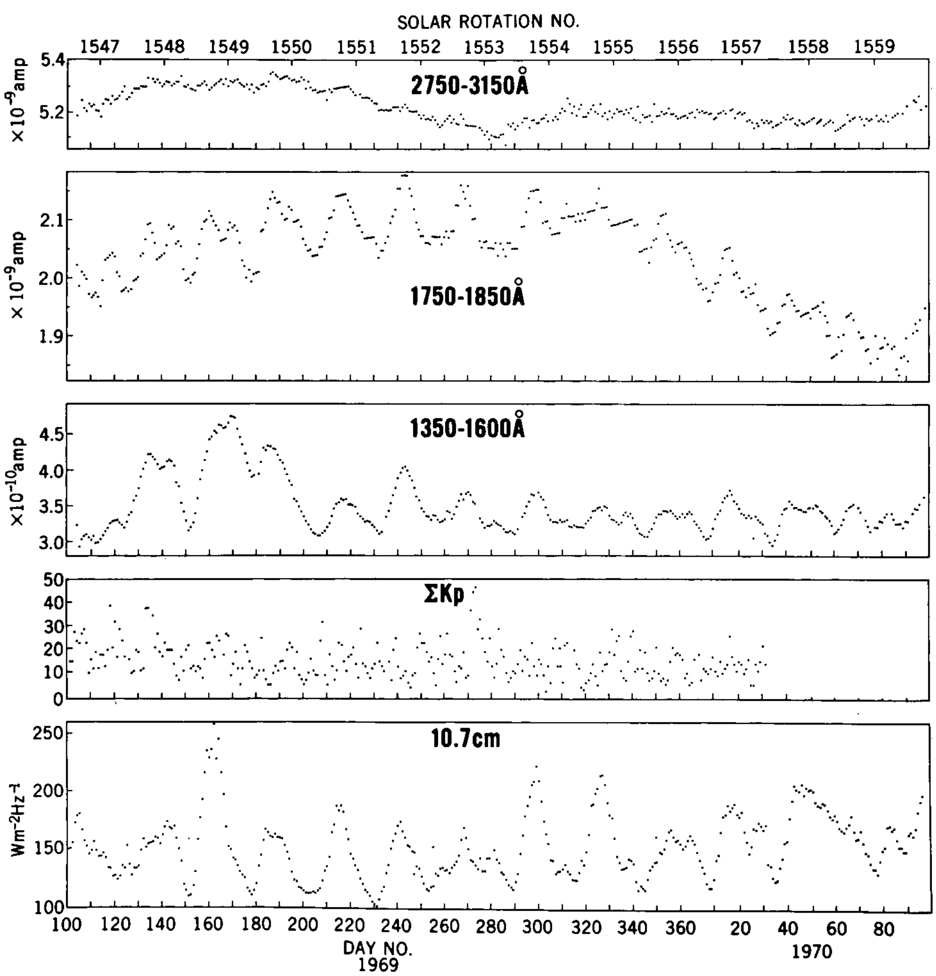

The figure below shows the variation in solar longitude of two ultraviolet active regions on the sun as observed by the MUSE experiment on Nimbus III and IV. The longitude is determined by the average rotation rate of sunspots. The slope of these lines indicates that the ultraviolet active regions possess a different rotation rate than the sunspot region used to define the solar longitude.

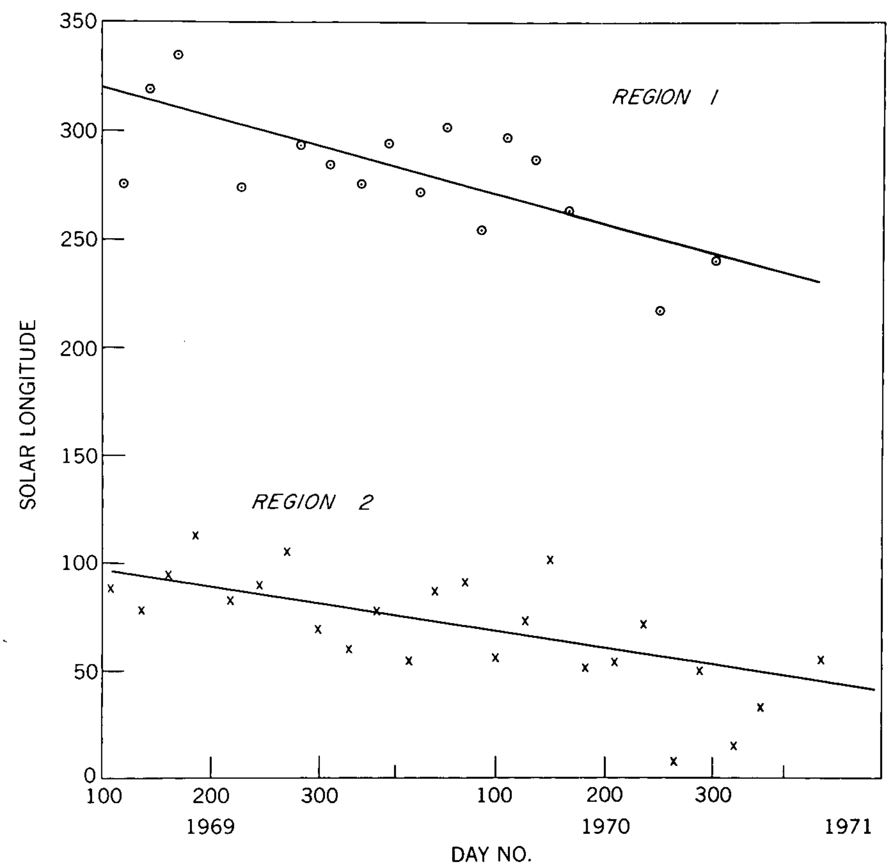

MUSE Measurements of the variations of the solar flux at hydrogen Lyman alpha (1216 Å) and the 1350-1600 Å solar continuum for the same two ultraviolet active regions are shown below. The approximate solar rotation rate is 27 days, which is the time interval between successive ultraviolet maxima.

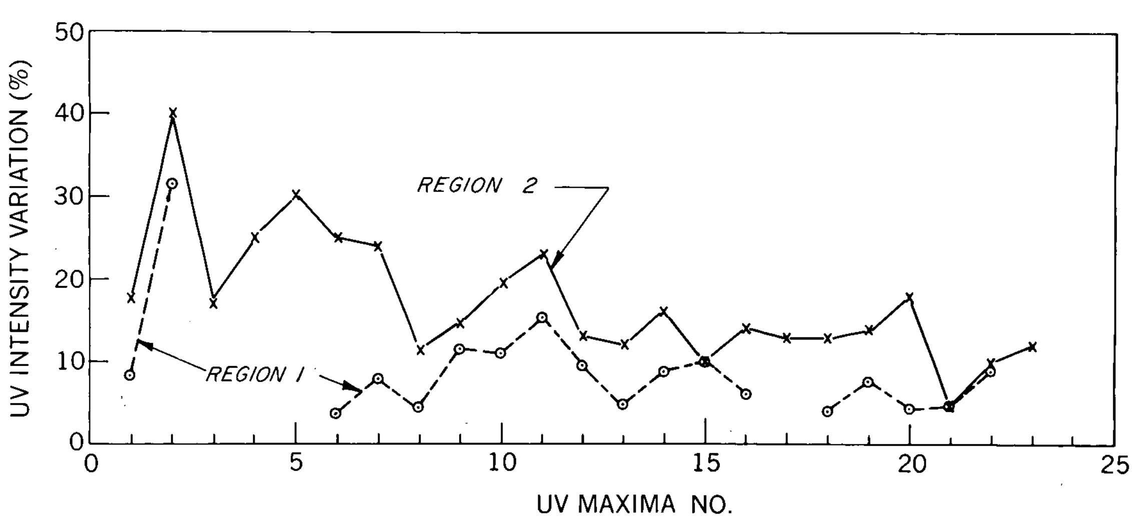

Filter Wedge Spectrometer (FWS)

The purpose of the experiment was to accurately measure radiance from the earth, as a function of wavelength, in the 1.2 to 2.4 and 3.2 to 6.4 μm regions of the spectrum for meteorological purposes. The 1.2 to 2.4 μm interval observed only energy of solar origin reflected from the earth or clouds. The 3.2 to 6.4 μm interval was designed to cover the emission spectrum due to the water vapor band centered at 6.3 μm.

At activation during orbit 5, the data output was degraded, showing patterns typical of ice absorption in both channels. Ice which had apparently collected on the detectors rendered the long wavelength channel insensitive by orbit 89 but data from the short wavelength channel were still usable. The figures show different FWS short wavelength spectral response curves for two different cloud types.

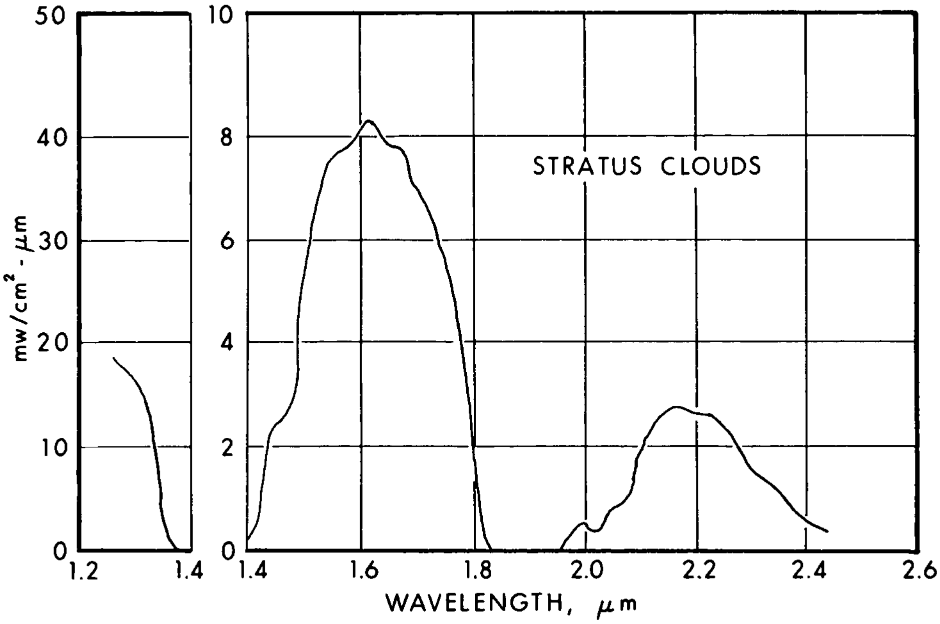

FWS SHORT WAVELENGTH DATA, ORBIT 28

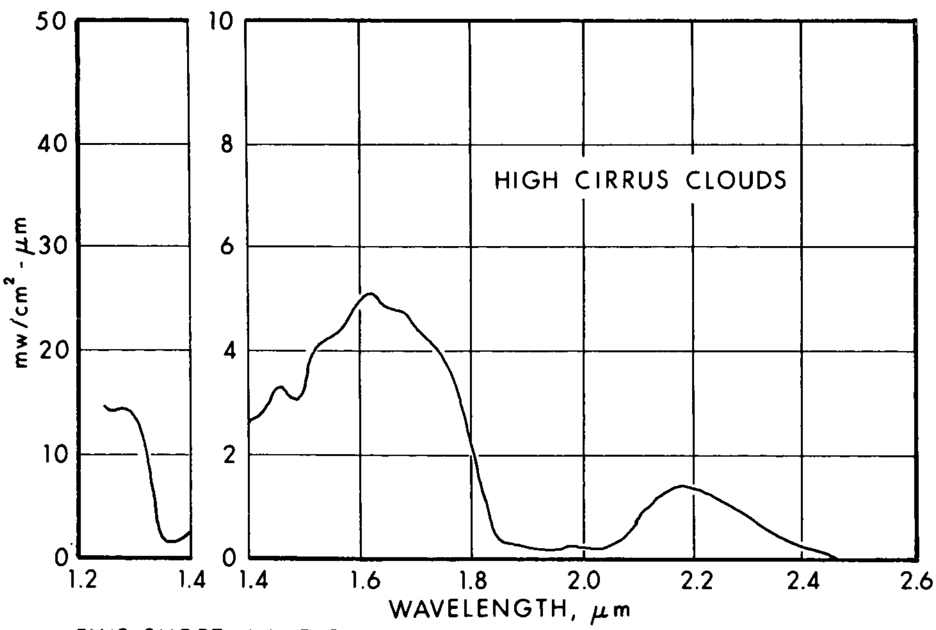

FWS SHORT WAVELENGTH DATA, ORBIT 33

Nimbus IV FWS   10 April 1970

Interrogation, Recording and Location System (IRLS)

The purpose of the IRLS package was to demonstrate the feasibility of using polar-orbiting satellites to determine position-location and to collect data from remote instrumented platforms deployed around the globe, either on or above the earth's surface.

Five types of platforms were utilized:

- Balloons
- Ships
- The T-3 Ice Island
- Buoys
- Land-Developed Packages

Over 440,000 bits of data were received during the first two months from platforms which recorded and stored data and then relayed the information to the satellite upon command. The experiments were as follows:

Balloons

A balloon was released from Christchurch, New Zealand, during April 1970 and, at the time of writing, had been tracked over a six-week period across the South Pacific to South America. The balloon was stabilized at 50 millibars (approximately 67,000 feet). Multiple future releases are scheduled from Ascension Island, in the South Atlantic Ocean, and are expected to provide wind speeds and directions in an area currently sparse in information.

The first Nimbus IV balloon platform was launched at Christchurch, New Zealand on 22 April 1970 and was still being tracked on 22 May 1970. The payload weight of the system was 10.5 lbs and the gross system weight was 61 lbs.

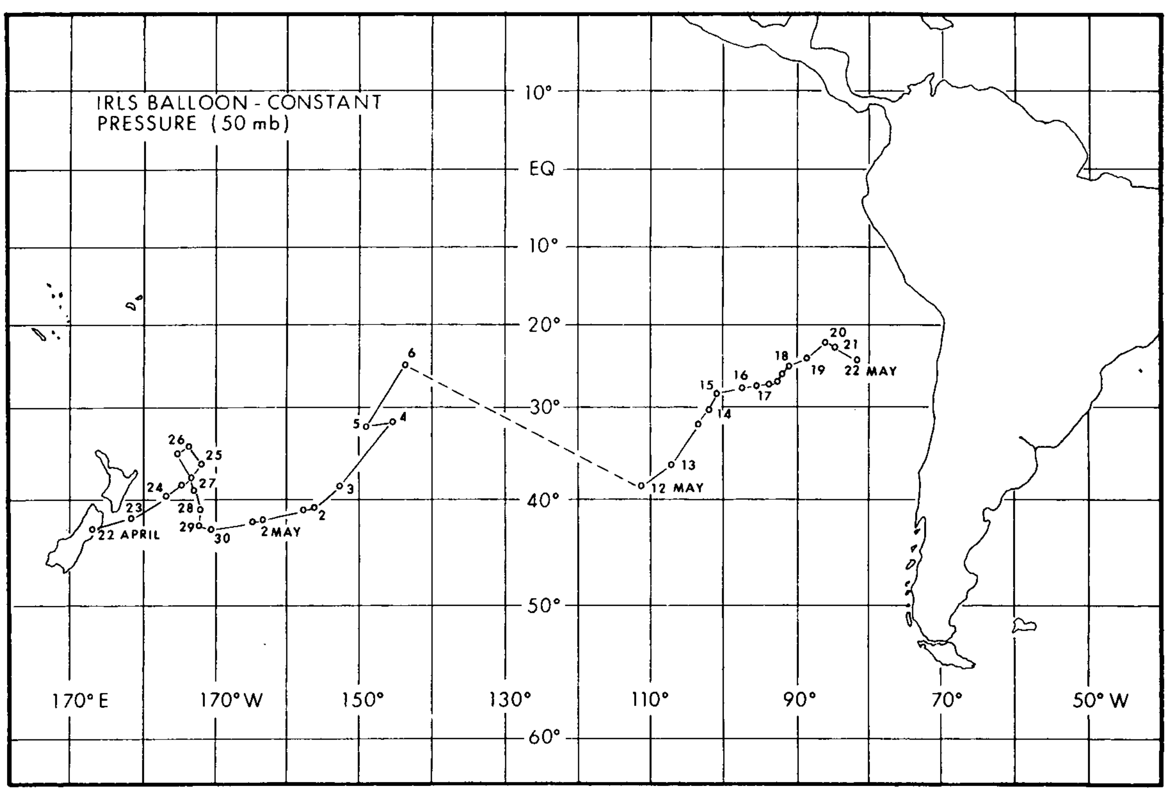

Nimbus IV IRLS 1970

USNS Eltanin Experiment

The Eltanin, which was cruising off Australia during June, July and August 1969, was utilized to demonstrate the capability of relaying weather information to the U. S. Weather Bureau (NOAA). Positions of the ship as determined by IRLS compared favorably to positions obtained by Transit (a navigation satellite system) as shown in accompanying figure. During mid-July, while the ship was on an east-west course south of Tasmania, a crew member became ill, occasioning an unscheduled stop at Hobart on the 16th. The IRLS experimenter at Goddard Space Flight Center was aware of the course change through his IRLS data some hours before routine communications confirmed the fact.

T-3 Ice Island Experiment

T-3, a floating island of ice in the Beaufort Sea, has had a long history in meteorological research. It was used in the IRLS evaluation process to demonstrate the capability to collect and disseminate seismometer data from Arctic regions within hours rather than the normal days or weeks. IRLS and Transit positions again compared favorably.

Drifting Buoy

An unanticipated application of the IRLS system occurred in August 1969 when the IRLS Puerto Rico buoy of the Naval Oceanographic Office was inadvertently separated from its anchor by a passing ship. The buoy, which might have been permanently lost, was easily recovered by IRLS tracking (see accompanying figure). It is also interesting to note that IRLS tracking confirmed the swirls and currents off the southwest tip of the island as shown in oceanographic charts of the area.

Land-Deployed Packages

A 24-pound collar was placed around the neck of an elk in the National Elk Refuge, Jackson Hole, Wyoming and it was successfully tracked over a 30-day period. The instruments recorded and passed to the satellite such information as position, temperature and light intensity readings. The ambient air temperature, the internal package temperature and the skin temperature of the elk were recorded; the latter to within 1° Fahrenheit. A photo-electric device was utilized to estimate general light conditions, such as whether the animal was in heavy woods or open areas.

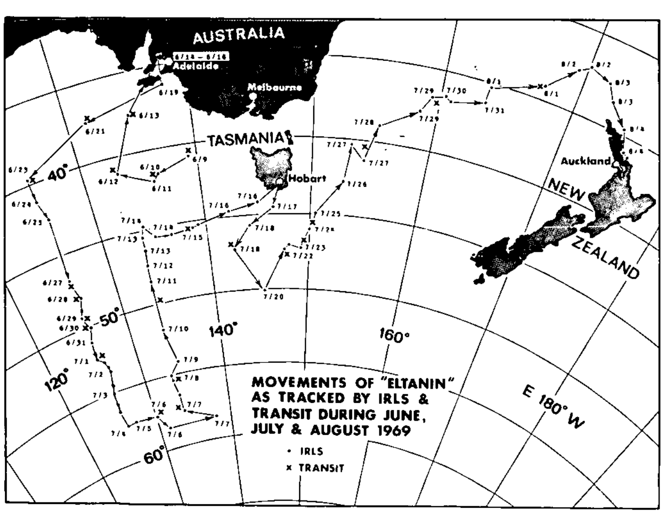

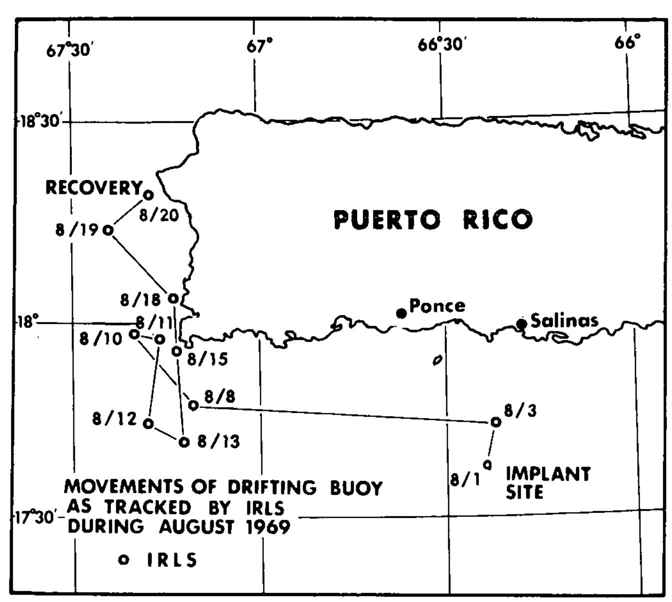

Color Enhancement

This is an example of a color enhancement technique now being used to display selected Nimbus HRIR and THIR radiation data. In this Nimbus III HRIR image of Hurricane Camille, 20 easily distinguishable color tones replace the previously used eight-level gray scale. The resulting presentation permits quick identification of those very high, cold cloud surfaces usually associated with areas of the most violent weather, such as in hurricanes and tornado-spawning clouds. In this picture the spiraling cloud pattern of Hurricane Camille is seen as the storm crossed the Mississippi Gulf Coast, near midnight on August 18, 1969. The gray areas define the core of the hurricane, and other high, very cold storm clouds to the southeast and northeast. The warm cloud-free Gulf waters and land areas appear violet to red.

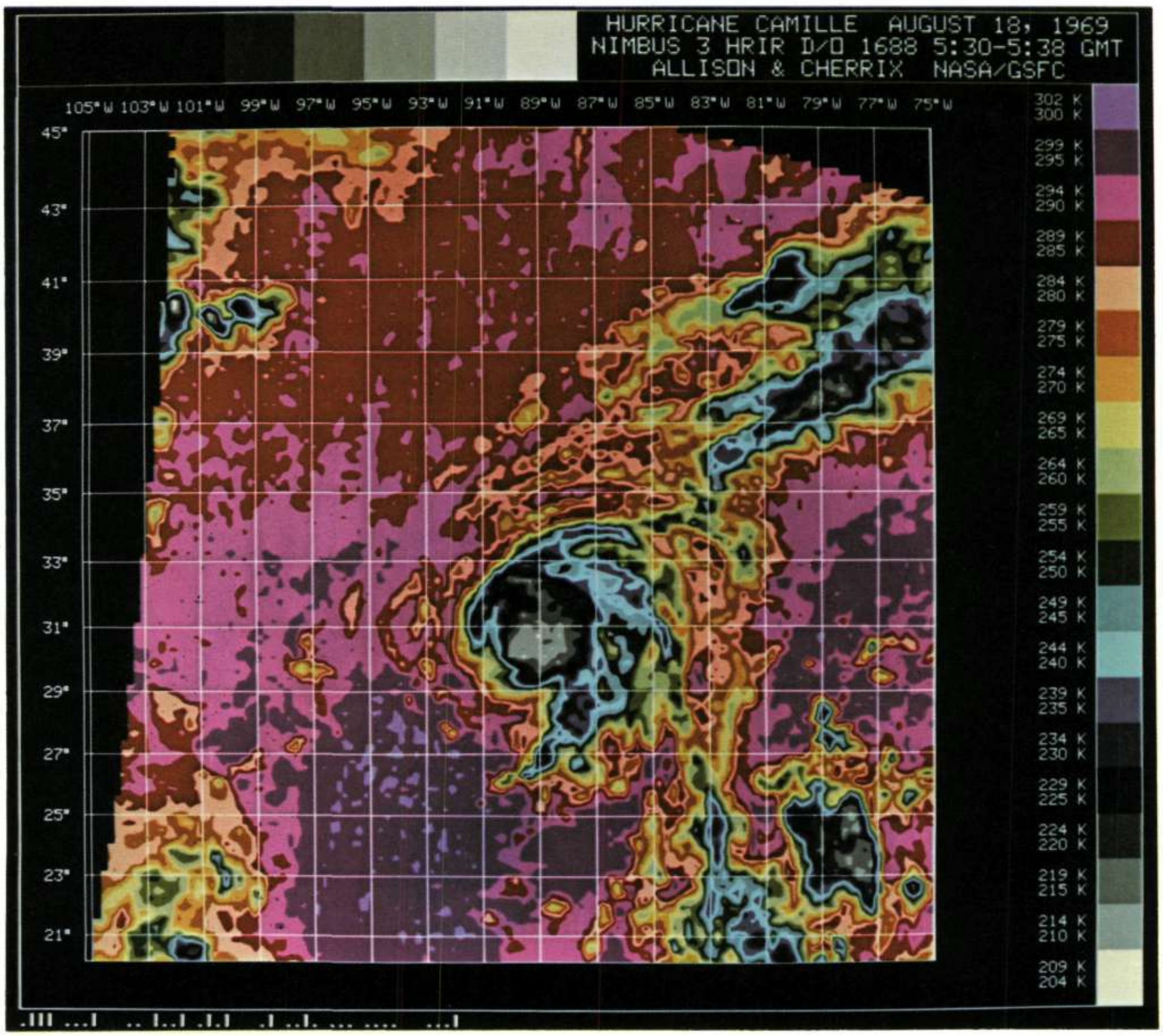

CATALOGS AND USER'S GUIDES

National Aeronautics and Space Administration, 1965: Nimbus I User's Catalog: AVCS and APT, Goddard Space Flight Center, Greenbelt, Maryland.

National Aeronautics and Space Administration, 1965: Nimbus I High Resolution Radiation Data Catalog and User's Manual, Goddard Space Flight Center.

National Aeronautics and Space Administration, 1966: Nimbus II User's Guide, Goddard Space Flight Center.

National Aeronautics and Space Administration 1966: Nimbus II Data Catalog (Vols. 1 through 5), Goddard Space Flight Center.

National Aeronautics and Space Administration, 1967: Nimbus II Medium Resolution Infrared Pictorial Data Catalog (Vols. 1 and 2), Goddard Space Flight Center.

National Aeronautics and Space Administration, 1967: Nimbus II Advanced Vidicon Camera System Data World Montage Catalog, Goddard Space Flight Center.

National Aeronautics and Space Administration, 1967: Nimbus II HRIR World Montage Catalog, Goddard Space Flight Center.

National Aeronautics and Space Administration, 1969: Nimbus III User's Guide, Goddard Space Flight Center.

National Aeronautics and Space Administration, 1969: Nimbus III Data Catalogs (Vols. 1 through 6), Goddard Space Flight Center.

National Aeronautics and Space Administration, 1970: Nimbus IV User's Guide, Goddard Space Flight Center.

National Aeronautics and Space Administration 1970: Nimbus 4 Data Catalogs (Vols. 1 through 3), Goddard Space Flight Center. (Succeeding Nimbus 4 Data Catalogs are being prepared.)

A SELECTED BIBLIOGRAPHY OF PUBLICATIONS BASED UPON NIMBUS DATA

Nordberg, W. and R. E. Samuelson, 1965: Observations from the Nimbus I Meteorological Satellite, NAS SP-89, National Aeronautics and Space Administration.

Woloshin, A. J., 1965: Notes on Geologic Interpretation of Nimbus AVCS Image of Southern California, Geonautics, Inc., Falls Church, Virginia.

Chief Topographic Engineer, 1965: "Cartographic and Geologic Uses of Nimbus I AVCS Data," Space Applications, NAS SP-137, pp. 60-61.

Popham, R. and R. E. Samuelson, 1965: "Polar Exploration with Nimbus," Observations from the Nimbus I Meteorological Satellite, NASA SP-89.

Kunde, V. G., 1965: "Theoretical Relationship Between Equivalent Blackbody Temperatures and Surface Temperatures Measured by the Nimbus High Resolution Infrared Radiometer," Observations from the Nimbus I Meteorological Satellite, NASA SP-89, pp. 23-36.

Kennedy, J. S., 1965: HRIR Noise, Memorandum of 16 April 1965, Goddard Space Flight Center, Greenbelt, Maryland.

Fujita, T. and W. Bandeen, 1965: "Resolution of the Nimbus High Resolution Infrared Radiometer," J. of Appl. Meteoro., 4(4).

Taggart, C. I., 1965: "Interpretation of Geological Features on a Satellite Photograph," Nature, 2071 (4996), pp. 513-514.

Lewis, C. R. and W. E. Davies, 1966: Geological Evaluation of Nimbus Vidicon Photography-Chesapeake-Blue Ridge, U. S. Geological Survey.

Widger, W. K., J. C. Barnes, E. S. Merritt and R. B. Smith, 1966: Meteorological Interpretation of Nimbus HRIR Data, Contract No. 5-9554, Allied Research Associates, Inc.

Predoehl, M., 1966: "Antarctic Pack Ice: Boundaries Established from Nimbus I Pictures," Science, 153, pp. 861-863.

Conti, M. A., 1967: Evaluation of Nimbus I High Resolution Infrared Radiometer (HRIR) Imagery, U. S. Geological Survey.

Raschke, E. and M. Pasternak, 1967: The Global Radiation Balance of the Earth Atmosphere System Obtained from Radiation Data of the Meteorological Satellite Nimbus II, Doc. X-622-67-383, NASA, Goddard Space Flight Center.

Raschke, E., F. Moller and W. R. Bandeen, 1967: The Radiation Balance of the Earth Atmosphere System Over Both Polar Regions Obtained from Radiation Measurements of the Nimbus II Meteorological Satellite, Doc. X-622-67-460, NASA, Goddard Space Flight Center.

Pasternak, M., 1967: An Atlas of Total Outgoing Long-Wave Radiation and of Short-Wave Reflectance from Nimbus II Observations, Doc. X-622-67-500, NASA, Goddard Space Flight Center.

Vickers, R. S. and R. J. P. Lyon, 1967: "Infrared Sensing from Spacecraft. A Geological Interpretation," AIAA Thermophysics Specialists Conference, Paper No. 67-284, New Orleans, Louisiana.

Greaves, J. R., J. H. Willand and D. T. Chang, 1968: Observations of Sea Surface Temperature Patterns and Their Synoptic Changes Through Optimal Processing of Nimbus II Data, Final Report, Contract No. NASW-1651, Allied Research Associates, Inc.

Kuers, G., 1968: Interpretation of Daytime Measurements by the Nimbus I and II HRIR, NASA TN D-4552.

Pouquet, J. and E. Raschke, 1968: A Preliminary Study of the Detection of Geomorphological Features Over Northeast Africa by Satellite Radiation Measurements in the Visible and Infrared, NASA Tech. Note, NASA TN04648.

Pouquet, J., 1968: An Approach to the Remote Detection of Earth Resources in Sub-Arid Lands, NASA Tech. Note, NASA TN D-4647.

Pouquet, J., 1968: Remote Detection of Terrain Features from Nimbus I High Resolution Infrared Radiometer Nighttime Measurements, NASA Tech. Note TN D4603.

Sabatini, R. R. and J. E. Sissala, 1968: Project NERO, Nimbus Earth Resources Observations, Tech. Report No. 7, Contract No. NAS 5-10343, NASA, Allied Research Associates, Inc.

Pouquet, J., 1969: Geopedological Features Derived from Satellite Measurements in the 3.4 to 4.2 micron and 0.7 to 1.3 micron Spectral Regions, Communication, 6th Symposium on Remote Detection, Ann Arbor, Michigan.

Pouquet, J., 1969: Possibilities for Remote Detection of Water in Arid and Sub-Arid Lands Derived from Satellite Measurements in the Atmospheric Window 3.5 to 4.2 microns, International Conference on Arid Lands in a Changing World, Tuscon, Arizona.

Pouquet, J., 1969: "Near Infrared Daytime Surface Characteristics from Nimbus III High Resolution Infrared Radiometer Data: Geological Aspects," Abstracts - AGU 1969 National Fall Meeting, Trans. Am. Geophys. Union, 50.11; p. 623.

MacLeod, N. H., 1969: "Ecological Analysis of Daytime HRIR Imagery from Nimbus III," Abstracts - AGU 1969 National Fall Meeting, Trans. Am. Geophys. Union, 50.11; p. 623.

Knapp, W. W., 1969: "A Satellite Study of the Ice in Antarctic Coastal Waters," Antarctic Journal, Sept-Oct, pp. 222-223.

Bowley, C. J., 1969: Use of Nimbus II APT to Determine the Rate of Ice Disintegration and Dispersion in Hudson Bay, Tech. Report No. 8, Contract No. NAS 5-10343, Allied Research Associates, Inc.

Barnes, J. C., D. T. Chang and J. H. Willand, 1969: Use of Satellite High Resolution Infrared Imagery to Map Arctic Sea Ice, Final Report, Contract No. N62306-38-C-0276, Allied Research Associates, Inc.

Hanson, D. M., 1963: The Use of Meteorological Satellite Data in Analysis and Forecasting, Tech. Note 13, Office of Forecast Development, U. S. Weather Burea.

Sissala, J. E., 1969: "Observation of an Antarctic Ocean Tabular Iceberg from the Nimbus II Satellite," Nature, 224, pp. 1285-1287.

Rabchevsky, G., 1970: Comments on the Geological Use of Nimbus I Television Photography, Allied Research Associates, Inc.

Prabhakara, C., V. V. Salomonson, B. J. Conrath, J. Steranka and L. J. Allison, 1970: Nimbus 3 Satellite Observations of Ozone Associated with the Easterly Jet Stream over India During the 1969 Summer Monsoon, NASA Publication X-651-70-464, Goddard Space Flight Center, Greenbelt, Maryland.

Thekaekara, M. P., 1970: The Solar Constant and the Solar Spectrum Measured from a Research Aircraft, NASA Tech. Report No. TR R-351, Goddard Space Flight Center, Greenbelt, Maryland.

Prabhakara, C., B. J. Conrath, L. J. Allison and J. Steranka, 1971: Seasonal and Geographic Variation of Atmospheric Ozone Derived from Nimbus 3, NASA Publication X-651-71-38, Goddard Space Flight Center, Greenbelt, Maryland.

Heath, D. F., A. J. Krueger and C. L. Mateer, 1971: Observations of Earth Radiance and Solar Irradiance in the 2550-3800A Region from Nimbus 4, Fifty-Second Annual Meeting of the American Geophysical Union 12-16 April, 1971, Washington, D. C.

Mateer, C. L., D. F. Heath and A. J. Krueger, 1971: Total Ozone from Nimbus Ultraviolet Earth Radiances and Comparison with Dobson Spectrophotometer Data, Fifty-Second Annual Meeting of the American Geophysical Union, 12-16 April 1971, Washington, D. C.

Krueger, A. J., D. F. Heath and C. L. Mateer, 1971: High-Level Ozone Distribution from Nimbus 4 and Comparison with Simultaneous Rocket Data, Fifty-Second Annual Meeting of the American Geophysical Union, 12-16 April 1971, Washington, D. C.

Heath, D. F., C. L. Mateer and A. J. Krueger, 1971: Satellite Spectrophotometric Measurements of the Earth Radiance and Solar Irradiance in Near Ultraviolet, 1971 Spring Meeting of the Optical Society of America, 5-8 April 1971, Tucson, Arizona.

Heath, D. F., 1971: "Observations of the Solar Long-Term Variability and Irradiance in the Near and Far Ultraviolet (to be published in) J. of Geophysical Research. Preprint: NASA X-651-71-116.

GLOSSARY OF TERMS

Å	Angstrom
APT	Automatic Picture Transmission
AVCS	Advanced Vidicon Camera System
BUV	Backscatter Ultraviolet Spectrometer
CDA	Command and Data Acquisition Station
CMS	Canadian Meteorological Service
(D)	Day
DRID	Direct Readout Image Dissector
DRIR	Direct Readout Infrared Radiometer
ERTS	Earth Resources Technology Satellite
FWS	Filter Wedge Spectrometer
GMT	Greenwich Mean Time
GSFC	Goddard Space Flight Center
HRIR	High Resolution Infrared Radiometer
IDCS	Image Dissector Camera System
IRIS	Infrared Interferometer Spectrometer
IRLS	Interrogation Recording and Location System
K	Kelvin
μm	Micrometer
MRIR	Medium Resolution Infrared Radiometer
MUSE	Monitor of Ultraviolet Solar Energy
NASA	National Aeronautics and Space Administration
(N)	Night
NESS	National Environmental Satellite Service
RTTS	Real Time Transmission System
SCR	Selective Chopper Radiometer
SIRS	Satellite Infrared Spectrometer
STP	Standard Temperature Pressure
THIR	Temperature Humidity Infrared Radiometer
TIROS	Television Infra-Red Observation Satellite